5 October 2007 | $10

Science

Cell Signaling

AAAS

Volume 318, Issue 5847

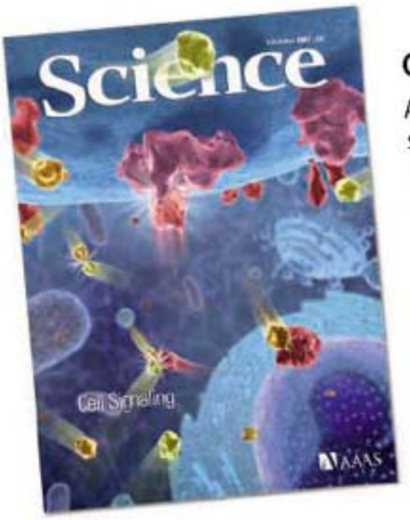

COVER

Artist's representation of the molecular signaling initiated by cell surface receptors. Four Perspectives in this issue and their associated Connections Maps in *Science*'s STKE highlight pathways that regulate diverse functions—from cell motility and survival to development in mammals, plants, and insects. See the special section beginning on page 61.

Illustration: Chris Bickel/Science

For related online content, see page 11 or go to www.sciencemag.org/sciext/cellsignaling07/

DEPARTMENTS

11 *Science* Online
13 This Week in *Science*
19 Editors' Choice
22 Contact *Science*
25 Random Samples
27 Newsmakers
121 New Products
122 *Science* Careers

EDITORIAL

17 Sputnik Nostalgia
by Donald Kennedy
>> Book Review p. 48; Perspectives pp. 51, 52, 53

SPECIAL SECTION

Cell Signaling

INTRODUCTION

An Insider's View 61

PERSPECTIVES

Life with Oxygen 62
G. L. Semenza

PI3Kγ Is a Key Regulator of Inflammatory Responses and Cardiovascular Homeostasis 64
P. T. Hawkins and L. R. Stephens

Deconstructing the Hedgehog Pathway in Development and Disease 66
L. Jacob and L. Lum

Advances in Cytokinin Signaling 68
B. Müller and J. Sheen

CONNECTIONS MAPS

Hypoxia-Inducible Factor 1 (HIF-1) Pathway
G. L. Semenza
Sci. STKE, http://stke.sciencemag.org/cgi/cm/stkecm;CMP_19178

PI3K Class IB Pathway
S. Andrews, L. Stephens, P. Hawkins
Sci. STKE, http://stke.sciencemag.org/cgi/cm/stkecm;CMP_19912

PI3K Class IB Pathway in Neutrophils
S. Andrews, L. Stephens, P. Hawkins
Sci. STKE, http://stke.sciencemag.org/cgi/cm/stkecm;CMP_20127

Hedgehog Signaling Pathway
L. Jacob and L. Lum
Sci. STKE, http://stke.sciencemag.org/cgi/cm/stkecm;CMP_19889

Hedgehog Signaling Pathway in *Drosophila*
L. Jacob and L. Lum
Sci. STKE, http://stke.sciencemag.org/cgi/cm/stkecm;CMP_20386

Cytokinin Signaling Pathway
B. Müller and J. Sheen
Sci. STKE, http://stke.sciencemag.org/cgi/cm/stkecm;CMP_9724

Arabidopsis Cytokinin Signaling Pathway
B. Müller and J. Sheen
Sci. STKE, http://stke.sciencemag.org/cgi/cm/stkecm;CMP_10021

NEWS OF THE WEEK

Promising AIDS Vaccine's Failure Leaves Field Reeling 28
Myanmar's Secret History Exposed in Satellite Images 29
At Long Last, Pathologists Hear Plants' Cry for Help 31
>> Report p. 113

SCIENCESCOPE 31
Nariokotome Boy to Go on the Road Despite Protests 32
Is Battered Arctic Sea Ice Down for the Count? 33
European Science by the Numbers 34
Europeans Lay Down Their Wish List for Next 2 Decades 35

NEWS FOCUS

Greening the Meeting 36
Offsets: Worth the Price of Emission?

This Man Wants to Green Your Lab 39
Energy-Efficient Freezers for Everyone
Do-It-Yourself Recycling

CONTENTS continued >>

Science

SCIENCE EXPRESS

www.sciencexpress.org

MOLECULAR BIOLOGY

Telomeric Repeat–Containing RNA and RNA Surveillance Factors at Mammalian Chromosome Ends
C. M. Azzalin, P. Reichenback, L. Khoriauli, E. Giulotto, J. Lingner
In mammals, RNA is transcribed from repetitive DNA at the ends of chromosomes and, along with other regulatory proteins, is incorporated locally into silenced chromatin.
10.1126/science.1147182

BIOCHEMISTRY

Nanomechanical Basis of Selective Gating by the Nuclear Pore Complex
R. Y. H. Lim, B. Fahrenkrog, J. Köser, K. Schwarz-Herion, J. Deng, U. Aebi
Regulators of nuclear permeability reversibly collapse parts of nuclear pore proteins, a process that may underlie control of nuclear transport in cells.
10.1126/science.1145980

ECOLOGY

BREVIA: Video Cameras on Wild Birds
C. Rutz, L. A. Bluff, A. A. S. Weir, A. Kacelnik
Miniaturized video cameras harnessed to wild New Caledonian crows show that they often use twigs as tools in their natural habitat.
10.1126/science.1146788

CELL BIOLOGY

Ordered Phosphorylation Governs Oscillation of a Three-Protein Circadian Clock
M. J. Rust, J. S. Markson, W. S. Lane, D. S. Fisher, E. K. O'Shea
The cycling of three protein components comprising the circadian clock in cyanobacteria is driven by a pattern of sequential phosphorylation that can be described mathematically.
10.1126/science.1148596

LETTERS

A World with Corals: What Will It Take? 42
H. Schuttenberg and O. Hoegh-Guldberg
Pseudoscience in Bosnia *P. V. Heinrich*
Effect of Poor Census Data on Population Maps
A. J. Tatem Response *S. Riley*
Light-Splitting Method Not New *P. Borden*
CORRECTIONS AND CLARIFICATIONS 44

BOOKS *ET AL.*

Breathing Space How Allergies Shape Our Lives and Landscapes *G. Mitman*; **Toxic Exposures** Contested Illnesses and the Environmental Health Movement *P. Brown*, reviewed by *P. Anker* 46

A Disappearing Number *Conceived and directed by S. McBurney, devised by Complicite*, reviewed by *L. Whiteley* 47

Epic Rivalry The Inside Story of the Soviet and American Space Race *V. Hardesty and G. Eisman* >> Editorial p. 17 48

POLICY FORUM

Learning from 10 Years of Climate Outlook Forums in Africa 49
A. G. Patt, L. Ogallo, M. Hellmuth

PERSPECTIVES

Sputnik and the Soviets 51
R. Sagdeev >> Editorial p. 17

Science and Sputnik 52
J. C. Mather >> Editorial p. 17

Sputnik and Satellite Astronomy 53
G. F. Bignami >> Editorial p. 17

Feathers, Females, and Fathers 54
M. G. Ritchie >> Report p. 95

Testing Hypotheses About Autism 56
J. N. Crawley >> Research Article p. 71

Going with the Flow 57
R. G. Larson

There's Room in the Middle 58
A. K. Cheetham and C. N. R. Rao

TECHNICAL COMMENT ABSTRACTS

NEUROSCIENCE

Comment on "Top-Down Versus Bottom-Up Control of Attention in the Prefrontal and Posterior Parietal Cortices" 44
J. D. Schall, M. Paré, G. F. Woodman
full text at www.sciencemag.org/cgi/content/full/318/5847/44b

Response to Comment on "Top-Down Versus Bottom-Up Control of Attention in the Prefrontal and Posterior Parietal Cortices"
E. K. Miller and T. J. Buschman
full text at www.sciencemag.org/cgi/content/full/318/5847/44c

BREVIA

PLANT SCIENCE

Odor-Mediated Push-Pull Pollination in Cycads 70
I. Terry, G. H. Walter, C. Moore, R. Roemer, C. Hull
To ensure pollination of female plants, male Australian cycads periodically heat up, volatilizing a toxic chemical that repels resident beetle pollinators.

RESEARCH ARTICLE

MEDICINE

A Neuroligin-3 Mutation Implicated in Autism Increases Inhibitory Synaptic Transmission in Mice 71
K. Tabuchi et al.
A mouse model reveals that a mutation that changes the balance of excitatory and inhibitory synapses affects learning skills, a finding that may help understand autism. >> Perspective p. 56

CONTENTS continued >>

REPORTS

MATERIALS SCIENCE

Polymer Gate Dielectric Surface Viscoelasticity Modulates Pentacene Transistor Performance 76

C. Kim, A. Facchetti, T. J. Marks

The electrical properties of an organic semiconductor depend on whether it is formed above or below its glass-transition temperature, offering a means to improve thin-film transistors.

MATERIALS SCIENCE

Ultrastrong and Stiff Layered Polymer Nanocomposites 80

P. Podsiadlo et al.

Deposition of alternating nanoscale layers of clay particles and a polymer yields a transparent composite that is as stiff and strong as steel.

GEOPHYSICS

Major Australian-Antarctic Plate Reorganization at Hawaiian-Emperor Bend Time 83

J. M. Whittaker et al.

Subduction of a spreading ridge and development of the Marianas-Tonga subduction zone may have initiated a major change in Pacific plate motion 50 million years ago.

ATMOSPHERIC SCIENCE

Absence of Cooling in New Zealand and the Adjacent Ocean During the Younger Dryas Chronozone 86

T. T. Barrows, S. J. Lehman, L. K. Fifield, P. De Deckker

Dating of a New Zealand moraine and nearby ocean core data show that a major cool period after the end of the last Ice Age affected only the Northern Hemisphere.

ATMOSPHERIC SCIENCE

Toward Direct Measurement of Atmospheric Nucleation 89

M. Kulmala et al.

A ubiquitous pool of neutral, nanometer-sized particle clusters dominates the process of aerosol formation over boreal forests.

PALEONTOLOGY

A Cretaceous Scleractinian Coral with a Calcitic Skeleton 92

J. Stolarski, A. Meibom, R. Przeniosło, M. Mazur

Modern reef-building corals deposit aragonite, but a fossil reef-builder formed calcite, suggesting that it arose from the extinct, calcite-depositing horn corals.

EVOLUTION

Sex Chromosome–Linked Species Recognition and Evolution of Reproductive Isolation in Flycatchers 95

S. A. Sæther et al.

Female hybrids of two flycatcher species choose mates of their fathers' species because recognition traits reside on the paternally inherited sex chromosome, maintaining speciation. >> *Perspective p. 54*

ECOLOGY

Microbial Population Structures in the Deep Marine Biosphere 97

J. A. Huber et al.

Rapid sequencing of microbial populations shows differences in archaeal diversity between two deep sea vents, but fails to provide a full inventory of the bacterial population.

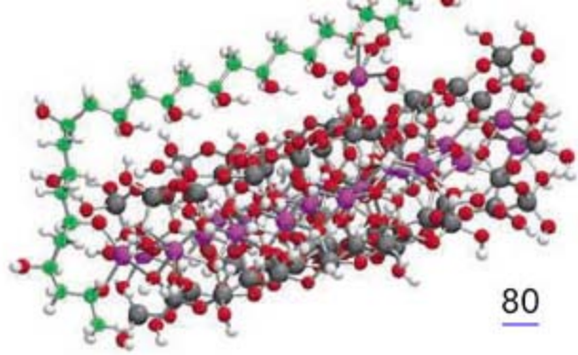

80

GENETICS

Genetic Effects of Captive Breeding Cause a Rapid, Cumulative Fitness Decline in the Wild 100

H. Araki, B. Cooper, M. S. Blouin

Steelhead trout bred in captivity and then released reproduced poorly in comparison to wild fish; these rapid negative effects may prevent use of captive fish for repopulation.

NEUROSCIENCE

Glia Promote Local Synaptogenesis Through UNC-6 (Netrin) Signaling in *C. elegans* 103

D. A. Colón-Ramos, M. A. Margeta, K. Shen

Glial cells can orchestrate neuron-to-neuron connections by attracting processes from the postsynaptic cell and triggering synapse formation in the presynaptic cell.

BEHAVIOR

Chimpanzees Are Rational Maximizers in an Ultimatum Game 107

K. Jensen, J. Call, M. Tomasello

In a game of fairness, chimpanzees act only to maximize their own benefits, whereas human toddlers also value social norms like cooperation and parity.

MOLECULAR BIOLOGY

Widespread Role for the Flowering-Time Regulators FCA and FPA in RNA-Mediated Chromatin Silencing 109

I. Bäurle, L. Smith, D. C. Baulcombe, C. Dean

Two proteins known to participate in flowering are also required for chromatin silencing at various genetic loci early in *Arabidopsis* development.

PLANT SCIENCE

Methyl Salicylate Is a Critical Mobile Signal for Plant Systemic Acquired Resistance 113

S.-W. Park, E. Kaimoyo, D. Kumar, S. Mosher, D. F. Klessig

In response to viral infection, tobacco plants locally produce methyl salicylate, which then spreads and renders the whole plant more resistant to subsequent infections. >> *News story p. 31*

IMMUNOLOGY

In Situ Imaging of the Endogenous CD8 T Cell Response to Infection 116

K. M. Khanna et al.

Imaging of the spleen during bacterial infection reveals where immune cell percursors divide and are activated by antigens, and how they migrate through channels to the blood.

AAAS

ADVANCING SCIENCE, SERVING SOCIETY

SCIENCE (ISSN 0036-8075) is published weekly on Friday, except the last week in December, by the American Association for the Advancement of Science, 1200 New York Avenue, NW, Washington, DC 20005. Periodicals Mail postage (publication No. 484460) paid at Washington, DC, and additional mailing offices.

Copyright © 2007 by the American Association for the Advancement of Science. The title SCIENCE is a registered trademark of the AAAS. Domestic individual membership and subscription (51 issues): $142 ($74 allocated to subscription). Domestic institutional subscription (51 issues): $710; Foreign postage extra: Mexico, Caribbean (surface mail) $55; other countries (air assist delivery) $85. First class, airmail, student, and emeritus rates on request. Canadian rates with GST available upon request, GST #1254 88122. Publications Mail Agreement Number 1069624. SCIENCE is printed on 30 percent post-consumer recycled paper. **Printed in the U.S.A.**

Change of address: Allow 4 weeks, giving old and new addresses and 8-digit account number. **Postmaster:** Send change of address to AAAS, P.O. Box 96178, Washington, DC 20090–6178. **Single-copy sales:** $10.00 current issue, $15.00 back issue prepaid includes surface postage; bulk rates on request. **Authorization to photocopy** material for internal or personal use under circumstances not falling within the fair use provisions of the Copyright Act is granted by AAAS to libraries and other users registered with the Copyright Clearance Center (CCC) Transactional Reporting Service, provided that $18.00 per article is paid directly to CCC, 222 Rosewood Drive, Danvers, MA 01923. The identification code for *Science* is 0036-8075. *Science* is indexed in the *Reader's Guide to Periodical Literature* and in several specialized indexes.

Printed on 30% post-consumer recycled paper.

CONTENTS continued >>

Mentoring at U.S. agencies.

SCIENCE CAREERS

www.sciencecareers.org CAREER RESOURCES FOR SCIENTISTS

US: Making Mentoring Mandatory
B. Benderly
A new law makes mentoring matter at NSF, while NIH's view of mentoring remains fuzzy.

EUROPE: Studying the Self Scientifically
E. Pain
Ph.D. student Bigna Lenggenhager has a unique area of research and has already published her work in a top journal.

US: Education Research—A New (Tenure) Track for Scientists
S. Webb
Physics has carved out a place for science-education researchers on traditional science faculties.

GRANTSNET: October 2007 Funding News
GrantsNet Staff
Learn about the latest in research funding, scholarships, fellowships, and internships.

SCIENCENOW

www.sciencenow.org DAILY NEWS COVERAGE

Once More Into the Fray
Meerkats sprint toward danger and learn in the process.

Solving the Antidepressant Paradox
Variations in two genes help explain why some people who take the drugs become more suicidal.

Dust Bowl Writ Large?
Modern conservation could head off global soil crisis.

SCIENCE PODCAST

Download the 5 October *Science* Podcast to hear about tool use by wild crows, the downsides of captive fish breeding, labs and scientific meetings going green, and more.
www.sciencemag.org/about/podcast.dtl

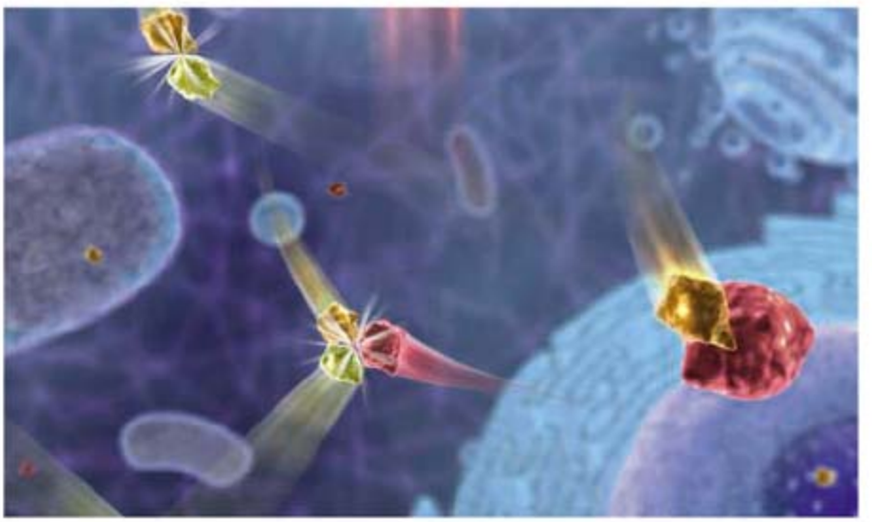

CREDIT: (SCIENCE CAREERS) AGRICULTURAL RESEARCH SERVICE

SPECIAL SECTION

Cell Signaling

SCIENCE'S STKE

www.stke.org SIGNAL TRANSDUCTION KNOWLEDGE ENVIRONMENT

EDITORIAL GUIDE: Cell Signaling—Details, Details, Details
N. R. Gough, E. M. Adler, J. F. Foley
New pathways and updates to the Database of Cell Signaling highlight how cells respond to stimuli and changing environmental conditions.

Separate individual or institutional subscriptions to these products may be required for full-text access.

EDITED BY STELLA HURTLEY AND PHIL SZUROMI

CREDITS (TOP TO BOTTOM): JAROSLAW STOLARSKI; CHOONGIK KIM/NORTHWESTERN UNIVERSITY

Rethinking Coral Composition

Modern coral reefs are built primarily by scleractinian corals, which arose in the Triassic after the Permian extinction. Today, all of these corals form skeletons of aragonite, and this composition has been thought to be typical of fossil scleractinians as well. **Stolarski *et al.*** (p. 92) now have identified a Cretaceous scleractinian coral with a primary calcite skeleton. The fine preservation of internal structures and the Mg and Sr chemistry show that the calcite is primary, not diagenetic. This result tightens the evolutionary connection between these corals and rugose corals, which formed calcite skeletons but were eliminated in the Permian extinction. These results suggest that corals may be able to alter their biochemistry in response to changes in seawater chemistry.

Intimate Contact

Composite materials commonly consist of strong or stiff particles or fibers surrounded by a matrix material. Often the best properties are observed when the contact between the reinforcing materials and the matrix are maximized, but in many cases, poor distribution and adhesion of the reinforcing material limit dispersion. **Podsiadlo *et al.*** (p. 80) used a layer-by-layer deposition technique to distribute clay platelets into a polymer matrix, and obtain nearly the idealized properties for a series of thin, transparent films. The nanometer-scale clay platelets formed ordered sheets that allow very strong hydrogen bonding with the polymer matrix, which ensured efficient load transfer between the polymer and clay.

The Importance of Neutrality

Atmospheric aerosol particles, which have diameters between 3 and 10 nanometers (nm), are formed continually in all parts of the troposphere. These particles play key roles in climate because they can absorb or reflect sunlight and affect cloud formation and atmospheric chemical reactions. However, how and in what quantities aerosols form are poorly understood, largely because of the difficulty in observing the smaller particles from which they grow. **Kulmala *et al.*** (p. 89, published online 30 August) investigated the distribution of particles smaller than 3 nm in diameter and found that an abundant pool of neutral clusters is present at almost all times. These clusters dominate the process of atmospheric aerosol formation, at least over boreal forests. These findings dispel the suggestion that aerosol production is driven mainly by processes involving ion clusters.

Check the Substrate Before You Grow

Organic thin-film transistors (TFTs) can be fabricated by depositing an organic semiconductor layer on a polymeric insulator such as polystyrene (PS) or polymethylmethacrylate that coats the gate electrode. **Kim *et al.*** (p. 76) show that these thin insulating layers have glass transition temperatures, T_g, well below that of the corresponding bulk material and in the range of temperatures normally used for deposition of the semiconductor layer. Pentacene layers grown at temperatures below the surface-depressed T_g exhibited much higher carrier mobilities and grain sizes than those layers grown at higher temperatures, where the material is rubbery and has greater polymer chain motion. Surface treatments that cross-link the chains of the insulating layer, such as oxygen-plasma treatment of PS films, increased the surface T_g and restored higher mobility.

Missing Jigsaw Piece

The Pacific tectonic plate apparently underwent a shift about 50 million years ago, as evidenced in the changing of the track of the Hawaiian-Emperor chain of seamounts. Why this happened has not been clear. **Whittaker *et al.*** (p. 83) show that additional plate movement between Australia and Antarctica around this time can be gleaned from magnetic and satellite gravity data, which would indicate that a major plate reorganization occurred between 50 and 53 million years ago. Revised Pacific Ocean–floor reconstructions suggest that subduction of the Izanagi spreading ridge and subsequent Marianas/Tonga-Kermadec subduction initiation may have been the ultimate causes of these events.

Learning, Autism, and the Synapse

A small number of individuals with autism harbor mutations in genes encoding neuroligins and neurexins, cell adhesion proteins that facilitate neuronal communication across synapses. **Tabuchi *et al.*** (p. 71, published online 6 September; see the Perspective by **Crawley**) studied the functional consequences of one of these mutations, an R451C substitution in neuroligin-3, by introducing the mutant protein into mice. The mice displayed enhanced spatial learning skills but impaired social interactions, and these behavioral changes were accompanied by a selective increase in inhibitory synaptic transmission. Thus, alterations in the balance of exci-

Continued on page 15

Continued from page 13

tatory and inhibitory synapses can affect learning and such alterations may be a contributing factor in the pathogenesis of autism.

Neuronal Roadmap

As the neural system develops, a distinctive network of interneuron connections is created. **Colón-Ramos *et al.*** (p. 103) now find that, in the nematode worm *Caenorhabditis elegans*, the supporting glial cells provide the requisite road map for making these connections. Particular glial cells express netrin, a signaling molecule, which tells the postsynaptic neuron where to find its connection and tells the presynaptic neuron where to build the substructures required for the connection. Localization of the netrin expression in the glial cells serves to focus the neuronal synapse-building capacity in the right spot.

Captive Breeding Reduces Reproductive Fitness

Captive breeding programs to prevent extinction are now in place for restoring many endangered wild populations and species, although the impact of such programs remains largely untested. **Araki *et al.*** (p. 100) evaluated the reproductive success of captive-bred fish when they breed in natural environments. Captive-reared individuals with captive-reared parents have half the reproductive success of captive-reared fish with wild parents. The rate of fitness decline can be ~40% per captive-reared generation, which suggests that breeding programs need further evaluation of their impact when used to restore declining wild populations.

CREDIT: HITOSHI ARAKI

Fair's Fair…or Not

The experimental benchmark for demonstrating that humans have developed a sense of fairness is their behavior when playing the ultimatum game. If the division of spoils proposed by the first player is not generous enough (roughly 40 to 50% of the total), the second player will usually refuse to accept the proposal (giving up any hope of a gain), which has the consequence of depriving the first player of any payout as well. **Jensen *et al.*** (p. 107) have now implemented a trimmed-down version of the ultimatum game in chimpanzees. When in the role of player 2, our nearest relatives, unlike human subjects, will accept any number of raisins, and, perhaps as a consequence, chimps show little propensity to make fair offers.

Plant Protector Identified

Plants that survive an initial pathogen attack often develop enhanced resistance to subsequent infections. For example, prior infection of tobacco plants by tobacco mosaic virus (TMV) exhibit enhanced resistance elsewhere in the plant to subsequent challenge by TMV or other pathogens, which is termed systemic acquired resistance (SAR). The development of SAR requires the movement of a signal made in the primary infected tissue through the phloem to the distal systemic tissue. **Park *et al.*** (p. 113; see the news story by Leslie) show that the mobile signal for SAR is a biologically inactive form of salicylic acid, methyl salicylate (MeSA), a key hormone for activating host defenses to many plant pathogens.

Anatomy of an Immune Response

Intravital imaging techniques allow experimentally induced immune responses to be traced in real time. Nevertheless, the techniques have often relied on the transfer of nonphysiological numbers of artificially labeled immune cells into animals. **Khanna *et al.*** (p. 116) report the use of in situ confocal microscopy of the spleen with a sufficient level of resolution to detect fine features of an immune response to a bacterial infection. Endogenous primary and secondary (memory) T cell responses could be compared, revealing unexpected relocalization within the spleen, as T cells underwent activation, expansion, and then migration out to peripheral anatomical sites.

www.cellsciences.com

Cytokine Center

Cell Sciences offers thousands of immunochemicals for life science research. Browse our web site showcasing recombinant cytokines, chemokines and growth factors, as well as enzymes, hormones, kinases, phosphatases and more.

Cell Sciences also carries corresponding antibodies, ELISA & ELISPOT kits and matched antibody pairs for assays. Competitive pricing and quick shipping worldwide!

Cell Lysates
Chemokines
Cytokines
ELISA Kits
ELISPOT Kits
Enzymes
Growth Factors
Hormones
Ion Channel Products
MonoclonalAbs
PolyclonalAbs
Proteins & Peptides
Small Molecule Antibodies
Small Molecule Antigens
Tissue Lysates

cell sciences®
480 Neponset St., Bldg. 12A
Canton, MA 02021
TEL (781) 828-0610
EMAIL info@cellsciences.com
Toll free (888) 769-1246
www.cellsciences.com

Donald Kennedy is Editor-in-Chief of *Science*.

Sputnik Nostalgia

HERE WE ARE, IN THE MIDDLE OF AN INTENSE STRUGGLE OVER HOW WE CAN IMPROVE the education of young men and women about science. In the United States, we have the America COMPETES legislation, with its emphasis on STEM, the rather dull acronym for science, technology, engineering, and mathematics education. Some nations thought to be better at STEM than the United States seem to be worrying too. My present job sometimes leads people who are concerned about the quality of science education to ask me questions like this: "What must happen to wake us up and get us really committed to this?"

Well, once upon a time, an event of that kind really did happen. On 4 October 1957, the Soviet Union launched a 183-pound Earth-orbiting satellite named Sputnik, an event whose anniversary is saluted from different national perspectives in this issue. Sputnik's appearance, and its annoying "beep-beep" as it passed overhead, produced a striking reaction in the United States that was only enhanced when the Project Vanguard rocket—a much-advertised U.S. contribution to the International Geophysical Year—blew up trying to launch a satellite much smaller than Sputnik only months later. Trumped first, then humiliated!

The response was one of those political improbabilities. Congress promptly passed the National Defense Education Act, as well as legislation that established the National Aeronautics and Space Administration. The post of Science Adviser to the President was created, though not in statute, and President James Killian of the Massachusetts Institute of Technology came to occupy it. Almost immediately, the National Science Foundation (NSF) budget for science education tripled. That soon altered lives; one of them was mine, and I hope you will forgive a few personal reflections.

The physicists quickly got to work, the CHEMStudy curriculum came along, and new opportunities for biologists appeared. Sputnik had scarcely fallen out of orbit (leaving a part or two in Los Angeles) when I found myself on a trip to Fishs Eddy, New York, which hadn't seen many college professors. There, talking with a high-school biology teacher in a downtown bar after a day in various classrooms, I found him thinking about his job in much the same way that I thought about mine. NSF later sent me to Hamilton West High in Trenton, New Jersey, showing me how tough it is to teach seven classes in a row.

Soon organizations came together to build intellectual momentum behind the sense of urgency. The Biological Sciences Curriculum Study (BSCS), founded the year after Sputnik and celebrating its 50th anniversary next year, brought together some thoughtful curriculum planners and textbook writers. That resulted in series of texts focusing on cell biology, diversity, and ecology (although its "three-colors" approach of blue, yellow, and green, respectively, produced an occasional jest). But the development of challenging curricula focusing on different levels of organization and student interests turned out to be a science education milestone.

In the early to mid-1960s, Stanford became a destination for hundreds of high-school teachers enrolling in in-service NSF summer programs. My colleague Paul Hurd in the School of Education would ask me to offer a seminar course for 15 or 20 of these students. I got to pick a topic that interested me and might perhaps be introduced into classes, should it inspire teachers. A couple of times I taught animal navigation and orientation; the seminars were fun and even interesting for some graduate students, one of whom later went with me to teach an NSF summer institute in neurobiology at Carleton College.

Lively times—but 50 years later, what can be learned from the post-Sputnik attention to science education? I think the schools improved through teacher training and curricular innovation, largely due to strong federal engagement. First lesson for today: Let's lose our national wariness about letting the feds into K-12 education. The second lesson comes from perhaps the greatest reward of the Sputnik experience: the establishment of a real community of professional engagement among committed people who taught science at different levels. In the current movement toward school reform, revitalizing that sense of shared mission may be the most important policy goal of all.

– Donald Kennedy

10.1126/science.1150389

CREDIT: DARIN FONG/ISTOCKPHOTO

EDITED BY GILBERT CHIN AND JAKE YESTON

PSYCHOLOGY

State of Reference

Students in elementary physics classes are introduced to the concept of frame of reference—the spatial coordinate system used by an observer to describe events—for instance, in the context of the perceived motion of trees by a passenger in a moving automobile. Adding in the dimension of time leads into nonintuitive territory, as in the example of a traveling astronaut who returns to Earth younger than her stay-at-home twin.

Building on previous work that demonstrated that internal physiological states can influence one's perception of physical quantities (such as thirsty people being more likely to characterize objects as transparent; that is, resembling water), Balcetis and Dunning show that internal psychological states are also capable of altering our perception of the external world. They induced states of high or low cognitive dissonance (a mismatch between thought and action) by asking or telling two groups of students to walk across campus wearing various fruit- and vegetable-themed adornments. In order to render a freely chosen yet somewhat embarrassing task less unpleasant to fulfill, the first set of students mentally shortened the distance they had to cover by estimating it to be fully 40% less than the average estimate made by the second group. Intriguingly, the route to ameliorating the state of dissonance appeared to be purely perceptual, as the free-choice students did not shorten their time of exposure by walking faster; in fact, they took about 10% longer. — GJC

Psychol. Sci. **18**, 917 (2007).

MATERIALS SCIENCE

Thin and Fast

Temperature changes in gas-phase chemical processes such as combustion and explosions can evolve on the submicrosecond time scale, but commercial thermocouples (TCs) are limited to millisecond response times. Thin-film TCs can achieve submicrosecond responses, but extreme film thinness (less than 100 nm) affects sensitivity through decreases in the thermopower. In principle, TCs made from submicrometer-diameter wires (SMTCs) would have a more favorable change in thermal mass and could be thicker (1.0 to 0.5 μm). Bourg *et al.* fabricated SMTCs by first electrodepositing silver wires 1.0 to 0.5 μm in diameter onto half of a stepped graphite surface. A mask covering the other half of the substrate was removed, the silver wires were coated with a self-assembled alkanethiol monolayer, and nickel wires were deposited. The arrays were then pressed into a cyanoacrylate adhesive, and after hardening, the graphite was removed. Scanning electron microscopy revealed a robust weld at the silver/nickel interface. The success rate for SMTCs ranged up to 80%, and these junctions were functional after months of air exposure. In laser-heating tests, response times varied from tenths of microseconds to several microseconds, with outputs of 20 μV/°C. — PDS

Nano Lett. **7**, 10.1021/nl071990q (2007).

CREDITS (TOP TO BOTTOM): ERICH LESSING / ART RESOURCE, NY; SUN *ET AL.*, *NAT. CELL BIOL.* **9**, 1057 (2007)

CELL BIOLOGY

Death Throes in Living Color

Mitochondria—the tiny double-membrane–bounded organelles that provide healthy cells with a ready supply of energy—also play a key role in the triggering of programmed cell death or apoptosis. Sun *et al.* have combined light microscopy and three-dimensional electron microscopic tomography to record in detail the structural changes in mitochondria in cells that have been stimulated to undergo apoptosis. One of the first events observed after stimulation was a rearrangement of submitochondrial morphology: The inner mitochondrial membrane changed from an organized arrangement of folded membrane cristae into a vesicular patchwork, which was accompanied by the release of several mitochondrial proteins into the cytosol. However, one key mitochondrial protein involved in the apoptosis pathway, cytochrome c, was released efficiently independently of and before this remodeling. Swelling of the mitochondria occurred after the collapse of the membrane potential and was accompanied by a dissolution of the intramitochondrial structure. This generation of a composite time-course overview of morphological changes within single cells should help to dissect a variety of nonsynchronous cellular events. — SMH

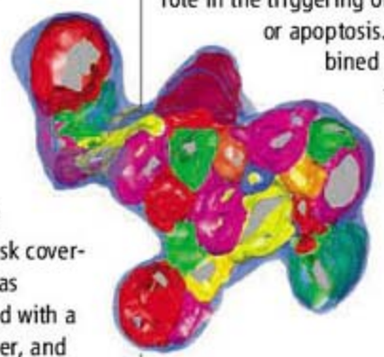

Vesiculated reconstructed mitochondria.

Nat. Cell Biol. **9**, 1057 (2007).

ECOLOGY/EVOLUTION

Something Fishy in Speciation

Adaptation to environmental conditions is believed to drive population divergence and hence demonstrates the predictability of evolutionary change. By investigating the morphology, genetic divergence, and mate choice of Bahamas mosquitofish, which live in isolated pools, Langerhans *et al.* demonstrate parallel speciation events among pools, in which the presence or absence of a fish predator appears to be driving speciation. In pools with strong predation, mosquitofish have evolved a morphology conducive to high-speed escape swim-

Continued on page 21

Continued from page 19

ming. Haplotype and allozyme analyses show that these morphological changes in response to predation have occurred multiple times. As these fish prefer to mate with similar individuals, the presence or absence of a predator drives speciation through mate selection. Taken all together, this set of results shows a direct link between natural selection and speciation: The traits under divergent selection between environments are the same traits used in mate choice, resulting in reproductive isolation between populations inhabiting different environments. — LMZ

Evolution **61**, 2056 (2007).

APPLIED PHYSICS

A Bigger Photonic Playground

In metallic nanostructures, surface plasmons, the collective oscillations of free electrons, can induce such phenomena as enhanced optical transmission and collimation of light through a subwavelength aperture. Though the structures are patterned on length scales of 100 nm, surface plasmons can interact over much longer distances. Henzie *et al.* cleverly combined a series of standard lithographic techniques to make larger photonic structures. Using interference lithography, they patterned high-quality silicon masters from which hundreds of photomasks could be made for patterning over centimeter length scales. Patterns of holes were created in both Si and Au films, either as infinite arrays or as a set of islands or patches. The patterned Au arrays exhibited an order-of-magnitude enhancement of optical transmission, a feature comparable to the optical quality seen in nanohole films produced by ion milling. When patches were not too far apart, plasmon interactions between them also led to much higher sensitivity in refractive index sensing. — MSL

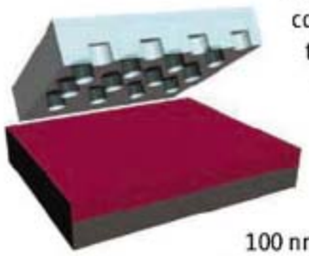

CREDIT: HENZIE *ET AL., NAT. NANOTECHNOL.* **2**, 549 (2007)

Nat. Nanotechnol. **2**, 549 (2007).

ECOLOGY

Millennium Bugs

One thousand years ago, the Emperor of China ordered that locust abundance be recorded so as to predict swarms. Although wetland management techniques reduced locust outbreaks in the second half of the 20th century, they have recently become troublesome again in the Yangtze and Yellow River basins, perhaps as a consequence of global climate change. Locust numbers peak during drought years and in years after floods, reflecting differential effects of moisture and warmth on different life cycle stages. This discrepancy has made it difficult to predict how the warmer and wetter conditions that are projected to prevail in East Asia will affect locust numbers.

Stige *et al.* combined the millennial time-series data with recent temperature and precipitation reconstructions of historical weather and discovered that locust abundance is highest during periods with a high frequency of floods and droughts. The records reveal that these more variable climates actually tended to occur during the coldest and wettest decades. So, warmer conditions will not necessarily favor locust breeding. — CA

Proc. Natl. Acad. Sci. U.S.A. **104**, 10.1073/pnas0706813104 (2007).

Science STKE AAAS

www.stke.org

<< Gut Sensations

Recent studies have helped to define the proteins that transform the arrival of sugars on the tongue into a sensation of sweetness. Two studies suggest that the same pathway functions in the intestinal tract. Jang *et al.* found that the sugar-sensitive G protein–coupled receptor (T1R2/T1R3) and the G protein subunit gustducin could be detected in enteroendocrine cells—specifically, the L cells, which secrete the appetite-regulating glucagon-like peptide (GLP-1) of the human duodenum. Application of glucose to human L cells resulted in GLP-1 release, which was blocked by an antagonist of T1R3. In mice, gustducin was also present in L cells, and delivering glucose directly into the duodenums (to bypass the tongue) of normal mice and of gustducin-deficient mice showed that GLP-1 secretion was absent in the latter group of animals and that the temporal pattern of insulin secretion was altered. Margolskee *et al.* connect glucose absorption to glucose sensing via the T1R2/T1R3 pathway. Normal mice, unlike those deficient in gustducin or T1R3, showed an increase in sodium-glucose cotransporter 1 (SGLT1) mRNA and protein and in glucose uptake when fed a high-carbohydrate diet or a low-carb diet containing artificial sweeteners. — NRG

Proc. Natl. Acad. Sci. U.S.A. **104**, 15069; 15075 (2007).

High photostability and unsurpassed brightness!

NOVEL FAR-RED FLUORESCENT PROTEINS

TurboFP635

superbright and fast-maturing far-red fluorescent reporter for cell labeling within living tissues

TagFP635

bright monomeric far-red fluorescent tag for protein localization studies

Excitation max	588 nm
Emission max	635 nm

Published in Shcherbo *et al.* (2007) Bright far-red fluorescent protein for whole-body imaging. Nat. Methods 4(9): 741-746

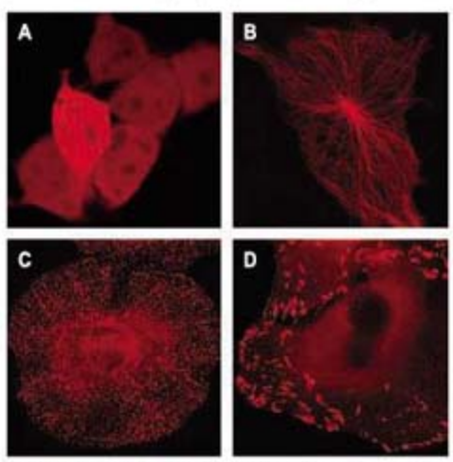

Cell and protein labeling using far-red proteins

Phoenix cells expressing TurboFP635 (A); 3T3 cells expressing TagFP635 fusion with alpha-tubulin (B); HeLa cells expressing TagFP635 fusions with clathrin (C) and vinculin (D).

Images C-D were kindly provided by Michael W. Davidson (Florida State University).

Evrogen JSC
Tel: +7(495) 336 6388
Fax: +7(495) 429 8520
www.evrogen.com

evrogen

www.sciencemag.org

Science

1200 New York Avenue, NW
Washington, DC 20005
Editorial: 202-326-6550, FAX 202-289-7562
News: 202-326-6581, FAX 202-371-9227

Bateman House, 82-88 Hills Road
Cambridge, UK CB2 1LQ
+44 (0) 1223 326500, FAX +44 (0) 1223 326501

SUBSCRIPTION SERVICES For change of address, missing issues, new orders and renewals, and payment questions: 866-434-AAAS (2227) or 202-326-6417, FAX 202-842-1065. Mailing addresses: AAAS, P.O. Box 96178, Washington, DC 20090-6178 or AAAS Member Services, 1200 New York Avenue, NW, Washington, DC 20005

INSTITUTIONAL SITE LICENSES please call 202-326-6755 for any questions or information

REPRINTS: Author Inquiries 800-635-7181
Commercial Inquiries 803-359-4578

PERMISSIONS 202-326-7074, FAX 202-682-0816

MEMBER BENEFITS Bookstore: AAAS/BarnesandNoble.com bookstore www.aaas.org/bn; Car purchase discount: Subaru VIP Program 202-326-6417; Credit Card: MBNA 800-847-7378; Car Rentals: Hertz 800-654-2200 CDP#343457, Dollar 800-800-4000 #AA1115; AAAS Travels: Betchart Expeditions 800-252-4910; Life Insurance: Seabury & Smith 800-424-9883; Other Benefits: AAAS Member Services 202-326-6417 or www.aaasmember.org.

science_editors@aaas.org	(for general editorial queries)
science_letters@aaas.org	(for queries about letters)
science_reviews@aaas.org	(for returning manuscript reviews)
science_bookrevs@aaas.org	(for book review queries)

Published by the American Association for the Advancement of Science (AAAS), *Science* serves its readers as a forum for the presentation and discussion of important issues related to the advancement of science, including the presentation of minority or conflicting points of view, rather than by publishing only material on which a consensus has been reached. Accordingly, all articles published in *Science*—including editorials, news and comment, and book reviews—are signed and reflect the individual views of the authors and not official points of view adopted by the AAAS or the institutions with which the authors are affiliated.

AAAS was founded in 1848 and incorporated in 1874. Its mission is to advance science and innovation throughout the world for the benefit of all people. The goals of the association are to: foster communication among scientists, engineers and the public; enhance international cooperation in science and its applications; promote the responsible conduct and use of science and technology; foster education in science and technology for everyone; enhance the science and technology workforce and infrastructure; increase public understanding and appreciation of science and technology; and strengthen support for the science and technology enterprise.

INFORMATION FOR AUTHORS

See pages 120 and 121 of the 5 January 2007 issue or access www.sciencemag.org/feature/contribinfo/home.shtml

EDITOR-IN-CHIEF **Donald Kennedy**
EXECUTIVE EDITOR **Monica M. Bradford**
DEPUTY EDITORS **R. Brooks Hanson, Barbara R. Jasny, Katrina L. Kelner**
NEWS EDITOR **Colin Norman**

EDITORIAL SUPERVISORY SENIOR EDITOR Phillip D. Szuromi; **SENIOR EDITOR/PERSPECTIVES** Lisa D. Chong; **SENIOR EDITORS** Gilbert J. Chin, Pamela J. Hines, Paula A. Kiberstis (Boston), Marc S. Lavine (Toronto), Beverly A. Purnell, L. Bryan Ray, Guy Riddihough, H. Jesse Smith, Valda Vinson, David Voss; **ASSOCIATE EDITORS** Jake S. Yeston, Laura M. Zahn; **ONLINE EDITOR** Stewart Wills; **ASSOCIATE ONLINE EDITORS** Robert Frederick, Tara S. Marathe; **BOOK REVIEW EDITOR** Sherman J. Suter; **ASSOCIATE LETTERS EDITOR** Etta Kavanagh; **EDITORIAL MANAGER** Cara Tate; **SENIOR COPY EDITORS** Jeffrey E. Cook, Cynthia Howe, Harry Jach, Barbara P. Ordway, Jennifer Sills, Trista Wagoner; **COPY EDITORS** Lauren Kmec, Peter Mooreside; **EDITORIAL COORDINATORS** Carolyn Kyle, Beverly Shields; **PUBLICATIONS ASSISTANTS** Ramatoulaye Diop, Chris Filiatreau, Joi S. Granger, Jeffrey Hearn, Lisa Johnson, Scott Miller, Jerry Richardson, Brian White, Anita Wynn; **EDITORIAL ASSISTANTS** Emily Guise, Patricia M. Moore, Jennifer A. Seibert; **EXECUTIVE ASSISTANT** Sylvia S. Kihara; **ADMINISTRATIVE SUPPORT** Maryrose Madrid

NEWS SENIOR CORRESPONDENT Jean Marx; **DEPUTY NEWS EDITORS** Robert Coontz, Eliot Marshall, Jeffrey Mervis, Leslie Roberts; **CONTRIBUTING EDITORS** Elizabeth Culotta, Polly Shulman; **NEWS WRITERS** Yudhijit Bhattacharjee, Adrian Cho, Jennifer Couzin, David Grimm, Constance Holden, Jocelyn Kaiser, Richard A. Kerr, Eli Kintisch, Andrew Lawler (New England), Greg Miller, Elizabeth Pennisi, Robert F. Service (Pacific NW), Erik Stokstad; **INTERNS** Benjamin Lester, Marissa Cevallos, Veronica Raymond; **CONTRIBUTING CORRESPONDENTS** Barry A. Cipra, Jon Cohen (San Diego, CA), Daniel Ferber, Ann Gibbons, Robert Irion, Mitch Leslie, Charles C. Mann, Evelyn Strauss, Gary Taubes; **COPY EDITORS** Rachel Curran, Linda B. Felaco, Melvin Gatling; **ADMINISTRATIVE SUPPORT** Scherraine Mack, Fannie Groom; **BUREAUS** New England: 207-549-7755, San Diego, CA: 760-942-3252, FAX 760-942-4979, Pacific Northwest: 503-963-1940

PRODUCTION DIRECTOR James Landry; **SENIOR MANAGER** Wendy K. Shank; **ASSISTANT MANAGER** Rebecca Doshi; **SENIOR SPECIALISTS** Jay Covert, Chris Redwood; **SPECIALIST** Steve Forrester; **PREFLIGHT DIRECTOR** David M. Tompkins; **MANAGER** Marcus Spiegler; **SPECIALIST** Jessie Mudjitaba

ART DIRECTOR Kelly Buckheit Krause; **ASSOCIATE ART DIRECTOR** Aaron Morales; **ILLUSTRATORS** Chris Bickel, Katharine Sutliff; **SENIOR ART ASSOCIATES** Holly Bishop, Laura Creveling, Preston Huey, Nayomi Kevitiyagala; **ASSOCIATE** Jessica Newfield; **PHOTO EDITOR** Leslie Blizard

***SCIENCE* INTERNATIONAL**

EUROPE (science@science-int.co.uk) **EDITORIAL: INTERNATIONAL MANAGING EDITOR** Andrew M. Sugden; **SENIOR EDITOR/PERSPECTIVES** Julia Fahrenkamp-Uppenbrink; **SENIOR EDITORS** Caroline Ash, Stella M. Hurtley, Ian S. Osborne, Stephen J. Simpson, Peter Stern; **ASSOCIATE EDITOR** Joanne Baker; **EDITORIAL SUPPORT** Deborah Dennison, Rachel Roberts, Alice Whaley; **ADMINISTRATIVE SUPPORT** Janet Clements, Jill White; **NEWS: EUROPE NEWS EDITOR** John Travis; **DEPUTY NEWS EDITOR** Daniel Clery; **CONTRIBUTING CORRESPONDENTS** Michael Balter (Paris), John Bohannon (Vienna), Martin Enserink (Amsterdam and Paris), Gretchen Vogel (Berlin)

ASIA Japan Office: Asca Corporation, Eiko Ishioka, Fusako Tamura, 1-8-13, Hirano-cho, Chuo-ku, Osaka-shi, Osaka, 541-0046 Japan; +81 (0) 6 6202 6272, FAX +81 (0) 6 6202 6271; asca@os.gulf.or.jp; **ASIA NEWS EDITOR** Richard Stone +66 2 662 5818 (rstone@aaas.org); **CONTRIBUTING CORRESPONDENTS** Dennis Normile (Japan: +81 (0) 3 3391 0630, FAX 81 (0) 3 5936 3531; dnormile@goL.com); Hao Xin (China: + 86 (0) 10 6307 4439 or 6307 3676, FAX +86 (0) 10 6307 4358; cindyhao@gmail.com); Pallava Bagla (South Asia: +91 (0) 11 2271 2896; pbagla@vsnl.com)

AFRICA Robert Koenig (contributing correspondent, rob.koenig@gmail.com)

EXECUTIVE PUBLISHER **Alan I. Leshner**
PUBLISHER **Beth Rosner**

FULFILLMENT SYSTEMS AND OPERATIONS (membership@aaas.org) **DIRECTOR** Waylon Butler; **CUSTOMER SERVICE SUPERVISOR** Pat Butler; **SPECIALISTS** Laurie Baker, Latoya Casteel, Lavanda Crawford, Vicki Linton; **DATA ENTRY SUPERVISOR** Cynthia Johnson; **SPECIALISTS** Tomeka Diggs, Tarrika Hill, Erin Layne, Sheila Thomas; **SYSTEMS ANALYST** Tim Popoola

BUSINESS OPERATIONS AND ADMINISTRATION DIRECTOR Deborah Rivera-Wienhold; **ASSISTANT DIRECTOR, BUSINESS OPERATIONS** Randy Yi; **SENIOR FINANCIAL ANALYSTS** Michael LoBue, Jessica Tierney; **FINANCIAL ANALYSTS** Nicole Nicholson, Farida Yeasmin; **RIGHTS AND PERMISSIONS: ADMINISTRATOR** Emilie David; **ASSOCIATE** Elizabeth Sandler; **MARKETING DIRECTOR** John Meyers; **MARKETING MANAGERS** Darryl Walter, Allison Pritchard; **MARKETING ASSOCIATES** Julianne Wielga, Mary Ellen Crowley, Alison Chandler, Marcia Leach, Wendy Wise; **INTERNATIONAL MARKETING MANAGER** Wendy Sturley; **MARKETING EXECUTIVE** Jennifer Reeves; **MARKETING/MEMBER SERVICES EXECUTIVE** Linda Rusk; **JAPAN SALES** Jason Hannaford; **SITE LICENSE SALES DIRECTOR** Tom Ryan; **SALES MANAGER** Russ Edra; **SALES AND CUSTOMER SERVICE** Mehan Dossani, Iquo Edim, Kiki Forsythe, Catherine Holland, Phillip Smith; **ELECTRONIC MEDIA: MANAGER** Lizabeth Harman; **PROJECT MANAGER** Trista Snyder; **ASSISTANT MANAGER** Lisa Stanford; **SENIOR PRODUCTION SPECIALIST** Walter Jones; **PRODUCTION SPECIALISTS** Nichele Johnston, Kimberly Oster

ADVERTISING DIRECTOR WORLDWIDE AD SALES Bill Moran

PRODUCT (science_advertising@aaas.org); **CONSUMER & SPONSORSHIP SALES MANAGER** Tina Morra: 202-326-6542; **MIDWEST** Rick Bongiovanni: 330-405-7080, FAX 330-405-7081; **WEST COAST/W. CANADA** Teola Young: 650-964-2266; **EAST COAST/E. CANADA** Christopher Breslin: 443-512-0330, FAX 443-512-0331; **UK/EUROPE/ASIA** Michelle Field: +44 (0) 1223-326-524, FAX +44 (0) 1223-325-532; **JAPAN** Mashy Yoshikawa: +81 (0) 33235 5961, FAX +81 (0) 33235 5852; **SENIOR TRAFFIC ASSOCIATE** Deiandra Simms

COMMERCIAL EDITOR Sean Sanders: 202-326-6430

CLASSIFIED (advertise@sciencecareers.org); **U.S.: RECRUITMENT SALES MANAGER** Ian King: 202-326-6528, FAX 202-289-6742; **INSIDE SALES MANAGER: MIDWEST/CANADA** Daryl Anderson: 202-326-6543; **NORTHEAST** Alexis Fleming: 202-326-6578; **NORTHEAST** Allison Millar: 202-326-6572; **SOUTHEAST** Tina Burks: 202-326-6577; **WEST** Nicholas Hintibidze: 202-326-6533; **SALES COORDINATORS** Erika Foard, Rohan Edmonson, Leonard Marshall, Shirley Young; **INTERNATIONAL: SALES MANAGER** Tracy Holmes: +44 (0) 1223 326525, FAX +44 (0) 1223 326532; **SALES** Marium Hudda, Alex Palmer, Alessandra Sorgente; **SALES ASSISTANT** Louise Moore; **JAPAN** Jason Hannaford: +81 (0) 52 757 5360, FAX +81 (0) 52 757 5361; **ADVERTISING PRODUCTION OPERATIONS MANAGER** Deborah Tompkins; **SENIOR PRODUCTION SPECIALISTS** Robert Buck, Amy Hardcastle; **SENIOR TRAFFIC ASSOCIATE** Christine Hall; **PUBLICATIONS ASSISTANT** Mary Lagnaoui

AAAS BOARD OF DIRECTORS RETIRING PRESIDENT, CHAIR John P. Holdren; **PRESIDENT** David Baltimore; **PRESIDENT-ELECT** James J. McCarthy; **TREASURER** David E. Shaw; **CHIEF EXECUTIVE OFFICER** Alan I. Leshner; **BOARD** John E. Dowling, Lynn W. Enquist, Susan M. Fitzpatrick, Alice Gast, Linda P. B. Katehi, Cherry A. Murray, Thomas D. Pollard, Kathryn D. Sullivan

AAAS
ADVANCING SCIENCE, SERVING SOCIETY

SENIOR EDITORIAL BOARD

John I. Brauman, *Chair, Stanford Univ.*
Richard Losick, *Harvard Univ.*
Robert May, *Univ. of Oxford*
Marcia McNutt, *Monterey Bay Aquarium Research Inst.*
Linda Partridge, *Univ. College London*
Vera C. Rubin, *Carnegie Institution*
Christopher R. Somerville, *Carnegie Institution*
George M. Whitesides, *Harvard Univ.*

BOARD OF REVIEWING EDITORS

Joanna Aizenberg, *Harvard Univ.*
R. McNeill Alexander, *Leeds Univ.*
David Altshuler, *Broad Institute*
Arturo Alvarez-Buylla, *Univ. of California, San Francisco*
Richard Amasino, *Univ. of Wisconsin, Madison*
Meinrat O. Andreae, *Max Planck Inst., Mainz*
Kristi S. Anseth, *Univ. of Colorado*
John A. Bargh, *Yale Univ.*
Cornelia I. Bargmann, *Rockefeller Univ.*
Marisa Bartolomei, *Univ. of Penn. School of Med.*
Brenda Bass, *Univ. of Utah*
Ray H. Baughman, *Univ. of Texas, Dallas*
Stephen J. Benkovic, *Pennsylvania St. Univ.*
Michael J. Bevan, *Univ. of Washington*
Ton Bisseling, *Wageningen Univ.*
Mina Bissell, *Lawrence Berkeley National Lab*
Peer Bork, *EMBL*
Dianna Bowles, *Univ. of York*
Robert W. Boyd, *Univ. of Rochester*
Paul M. Brakefield, *Leiden Univ.*
Dennis Bray, *Univ. of Cambridge*
Stephen Buratowski, *Harvard Medical School*
Jillian M. Buriak, *Univ. of Alberta*
Joseph A. Burns, *Cornell Univ.*
William P. Butz, *Population Reference Bureau*
Peter Carmeliet, *Univ. of Leuven, VIB*
Gerbrand Ceder, *MIT*
Mildred Cho, *Stanford Univ.*
David Clapham, *Children's Hospital, Boston*
David Clary, *Oxford University*
J. M. Claverie, *CNRS, Marseille*
Jonathan D. Cohen, *Princeton Univ.*
Stephen M. Cohen, *EMBL*
Robert H. Crabtree, *Yale Univ.*
E. Fleming Crim, *Univ. of Wisconsin*
William Cumberland, *UCLA*
George Q. Daley, *Children's Hospital, Boston*
Edward DeLong, *MIT*
Emmanouil T. Dermitzakis, *Wellcome Trust Sanger Inst.*
Robert Desimone, *MIT*
Dennis Discher, *Univ. of Pennsylvania*
Scott C. Doney, *Woods Hole Oceanographic Inst.*
W. Ford Doolittle, *Dalhousie Univ.*
Jennifer A. Doudna, *Univ. of California, Berkeley*
Julian Downward, *Cancer Research UK*
Denis Duboule, *Univ. of Geneva/EPFL Lausanne*
Christopher Dye, *WHO*
Richard Ellis, *CalTech*
Gerhard Ertl, *Fritz-Haber-Institut, Berlin*
Douglas H. Erwin, *Smithsonian Institution*
Mark Estelle, *Indiana Univ.*
Barry Everitt, *Univ. of Cambridge*
Paul G. Falkowski, *Rutgers Univ.*
Ernst Fehr, *Univ. of Zurich*
Tom Fenchel, *Univ. of Copenhagen*
Alain Fischer, *INSERM*
Jeffrey S. Flier, *Harvard Medical School*
Scott E. Fraser, *CalTech*
Chris D. Frith, *Univ. College London*
John Gearhart, *Johns Hopkins Univ.*
Wulfram Gerstner, *EPFL Lausanne*
Charles Godfray, *Univ. of Oxford*
Christian Haass, *Ludwig Maximilians Univ.*
Dennis L. Hartmann, *Univ. of Washington*
Chris Hawkesworth, *Univ. of Bristol*
Martin Heimann, *Max Planck Inst., Jena*
James A. Hendler, *Rensselaer Polytechnic Inst.*
Ray Hilborn, *Univ. of Washington*
Ove Hoegh-Guldberg, *Univ. of Queensland*
Ary A. Hoffmann, *La Trobe Univ.*
Ronald R. Hoy, *Cornell Univ.*
Evelyn L. Hu, *Univ. of California, Santa Barbara*
Olli Ikkala, *Helsinki Univ. of Technology*
Meyer B. Jackson, *Univ. of Wisconsin Med. School*
Stephen Jackson, *Univ. of Cambridge*
Steven Jacobsen, *Univ. of California, Los Angeles*
Peter Jonas, *Universität Freiburg*
Daniel Kahne, *Harvard Univ.*
Bernhard Keimer, *Max Planck Inst., Stuttgart*
Elizabeth A. Kellog, *Univ. of Missouri, St. Louis*
Alan B. Krueger, *Princeton Univ.*
Lee Kump, *Penn State*
Mitchell A. Lazar, *Univ. of Pennsylvania*
Virginia Lee, *Univ. of Pennsylvania*
Anthony J. Leggett, *Univ. of Illinois, Urbana-Champaign*
Michael J. Lenardo, *NIAID, NIH*
Norman L. Letvin, *Beth Israel Deaconess Medical Center*
Olle Lindvall, *Univ. Hospital, Lund*
John Lis, *Cornell Univ.*
Richard Losick, *Harvard Univ.*
Ke Lu, *Chinese Acad. of Sciences*
Andrew P. MacKenzie, *Univ. of St. Andrews*
Raul Madariaga, *École Normale Supérieure, Paris*
Anne Magurran, *Univ. of St. Andrews*
Michael Malim, *King's College, London*
Virginia Miller, *Washington Univ.*
Yasushi Miyashita, *Univ. of Tokyo*
Richard Morris, *Univ. of Edinburgh*
Edvard Moser, *Norwegian Univ. of Science and Technology*
Naoto Nagaosa, *Univ. of Tokyo*
James Nelson, *Stanford Univ. School of Med.*
Roeland Nolte, *Univ. of Nijmegen*
Helga Nowotny, *European Research Advisory Board*
Eric N. Olson, *Univ. of Texas, SW*
Erin O'Shea, *Harvard Univ.*
Elinor Ostrom, *Indiana Univ.*
Jonathan T. Overpeck, *Univ. of Arizona*
John Pendry, *Imperial College*
Philippe Poulin, *CNRS*
Mary Power, *Univ. of California, Berkeley*
Molly Przeworski, *Univ. of Chicago*
David J. Read, *Univ. of Sheffield*
Les Real, *Emory Univ.*
Colin Renfrew, *Univ. of Cambridge*
Trevor Robbins, *Univ. of Cambridge*
Barbara A. Romanowicz, *Univ. of California, Berkeley*
Nancy Ross, *Virginia Tech*
Edward M. Rubin, *Lawrence Berkeley National Lab*
J. Roy Sambles, *Univ. of Exeter*
Jürgen Sandkühler, *Medical Univ. of Vienna*
David S. Schimel, *National Center for Atmospheric Research*
Georg Schulz, *Albert-Ludwigs-Universität*
Paul Schulze-Lefert, *Max Planck Inst., Cologne*
Terrence J. Sejnowski, *The Salk Institute*
David Sibley, *Washington Univ.*
Montgomery Slatkin, *Univ. of California, Berkeley*
George Somero, *Stanford Univ.*
Joan Steitz, *Yale Univ.*
Elsbeth Stem, *ETH Zürich*
Thomas Stocker, *Univ. of Bern*
Jerome Strauss, *Virginia Commonwealth Univ.*
Marc Tatar, *Brown Univ.*
Glenn Telling, *Univ. of Kentucky*
Marc Tessier-Lavigne, *Genentech*
Michiel van der Klis, *Astronomical Inst. of Amsterdam*
Derek van der Kooy, *Univ. of Toronto*
Bert Vogelstein, *Johns Hopkins*
Christopher A. Walsh, *Harvard Medical School*
Graham Warren, *Yale Univ. School of Med.*
Colin Watts, *Univ. of Dundee*
Julia R. Weertman, *Northwestern Univ.*
Detlef Weigel, *Max Planck Inst., Tübingen*
Jonathan Weissman, *Univ. of California, San Francisco*
Ellen D. Williams, *Univ. of Maryland*
R. Sanders Williams, *Duke University*
Ian A. Wilson, *The Scripps Res. Inst.*
Jerry Workman, *Stowers Inst. for Medical Research*
John R. Yates III, *The Scripps Res. Inst.*
Martin Zatz, *NIMH, NIH*
Huda Zoghbi, *Baylor College of Medicine*
Maria Zuber, *MIT*

BOOK REVIEW BOARD

John Aldrich, *Duke Univ.*
David Bloom, *Harvard Univ.*
Angela Creager, *Princeton Univ.*
Richard Shweder, *Univ. of Chicago*
Ed Wasserman, *DuPont*
Lewis Wolpert, *Univ. College, London*

Beetle Battles

Collecting stag beetles is a long-established hobby for Japanese boys. But things are now getting out of hand: Thanks to an arcade game called Mushi (insect) King, the beetles are all over Japan, and one subspecies is becoming endangered in its native habitat in Turkey.

In Mushi King, players collect cards with the picture and vital statistics of one of various beetle species. By inserting the card into the game machine, players control their bug in virtual fights. The game has spurred interest in exotic beetles, leading to imports of more than a million a year, according to Koichi Goka, an entomologist at the National Institute for Environmental Studies in Tsukuba. Prize bugs sell over the Internet for $400 or more.

This year's hottest beetle is *Lucanus cervus akbesianus*, a rare subspecies found only in the Amanos Mountains of southern Turkey. The Amanos Environmental Protection Association has warned that overharvesting is pushing this beetle toward extinction.

In Japan, meanwhile, Goka worries that the beetle battle might move into the real world if the aliens escape and breed, with the big foreign bugs muscling out their weaker domestic rivals. "It is not an actual problem yet, but there is a big risk," Goka says. But, he says, the Environment Ministry hesitates to designate stag beetles as an invasive species because "the market has already become too large to control."

Hot beetle.

NET WATCH

Posthumous Peer Review

Remembrances of deceased members written since 1995 have been available at the U.S. National Academy of Sciences Biographical Memoirs Web site. Now the site is adding more than 900 accounts dating back to 1877. They aren't your typical sketchy Web bios but are hefty appreciations of the subject's work and life, typically written shortly after the person's death by colleagues or friends.

The former chief engineer at AT&T offers his take on Alexander Graham Bell, for example, and physics heavyweight Hans Bethe recalls J. Robert Oppenheimer, who headed the Manhattan Project. >> www.nasonline.org/site/PageServer?pagename=MEMOIRS_A

Our Ancestral Brains

Evolutionary psychologists have come up with a new piece of evidence that we are still operating with our old hunter-gatherer brains: We notice animals more than we notice objects.

Graduate student Joshua New, along with John Tooby and Leda Cosmides, both of the University of California, Santa Barbara, theorized that human beings have evolved a "category-specific" attention system that pays especially close heed to other animals. To test the idea, they showed volunteers scenes for a fraction of a second and then the same scenes with changes in the position of an animal or an object, including a car. Even when the animals were smaller than or not contrasted as much as the objects, the viewers spotted changes in their position more quickly and accurately than they did changes in inanimate targets.

The authors, in a paper published online last week in the *Proceedings of the National Academy of Sciences*, say animals are detected faster not simply because they are more interesting. "Even dull animals like pigeons … recruit a surprising amount of attention—as do turtles resembling rocks," Tooby says.

Viewers notice changes in the elephant (circled, *above*) more often than in the van (*below*).

David Buss, an evolutionary psychologist at the University of Texas, Austin, says the work bolsters the theory that humans evolved "specialized psychological mechanisms … for solving distinct adaptive problems." The alternative view is that human information-processing machinery is "domain-general" and did not evolve to process specific types of information.

WORLD OF WATER

Replicas of distinctive towers that rise from California's extremely salty Mono Lake will be featured at a major exhibit on water at the American Museum of Natural History in New York City. The massive pillars, of a type of limestone called tufa, form underwater from an interaction of calcium from freshwater springs with carbonates in the lake water. Up to 10 meters high, they now poke out because of water diversions.

The exhibit, called Water: H_2O = Life, is designed to explore water from every angle, from its various cultural and spiritual aspects to the shortage of clean water facing most of the world's poor. It opens on 3 November and leaves for a world tour next June.

CREDITS (TOP TO BOTTOM): BENJAMIN HARINK; *PNAS*; R. MICKENS/AMNH

EDITED BY YUDHIJIT BHATTACHARJEE

MOVERS

GEMS FROM THE PAST. Working with artifacts including Egyptian mummies and Australian Aboriginal bark paintings, conservation scientist Eric Hansen spent 20 years at the Getty Conservation Institute in Los Angeles, California, figuring out ways to preserve rare objects. Now Hansen has taken over preservation research at another treasure vault: the U.S. Library of Congress, the largest library in the world.

Hansen, a chemist and archaeologist, says one major project will be to conserve magnetic tapes that are degrading. "You lose all information because you can't run it through a machine," he says. Bolstered by a planned doubling of the Ph.D. research staff to six, Hansen will also be trying to pin down the shelf life of CDs, DVDs, and recycled paper and find ways to strengthen millions of books weakened by age. "The challenge here is the sheer amount in the collections," he says.

THEY SAID IT

"It took me 8 years at Harvard to figure out I'm not that stupid."

—Anthropologist Sven Haakanson, a member of the Alutiiq community in Alaska and one of 24 winners of this year's MacArthur fellowships. Haakanson, 40, directs the Alutiiq Museum in Kodiak and works to erase the culture's self-perception that native people are "worthless." A full list of the fellows, who will receive $500,000 each, is at www.macfound.org.

MONEY MATTERS

STRIKING SILVER. An international mining company has promised to pay $10 million for a clean and cost-effective way to extract silver from its Veladero mine in Argentina. The usual method uses a cyanide solution to leach out the precious metal. But the mine's estimated 180 million ounces of silver are encrusted with silica in particles a few micrometers in diameter, and the mineral has resisted every trick tried by scientists at the Barrick Gold Corp. in Toronto. The price of silver makes it too expensive to grind the ore down to the size necessary to make traditional leaching viable. "Our in-house metallurgists can't figure it out," says Barrick spokesperson Vincent Borg. "The best way to solve [the problem] is to reach out" to the scientific community, he says.

Tibor Rozgonyi, a mining engineer at the Colorado School of Mines in Golden, says Barrick's offer is "a good approach" because it's likely to get many different heads thinking about a difficult problem. In addition to the prize, the company has announced that it will fund development and testing of promising techniques. "We are definitely considering [submitting] a proposal," says Rozgonyi, who has been working with colleagues on using bacteria to extract ore.

FIGHTING DISEASE. A. Alfred Taubman, who made a fortune developing real estate, has given $22 million to the University of Michigan Health System to help found a new institute that will conduct basic research on human disease. A portion of the gift will go to five scholars at the university's medical school, each of whom will receive a research award of $200,000 per year for 3 years. Taubman's previous gifts to his alma mater add up to more than $38 million.

Got a tip for this page? E-mail people@aaas.org

Pioneers >>

NAMING RIGHTS. Shiva Balak Misra was a graduate student at Memorial University in Newfoundland, Canada, when he discovered the 565-million-year-old fossils of soft-bodied organisms shaped like leaves and spindles. Misra published his findings in the *Geological Society of America Bulletin* but returned to his native village in north India in 1971 to build a school.

Now, 40 years after the discovery, the fossils bear his name. *Fractofusus misrai* belongs to a class of fossils known as Ediacaran life forms: creatures that emerged about 600 million years ago and thrived until the dawn of the Cambrian 540 million years ago. "We needed a formal nomenclature, and we didn't want to forget the people associated with past discoveries," says Guy Narbonne, a paleontologist at Queen's University in Kingston, who led the naming initiative.

Misra says he left research to realize his dream of founding a school in Kunaura, the village where he spent his childhood. "I had to walk 10 kilometers to school until class [grade] eight," says Misra. Five years after founding the school, however, he needed an income and became a geology professor at Kumaon University in Nainital, a town in the foothills of the Himalayas. His wife now manages the school, which has 700 students in grades 1 to 10.

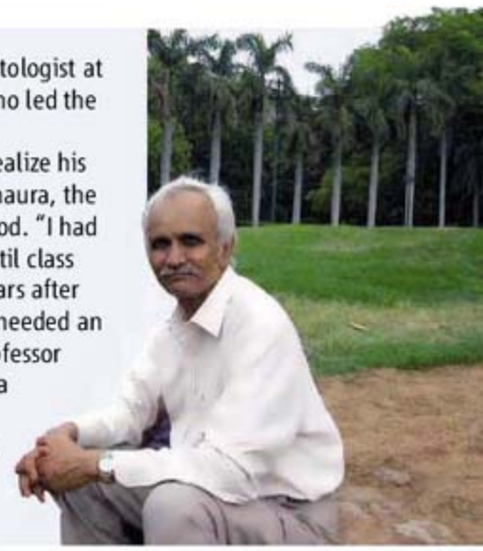

CREDITS (CLOCKWISE FROM TOP): DENNIS KEELEY/J. PAUL GETTY TRUST; S. MISRA; G. M. NARBONNE/QUEEN'S UNIVERSITY

Plants' alarm bell 31

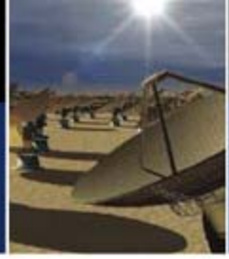

A wish list for European astronomy 35

AIDS RESEARCH

Promising AIDS Vaccine's Failure Leaves Field Reeling

On Tuesday 18 September, AIDS vaccine research suffered one of its most devastating setbacks.

That day, an interim safety analysis that no one expected would reveal anything significant showed that the vaccine widely thought to have the best shot at success had failed in a large human trial. "We were all in shock and devastated," says Peggy Johnston, who heads AIDS vaccine research at the National Institute of Allergy and Infectious Diseases (NIAID) in Bethesda, Maryland, which was one of three partners conducting the multicountry trial of the vaccine, made by the pharmaceutical giant Merck.

Three days later, Merck, NIAID, and an academic consortium known as the HIV Vaccine Trials Network (HVTN) announced that the trial, dubbed STEP, had been halted. Started in December 2004, the trial involved 3000 HIV-negative men and women from North and South America, the Caribbean, and Australia who were at high risk of becoming infected.

AIDS researchers around the world were stunned by the trail's results. "This was the first AIDS vaccine clinical trial in history where most people thought they'd at least see something positive," says John Moore, an AIDS researcher at Weill Cornell Medical College in New York City. "It's very dispiriting for the field," says Lawrence Corey, an AIDS researcher at the University of Washington, Seattle, who also heads HVTN. "It will take time to unravel where this leaves us and how we move forward."

Knocked out. Disappointing interim results abruptly ended a Merck vaccine trial that used this recruiting poster.

Researchers had pinned their hopes on Merck's vaccine because it uses a novel strategy. Instead of trying to trigger antibodies to HIV, as most other candidates do to some degree, this one relies exclusively on another arm of the immune system that stimulates what are known as killer T cells. HIV has so many mutant types that it's easy for the virus to dodge antibodies. Killer T cells, in contrast, appear to work against a wide array of variants, selectively targeting and destroying cells that the virus has managed to infect. Although only antibodies can actually prevent infections, the hope was that a T-cell vaccine might beat back HIV before it could get a foothold, or at least keep levels of the virus (the viral load) in check.

To trigger the T-cell response, the vaccine uses a modified adenovirus, or cold virus, as a vector to shuttle three HIV genes into the body. But many people have strong immunity to that adenovirus, which theoretically could cripple the vector and render the vaccine ineffective. To assess the magnitude of this problem and increase chances that the vaccine would work, half of the people enrolled in the study had to have low antibody levels against that adenovirus. The interim analysis focused on only those 1500 people, most of whom were men who have sex with men.

In participants who received at least one dose of the vaccine, 24 of the 741 vaccinated people became infected, compared with 21 of the 762 participants who received a dummy shot. More discouraging still, there was virtually no difference in viral loads between the two groups. "I was hopeful we'd see *some* dampening of viral replication," says Norman Letvin, an AIDS vaccine researcher at Harvard Medical School in Boston, Massachusetts, whose earlier monkey studies with the vaccine did show such a decline.

Letvin and his colleagues vaccinated monkeys and then challenged them with a lab virus, SHIV, which combines HIV with its simian cousin SIV. But when another group later tested the Merck vaccine against a more potent SIV, it failed. To Ronald Desrosiers, head of Harvard's New England Primate Research Center in Southborough, Massachusetts, that failure should have raised more red flags. "Everything protects against SHIVs," says Desrosiers.

Anthony Fauci, NIAID's director, worries that the Merck failure will give the broader T-cell vaccine concept a bad rap. "Clearly this indicates the failure of a product. Whether or not it indicates the failure of a concept, we don't know at this point," Fauci says. NIAID researchers have developed another T-cell vaccine that has more HIV genes and differs in several other key features. A large-scale trial was slated to ▶

CREDIT: COURTESY OF HVTN

SCIENCE OPENS CHINA BUREAU

Science has opened a news bureau in Beijing to report on science and science policy developments in China. The bureau is staffed by Asia News Editor Richard Stone, who has been based in Bangkok, Thailand, for the past 2 years. Before that, Stone spent 4 years in Cambridge, U.K, as *Science*'s European News Editor and a year teaching in Kazakhstan on a Fulbright fellowship. He can be reached at rstone@aaas.org.

start this fall but has been delayed pending a more thorough analysis of the STEP results. HVTN has also put on the back burner its plans for a trial of the Merck vaccine in South Africa.

Fauci worries, too, that the failure could have reverberations throughout the pharmaceutical industry, which already is wary of investing in AIDS vaccine research and development. "There's certainly a danger of industry scratching its head and saying before we put substantial resources in, we need more sound scientific data," says Fauci.

Merck, based in Whitehouse Station, New Jersey, would not speculate about the future of its AIDS vaccine program. "The best thing we can contribute to the field overall is a thorough analysis of the data," says Mark Feinberg, the company's vice president of medical affairs. Many intriguing questions remain, he notes, such as what happened in the other 1500 participants, what was the immune responses in the "breakthrough" infection cases, and are there differences in heterosexual transmission (so far, only one woman out of the 1000 volunteers became infected). "It's not like we're not interested in the questions anymore, but it's unclear where the next breakthrough will come from," he says. "And that's not just a question for Merck. It's a question for the entire field."

–JON COHEN

HUMAN RIGHTS

Myanmar's Secret History Exposed in Satellite Images

When militiamen backed by Sudan's government attacked non-Arab villages in the country's Darfur region in 2003, Sudanese officials dismissed international criticism and called the reports of violence propaganda. Earlier this year, Sudan's denials lost all credibility when the world saw before-and-after satellite images showing that scores of settlements in the region had indeed been destroyed. Observers say the images played an important role in persuading the United Nations Security Council to authorize a new peacekeeping mission in Darfur this summer.

Last week, AAAS (the publisher of *Science*) released similar satellite images of Myanmar—also known as Burma—showing that dozens of villages in the eastern part of the country had been uprooted or razed to the ground. The images, taken over the past year by commercial high-resolution satellites, strengthen field accounts of a military campaign by Myanmar's dictatorship against the country's ethnic minorities, which has claimed thousands of lives and forced many more to flee to refugee camps in Thailand.

Human rights organizations hope the evidence will help prod the international community into taking tougher measures against Myanmar's government, which in recent days has cracked down on pro-democracy protestors in the capital city of Yangon. "We are following the example provided by the Darfur images," says Aung Din, policy director for the U.S. Campaign for Burma in Washington, D.C., one of AAAS's partners on the project. "We have two intentions: Convincing the international community to do more to stop human rights abuses in Myanmar, and letting the military junta know that we have satellites in the sky watching this territory."

At 25 of the 31 locations in east Myanmar that were examined in the study, researchers found visual evidence confirming eyewitness accounts of villages having been burned or shifted and showing military camps that have been set up near minority settlements. In one set of photos, for example, blackened scars of buildings appear in a village in Papun district after attacks were reported on 22 April.

"Eighteen of the locations showed evidence consistent with destroyed or damaged villages," says AAAS's Lars Bromley, who directed the project. "We found evidence of expanded military camps in four other locations as well as multiple possibly relocated villages, and we documented growth in one refugee camp on the Thai border." Bromley says the images help to "discredit the denials" issued by Myanmar's government.

Satellite images helped in the same way to counter Sudan's denials, says Ariela Blatter of Amnesty International, which teamed up with AAAS for a project called Eyes on Darfur. Blatter says that although Sudanese officials have "downplayed the validity" of the project, they have found it hard to reject the evidence altogether.

Myanmar's government may prove to be more unyielding. Last year, after AAAS launched the project, Myanmar's information minister, Kyaw Hsan, predicted that critics would use "fabricated satellite photos" to claim "that the [military] is dislodging villages by force and torturing the village people." This week, Myanmar had no comment on the evidence.

–YUDHIJIT BHATTACHARJEE

Wiped out. The village near Kewy Kee in east Myanmar photographed by a commercial satellite on 5 May 2004 (*left*) has disappeared in an image taken on 23 February 2007.

CREDITS (LEFT TO RIGHT): COPYRIGHT GEOEYE INC. (NASDAQ:GEOY); COPYRIGHT 2007 DIGITAL GLOBE

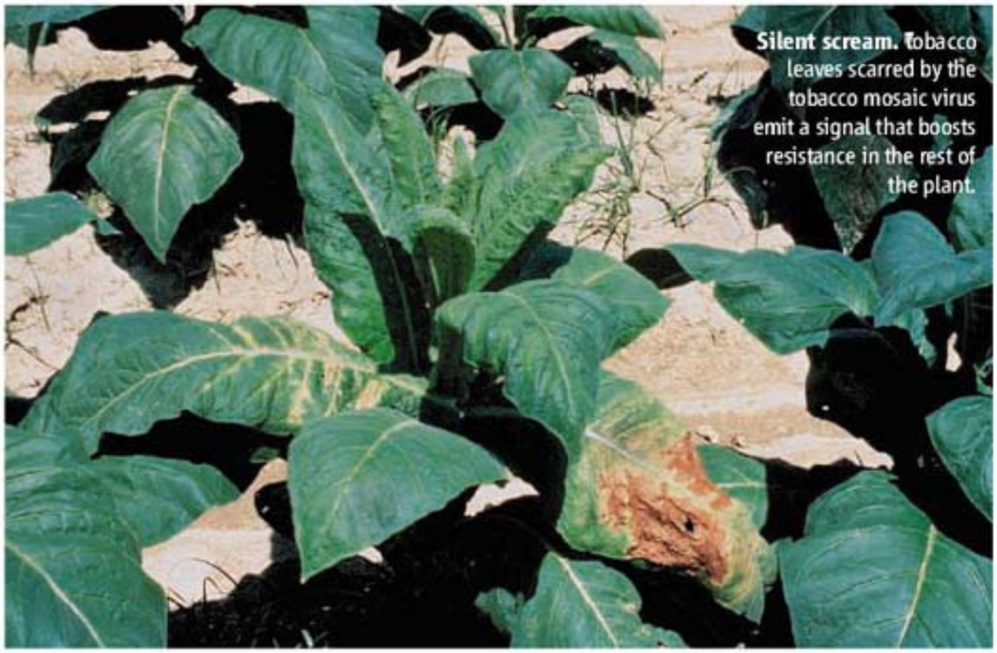

Silent scream. Tobacco leaves scarred by the tobacco mosaic virus emit a signal that boosts resistance in the rest of the plant.

CREDIT: COURTESY H. D. SHEW. REPRINTED BY PERMISSION FROM COMPENDIUM OF TOBACCO DISEASES, 1991, AMERICAN PHYTOPATHOLOGICAL SOCIETY, ST. PAUL, MINNESOTA

PLANT BIOLOGY

At Long Last, Pathologists Hear Plants' Cry For Help

A sick plant has something in common with an athlete who slathers on stinky sports balms. Both are counting on the salutary effects of methyl salicylate, the pungent oil of wintergreen. This compound turns out to be a long-sought distress call that rouses plant resistance against disease, researchers report on page 113. "Finally, we've been able to identify a signal that activates this plant-wide defense," says co-author and plant pathologist Daniel Klessig of the Boyce Thompson Institute for Plant Research in Ithaca, New York.

Unlike animals, plants can't mobilize a cadre of targeted immune cells to fight infection. But that doesn't mean that they just stand there and take it. When a pathogen infects one part of the plant, say a leaf, that tissue sounds the alarm, and other parts beef up their defenses, not only to that pathogen but also to other potential attackers. Some evidence even indicates that nearby plants can heed the alert.

For more than 50 years, scientists have pursued the so-called mobile signal that wends through the plant's phloem, or food-transporting tissue, and spreads the alarm. In the 1990s, they thought they had nabbed this molecular messenger: salicylic acid, a key plant hormone and a close relative of the main ingredient in aspirin. However, grafting experiments proved them wrong: The graft still exhibited systemic resistance even if the infected part of the plant lacked the supposed messenger.

Klessig and colleagues came upon what seems to be a real messenger while chasing the receptor for salicylic acid. The team's experiments eliminated one candidate receptor, the enzyme SABP2. However, they discovered that SABP2 transforms methyl salicylate into salicylic acid and that the enzyme is necessary for systemic resistance, suggesting that methyl salicylate might be the signal.

To determine whether methyl salicylate indeed delivers a warning from the site of an infection to the rest of the plant, the team performed grafting experiments on tobacco plants and then exposed the graft recipient, or rootstock, to tobacco mosaic virus. Systemic resistance still occurred when the graft was missing an enzyme that makes methyl salicylate, but not if this protein was absent from the rootstock, indicating a need for methyl salicylate only where the infection occurred.

The researchers engineered plants to make an overactive form of SABP2 that uses up methyl salicylate. When they used those plants as rootstock, no systemic resistance developed after the rootstock was infected. But if the graft alone manufactured this unstoppable enzyme, resistance appeared, again arguing for the need for methyl salicylate at the infection site.

The scientists also used RNAi to banish SABP2 from the graft or the rootstock. After infection of the rootstock, the graft developed resistance only if it could make SABP2. It didn't matter whether the rootstock could produce the enzyme. ▶

Boycott: Blocked

The British University and College Union (UCU) last week dropped efforts to boycott exchanges with Israeli researchers, terminating debate on the issue after lawyers advised that UCU risked violating British antidiscrimination laws. Conceived as a protest of Israeli policies toward Palestinians, the current proposal was circulated in May, following two similar attempts in Britain in 2005 and 2006. Opponents of the idea included the British and Israeli governments, scientists, and AAAS, the publisher of *Science*.

"We are really happy," says chemist Yoram Cohen of Tel Aviv University in Israel, adding that collaborations have continued despite the talk of barriers. He adds, "Some of the biggest criticisms of Israeli policy come from Israeli academia." **–BENJAMIN LESTER**

Budget: Boosted

The acting chief of the National Institute of Environmental Health Sciences (NIEHS) assured Congress last week that he will partly reverse $11.1 million in funding cuts made by his controversial predecessor, David Schwartz. Acting director Samuel Wilson said at a House hearing that he will restore cuts, including $966,000 slashed from the $3.1 million budget of the institute's journal, *Environmental Health Perspectives*. Schwartz, who has come under fire for ethics issues and for shifting NIEHS's focus from disease prevention to clinical research, is on temporary leave as director as he awaits a high-level review of the institute's management. **–JOCELYN KAISER**

Regulation: Required?

At an international meeting in Washington, D.C., last week, the Bush Administration emphasized voluntary measures to tackle climate change—a hands-off approach that has been widely used by the Environmental Protection Agency (EPA) to deal with environmental problems. But clear examples of success are rare, according to a report released last week by the EPA's inspector general. The report finds that EPA lacks a system for determining whether its 54 voluntary programs—which cover everything from reducing air pollution to creating safer detergents—are improving the environment. EPA associate administrator Brian Mannix agreed that stronger management is needed but noted that White House officials already review voluntary programs. That's not good enough oversight, says William Pizer of Resources for the Future, calling the inspector general's report "damning criticism."

–ERIK STOKSTAD

Overall, the experiments indicate that the infected tissue requires the ability to make methyl salicylate, whereas the target tissue needs to be able to break it down. "I'd say we were quite confident that methyl salicylate is a signal [for resistance]," says Klessig.

"It's a pretty persuasive series of experiments," says molecular plant pathologist Terrence Delaney of the University of Vermont, Burlington.

Raising the alarm probably involves two steps, Klessig says. The tissue under attack first produces methyl salicylate and releases it into the phloem for distribution. When this messenger arrives in target tissues, SABP2 converts it into salicylic acid, which triggers systemic resistance. The work is "an elegant solution" to the question of how to reconcile earlier evidence implicating salicylic acid in systemic resistance, says plant pathologist Luis Mur of the University of Wales in Aberystwyth, U. K.

Agriculture could benefit from the discovery, says Klessig. Fine-tuning methyl salicylate levels—either through genetic engineering or selective breeding—might fortify crop defenses and reduce the amount of pesticides farmers need to apply.

However, the methyl salicylate pathway may not be the whole story. Some data suggest that the signal is a lipid—methyl salicylate is not—and that a lipid called jasmonic acid might serve as an independent signal or as a partner. "The key question is, are we looking at a parallel system?" Mur asks. Klessig doesn't have an answer, at least not yet. "It's quite possible, even likely," he notes, "that there are multiple signals."

–MITCH LESLIE

PALEOANTHROPOLOGY

Nariokotome Boy to Go on the Road Despite Protests

When Ethiopian officials announced plans last year to send the famous human ancestor "Lucy" to the Houston Museum of Natural Science in Texas, many paleoanthropologists were furious at the risk to an irreplaceable specimen. The late F. Clark Howell of the University of California, Berkeley, predicted that Lucy's journey would "start an avalanche" of exhibits of original hominid fossils. Last week, Howell's remark began to seem prescient: Officials at the National Museums of Kenya announced government approval for their plans to send Nariokotome Boy, the partial skeleton of a 12-year-old, to The Field Museum in Chicago, Illinois.

Chicago-bound. This rare skeleton of *Homo erectus* may travel from Kenya to Chicago, Illinois.

The 1.5 million-year-old fossil, the most complete skeleton of *Homo erectus* found, continues to be a source of scientific data, and many researchers are angry at the news. A traveling exhibit is "prostitution" of the fossils, charges Kenyan paleoanthropologist Richard Leakey, whose team discovered the skeleton in 1984.

No formal agreement has been signed, and Field Museum officials say the announcement in Nairobi last week took them by surprise, as they are still in negotiations and have yet to raise funds for the exhibit. But the proposal under discussion includes exhibiting Nariokotome Boy and its retinue of fossils from Kenya for 18 months, perhaps as early as 2009. "The Field Museum is indeed currently at an initial stage of discussions … with the aim of organizing a traveling exhibit in the U.S.A.," says Robert D. Martin, curator of biological anthropology at The Field Museum. He says The Field has great experience in caring for fragile fossils and will strive to make sure that profits benefit Kenyan science. The Field is also considering exhibiting Lucy, who is now drawing 2000 people each weekend day in Houston.

With regard to the Lucy exhibit, many researchers argued that original fossils are too fragile to be packed up and sent around the world. Several museums declined to exhibit Lucy because of the risk of damage and because there was no compelling scientific reason to take her out of Ethiopia (*Science*, 27 October 2006, p. 574).

The Nariokotome Boy announcement, made by National Museums of Kenya Director General Idle Omar Farah, is drawing similar reactions. Says co-discoverer Alan Walker of Pennsylvania State University in University Park: "Like many others, I don't approve. It took about a century after [finding] the first bones of *H. erectus* for us to find a partial skeleton, and it would be a disaster if we lost it."

The Lucy exhibit and any display of Nariokotome Boy outside their homelands also violate a 1999 international agreement that original hominid fossils should not be transported from their country of origin without compelling scientific reasons. Many African researchers oppose sending fossils overseas because such exhibits do little to spark investment in African scientific infrastructure, says paleoanthropologist Frederick Kyalo Manthi of the National Museums of Kenya. Meave Leakey, also of the National Museums of Kenya, adds that "the timing is unfortunate since the specimens will be seen overseas just at the time that they are planned to be put on exhibit for the first time in Kenya."

Field Museum Provost Neil Shubin says he and Martin are working to make sure the fossils would be available for study. They also would create an exhibit in Nairobi and have payments go to the National Museums of Kenya, which, according to Farah, is seeking a total endowment of $3.5 million.

Some researchers do support traveling exhibits if done right. Lucy and Nariokotome Boy are the "patrimony for all of humankind" and should occasionally travel for study and short exhibits, says paleoanthropologist Ian Tattersall of the American Museum of Natural History in New York City. So far, however, neither the American Museum nor the Smithsonian Institution in Washington, D.C., has signed on for either exhibit.

ANN GIBBONS

CREDIT: (PHOTO) ALAN WALKER, COPYRIGHT NATIONAL MUSEUMS OF KENYA

CLIMATE CHANGE

Is Battered Arctic Sea Ice Down For the Count?

A few years ago, researchers modeling the fate of Arctic sea ice under global warming saw a good chance that the ice could disappear, in summertime at least, by the end of the 21st century. Then talk swung to summer ice not making it past mid-century. Now, after watching Arctic sea ice shrink back last month to a startling record-low area, scientists are worried that 2050 may be overoptimistic.

"This year has been such a quantum leap downward, it has surprised many scientists," says polar researcher John Walsh of the University of Alaska, Fairbanks. "This ice is more vulnerable than we thought." And that vulnerability seems to be growing from year to year, inspiring concern that Arctic ice could be in an abrupt, irreversible decline. "Maybe we are reaching the tipping point," says Walsh.

There's no doubt that 2007 was a special summer melt season. The ice area remaining in September—the year's low point—had been shrinking since satellite monitoring began in 1979. Some years it recovered a bit, others it declined further, but overall it shrank 8.6% per decade. In 2005, it hit a record low of 5.6 million square kilometers, down 20% from 1979. But last month, "we completely blew 2005 out of the water," says sea ice specialist Mark Serreze of the University of Colorado, Boulder. Ice area plummeted to 4.13 million square kilometers, down 43% from 1979. That's a loss equivalent to more than two Alaskas. The new low is more than one Alaska below the trend line. Nothing else like that appears in the satellite record or, for that matter, in monitoring from ships and planes during the rest of the 20th century, says Walsh.

An immediate cause of the record-breaking year is clear enough. As Serreze explains, an unusually strong high-pressure center sat over the central Arctic Ocean while a strong low hovered over Siberia. This weather pattern allowed more solar heat through the clear skies beneath the high-pressure center and pumped warm air up from the south between the high and the low.

The vicissitudes of weather may have enhanced ice loss this year, but there's more going on than that, scientists are realizing. For one thing, their models underestimate how fast summer ice has been disappearing in the warming Arctic. "It's very alarming the way things are changing so fast," says polar oceanographer D. Andrew Rothrock of the University of Washington (UW), Seattle. "We've thought we have the important physics in the models, but … it seems our models aren't very good in the Arctic."

Researchers say the models probably lack some realistic feedbacks, natural processes that can amplify a climatic nudge—whether natural or humanmade—into a shove. And that shove could send the ice past a tipping point. "You get a kick in the right direction," says Serreze, "and it sends the ice over the edge" and into a meltdown from which it cannot recover.

Last December, researchers reported finding that at least one climate model includes feedbacks that can accelerate sea ice into a ▶

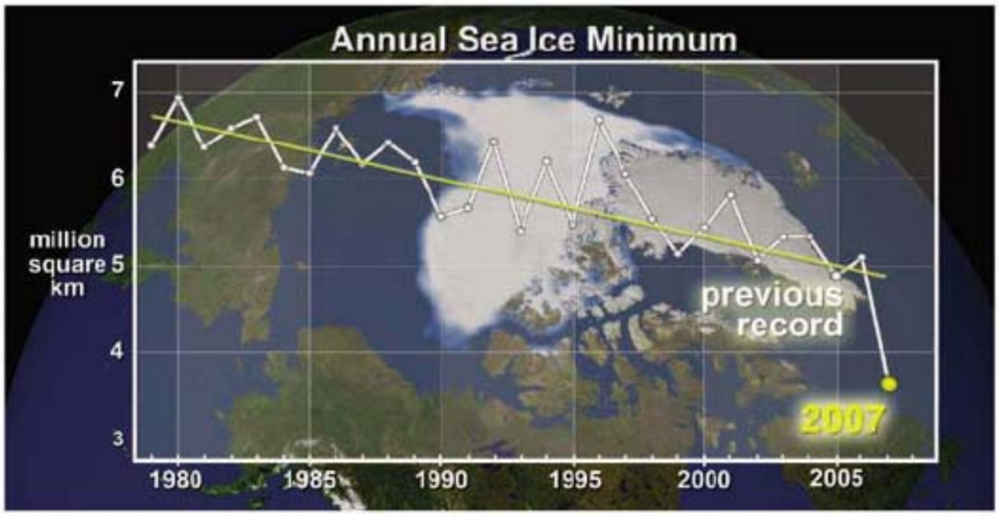

CREDIT: NASA/GODDARD SPACE FLIGHT CENTER SCIENTIFIC VISUALIZATION STUDIO; (DATA) ROB GERSTON, GSFC

Bad sign. Arctic sea ice (gauged here using NASA's measurement techniques) has been declining, but 2007's unfavorable weather drove the increasingly vulnerable ice to a new record low.

In the Navy

The University of Hawaii (UH) is moving ahead with plans to build a Navy-affiliated research laboratory near one the system's 10 campuses. Approval by the university's Board of Regents last week followed more than 4 years of controversy over the Applied Research Laboratory (ARL), which is expected to bring in as much as $10 million per year for 3 to 5 years in research funds from the Navy and other agencies, including NASA and the National Institutes of Health. The ARL will be the fifth such University Affiliated Research Center; other hosts include sites at Johns Hopkins and Pennsylvania State universities.

But finalizing the Hawaii deal amidst opposition by community, student, and faculty groups wasn't easy; in 2005, anti-ARL protestors took over the university president's office for 6 days. Pressure from opponents led the university to specify in the contract that no classified research would occur during the first 3 years of operation. UH vice president for research James Gaines says the lab will raise the school's profile. Critics, however, accuse UH of disregarding what UH, Manoa, plant scientist Hector Valenzuela calls "general overwhelming opposition." The center, he says, "is against what the university is all about."

–BENJAMIN LESTER

Leszek is More

Leszek Borysiewicz is the new chief executive of Britain's Medical Research Council (MRC). Borysiewicz, an immunologist who helped develop vaccines against cervical cancer, was most recently deputy rector at Imperial College London. He takes over as MRC is attempting to respond to a government report last year that called for more emphasis on research with clinical and commercial applications. But Borysiewicz says that does not mean short-changing basic research. "We're not going to improve our translational science without keeping the basic research strong," he says.

Meanwhile, he will oversee the controversial relocation of the National Institute for Medical Research (NIMR) from the London suburb of Mill Hill into the city. NIMR researchers fought the original plans, saying the proposed site was too small (*Science*, 18 February 2005, p. 1028). But now MRC has joined forces with the Wellcome Trust/Cancer Research U.K. and University College London to bid for a site near the British Library that would eventually house 1500 scientists. The government, which is selling the property, should announce a decision on the sale in the coming weeks.

–GRETCHEN VOGEL

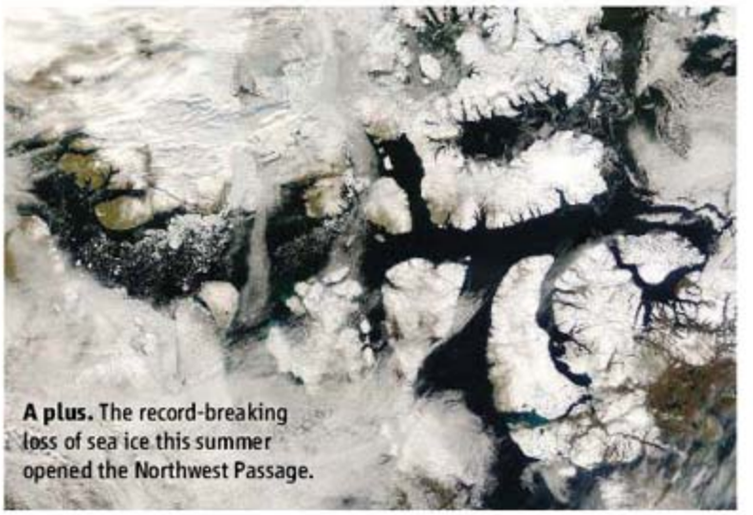

A plus. The record-breaking loss of sea ice this summer opened the Northwest Passage.

tipping point. Modeler Marika Holland of the National Center for Atmospheric Research (NCAR) in Boulder, Colorado, and colleagues wrote in *Geophysical Research Letters* (*GRL*) that when NCAR's Community Climate System Model, version 3—which has one of the most sophisticated ice components available—is run under a strengthening greenhouse, sea ice loss can suddenly accelerate, in one case cutting ice area by two-thirds in a decade and wiping out September ice by 2040.

Such accelerations were driven by two feedbacks in the model. In one, thinner ice one year made ice melt more easily the next year. In another, when white, highly reflective ice melted, the darker, more absorptive open water that replaced it absorbed more solar energy. The added heat could help melt more ice and keep new ice thinner that year—and even the next, if the heat lingered through the winter.

Holland and her colleagues "showed that in models, these abrupt changes can occur," says Walsh. Now, "this is the first time we may have seen it" in the real world.

In an in-press *GRL* paper, polar researcher Donald Perovich of the U.S. Army Cold Regions Research and Engineering Laboratory in Hanover, New Hampshire, and colleagues report estimates of increasing solar heating of the Arctic Ocean. They found that a large area of Arctic waters north of the Bering Strait had been absorbing increasing amounts of solar heat since 1979 as summer ice retreated, suggesting that the ice-reflectivity feedback has been operating there.

And in a paper appearing in *GRL* this week, Son Nghiem of the Jet Propulsion Laboratory in Pasadena, California, and colleagues report a continuing decline in the thicker, older ice that tends to persist from year to year. Much of the decline in perennial ice, they found, was due to winds blowing it out of the Arctic Ocean. But thinning from added heat had made it easier for the wind to blow the ice out. That would add a dynamical feedback to the thermal feedback of ice reflectivity.

Researchers suspect that these and other feedbacks are eroding sea ice's ability to resist the warming of recent decades. "Might we lose summer sea ice by 2030?" asks Serreze. "That is not unreasonable." Next September could tell whether natural variability just made for one bad year in the Arctic or whether it is pushing the ice over the edge. Meteorologist Ignatius Rigor of UW is worried. Given the beating the ice has taken of late, he says, "the chances of another extreme next year are pretty high."

–RICHARD A. KERR

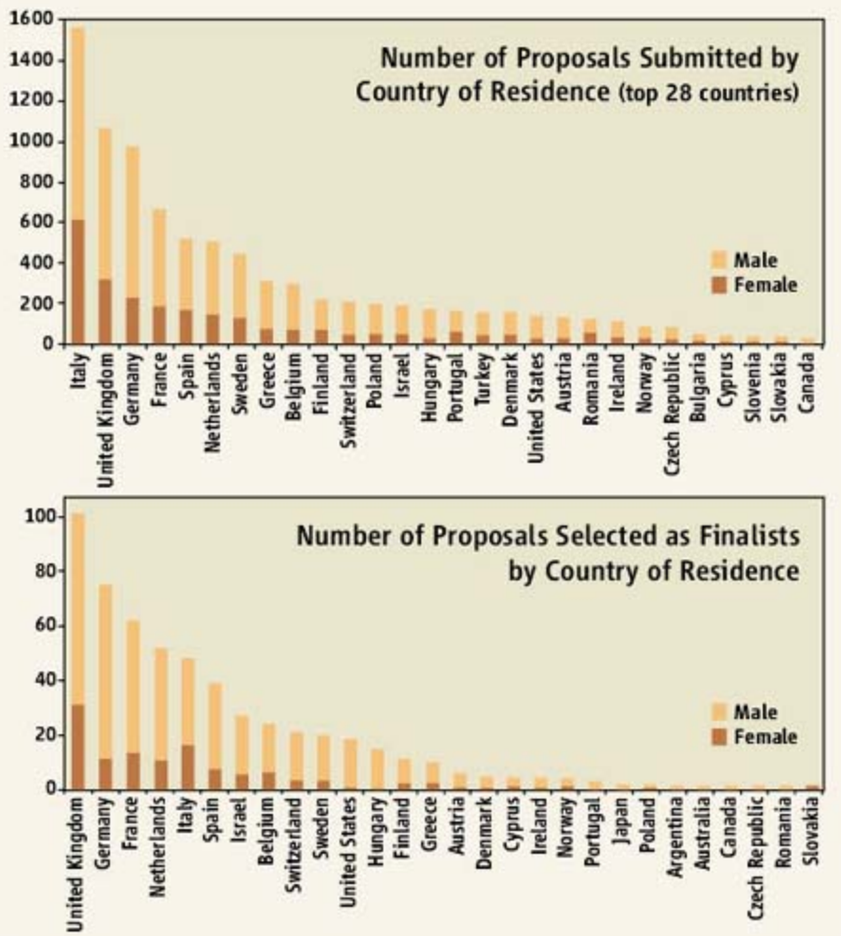

European Science by the Numbers

The first round of peer-reviewed grants from the European Research Council (ERC) is out, and the agency's analysis of applicants and finalists paints a revealing picture of Europe's scientific landscape. Nearly 9000 applications flooded in this spring (*Science*, 4 May, p. 672); review panels narrowed these down to just 559 finalists. The ERC will select about 250 young scientists from the list by January 2008 and award each of them roughly €1 million ($1.4 million). This week, the ERC released new figures about where the applicants come from and where they hope to work. Italians far outpaced all other nationalities, submitting more than 1700 applications—a sign, says ERC Vice President Helga Nowotny, of the dire lack of support for young researchers there. Italians were fairly successful, too: 70 made it to the final round, although just fewer than 50 plan to work in Italy. The U.K. has the best "brain-gain" statistics: More than 100 of the finalists work in the U.K. but just 42 are British. The big surprise, Nowotny notes, is Poland. Just three Polish researchers are finalists, and none plans to work in Poland. Michal Kleiber, president of the Polish Academy of Sciences and a member of the ERC scientific council, sees the results as disappointing; he thinks they reflect the salary caps in Poland that spur top applicants to work elsewhere. He also notes that although Poland has 8% of the E.U. population, its science budget accounts for less than 1% of overall E.U. research spending. More details are available at: http://erc.europa.eu/pdf/erc-stg-statistics-stage1-20071001_en.pdf

–GRETCHEN VOGEL

CREDITS (TOP TO BOTTOM): IMAGE COURTESY OF MODIS RAPID RESPONSE PROJECT AT NASA/GSFC; (DATA) ERC

ASTRONOMY

Europeans Lay Down Their Wish List for Next 2 Decades

European astronomers are in a buoyant mood. They have what is widely acknowledged to be the world's number one optical instrument—the Very Large Telescope (VLT) in Chile—and several other ambitious projects under construction or on the drawing board. And last week, following a consultation process that for the first time brought together European researchers from all branches of astronomy, a new umbrella body called Astronet laid out the continent's goals for the next decade or two. "It describes the sort of science we want to do and the sort of tools we will need," says Johannes Andersen, director of the Nordic Optical Telescope at La Palma in the Canary Islands and chair of the Astronet board.

Astronet's Science Vision poses four basic questions, including "Do we understand the extremes of the universe?" (which takes in dark matter, dark energy, regions of strong gravity and the source of high-energy cosmic rays) and "How do we fit in?" (covering the heliosphere, Earth-sun interactions, minor bodies, and planetary atmospheres). Along the way, the vision dips into galaxy formation and evolution and how dust clouds form into stars and planets. The document also suggests a list of instruments needed to meet each question's science goals (see figure, below). More than two dozen of these instruments are still at the planning stage, and the report says building them all would cost "several billion euros" over the next 2 decades. But the report's authors readily acknowledge that this is a wish list. A construction schedule "wasn't the job of the Science Vision," says Astronet program coordinator Jean-Marie Hameury of the French research agency CNRS. "We won't be able to do it all. Hard choices will have to be made."

Those hard choices will fall to a Roadmap working group, which over the next year will hammer out realistic schedules and cost estimates under the watchful eye of Astronet's funding-agency sponsors. "We will be pushing the bounds, making the case where appropriate for increased astronomy spending in Europe," says the working group's head, astrophysicist Michael Bode of Liverpool John Moores University in the U.K.

European astronomy has in the past been a fragmented community. Optical astronomers work together through the European Southern Observatory; the European Space Agency handles most space missions; and national research agencies fund those bodies as well as their own astronomy programs. Europeans watched enviously as their American counterparts laid out plans in a series of decadal reviews drawn up by the U.S. National Research Council. Andersen says that plans for a similar European effort were discussed a decade ago, but it was not until 2005 that a group of national funding agencies for astronomy grew impatient, set up Astronet, and told astronomers to get organized. "Funding agencies want a comprehensive long-term plan so they can act rationally," says Andersen.

There are several key differences between the European and American planning efforts, Andersen says. First, Astronet was instigated by funding agencies (now numbering 17) rather than by the research community. The agencies will be involved in framing the Roadmap document, so they "will have signed up to it in principle," says Bode, although Andersen adds that "there are no guarantees."

The Astronet process also differs from the decadals in that first a panel, consulting with the whole community, works out the scientific priorities, and then a new panel has to whittle those aspirations down to a realistic program in the Roadmap. The Science Vision—coordinated by Tim de Zeeuw, director of ESO since last month—involved a draft report, extensive consultation via a Web site, and a meeting in Poitiers, France, last January attended by 228 scientists from 31 countries. "This has never been done before in Europe," says Bode. "Some were very skeptical, but it worked very well. People learned to think more strategically." The Roadmap will follow a similar trajectory culminating in a symposium in Liverpool next June. And finally, whereas the decadals prioritize projects and list construction costs, the Roadmap will go into much more detail and will also cover operating costs, schedules, management, research and development, and industry involvement. "The Roadmap is going to bite all those bullets. That's why it's going to be so tough," says Andersen.

With U.S. astronomers facing a flat budget and possible facility closures to pay for new projects (*Science*, 10 November 2006, p. 904), Britain's Astronomer Royal Martin Rees of the University of Cambridge, U.K., who has not been directly involved in Astronet, thinks Europe has reason to be optimistic. "The VLT is a symbol of what Europe can do when it works together," he says. "It's important that Europe thinks big and long term."

–DANIEL CLERY

Questions	Do we understand the extremes of the universe?	How do galaxies form and evolve?	What is the origin and evolution of stars and planets?	How do we fit in?
Proposed ground-based facilities	Extremely Large Telescope (ELT)			
	Square Kilometer Array (SKA)			Solar radio spectral imaging
	Cherenkov Telescope Array (CTA)		High-precision radial velocity monitors	Large-aperture solar telescope
	Very long baseline sub-mm interferometer			Network of ground-based radars
Proposed space missions	X-ray survey satellite	Gamma-ray burst satellites	Next generation UV and x-ray satellites	High-latitude solar encounter satellite
	Wide-field imaging telescope	X-ray spectrometry satellite	High-res IR interferometer in space	Medium-aperture UV satellite
	CMB polarization satellite	Large UV space telescope	High-precision photometry satellite	Magnetospheric satellite fleet
	Laser Interferometer Space Antenna	Large IR spectroscopy satellite		Plasma interchange sensors
	Large x-ray observatory			Missions to minor bodies
				Missions to Jovian and Saturnian systems
				Mars sample return mission

CREDITS: (PHOTOS, TOP AND BOTTOM) LHEA AT NASA/GSFC; (MIDDLE) SKA

Stargazing. The Astronet Science Vision describes what European astronomers want to find out and what tools they need for the job.

Greening the Meeting

Scientific travel pours huge amounts of greenhouse gases into the atmosphere. Some societies are changing the way they run their annual meetings—and a few scientists are proposing even more drastic changes

EVERY DECEMBER, GEOSCIENTISTS DESCEND on San Francisco for the Fall Meeting of the American Geophysical Union (AGU). In 2002, the 9500 participants traveled an average of 7971 kilometers to get there and back. That means their share of the carbon dioxide emitted by the planes they flew on totals about 11,000 metric tons—roughly the same as 2250 Honda Civics during a year's worth of normal driving.

Flying is a carbon-intensive activity. Scientists may not rack up as many frequent-flier miles as international business travelers, but one thing every field has in common is the big annual meeting and numerous smaller workshops and conferences. Add up the CO_2 emitted in traveling to all those gatherings, and it amounts to a sizable contribution to global warming. Scientists have been instrumental in raising public consciousness about air travel and CO_2 emissions. Now they are beginning to examine the consequences of their own jetting around the globe.

Several scientific organizations are trying to reduce the carbon footprint of their gatherings. The approaches include tinkering, such as reducing the use of plastic cups and reusing tote bags, and offering attendees the chance to pay to compensate for the carbon emissions their travel generates. More radical ideas include shrinking or eliminating some meetings. A few virtual meetings have taken off, but they sacrifice networking and brainstorming. Until there's a quick, convenient, and carbon-neutral way to travel, self-restraint may be the solution, says David Reay, a climate scientist at the University of Edinburgh, U.K.

A growing problem

Scientific conferences are a booming business. Conference Service Mandl, a scientific conference service provider, lists nearly 4000 upcoming events over the next 2 years or so in its online directory. They range from tiny, highly focused Gordon Research Conferences (GRC) to the 800-pound gorilla of the conference world: the annual meeting of the Society for Neuroscience. (AAAS, publisher of *Science*, runs an annual general scientific meeting that drew 8000 attendees in 2007.)

Conferences are also growing in size. Since 1971, Neuroscience attendance has burgeoned from less than 1500 to a 2005 peak of nearly 35,000—a small city's worth of researchers, flying in from all over the planet. AGU's Fall Meeting has added 6000 participants over the past 5 years, an increase of more than 60%. And since 1995, the number of Gordon conferences in the United States and overseas has jumped from 130 to 180, with a surge in combined attendance of 40%. In short, even as the globe warms, more scientists than ever are on the move.

The Ecological Society of America (ESA) has taken a hard look at the environmental impact of its annual meeting. In response, it slimmed down the program book, began using soy-based inks, and now distributes its advertiser kit only electronically. The society also arranges with hotels to change linen less frequently and has removed Styrofoam from the meeting entirely. Some of the changes make more of a difference than others, but "every little bit helps," says Michelle Horton, a meeting organizer at ESA.

Other organizations are moving in similar directions, albeit more slowly. AGU paid little attention to the environmental impact of its meeting until recently, according to a spokesperson, but at its next meeting in December the organizers intend to try

CREDIT: TED HOROWITZ/CORBIS

Offsets: Worth the Price of Emission?

With society's environmental conscience outpacing its willingness to cut down on carbon-intensive travel, carbon offsetting is coming to the fore as a way for concerned citizens and organizations to reduce their contributions to global warming. The most popular approaches are planting trees to sequester carbon from the atmosphere or paying energy companies to pump renewable energy onto the grid. A new crop of companies has sprung up to cater to the need.

It's a simple idea that's fraught with problems. For instance, the Society for Conservation Biology (SCB) offsets members' emissions from travel to the annual meeting by hiring locals to replant goat-decimated World Heritage Area habitat in South Africa's Baviaanskloof (Baboon Valley). According to offset committee chair Paul Beier, the project provides real, verifiable carbon reductions. However, trees die, so organizations that use offset schemes like SCB's must commit to maintaining their investment and replanting in case of fire or disease. Offsets based on renewable energy technology only work if every dollar spent on an offset actually translates into an increase in the number of green kilowatts a provider pumps onto the grid—tricky to verify if the offset provider is half a world away.

Issues like these have led governments and nongovernmental organizations around the world to introduce offset-certification schemes to give consumers confidence that their money won't be wasted. Technical matters aside, however, some, like British environmentalist George Monbiot, argue that the very concept of offsets—allowing people to feel better about causing carbon emissions—saps the will to conserve or consume less. **–B.L.**

CREDIT: K. KRAUSE/SCIENCE

webcasting some conference sessions to make it easier for people to tune in from home, as well as asking shuttle-bus drivers to turn off their engines while waiting to load.

These measures only address the conference itself, of course, rather than the larger impact of people traveling to it. According to the Society for Conservation Biology (SCB), 95% of the society's entire emissions comes from jet fuel used in getting members to the annual meeting. Everything else—running the executive offices for an entire year, for instance—pales in comparison. So SCB, as well as ESA, has begun offering carbon offsets to its members to compensate for the emissions related to their air travel. Check a box on either organization's meeting registration form, and they'll tack a maximum of $20 on to the admission fee, putting it toward projects that help offset carbon. However, offsetting is still new, and some environmentalists think the practice is so plagued by flaws that it is little more than feel-good greenwashing (see sidebar).

Even within ESA, the idea has been slow to catch on. Last year, only six ESA members ponied up extra cash to offset their trip, meeting organizers say. At this year's conference, held in August in San Jose, California, greater awareness pushed that number up to 500—a huge increase but still less than 15% of the meeting's 3600 registrants. Members of SCB seem to feel more strongly; in the program's debut in July, 97% of the 1600 attendees at the meeting held in Port Elizabeth, South Africa, checked the offset box on their registration form.

Make the meeting count

Another option would be to hold annual meetings less frequently. But that can be a tough sell. When SCB's Board of Governors voted on this idea in South Africa, some members considered the meeting's exchange of ideas too important to forgo. "We tied eight to eight," says Paul Beier, a conservation biologist at Northern Arizona University in Flagstaff and chair of the SCB carbon-offset committee. So the issue was tabled until the next meeting. In any case, Beier thinks his society should restrict meetings to major cities because holding them in scenic outlying areas such as Port Elizabeth means more connecting flights and more emissions. "Nearly everyone flew through Johannesburg," he says, so "in the future, we should hold any meeting in southern Africa in Jo'burg."

The importance of location is also evident from the unpublished analysis of the 2002 AGU and ESA meetings by David Scott and Lawrence Plug, both of Dalhousie University in Halifax, Canada. They found that ESA could have reduced its meeting's emissions more than 13% by changing the venue from Tucson, Arizona, to the more central spot of Omaha, Nebraska.

Edward Hall, a geographer at the University of Dundee, U.K., suggests a more radical approach: Limit attendance, especially by international travelers. Earlier this year, Hall published a breakdown of the environmental impact of the 2006 annual meeting of the Royal Geographical Society in *Area*, the society's journal. He found that more than 95% of the 810 metric tons of carbon emitted during 4 million kilometers of conference travel resulted from foreign attendees flying into the U.K.

TRAVEL TIPS

1. Skip meetings when you can.
2. When you can't, combine trips to get the most out of your air miles.
3. Avoid conferences in far-flung lands.
4. For conferences close to home, carpool or take a train.
5. Choose a hotel close to the conference to avoid commuting.
6. Ask conference organizers to team with local hotels to reduce linen changes and other waste for conference attendees.
7. Avoid using disposables such as plastic tableware and Styrofoam cups.
8. Don't collect brochures that will only get thrown out.

That idea might have trouble getting off the ground. Case in point is a small conference concerning, ironically, greenhouse gases. The organizers of the conference—the groups Chemical Research Applied to World Needs and the International Conference on Carbon Dioxide Utilization (ICCDU)—had some discretionary funds at their disposal, and several of the 151 delegates suggested carbon offsets for travel to the conference in Ontario. Instead, the organizers decided to offer travel scholarships to delegates from developing countries, which will be less equipped to cope with warming. "We felt it was very important for them to attend," says Philip Jessop, an ICCDU member and chemist at Queen's University in Kingston, Canada.

Poster child. The Society for Neuroscience hosts the largest scientific meeting, but all such gatherings consume copious jet fuel and other resources.

Virtually there

Researchers don't necessarily have to attend a meeting in person to get something out of it. Virtual conferences are a growing trend; they have recently been held on topics including nanoscale structures, animal diseases, amphibian conservation, and climate change.

One of the largest such events is the Virtual Conference on Genomics and Bioinformatics (VCGB). In 2001, a Peruvian geneticist named Willy Valdivia-Granda, then associated with North Dakota State University in Fargo, founded the conference to enable researchers from poorer nations to attend scientific conferences in developed countries. The most recent conference, held in 2005, included 3000 people in more than 50 countries. Valdivia-Granda, now of Orion Integrated Biosciences in New York, recalls a particularly jam-packed venue in India. "They had so many people participating that they had to show the conference in city hall," he says.

Face to face. Virtual meetings, like this one at the Access Grid site in Arlington, Virginia, save on travel—at the expense of hallway brainstorming.

Attendees to VCGB gather at local nodes linked together using Access Grid, a virtual collaboration system developed at Argonne National Laboratory in Illinois. A simple node typically consists of a laptop with a webcam, says project lead Thomas Uram of Argonne, but a top-of-the-line installation might feature a dedicated conference room sporting several computers linked to large flat-panel displays with motorized webcams, microphones, and sophisticated echo-cancellation equipment. All that can cost as much as $20,000—much more than the cost of getting to a conference.

The system creates a permanent virtual meeting space on the Internet, which can house collaborators' data and files, that allows participants to talk things over via video, audio, and chat. Although the original purpose was to facilitate collaboration between small groups of researchers, Access Grid also works for an international multicast on the scale of VCGB.

In addition to broadening its audience, VCGB has had an environmental payoff. According to an analysis by climate scientist Reay, the 2001 conference prevented the release of 900 metric tons of CO_2. The savings have increased with subsequent years' growing attendance.

Lower tech virtual formats avoid some of the costs and technical savvy required to set up a conference using Access Grid, but they have the same basic shortcomings: They lack impromptu conversations and networking between sessions. "I'm nervous of virtual conferences," says plant biologist Gregory Copenhaver of the University of North Carolina, Chapel Hill. Although he has never participated in a conference like VCGB, he says he worries that "you lose that sense of catching someone in a hallway" and sitting down for a chat.

Reay agrees. "I can't see a future where we don't have conferences," he says. "A lot of the best scientific ideas I've been privy to have come over a glass of wine at a conference dinner or a bar later on." The problem is magnified at small, focused meetings like the Gordon conferences, whose main focus is on that kind of direct personal interaction. According to a GRC organizer, linking in an attendee remotely has been tried: It "failed miserably."

At their best, conferences put minds in close proximity and can foster the kind of environment that leads to new ideas. Sometimes, they just rehash information that is already published or easily accessible online. Researchers concerned with the environmental impact they make should pose a question before they register, says Reay. "Ask yourself, 'Do I really need to go to this meeting?'" **–BENJAMIN LESTER**

CREDITS (TOP TO BOTTOM): JOE SHYMANSKI, SOCIETY FOR NEUROSCIENCE; ACCESS DC

Treasure hunt. If there's anything reusable in this dumpster, Allen Doyle will find it.

SUSTAINABILITY

This Man Wants to Green Your Lab

Allen Doyle and his team spread the gospel of sustainability from lab to lab, but it's no easy task in the competitive world of research

SANTA BARBARA, CALIFORNIA—For the price of a few pizzas, Allen Doyle saved his science building $16,000 in electricity costs this year—and kept more than 6 metric tons of carbon from entering the atmosphere. The six-story structure where Doyle manages a soil ecology lab at the University of California, Santa Barbara (UCSB), houses 55 fume hoods, each of which burns through as much energy as three averaged-sized U.S. homes. "I offered pizza to anyone who would let us shut off their [unused] hoods for 6 months or more," he says. "I was hoping for three hoods; we got nine."

Doyle hates to see anything wasted. The typical lab consumes four to five times as much energy as an equivalent-sized office or classroom, to say nothing of the huge amount of plastic, paper, and hazardous chemicals researchers go through. Yet in Doyle's experience, scientists are blasé about reducing their environmental footprint while at work. "There's a bit of a 'Don't ask, don't tell' culture out there," he says. Many researchers chastise the government for not doing more for sustainability, says Doyle, "but we're ignoring the same issues in our own labs."

In the spring of 2006, Doyle co-founded a program called Laboratory Assessments for Research Sustainability (LARS)* with campus sustainability coordinator Katie Maynard. Assisted by a team of interns, Doyle goes from lab to lab on campus, identifying trouble spots, offering advice, and throwing in cookies and coffee when necessary. "We're just looking for simple answers that may have a significant impact on campus," he says.

LAB TIPS

1. Close hood sashes and disable unused hoods.
2. Defrost freezers regularly.
3. Turn off equipment at night.
4. Borrow and lend used equipment.
5. Share surplus chemicals and use environmentally friendly reagents.
6. Request removal of unused light bulbs from ceiling fixtures.
7. Print double-sided.

* http://www.sustainability.ucsb.edu/LARS/

What makes Doyle's program stand out from other sustainability efforts around the country is its student-driven approach, says Dale Sartor of the U.S. government–sponsored Labs21 Program, which aims to improve the sustainability of research laboratories (see p. 40). Already, LARS has helped shut down unused vacuum systems and other utilities, saving departments thousands of dollars in electricity. And by helping researchers trade surplus materials, Doyle has cut down on industrial waste.

Still, the grassroots effort has its limits. Doyle says his team has been stymied by scientists more concerned with cost and competition than conservation. But he remains optimistic that his program is a model for what scientists with a green streak across the country can do to help their labs go easier on the environment.

Campus crusader

Tag along with Doyle for a day, and you can't help but catch a bit of his sustainability fever. The lanky 49-year-old credits his environmental passion to "Jacques Cousteau, Marlin Perkins, and the brook across the street." After earning a master's degree in chemical oceanography from the University of Alaska, Fairbanks, Doyle came to UCSB almost a decade ago. Since then, he has somewhat obsessively turned the lab he manages into a shrine to conservation. Old wooden shelves

CREDITS (TOP TO BOTTOM): D. GRIMM/SCIENCE; JUPITER IMAGES

overflow with opaque plastic tubes, each sporting numerous black marks indicating the number of times they have been reused. And almost every scrap of paper in the room has been printed on at least twice: readouts from a spectrophotometer bleed through to a lab inventory list.

In June, Doyle was spreading the gospel to a neuroscience lab run by Kenneth Kosik. Doyle sees opportunities for conservation around every corner; sometimes he gets so fired up, he can't get his suggestions out fast enough. As third-year graduate student Fernando Santiago shows the team around Kosik's lab, two of Doyle's undergraduate volunteers pepper Santiago with questions. *Is there a labwide policy for shutting the lights off? Do you recycle unused chemicals? How does everyone commute?*

Inside the tissue-culture room, two large hoods glow aquamarine with UV light. Doyle immediately zooms in on a glass vacuum trap that isn't working efficiently. By simply repositioning it, he tells Santiago, the lab could avoid clogging the building's vacuum system and cut down on wasted energy. "It made a lot of sense and hadn't occurred to me," Santiago says later.

Elsewhere in the lab, Doyle's team offers more obvious suggestions. *Turn your computers off at night.* The average computer uses at least 100 watts. If the members of the Kosik lab powered down its four desktop computers when they left for the night, the lab could keep a maximum of 700 kilograms of carbon out of the atmosphere each year. *Defrost your freezers regularly.* The frost insulates the coils and makes the compressor work harder to pull heat away. *Make yourself aware of the electricians on campus.* Sometimes a simple tweak can help a piece of equipment run more efficiently or save a gadget that would otherwise end up as industrial waste.

Waste stream. Plastic tubes and old electronics can become huge sustainability problems for biomedical labs.

Other issues don't lend themselves to simple solutions. For example, Santiago guesses his lab goes through somewhere between 20 and 40 kilograms of plastic a month—in the form of pipette tips, polypropylene tubes, and tissue culture plates (not to mention the packaging). "Plastic use is a huge issue in biomedical labs," says Doyle. But when he suggests that the Kosik lab switch to glass, Santiago looks skeptical. Reusing glass opens the lab up to the risk of contamination. "If we lost even a few cell lines because of this, it would be a big punch to the stomach," Santiago says. "Nobody wants to take that kind of blow to their science in the name of sustainability." Plus, hiring a dishwasher would cost $7 to $8 an hour.

Doyle admits that the issue is not clear-cut. Washing glass has its own environmental impact in terms of water use—especially in southern California. Still, he doesn't give up easily. "I could reuse your plastic for my work," he says, explaining that because his lab studies dirt, it doesn't have major contamination issues. "I could live downstream of you." Santiago agrees, and a new sustainability relationship is born.

Not easy being green

Even with the best intentions, Doyle's program is struggling to grow beyond its pilot phase. LARS currently operates on about $40,000 and is largely staffed by interns,

Energy-Efficient Freezers for Everyone

If you live in the United States, it's easy to spot the most energy-efficient appliances at your local home electronics store. Thanks to a joint program of the Environmental Protection Agency (EPA) and the Department of Energy, more than 50 types of products—from computer monitors to air conditioners—sport an "Energy Star" label if they are among the most energy-efficient items in their line. But leaf through a catalog of lab equipment, and you'll find no such guides.

Paul Mathew hopes to change that. The staff scientist at Lawrence Berkeley National Laboratory has been working with EPA for more than a year to put Energy Star labels on lab appliances. "People are clamoring for energy-efficient equipment," he says, "and the best way to do this is to have labels." Starting in 2008, researchers should have their wish—at least as far as fridges and freezers are concerned.

That still leaves out a host of other lab gadgets, including ovens and centrifuges. The short-term prospects for getting Energy Star labels on these products are dim, says Mathew, because they represent a niche market. So he and colleagues at Labs21,* a federal green-labs program, have been calling manufacturers and plugging in watt meters to obtain energy-use figures for as much lab equipment as they can. Those data should start appearing on the Labs21 Web site in about a year, meaning scientists will soon be able to tell which water bath is likely to send their energy bills off the deep end. **–D.G.**

* www.labs21century.gov

CREDITS (TOP TO BOTTOM): ALLEN DOYLE

who call themselves the Laboratory Research and Technical Staff (LabRATS). Doyle and his helpers scrounge most of the money from receptive departments and grants from foundations. The university won't commit hard funding until more labs are eager for assessments.

That's been a big challenge. In its first year, Doyle and his crew only visited labs they were friendly with, racking up 11 assessments. But in early January, the program started cold-calling professors, and the reception was far more chilly. Out of 27 invitations, only four labs have said yes.

Why the cold shoulders? "People don't want to take time away from their projects," says LARS co-founder Maynard, even if it's only for a couple of hours. And researchers just don't give conservation a high priority, adds UCSB paleobotanist and campus sustainability crusader Bruce Tiffney: "Scientists think about being green in their personal lives, but when it comes to work, they start thinking about publications and promotions." To that end, they typically don't want to risk using recycled reagents or tweaking delicate equipment just to save a few watts.

The lack of tangible incentives is also a roadblock, says Doyle. Sustainable lab practices often save money, especially when energy is involved, he says, but labs don't see those savings because the university pays the bills. UCSB campus energy manager Jim Dewey agrees. "Researchers aren't going to make compromises just to save the campus money," he says. And if making a change costs the lab itself cash, forget it. "Researchers are not held responsible for meeting carbon goals," Dewey says. "They're held responsible for meeting their budget."

Labs in hot fields—especially those run by young professors—also worry about competition. Doyle recommends that researchers turn off their water baths at night to save energy. But heating those baths back up in the morning can take precious time. "The pressures on productivity are huge," he says. "If you ask a lab to do something that will slow them down, it won't work out."

Spreading the word

Despite faculty resistance, Doyle's program has begun to win converts on campus. After the LabRATS visited a soil science lab in the fall of 2006, the researchers began pestering the recycling office about recycling pipettes, paper, and electronics. "Apparently, we got them thinking, and they started calling every other day," says Maynard. In other instances, lab members have become LabRATS themselves and have helped spread the word to other labs. "Once you tune people in, some people get really turned on," says Doyle.

Over the next year, Doyle hopes to reach even more scientists. One goal is to incorporate "eco-training" into the safety course that all faculty members and students must complete before working in a lab. Another project involves creating a Web site for surplus equipment to make it easier for scientists around campus to find and trade used equipment.

Still, Doyle says that to make more than an incremental impact, he'll need to get the university involved. If UCSB were to mandate a similar program in every department—what Doyle describes as going from retail to wholesale—he predicts it could save the campus hundreds of thousands of dollars in utility bills and equipment purchases. So far, university officials have shown no sign of wanting to set any requirements. With enough faculty support, however, they just might. A positive sign is that LARS just got permission from the dean of the Division of Mathematical, Life, and Physical Sciences to assess all eight labs in the department's new marine science building.

Doyle thinks his approach could work at other institutions, too, at least on a similarly small scale. "The challenge is finding a blend of dedicated staff and students to make the communications happen and to look for the conservation opportunities," says Doyle, "but our experience is that there are strong personalities and dedicated conservationists on most campuses." They just need the right tools, says Doyle, and he is planning on publishing his survey questions and other techniques on the Web.

For now, however, Doyle is focused on the task at hand. A couple of hours after visiting the Kosik lab, the LabRATS finish an assessment of an ecology lab run by Bradley Cardinale. The lab runs out of a World War II Army barracks, and Doyle jokingly refers to it as a recycled building. Cardinale's lab has done a good job optimizing its equipment to save energy, but Doyle suggests decommissioning a few unused overhead lights and unclogging a cold-room compressor. Cardinale seems eager to comply. "I think it's going to be a very successful program, and it makes a lot of sense for academics to get involved," he says. "If we don't take leadership for sustainability, who will?"

–DAVID GRIMM

Do-It-Yourself Recycling

What if your lab went through enough plastic pipette tip boxes a month to fill a small backyard pool, and your university didn't recycle any of it? Such was the case in the Johns Hopkins University laboratory of Bert Vogelstein as it plowed hot and heavy into the cancer genome project in early 2006. "The sheer volume of what we were wasting was annoying to me," says postdoc Devin Dressman.

So Dressman took matters into his own hands. He hauled the plastic boxes to a local recycling pickup site and made reusable cardboard receptacles back in the lab. "Most people were really into it," Dressman says of his labmates.

Eventually, Dressman convinced his building manager that the program made financial sense. Johns Hopkins pays about 66 cents a kilogram to destroy biohazard trash, he notes, so the campus reduces those costs by recycling the harmless pipette boxes. The entire medical campus is now recycling the boxes, and efforts are under way to get the rest of the university involved. "It's a win-win situation for everybody, and it's self-sustaining," says Dressman. Best of all, he no longer has to schlep plastic across town himself. "My goal was to take myself out of the picture," Dressman says. "I'm not here to do recycling, I'm here to do research." **–D.G.**

Tip top. Devin Dressman sits on a throne of recyclable pipette tip boxes.

CREDIT: MELISSA WHALEN

Numerical creativity 47

50 years after Sputnik 51

LETTERS | BOOKS | POLICY FORUM | EDUCATION FORUM | PERSPECTIVES

LETTERS

edited by Jennifer Sills

A World with Corals: What Will It Take?

IF THE ARTICLE "A WORLD WITHOUT CORALS?" (NEWS FOCUS, R. STONE, 4 MAY, P. 678) LEFT YOU reaching for a stiff drink, you are not alone. The measures required to limit climate change can seem an eternity away to coastal communities left to deal with the consequences. Yet, since the 1997–98 mass bleaching—an unforgiving global event that destroyed 16% of the world's coral reefs—practitioners and scientists have worked to identify meaningful actions that can promote reef survival in the face of climate change.

We believe it is more useful to ask, "What would it take to have a world with corals?" In this respect, the community responsible for the sustainable management of reefs has recently produced a series of consensus viewpoints (*1*–*3*). The emerging agenda stresses the need for a two-pronged approach: (i) global actions to reduce climate change and (ii) local actions to support ecosystem resilience.

The challenge of achieving international action on climate should not overshadow the significance of local interventions. Growing evidence suggests that local management will assist coral reefs through the period where we, as a global society, struggle to stabilize Earth's atmosphere. Strategies as broad as retaining herbivores (*4*), protecting naturally resilient areas (e.g., the sidebar "Palau combats coral bleaching," C. Pala, 4 May, p. 680), and maintaining conditions for coral recruitment (*5*) appear to be effective for shoring up the resilience of reefs in preparation for the next 100 years of stress.

Although the current greenhouse trajectory is disastrous for coral reefs and the millions of people who depend on them for survival, we should not be lulled into accepting a world without corals. Only by imagining a world with corals will we build the resolve to solve the challenges ahead. We must avoid the "game over" syndrome and marshall the financial, political, and technical resources to stabilize the climate and implement effective reef management with unprecedented urgency.

HEIDI SCHUTTENBERG[1,2] AND OVE HOEGH-GULDBERG[2,3]

[1]School of Earth and Environmental Sciences, James Cook University, Townsville, QLD 4811, Australia. [2]World Bank Coral Reef Targeted Research Program (www.gefcoral.org). [3]Centre for Marine Studies, The University of Queensland, St. Lucia, QLD 4072, Australia.

References

1. "Coral Reefs and Climate Change, A Statement from the Third International Tropical Marine Ecosystem Management Symposium," available at www.itmems.org/Coral_Reefs_Climate_Change.pdf.
2. ICRI resolution on coral reefs and climate change, available at www.icriforum.org/library/Reso_CC_Tokyo_0407.pdf.
3. H. Schuttenberg *et al.*, "Building resilience into coral reef management: Key findings and recommendations," summary prepared for the conference proceedings of the International Tropical Marine Ecosystem Management Symposium 2006, Cozumel, Mexico; see Supporting Online Material at www.sciencemag.org/cgi/content/full/318/5847/42b/DC1.
4. T. P. Hughes *et al.*, *Curr. Biol.* **17**, 360 (2007).
5. T. McClanahan, N. Polunin, T. Done, *Conserv. Ecol.* **6**, 18 (Dec. 2002); available at www.consecol.org/vol6/iss2/art18.

Pseudoscience in Bosnia

IN THE NEWSMAKERS ITEM "DIGGING FOR pride" (27 July, p. 435), Bosnian Prime Minister Nedzad Brankovic is quoted as asking, "Why don't we recognize something that is visible to the naked eye?" An answer to his question is that Semir Osmanagic and his colleagues have so far failed to publish, in a peer-reviewed journal, a credible case that the ruins of a monument-constructing "supercivilization" are anything other than a haphazard collection of jointed bedrock, Leisegang banding, sole marks, concretions, and other geologic features mixed in with some unrelated medieval, Roman, and other artifacts and ruins (*1*).

For example, Osmanagic and his colleagues claim that giant, meter-scale, "stone balls" found near Zavidovici, Bosnia and Herzegovina, are man-made artifacts related to a Bosnian "supercivilization." Examination of petrographic thin sections of recently obtained samples of the Zavidovici "stone balls" and the bedrock that originally enclosed them found that they consist of litharenite (*2*). Typical thin sections of the "stone balls" exhibit pervasive carbonate cement, including poikilotopic calcite spar. The calcite cement has often replaced framework grains. The bedrock, either from which these objects came or in which they are still partially encased, consists of litharenite almost identical in composition to these spherical to subspherical boulders. Local bedrock differs from these objects in that it typically lacks the strongly developed carbonate cement. Their carbonate cements, their subspherical shape, and their having been embedded in local bedrock demonstrate that they are naturally formed, calcite-cemented cannonball concretions, which have been described from Egypt, Kansas, New Zealand, and the southwestern United States (*3*–*6*).

However, no matter how obviously natural the various features that comprise pseudoarchaeological sites are to conventional geologists and archaeologists, dismissing them as "pseudoscience" is not enough. Instead, we need to explain to the public—using empirical data and logical arguments published in either popular articles, field guidebooks, Web pages, or other media—how natural features are either being misidentified or misrepresented as cultural

CREDIT: PHOTOS.COM

Bird speciation

54

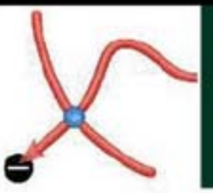

Rheology and biophysics

57

artifacts. The wide interest generated by Bosnian "pyramids," the "Phoenician Furnace and Fortress" of Oklahoma, and other pseudoarchaeological sites offers an opportunity to educate a curious public about the origin and significance of the geologic features such as systematic jointing, Leisegang banding, ripple marks, sole marks, and concretions that comprise them.

PAUL V. HEINRICH

Louisiana Geological Survey, Louisiana State University, Baton Rouge, LA 70803, USA.

References

1. Geology of the Bosnian "pyramids," Le site d'Irna, (2006), http://irna.lautre.net/Geology-of-the-Bosnian-pyramids.html (accessed 29 July 2007).
2. R. L. Folk, *Petrology of Sedimentary Rocks* (Hemphill's Bookstore, Austin, TX, ed. 2, 1981).
3. E. F. McBride, M. D. Picard, K. L. Milliken, *J. Sediment. Res.* **73**, 462 (2003).
4. E. F. McBride, K. L. Milliken, *Sedimentology* **53**, 1161 (2006).
5. J. R. Boles, C. A. Landis, P. Dale, *J. Sediment. Petrol.* **55**, 398 (1985).
6. A. Abdel-Wahab, E. F. McBride, *J. Sediment. Res.* **71**, 70 (2001).

Effect of Poor Census Data on Population Maps

THE REVIEW "LARGE-SCALE SPATIAL-TRANSMISSION models of infectious disease" (S. Riley, 1 June, p. 1298) states that "[f]or humans, an accurate estimate of population density is available for the entire Earth, up to a resolution of 1 arc sec." The differing modeling approaches and input data used in the many global human population surfaces (*1*–*3*) mean that the estimated spatial distribution of populations and consistency both within and between products varies markedly.

The spatial resolution of input census data is critical to the mapping accuracy (*4*). For many countries, contemporary census data collected at a high administrative unit level exist to facilitate "accurate," realistic-looking population mapping (e.g., fig. S1A) (*5*). For the majority of low-income countries, however, such data do not exist. This is especially true for much of Africa, where census data used for the production of global products are often over a decade old and at a resolution just below national level; a simple glance at the blocky and unrealistic-looking population distributions mapped for many African countries suggests that accuracy varies substantially (e.g., fig. S1B).

The lack of high-resolution data across much of the low-income regions of the world is likely to represent a significant limit to extending the reliable application of large-scale spatial transmission models of infectious diseases.

ANDREW J. TATEM

Spatial Ecology and Epidemiology Group, Tinbergen Building, Department of Zoology, University of Oxford, South Parks Road, Oxford, OX1 3PS, UK.

References and Notes

1. D. L. Balk *et al.*, *Adv. Parasitol.* **62**, 119 (2006).
2. J. E. Dobson, E. A. Bright, P. R. Coleman, R. C. Durfee, B. A. Worley, *Photogramm. Eng. Remote Sens.* **66**, 849 (2000).
3. M. Salvatore *et al.*, *Mapping Global Urban and Rural Population Distributions* (Food and Agriculture Organization, Rome, Italy, 2005).
4. S. I. Hay, A. M. Noor, A. Nelson, A. J. Tatem, *Trop. Med. Int. Health.* **10**, 1 (2005).
5. See Supporting Online Material at www.sciencemag.org/cgi/content/full/318/5847/43a/DC1.

Response

TATEM RAISES A POTENTIALLY IMPORTANT ISSUE. The accuracy of estimates of population density varies according to the quality of available supporting census data. However, current estimates for areas with poor census data may be sufficiently accurate to be used by studies based on large-scale spatial-transmission models.

Consider the potential transmission dynamics of reemergent smallpox. The main hypothesis supported in (*1*) is that, for the United Kingdom, spatial disc vaccination around known cases at either 15 or 50 km would not be an efficient addition to contact tracing, isolation, and vaccination. For the Central African Republic (CAR), results from a similar study would depend on the underlying assumptions of the human population model. Specifically, visual comparison of output from the global population model (*2*) for the CAR and northern Democratic Republic of Congo (immediately south of the CAR) suggests that heterogeneity between major roads in the CAR is underestimated. The sensitivity of predictions of disc vaccination efficacy for the CAR would have to be tested against this frailty, just as they would have to be tested against other key assumptions such as travel behavior and pathogen transmissibility. The post-hoc adjustment of global population data required for these sensitivity analyses would present particular technical challenges. However, given the much lower population densities in the CAR compared with the United Kingdom, if accurate travel data were available, it is entirely possible that a large-scale spatial-transmission model could be used with current global human population estimates to generate robust evidence in support of disc vaccination, perhaps with disc sizes greater than 50 km.

Another example where current population density estimates for Africa may be useful is in the analysis of the effects of sexual behavior change on the incidence of HIV in Uganda and Zimbabwe at different times (*3*). Did behavior changes affect the evolution of the regional incidence pattern over time, or is HIV incidence locally self-sustaining? If similar sustained behavior changes occur in other countries, can we predict spatial patterns of endemicity and/or eventual eradication of sexually transmitted infections? How useful could spatial targeting of resources across the region be in minimizing overall incidence? I do not suggest for a moment that large-scale spatial-transmission models can provide rapid definitive answers to these broad questions. However, using current population density estimates to construct large-scale models with these questions in mind might be a good starting point from which more specific relevant hypotheses could be generated.

STEVEN RILEY

Department of Community Medicine and School of Public Health, Faculty of Medicine, University of Hong Kong, Hong Kong, Special Administrative Region, People's Republic of China. E-mail: steven.riley@hku.hk

References and Notes

1. S. Riley, N. M. Ferguson, *Proc. Natl. Acad. Sci. U.S.A.* **103**, 12637 (2006).
2. J. E. Dobson, E. A. Bright, P. R. Coleman, R. C. Durfee, B. A. Worley, *Photogrammetric Eng. Remote Sens.* **66**, 849 (2000).
3. S. Gregson *et al.*, *Science* **311**, 664 (2006).
4. I thank G. Garnett for commenting on this response and The Research Fund for the Control of Infectious Diseases of the Government of the Hong Kong Special Administrative Region for funding.

Light-Splitting Method Not New

THE NEWS OF THE WEEK ARTICLE "LIGHT-splitting trick squeezes more electricity out of Sun's rays" (E. Kintisch, 3 August, p. 583) conveys the erroneous impression that a spectral splitting solar concentrator using a dichroic mirror is a novel, unproven method to achieve high efficiency. Although the group at the University of Delaware deserves commendation for setting an efficiency record, the approach is not new. In 1978, a group at Varian, working under a U.S. Department of Energy/Sandia contract, demonstrated an identical system using sili-

con and AlGaAs cells (*1*). The 28.5% module efficiency set a record at the time, which has been surpassed with the advent of stacked multijunction cells. Today, textbooks on photovoltaics describe such systems (*2*).

PETER BORDEN

Applied Materials, 118 Seville Way, Peter, CA 94402–2833, USA. E-mail: peter_borden@amat.com

References

1. R. C. Moon *et al.*, "Multigap Solar Cell Requirements and the Performance of AlGaAs and Si Cells in Concentrated Sunlight," Conference Record, 13th IEEE Photovoltaic Specialists Conference, Washington, DC, 1978, pp. 859–867.
2. M. A. Green, *Solar Cells: Operating Principles, Technology and System Applications* (University of New South Wales, Australia, 1998), p. 214.

Letters to the Editor

Letters (~300 words) discuss material published in *Science* in the previous 3 months or issues of general interest. They can be submitted through the Web (www.submit2science.org) or by regular mail (1200 New York Ave., NW, Washington, DC 20005, USA). Letters are not acknowledged upon receipt, nor are authors generally consulted before publication. Whether published in full or in part, letters are subject to editing for clarity and space.

CORRECTIONS AND CLARIFICATIONS

Reports: "Intra- and intermolecular band dispersion in an organic crystal" by G. Koller *et al.* (20 July, p. 351). The legend for Fig. 1 should have included the following information: The illustrative STM image of Fig. 1B was obtained at the Institute of Physics, Freie Universität Berlin, in collaboration with L. Grill.

Reports: "Food web–specific biomagnification of persistent organic pollutants" by B. C. Kelly *et al.* (13 July, p. 236). In Table 1, molecular weights were incorrectly reported for six chemicals. The corrected molecular weights (in parentheses) for the following compounds are: trifluralin (335); 1,2,4,5 TeCBz (216); PCB 180 (395); PBDE 47 (486); PBDE 99 (565); and PBDE 209 (960).

TECHNICAL COMMENT ABSTRACTS

Comment on "Top-Down Versus Bottom-Up Control of Attention in the Prefrontal and Posterior Parietal Cortices"

Jeffrey D. Schall, Martin Paré, Geoff F. Woodman

Buschman and Miller (Reports, 30 March 2007, p. 1860) described the activity of ensembles of neurons in parietal and frontal cortex of monkeys performing visual search for targets that were easy or hard to distinguish from distractors. However, their conclusions are called into question by discrepancies between their results and publications from other laboratories measuring the same neural process.

Full text at www.sciencemag.org/cgi/content/full/318/5847/44b

Response to Comment on "Top-Down Versus Bottom-Up Control of Attention in the Prefrontal and Posterior Parietal Cortices"

Earl K. Miller and Timothy J. Buschman

We reported latencies for target selection based on the earliest neurons to show effects, which Schall *et al.* mistakenly compare to latencies based on population averages. We show that there are actually no discrepancies across studies and also discuss the relative merits of single-electrode versus multiple-electrode approaches.

Full text at www.sciencemag.org/cgi/content/full/318/5847/44c

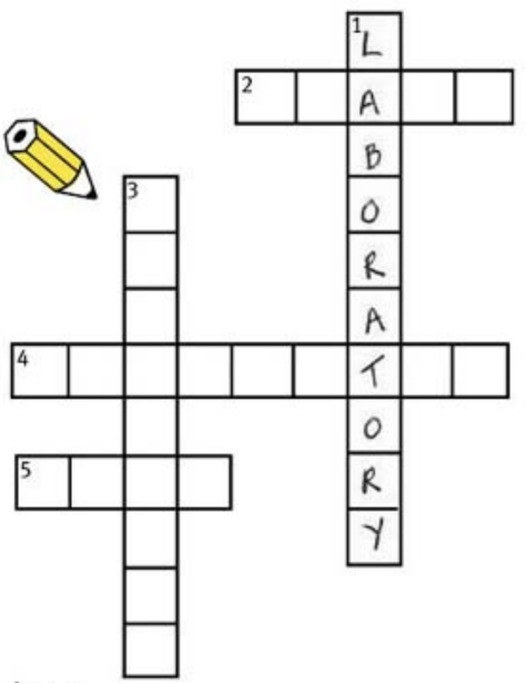

Across:
2. To impart knowledge
4. The science of matter
5. A method for trying or assessing

Down:
1. Place equipped to conduct scientific experiments
3. Variety; multiformity

1. laboratory, 2. teach, 3. diversity, 4. chemistry, 5. test

Searching for some fresh ideas about science education?

Find answers in *Science*'s Education Forum.

The *Science* Education Forum is a dynamic source of information and new ideas on every aspect of science education, as well as the science and policy of education. The forum is published in the last issue of every month and online, in collaboration with the Howard Hughes Medical Institute.

Keep up-to-date with the latest developments at:
www.sciencemag.org/education

What's your perspective?

Do you have ideas or research you'd like to share in the *Science* Education Forum? We're now looking for thoughtful, concise submissions (around 2,000 words) for 2007.

To submit your paper, go to:
www.submit2science.org

Science
AAAS

ENVIRONMENT AND HEALTH

On Sickness and Surroundings

Peder Anker

Breathing Space
How Allergies Shape Our Lives and Landscapes
by Gregg Mitman
Yale University Press, New Haven, CT, 2007. 330 pp. $30. ISBN 9780300110357.

Toxic Exposures
Contested Illnesses and the Environmental Health Movement
by Phil Brown
Columbia University Press, New York, 2007. 392 pp. $29.50, £19. ISBN 9780231129480.

Environmental health and justice have moved to the center stage of ecological concern. The current debate first flared with the dramatic events at Love Canal near Niagara Falls, New York. That polluted landscape became the scene of a social call to action against lethal living conditions that culminated in the 1980 evacuation of the Love Canal community. Phil Brown's *Toxic Exposures* documents the social movements that subsequently arose to improve people's environmental health in many other locations. Asthma has been a core issue for this movement, and Gregg Mitman's excellent study *Breathing Space* explores old and recent efforts to find relief for sufferers within allergenic landscapes.

The environmental health and justice movements brought new academic perspectives that address issues related to risk perception, landscape history, and the dynamics of a democratic society. They generally focus on the social and ecological complexity of environmental health problems, and they tend to conclude that one should seek interdisciplinary answers and solutions. Instead of equating an illness with the effect of a precise cause, as medicine tends to do, Mitman (a historian of science and medicine at the University of Wisconsin, Madison) recommends paying greater attention to the social and ecological relationships of diseases. Brown (a sociologist at Brown University) also emphasizes social and ecological complexity in dealing with toxic exposures.

The call for complex analysis tends to backfire when polluters answer with the same appeal to the complexity of their social or financial situations. Both authors readily admit this and recognize the importance of finding simple solutions to urgent problems. A quick medical or technical fix to toxic pollution is more helpful to those people exposed than ten sociological or historical studies. Yet swift scientific solutions lead to a state in which one is dealing only with the symptoms and not the underlying causes. As Mitman points out: "We take a pill or a puff, feel better, and conveniently ignore how that chemical moving inside our bodies connects us to a larger political economy and ecology of allergic disease." It is in locating these background issues that sociologists or historians of science may be of help to the scientific community.

Brown's sociological study shows the importance of laypeople's identification of toxic exposure and challenges to established medical perspectives. He analyzes three very different cases to demonstrate this: social movements addressing breast cancer, asthma, and Gulf War illness. In all three areas, he demonstrates, grassroots activity and mobilization played key roles in generating new scientific knowledge, finding solutions, and helping victims. Dealing with these toxic exposures required crossing specialist, social, and economic barriers. He explains why it is more likely that social, scientific, and policy-related answers to toxic exposures will be found when questions arise from those who have been exposed. Brown's argument is particularly convincing in his analysis of breast cancer, where he documents the importance of a social (as opposed to individual) call to action, the value of laypeople raising scientific questions, and the force of ground-level political mobilization among women.

In his analysis of asthma, Brown claims that "attention to the new asthma epidemic comes from empowered laypeople who are concerned about environmental triggers of the disease." This claim needs some qualification in view of Mitman's study, which shows that the asthmatic and allergic epidemic is an old phenomenon dating back to financially "empowered laypeople" with a different social and political setting than those Brown discusses. They both hold, though, that the call to action did not start in the scientific laboratory, but instead among the victims. Indeed, the thinking of the environmental health movement Brown describes looms large behind Mitman's historical analysis.

A combination of scholarly and engaging history, *Breathing Space* offers an alluring account of how allergies shape people and the environment. Mitman's historical research, archive work, and methodology are rigorous. His account is also witty (as in telling about the well-to-do's use of allergy as a convenient justification for going on vacation; I laughed out loud twice) and moving (as when address-

Mr. A. Wiper Weeps on a train. The hood sheltered him from the dust and smoke of the railway. Hay fever could be addressed humorously by those with the money to afford the holiday cure.

CREDIT: COURTESY OF EBLING LIBRARY, RARE BOOKS AND SPECIAL COLLECTIONS, UNIVERSITY OF WISCONSIN–MADISON

The reviewer is at the Forum for University History, University of Oslo, Post Office Box 1008 Blindern, NO-0315 Oslo, Norway. E-mail: peder.anker@ffu.uio.no

ing the racial bias and environmental injustice toward the urban poor).

Mitman takes the reader through six more or less independent stories describing how allergies came to shape people and spaces in the United States. He starts with the holiday resorts of the 1870s in which the leisure class searching for escape from hay fever created a substantial tourist economy in mountain environments. At the time, allergy was understood as a functional nervous disease best cured through travel to landscapes and hotels of leisure. Mitman turns this social history of allergy into an environmental history, arguing that the upper-class escape reshaped holiday landscapes into anything but allergy-safe places. Allergenic plants such as ragweed followed the infrastructure of large hotels (e.g., trains, roads, vegetable gardens, and tree cuttings). Mitman shows how botanical research into the life and spread of the giant ragweed (*Ambrosia trifida*) led to medical investigations of its allergenic powers. From these studies came new understanding of the importance of its pollen, followed by a social "war against ragweed" in the form of massive clearings and subsequent "vaccine" of nature in the form of herbicides.

Inspired by environmental justice methodology, Mitman develops a novel way of analyzing the urban history and ecology of ghetto cultures in New Orleans and New York City in the 1960s and 1970s. Instead of pinpointing one cause of asthma, the cockroach—which inevitably led to a narrow focus on its eradication—Mitman untangles a web of environmental, racial, social, and economic factors to explain the causes of allergies among the poor. Equally interesting is his history of air-conditioning and other attempts to engineer pollen- and dust-free indoor environments as refuges from allergic diseases. In these pages, Mitman argues that the one-size-fits-all technological fix of air-conditioning could not provide an asthma-safe zone inside buildings.

Neither could the billion-dollar pharmaceutical industry, to which Mitman devotes the last part of his book. Taking medicine against allergies, he argues, is an escape from place. In addition to addressing medical treatments of the body, the book offers a plea for addressing land use, the urban matrix, and building construction as well as the social and economic inequalities that in combination create an environment triggering allergic reactions. "Allergy is not a thing but a relation," Mitman stresses, and consequently one needs to take a broad social and ecological approach.

In reading these books, I was struck by their Amerocentric focus. Brown discusses the U.S. "environmental health movement," and in telling about "our lives and landscapes" Mitman only includes Americans. As the forces at work—plants, insects, animals, people, pollution, money, companies, politics, social movements, science—move around on a global scale, there is an urgent need to discuss environmental health concerns on the same international level.

Brown and Mitman show that environmental health advocacy groups have shaped not only the political and social dynamics of research but also the ways in which landscapes and society evolve. Their focus on the broad circumstances of scientific developments is both timely and important. *Toxic Exposures* and *Breathing Space* demonstrate that dreams about solving environmental problems through one medical or technological fix come at the expense of understanding the underlying social and ecological complexity of a problem.

10.1126/science.1145071

THEATER: MATHEMATICS

Variations on a Theorem

Louise Whiteley

A math lesson in southern India, circa 1900. The teacher is explaining what happens when you divide a number by itself—if you have ten fruits, and divide them between ten people, each gets one. Likewise with a thousand fruits and a thousand people, and for any other number you might care to mention. Srinivasa Ramanujan, a young boy already displaying unusual talent and a fondness for asking difficult questions, challenges: "But is zero divided by zero also one? If no fruits are divided among no one, will each still get one?" (*1*).

Ramanujan had put his finger on something that has troubled scholars as long as symbols have been used to stand for numbers: does zero really belong on the number line? How can something be nothing? Brilliant but unorthodox, he struggled to conform to the academic system in India and to attract the attention of the British establishment. Finally, in 1913, a letter from Ramanujan arrived in the tweedy lap of Cambridge mathematician G. H. Hardy, who recognized his genius and excitedly issued an invitation.

Srinivasa Ramanujan (Shane Shambhu) and G. H. Hardy (David Annen).

As a Brahmin, Ramanujan's religious beliefs forbade him leaving India, but eventually his mother received a vision that allowed him to follow his ambition to England, just as thousands of years before the concept of zero had traveled from East to West. *A Disappearing Number*, a play from Complicite and director Simon McBurney, tells the story of the famous collaboration that resulted—and of Ramanujan's ultimately tragic attempt to find intellectual fulfilment in cold, wartime Cambridge.

A Disappearing Number

Conceived and directed by Simon McBurney, devised by Complicite

Co-produced by Complicite, barbicanbite07, Wiener Festwochen, Holland Festival, Ruhrfestspiele, in association with Theatre Royal Plymouth. Barbican Theatre, London. Through 6 October 2007. www.complicite.org/productions/detail.html?id=43

The production follows Hardy and Ramanujan—along with an array of present-day characters including math lecturer Ruth, her husband Al, an Indian call center worker, and a particle physicist—in their struggles with loss, permanence, and identity and on journeys to and from India. The multiple narratives are knitted together through the use of repetition, overlap, and some ingenious staging. Projected scenes are used to evoke different places and times, and ordinary objects such as chairs are used to link them—serving as cars, trains, and airplanes; as dance partners; and even as the subject of musings on the essential nature of reality.

Al and Ruth's relationship is used to help the audience follow the math. We attend Ruth's lectures along with Al and follow his attempts to understand the ideas she is so pas-

The reviewer is at the Gatsby Computational Neuroscience Unit, University College London, Alexandra House, 17 Queen Square, London WC1N 3AR, UK. E-mail: louisew@gatsby.ucl.ac.uk

CREDIT: TRISTRAM KENTON/COURTESY THE BARBICAN

sionate about. One night, after Ruth has been trying to explain the infinite convergent series $1 + 1/2^1 + 1/2^2 + 1/2^3 + 1/2^4 + 1/2^5 + \ldots = 2$, Al suddenly exclaims that he understands: "In the end, it adds up to two!" No, says Ruth frustratedly from under the bedcovers, there is no "in the end"; the series adds up to two only in infinity. Later, alluding to her longed-for pregnancy, Ruth quips that the series might in fact add up to three, making the audience complicit in a mathematician's joke.

As is de rigueur for any film or play about mathematics, numbers are everywhere: in flight times, telephone numbers, turbulence, and the ripples on water. But the production also focuses on the links between the human themes it explores and the meanings of mathematical concepts integral to Ramanujan's work, such as infinity, nothingness, convergence, and partition. Mathematicians might complain that there is too much semantic slip here. For example, connecting the concept of infinity to the characters' desire to "leave something behind" doesn't really encompass the mysterious boundlessness that Al struggled to understand. But for the most part the two genuinely illuminate each other, both enriching the narrative and bringing the math alive.

Hardy believed that pure mathematics was a creative endeavor: as a poet makes patterns out of words, a mathematician makes patterns out of ideas (*2*). But in mathematics as well as in the arts, the process of pattern-making can be contentious. Ramanujan is famous for reaching his theorems through amazing leaps of intuition, which were baffling to Hardy, raised as he was on a strict diet of logical proofs. A scene in which Ramanujan scrawls off theorems at breakneck speed, while Nitin Sawhney's mathematically infused tabla music and Kathak dance unfolds around him, perfectly illustrated this and reflected the mixture of imaginative leaps and thorough research that characterizes Complicite's recent work.

It has been said that Hardy immediately recognized that Ramanujan's theorems must be true, because they were beautiful. *A Disappearing Number* may not enable us to look at an equation and see that it is beautiful. However, through our encounters with characters who can, we get some intriguing, and moving, glimpses of what this might mean.

References

1. R. Kanigel, *The Man Who Knew Infinity: A Life of the Genius Ramanujan* (Scribner, London, 1991).
2. G. H. Hardy, *A Mathematician's Apology* (Cambridge Univ. Press, Cambridge, 1940).

10.1126/science.1150152

SPACE EXPLORATION

How a Race Was Won

Epic Rivalry
The Inside Story of the Soviet and American Space Race

by Von Hardesty and Gene Eisman

National Geographic, Washington, DC, 2007. 367 pp. $28, C$36. ISBN 9781426201196.

We are now in the grips of a 21st-century space race, as many nations set their sights again on the Moon and then Mars. But 50 years after the launch of the Sputnik satellite, the first man-made object to orbit Earth, what might we learn from that achievement and the subsequent competition to dominate space it triggered? Why, after the early Soviet lead, was it the Americans who first walked on the Moon?

In *Epic Rivalry*, Von Hardesty and Gene Eisman (respectively, a curator and a researcher at the Smithsonian Institution's National Air and Space Museum) weave together historical details of the events that led to Sputnik's launch in 1957 and its subsequent impact on the human psyche. Following World War II, German missile technology was upgraded in parallel projects led in the United States by immigrant Wernher von Braun and in the USSR by Sergei Korolev. Both visionary engineers had the same goal: to fire a ballistic missile into space orbit during the International Geophysical Year, 1957. With Sputnik's successful launch, Korolev's team won the competition, perhaps because of his boldness in building a more powerful rocket capable of lofting large payloads.

Sputnik's orbit not only captured the public's imagination—people around the world marveled at it streaking across the night skies—but also instilled fear. The Americans in particular saw its global reach as a distinct threat. They responded by rapidly expanding their own space program. Although the Soviets' Luna 9 was the first craft to make a soft landing on the Moon, their program slipped into disarray—particularly after Korolev's untimely death in early 1966—and was eventually overtaken.

Hardesty and Eisman emphasize the different political approaches of the two countries. The communist Soviet Union could muster an effective work force, which triumphed under Korolev's inspirational leadership. But perhaps, they argue, its workers lacked the personal drive of the more individualistic Americans. Moreover, the entire Soviet project was shrouded in military secrecy, even located in a secret spaceport, Baikonur. Cosmonauts didn't grumble but gamely sealed themselves in their orbiting tin cans "like Spam," parachuting out individually as their capsules crashed to Earth in the Siberian snow. The more autonomous American astronauts demanded manual controls so they could wrestle the capsule down safely into the sea. The characters of the crews, mostly drawn from military test pilots, are striking for their bravery. All were extreme risk takers, astonishingly willing to gamble their own lives simply for the excitement and challenge of flying in space.

Today, the authors point out, such risks are deemed less acceptable, and space exploration has become an international collaborative exercise. The American style of carrying out space travel fully in the public glare has meant that appetites for failure are small, and accidental losses weigh heavily. The competitive aspects are, however, still alive in the private sector, with cash prizes driving the development of space technology and private space travel being a real possibility. The roles of national leaders in setting directions are also still relevant, as is pride. With more players at the table, let us see where the next space race will take us.

–Joanne Baker

First out of the gate. The Soviets launched Sputnik 1 on 4 October 1957.

CREDIT: SOVFOTO

10.1126/science.1149411

SUSTAINABILITY

Learning from 10 Years of Climate Outlook Forums in Africa

As new projects and programs are proposed to promote climate adaptation and disaster risk reduction in Africa, it is important to learn from the successes and failures of the Climate Outlook Forums.

Anthony G. Patt,[1,2] Laban Ogallo,[3] Molly Hellmuth[4]

In 1997, meteorologists and representatives from government ministries, nongovernmental organizations, and businesses held the first regional Climate Outlook Forum (COF), in Kadoma, Zimbabwe. Their goal was to negotiate a seasonal climate forecast, providing an indication of rainfall 3 to 6 months in advance, that would be useful in climate-sensitive sectors, such as agriculture, food security, health, and water-resource management. We describe examples of the uneven progress toward this goal during the 10 years since then and suggest lessons that apply to current efforts to promote sustainable development, climate-change adaptation, and disaster risk reduction in Africa.

By the 1990s, scientists had developed models to predict El Niño–Southern Oscillation (ENSO), a multiannual cycle in the tropical Pacific Ocean (*1*), and had identified climate anomalies in Africa associated with its different phases (*2*). During an El Niño, for example, much of southern Africa often experiences low seasonal rainfall and poor crop yields (*3*). Although models could not predict particular weather events more than about 10 days in advance, they could forecast likely seasonal conditions.

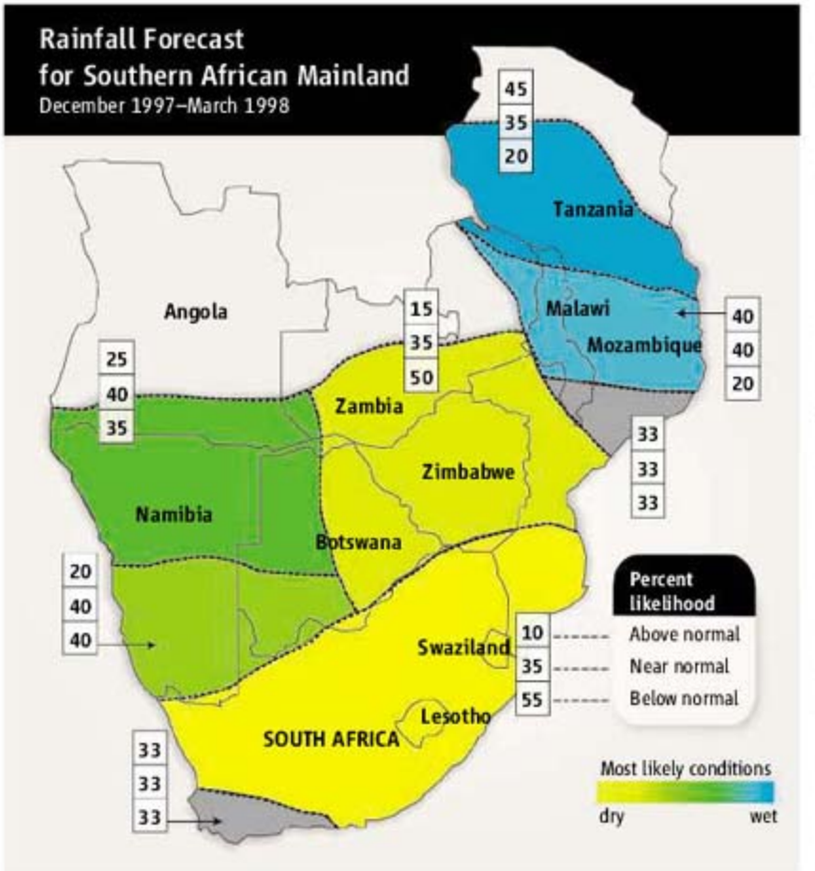

The seasonal forecast: Climatologists categorize the total quantity of seasonal rainfall as above normal, near normal, and below normal, defined for each measurement station such that historical measurements fall within each category, or tercile, with equal frequency. Based on how ENSO and other external factors affect different geographical zones, forecasters can depict the likelihood of rainfall falling within each tercile for the coming season, as well as the most likely outcome within each zone. The gray zones indicate areas where the effect of external factors is slight, and hence the probabilities remain at one-third for each tercile. This type of forecast provides potentially valuable information for a large geographical area, but can be difficult to use for many management decisions. Users need access to local historical data to know what range of actual rainfall each tercile represents, and then to incorporate this information into a probabilistic decision-making framework.

It was still unclear to the COF organizers (Note S1 in Supporting Online Material), however, whether people would trust the forecast and use it to improve decisions (*4*). The COF addressed the issue of trustworthiness by negotiating a single consensus forecast for the entire region (see figure, above), which would have the backing of the regional Drought Monitoring Centre (DMC) in Harare and the participating countries' national meteorological and hydrological services (NMHSs). They addressed the issue of forecast use by holding roundtable and panel discussions with potential forecast users. The COF generated enthusiasm among those who attended, and East and West Africa followed suit by holding COFs in February and May of 1998, respectively. Since then, COFs have taken place annually or biannually in three African regions, as well as in regions outside of Africa.

Unfortunately, the first efforts to apply forecasts were not encouraging. In mid-1997, El Niño conditions had led to a forecast of likely dry conditions over most of southern Africa. The response in Zimbabwe was that banks restricted credit, and farmers reduced their planting. When near-normal rains actually fell in much of the country, national-level harvests suffered because of the anticipatory action (*5*), and people accused the COF organizers of having misled them (*6*).

Lack of trust in the forecast created its own problems. War depleted Ethiopian food stocks in the late 1990s, and people feared that a drought could trigger famine. Sea surface temperatures in 1999 led to a forecast of likely dry conditions. But humanitarian organizations were unwilling to commit resources on the basis of probabilistic predictions, and relief efforts only began after the rains had failed, costing several months' time (*7*).

The use of forecasts has been a learning process, and the positive examples that emerged include the following five. As in 1999, the 2002 forecast in Ethiopia predicted a high likelihood of drought, suggesting the need for food relief. In contrast to 1999, an emergency management team began meeting shortly after the COF to identify specific actions (*8*), and donors were willing to begin making commitments before the situation had grown critical (Note S2).

In a pilot project in Mali operating since 1982, agricultural extension officers helped

[1]International Institute for Applied Systems Analysis Laxenburg 2361, Austria. [2]Department of Geography and Environment Boston University, Boston, MA, USA. [3]Intergovernmental Authority on Development Climate Prediction and Applications Centre, Nairobi, Kenya; [4]International Research Institute for Climate and Society, Columbia University, New York, NY, USA.

*Author for correspondence. E-mail: patt@iiasa.ac.at

farmers to base their decisions on forecasts of weather 10 days ahead (Note S3). Seasonal forecasts were also used, once they became available in 1998. A 2004 survey found income gains of 10 to 80% when participating farmers were compared with a control sample (*8*). A pilot project in Zimbabwe (2000–05) also showed gains from forecast use (Note S4). In collaboration with the agricultural extension service, the first author of this article held preseason climate workshops each year in four villages, inviting a random sample of subsistence farmers to participate. Postseason interviews revealed that farmers who made specific decisions on the basis of the forecast benefited, with gains in yields averaging 9% (*9*).

In 2001, Metéo France began to provide seasonal catchment forecasts for the Manantali Dam in West Africa, working with the dam authority to develop a management model for seasonal commitments in power generation and agriculture (Note S5). In the preoperational phase of the project, use of a model based on the forecast, rather than historical records, improved dam management considerably, and forecasts are now being used for actual dam operations (*10*).

Starting in the 1990s, the World Health Organization (WHO) began exploring the potential for climate information to guide malaria prevention and control efforts. A series of studies showed how malaria transmission rates are related to climatic conditions (*11*, *12*). The International Research Institute for Climate and Society (IRI), WHO, and DMC-Harare launched the Southern African Malaria Outlook Forum (MALOF) in 2004 (Note S6). The strategies developed at the MALOF influenced decisions and appear to have led to marked reductions in mortality and morbidity the following year (*8*).

Experience suggests three necessary conditions for forecasts to be useful. First, forecasts must provide information that is specific to particular users' needs, going beyond tercile probabilities (*13*). To predict crop yields, for example, one has to combine the forecast with indicators such as soil moisture (*14*). Seasonal forecasts could be useful for planning power generation in East Africa (*15*, *16*), but there is no formal operational use of forecasts because the information currently available is not catchment-specific. One factor explaining the successful response to the forecasted food insecurity for Ethiopia in 2002 was the development, shortly after the COF, of scenarios and specific action plans.

The second condition is institutional: Forecasters need to work in partnership with potential users to develop and interpret forecasts (*17*). The MALOF provides a good example. Public health organizations and forecasters organize each year's meeting. This has resulted in greater attention to historical climate and real-time weather data, which are often more relevant for malaria control efforts than the preseason forecast. The COFs, in contrast, have adapted less to user needs. Agricultural and food security planners have repeatedly identified the need for additional information, such as anomalies in the dates of rainfall onset or cessation. But such users have participated little in planning the agendas and forecasting activities for subsequent COFs, and attention has remained focused on predicting seasonal rainfall totals.

Inclusive communication is the third condition, because probabilistic forecasts of climatic anomalies are so hard to understand (*18*). A study of farmers in South Africa found that most people misinterpreted many of the basic forecast terms (*19*). In Zimbabwe, farmers who had participated in preseason forecast workshops were five times as likely to have changed decisions because of the forecasts as those who had learned the forecast from the media (*9*). Radio may be the most efficient communication medium in Africa, but organized listening groups, like the workshops in Mali and Zimbabwe, improve comprehension (*20*). Communication also needs to cover the forecast's reliability. A survey of South African water managers found that few understood or trusted the forecasts' reliability enough to use as the basis for decision-making (*21*).

Improving the capacity for forecast use may be an effective way for Africa to prepare for climate change (*22*), and several organizations engaged in development, disaster risk reduction, and climate-change adaptation in Africa are now launching programs that will incorporate climate forecasts into their activities. The largest of these, a partnership between the African Union, the United Nations Economic Commission for Africa, the African Development Bank, the United Kingdom Department for International Development, and the Global Climate Observing System, intends to spend up to $200 million over the next 12 years to spread out the use of climate information to help achieve the U.N. Millennium Development Goals.

The success of these new programs will depend on developing user-specific forecasts and interactive communication, but the emerging enthusiasm among development and humanitarian organizations creates the appropriate institutional conditions for partnerships with forecasters. Whether what follows is additional sector-specific meetings, like the MALOF, or shared responsibility for the multisector COFs, it may now be possible to extend the limited benefits of seasonal climate forecasts to reach many more people.

References

1. M. A. Cane, S. Zebiak, S. Dolan, *Nature* **321**, 827 (1986).
2. National Research Council, *Learning to Predict Climate Variations Associated with El Niño and the Southern Oscillation* (National Academy Press, Washington, DC, 1996).
3. M. Cane, G. Eshel, R. Buckland, *Nature* **370**, 204 (1994).
4. M. M. Betsill, M. H. Glantz, K. Crandall, *Environment* **39**, 6 (1997).
5. J. Phillips, D. Deane, L. Unganai, A. Chimeli, *Agric. Sys.* **74**, 351 (2002).
6. M. Glantz, *Once Burned, Twice Shy? Lessons Learned from the 1997–98 El Niño* [U.N, Environmental Programme/National Center for Atmospheric Research (USA)/U.N. University/World Meteorological Organizaiton/International Strategy for Disaster Reduction, Tokyo, Japan, 2000).
7. K. Broad, S. Agrawala, *Science* **289**, 1693 (2000).
8. M. Hellmuth, A. Moorhead, M. C. Thomson, J. Williams, Eds., *Climate Risk Management in Africa: Learning from Practice* (IRI, Columbia University, New York, 2007).
9. A. G. Patt, P. Suarez, C. Gwata, *Proc. Natl. Acad. Sci. U.S.A.* **102**, 12673 (2005).
10. J. Axel, J. P. Céron, in *Elements for Life*, J. Griffiths, Ed. (Tudor Rose, London, 2007), pp. 70–71.
11. G. Zhou, N. Minakawa, A. Githeko, G. Yan, *Proc. Natl. Acad. Sci. U.S.A.* **101**, 2375 (2004).
12. M. C. Thomson *et al.*, *Nature* **439**, 576 (2006).
13. C. Vogel, K. O'Brien, *Climate Res.* **33**, 111 (2006).
14. J. W. Hansen, M. Indeje, *Agric. Forest Meteorol.* **125**, 143 (2004).
15. C. Oludhe, S. Marigi, W. Ogana, D. Kimani, "An assessment of the potential benefits of seasonal rainfall prediction in relation to hydroelectric power generation in Kenya" [National Oceanic and Atmospheric Administration (NOAA), U.S. Department of Commerce, Washington, DC, 2001].
16. A. D. Babu, D. Korecha, "Evaluation of economic contributions of seasonal outlooks for the power industry in Ethiopia" (NOAA, Washington, DC, 2001).
17. D. Cash, J. Borck, A. G. Patt, *Sci. Technol. Hum. Values* **31**, 465 (2006).
18. C. Roncoli, *Climate Res.* **33**, 81 (2006).
19. S. Walker, E. Mukhala, W. J. V. d. Berg, C. R. Manley, "Assessment of communication and use of climate outlooks and development of scenarios to promote food security in the Free State province of South Africa" (NOAA, Washington, DC, 2001).
20. K. Ingram, C. Roncoli, P. Kirshen, *Agric. Sys.* **74**, 331 (2002).
21. P. Johnston, G. Ziervogel, M. Matthew, paper presented at the 30th Annual Applied Geography Conference, Indianapolis, IN, 17 to 20 October 2007.
22. R. Washington *et al.*, *Bull. Am. Meteorol. Soc.* **87**, 1355 (2006).

Supporting Onliee Material
www.sciencemag.org/cgi/content/full/318/5847/49/DC1

10.1126/science.1147909

HISTORY OF SCIENCE

Sputnik and the Soviets

The launch of Sputnik startled the world but did not lead to a healthy Soviet space program.

Roald Sagdeev

By launching a modest spherical capsule called Sputnik on 4 October 1957, the Soviets had no ambitions at all to shock the world. It was simply another routine test for the first intercontinental ballistic missile, known as R-7 [(*1*), p. 195]. Five preceding attempts failed to bring conclusive results, and the Kremlin desperately needed success. After the first explosions of American atomic bombs in the summer of 1945, the Soviet leadership under Stalin was paranoid over the perceived vulnerability of the USSR to nuclear attack. The United States not only had nuclear weapons and heavy bombers; its bases encircled the Soviet Union from locations in Europe, Turkey, and Japan. Yet the geostrategic configuration of the USSR did not favor a symmetrical approach with bombers. Rockets seemed the best asymmetric response to close the window of vulnerability. The Soviet nuclear bomb had already been tested in late 1949, and Andrei Sakharov's team was actively engaged in developing the ultimate weapon, the hydrogen bomb. If only the delivery vehicle had been available.

Shocking satellite. Postcard from 1958 commemorating the launches of Sputnik-1 and Sputnik-2. Although reported as a routine matter in the Soviet press, the launch of Sputnik-1 shocked the world.

That dream gained momentum with one of the lessons Stalin took from the Second World War: Even the imperfect V-2 rockets the Germans kept lobbing at the British became weapons of terror. With the Red Army entering East Germany, a large team of Soviet rocket engineers and technicians—including future heroes of the Space Age Sergei Korolev and Valentin Glushko—descended in 1945 on Peenemünde, the birthplace of the V-2. In the bombed-out ruins, the Soviets picked up every remaining piece of hardware and documentation (*2*). The Soviets, along with the remaining German rocket scientists and engineers, had to act like archaeologists to reconstruct Wernher von Braun's secrets. It took 18 months to reproduce the entire rocket design and finally successfully launch one. Then, in 1947, the Soviets shipped everything (including the key German personnel) to Russia, where a modified V-2 was produced and assembled. Both Korolev and Glushko were promoted to lead a much larger effort to develop a rocket program. This was quite a change for people who, until less than 3 years before, had been prisoners of the KGB's *sharaga*, a gulag where the inmates worked as intellectual serfs on defense projects.

The design of R-7 was initiated in 1953 to make a delivery vehicle for Soviet hydrogen bombs. At that time Sakharov and his colleagues did not yet know how heavy the warhead was going to be. The figure given to the rocket team was soon discovered to be a huge overestimate, and so the original R-7, later modified and renamed a few times, is still kept as an indispensable workhorse of the Soviet (now Russian) space program. Under the name "Soyuz" this rocket serves when needed as the lifeline for the International Space Station.

The work on R-7, the biggest liquid-propellant rocket of the 1950s, was under way when Korolev, urged by the leaders of the Soviet scientific community, persuaded the government to let him build and launch the first human-made object ever to orbit Earth. In May 1956, the Kremlin, in response to that request and in conjunction with the International Geophysical Year (IGY) of 1957–1958, adopted Korolev's plan as part of the R-7 program. This intent was confirmed in an official statement in September 1956 [(*3*), p. 4].

Although the Soviet press had announced the news about the launch of Sputnik-1 in a rather routine and businesslike fashion, the world was surprised and shocked. I had just started work at a classified location, which later became the Kurchatov Institute of Atomic Energy. We had no idea about the coming launch, and our reaction was surprise mixed with a feeling of pride (*2*).

Khrushchev quickly discovered that this was a new political propaganda vehicle and demanded another immediate spectacle for the eve of the 40th anniversary of the Great October Revolution (see the figure). The launch of Sputnik-2 was scheduled for 3 November 1957. This left no time to prepare even a modest scientific payload dedicated to the IGY program. As the veteran of Soviet rocketry Boris Chertok would later remark, the result was a death sentence for a poor dog named Laika, sent as a kamikaze passenger on that launch [(*1*), p. 198].

Sputnik-1 did not carry scientific instruments, and there would have been no practical scientific output had it not been for the indirect data on the gradual evolution of Sputnik's orbit due to atmospheric drag force. This phenomenon enabled researchers to reconstruct the atmospheric density at the satellite's altitude. With that, the whole of Earth's outer atmosphere became an object of scientific research. The USSR Academy of Sciences immediately

The author is in the Department of Physics, University of Maryland, College Park, MD 20742, USA. E-mail: rsagdeev@gmail.com

CREDIT: RYKOFF COLLECTION/CORBIS

started lobbying the government and the space industry for the opportunity to develop scientific instrumentation to be launched into space. Korolev firmly promised that a third Sputnik would be dedicated to scientific experiments. This came not a moment too soon: Despite initial setbacks, the American program was rapidly acquiring momentum. Scientific competition in space, on top of the military rocket race, was imminent.

In the spring of 1958, Korolev ran the last briefing before the final green light for the launch of Sputnik-3. It carried the first impressive collection of scientific instruments, each of which was reported to be functioning normally. However, trouble was discovered in a tape recorder, whose function was to gather and store the science data. The scientists were alarmed and wanted to postpone the launch. To their great disappointment, Korolev ordered that the countdown begin—and the tape recorder did not work in orbit. Consequently, the science data came only from the area of direct radio contact with the satellite. And within this area the cosmic ray detectors signaled extreme levels of enhanced radiation. Did it embrace the whole planet at altitudes above the atmosphere? With the lack of data, there was no way to tell. A few weeks later in 1958, a cosmic ray detector was launched to scan every bit of the satellite's orbit, but it was an American launch (*4*). It brought one of the most interesting developments of the early space era: the discovery of radiation belts, now named after James A. Van Allen.

A few years later, in conversation with one of the Sputnik-3 scientists, Korolev made a confession. On that unfortunate day, Khrushchev reached him on the phone at the Baikonur launch site. He said that the Italian Communist Party leaders had urged him to do something spectacular before the Italian parliamentary elections the next day. The priorities were thus established. Science was not simply a poor relative of the military-industrial complex, but a hostage to high-level politics too.

After Sputnik, the two superpowers in the Cold War embarked on very different approaches. The Soviet Union, by virtue of its closed system, did not establish a space program that was independent of the military. There was no legislation even remotely similar to the United States' 1958 Space Act, which instituted NASA as a civilian agency. The Soviet military owned and operated every launch site as well as the network of ground control centers. Planning and oversight for all aerospace programs was performed by departments and ministries of the Communist Party's Central Committee. Everything in the country's everyday life beyond defense contracts was given secondary priority. In certain areas of military technology, and with an almost unbearable burden on the Soviet economy, sometimes this approach did bring impressive results. But as we know, this modus vivendi finally proved unsustainable, and not only in space programs.

References

1. B. Chertok, *Rockets and People: Fili-Podlipki-Tyuratam* (Machinostroenie Publishing House, Moscow, ed. 2, 1999).
2. R. Z. Sagdeev, *The Making of a Soviet Scientist* (Wiley, New York, 1994).
3. S. Eisenhower, *Partners in Space: US-Russian Cooperation After the Cold War* (Eisenhower Institute, Washington, DC, 2004).
4. J. A. Van Allen, *Origins of Magnetospheric Physics* (Smithsonian Institution Press, Washington, DC, 1983).

10.1126/science.1149240

HISTORY OF SCIENCE

Science and Sputnik

Sputnik led to an energetic U.S. space program and new discoveries about the cosmos.

John C. Mather

A child of the atomic age, I was born a year and a day after Hiroshima, but I grew up in the seclusion of the Rutgers Agricultural Experiment Station, a mile from the Appalachian Trail. Science seemed exciting and a little dangerous, but not the force that would guide the fate of nations. Then in October 1957, Sputnik was launched, and America went into a frenzy. In 1958 Congress created NASA, in 1960 the (nonexistent) missile gap with the Soviet Union helped elect John Kennedy as president, in 1961 Kennedy endorsed NASA's Apollo program to go to the Moon before the decade was out, in 1962 there were Soviet missiles in Cuba, and a year later Kennedy was assassinated. The Apollo program was one side of an arms race that led to the collapse of the Soviet Union without nuclear war.

The events surrounding Sputnik stimulated a rich era in satellite-based astronomy. In 1970, at the University of California, Berkeley, I embarked on a thesis project with Paul Richards to measure the spectrum of the Big Bang's cosmic microwave background radiation discovered only 5 years before. Then in 1974, soon after I left Berkeley, NASA announced an opportunity to propose new satellite instruments. Pat Thaddeus, my postdoctoral advisor, told me to call Rainer Weiss, David Wilkinson, and Michael Hauser, and we put together a proposal to measure the cosmic microwave background spectrum and anisotropy (i.e., spatial fluctuations), and to find the cosmic infrared background from the first galaxies. In 1976, NASA chose members of our team and two other teams (from Berkeley and Jet Propulsion Laboratory) to define the Cosmic Background Explorer (COBE) mission (*1*) and assigned Goddard Space Flight Center to provide engineering.

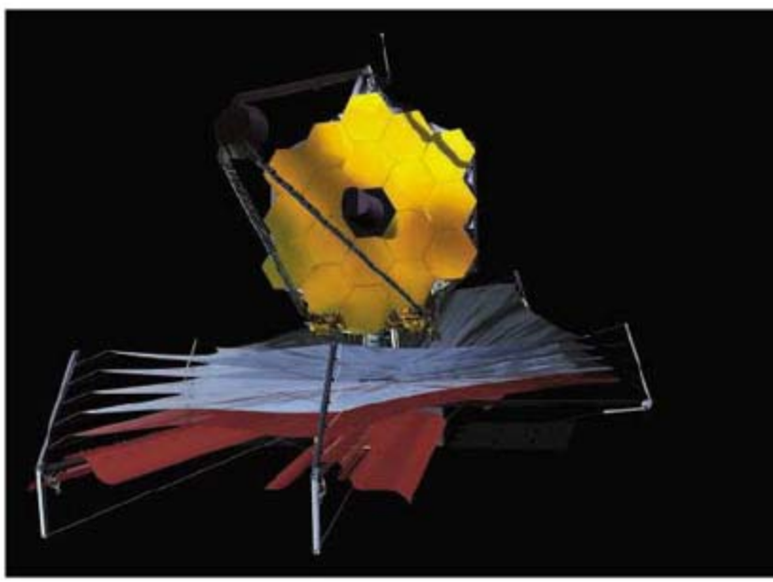

Next generation. The James Webb Space Telescope, scheduled for launch in 2013. It will have a 6.5-m hexagonal primary mirror with 18 beryllium segments that deploy after launch, and will occupy an orbit 1.5 million km from Earth.

CREDIT: NASA

The author is in the Astrophysics Science Division, Goddard Space Flight Center, NASA, Greenbelt, MD 20771, USA and the Science Mission Directorate, NASA Headquarters, Washington, DC 20546, USA. E-mail: John.C.Mather@nasa.gov

Infrared astronomy experienced a boom during this time, thanks to Nancy Boggess of NASA, and we owe her credit for four major projects: the Infrared Astronomical Observatory, COBE, the Spitzer Space Telescope, and the Stratospheric Observatory for Infrared Astronomy (SOFIA). To make a long story (*2*, *3*) short, the COBE spacecraft was launched in 1989, proved that the background radiation has a blackbody spectrum within 50 parts per million (ppm) and is therefore the remnant of the hot Big Bang, that it has anisotropies at 10 ppm presumably due to the quantum mechanics of the Big Bang, and that there is a cosmic infrared background radiation field twice as bright as expected. The COBE project opened the field of precision cosmology, which now offers new questions like: What is dark matter? What is dark energy? Was the evolution of the universe after the Big Bang simple or complex? The details may be detectable through their influence on the polarization of the background radiation, but the questions about dark matter and dark energy require different approaches (*4*).

After COBE, I worried that NASA might never again do anything so exciting, but in October 1995 Edward Weiler at NASA Headquarters asked me to work on the Next Generation Space Telescope, to follow the Hubble Space Telescope. This project is now named the James Webb Space Telescope (JWST), after the second NASA administrator, who persuaded Kennedy to start the Apollo program, and built up space science capabilities within NASA and universities. The JWST has reached technological maturity and is on its way to launch in 2013 (see the figure). The telescope will carry out infrared observations, from 0.6 to 29 μm, that even the mighty Hubble could not undertake. Most of this wavelength range cannot be observed from the ground, and the JWST will be far more sensitive than the Hubble and Spitzer telescopes that preceded it. The European Space Agency and Canadian Space Agency are contributing major components (*5*).

With the JWST, future observers might study the first objects to form after the Big Bang, the formation of galaxies like the Milky Way, the formation of stars and planets, and the development of planetary systems capable of supporting life. The JWST is built with unclassified technology, but without the national investment in detectors and space optics for military and surveillance purposes, the JWST could not be built. Swords are sometimes beaten into plowshares.

What does the future hold for science, and the world? One doesn't have to be a rocket scientist to know that science, engineering, and management are all required for the challenges of energy supply, environmental quality, and public health. Management of catastrophic events, from bridge collapse to wars, from volcanoes and earthquakes to tsunamis, storms, droughts, plagues, and killer rocks from the sky, is not out of range of human capability. If we can put a man on the Moon, why can't we do these other things? Technologically, we can, of course. Although there is no simple process for achieving worldwide consensus and taking worldwide action, nothing concentrates the mind like clear and impending doom. Perhaps climate change and energy supply will be the Sputnik for the next generation.

As to the long-term outcome, I'm cautiously optimistic. Kennedy challenged the United States to go to the Moon, not because it was easy, but because it was hard, and the nation responded. NASA's mission continues to expand the human sphere, both by observation and by travel, and I can imagine no discovery more fundamental than life on other planets, here in the solar system, or around some other star.

References

1. http://lambda.gsfc.nasa.gov/product/cobe/
2. J. Mather, J. Boslough, *The Very First Light* (Basic Books, New York, 1996).
3. http://nobelprize.org/nobel_prizes/physics/laureates/2006/index.html
4. *NASA's Beyond Einstein Program: An Architecture for Implementation* (National Research Council, Washington, DC, 2007).
5. www.jwst.nasa.gov/

10.1126/science.1148553

HISTORY OF SCIENCE

Sputnik and Satellite Astronomy

Giovanni F. Bignami

After Sputnik, European researchers emphasized basic research over politics and made important discoveries in space-based astronomy.

Few sounds have turned out to be more international than the "bip…bip" of the Sputnik satellite (*1*). Sputnik didn't speak Russian or English when it was launched in October 1957, yet it was clearly understandable and immediately popular. However, from the prestigious radio telescope at Jodrell Bank in the United Kingdom to amateur radio buffs in Turin, Italy, Sputnik's signals were regarded, at least in Europe, as a tribute more to science than to politics.

A generation of leading European physicists at the time, including Henk van de Hulst in the Netherlands, Giuseppe "Beppo" Occhialini in Italy, and Reimar Lust in Germany, immediately understood the science potential of space. Occhialini, for example, teamed up with an illustrious immigrant to the United States, Bruno Rossi, to start a space research program in Italy and Europe, the European Space Research Organization (ESRO), which later became the European Space Agency (ESA). Before Sputnik, the European school of physics had already been thinking about a unified particle physics laboratory (soon to become CERN) and now they turned their attention to space.

The author is at the Istituto Universitario di Studi Superiori, 27100 Pavia, Italy. E-mail: gfb@lambrate.inaf.it

NASA was coming together in the United States at about the same time. There was, however, a fundamental difference. NASA had been created from the start to counter not only Sputnik but also Laika the dog (1957) and Gagarin the man (1961). Europe was not under the same kind of pressure and could afford the luxury of creating ESRO in 1962, entirely dedicated to science. The European space science program lives on today as the sole mandatory part of ESA (created in 1975) and is a direct legacy of the reaction to Sputnik of those physicist "founding fathers."

When space astronomy started in the 1960s, the first goal was to search for high-energy photons invisible on the ground because they were being absorbed by our atmosphere. These x-rays carry information about truly fundamental processes in celestial objects, including the life and death cycles of stars. Enrico Fermi's Italian school of physics deserves credit for helping invent the technology for building telescopes to gather high-energy photons in space. Three graduates of this school, Rossi at MIT, and Giuseppe Vaiana and Riccardo Giacconi at Harvard, led groups that conceived and constructed x-ray detectors and telescopes later flown in space by NASA.

Astronomy with x-rays thus joined radio

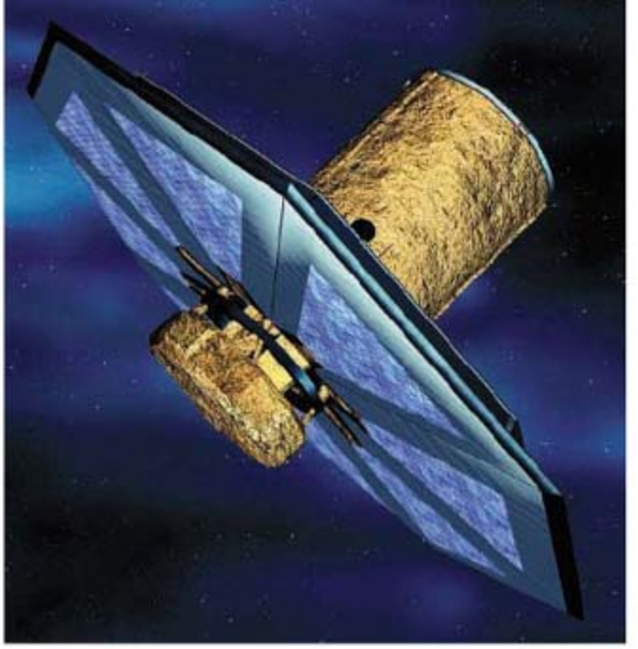

Other worlds. The proposed Darwin mission is a group of four satellites that will search for Earth-like planets and analyze their atmospheres for chemical signatures of life.

astronomy and moved us into an era of observing the invisible. Out of proportion with its modest budget, ESA's many missions have contributed to discoveries that poured in over the decades as detectors covering the full wavelength spectrum were launched from different continents. X-rays, for example, helped us understand the mechanisms of the solar corona. Stars, young and old, sometimes shine much brighter in x-rays than in the optical spectrum, and x-ray detectors provided a new look at their evolution and death. X-rays have shown us how stars collapse when they die and leave behind cores of a new state of matter, such as neutron stars. More important, x-rays from space gave the first evidence for black holes, objects so dense that not even light can escape them. Giacconi shared a Nobel prize for physics in 2002 for these and other discoveries.

Gamma-ray astronomy, another science of the invisible, has shown us objects emitting radiation that, on Earth, is produced only by radioactivity and particle accelerators. ESA's first mission, COS-B (1975), for example, showed the reality of "gamma-ray stars," that is, neutron stars that are only visible in gamma-rays (*2*).

Gamma-rays were also the protagonists of a unique success story in space science. During the Cold War, gamma detectors were launched to ferret out covert nuclear tests. Sure enough, the Vela spy satellites (a "secret" code name from the Spanish "velar," to monitor) launched by the United States detected suspicious bursts of gamma-rays. However, they came from the sky and not from the USSR (*3*), as was first disclosed at a 1973 conference where Soviet scientists admitted observing something similar. Gamma-ray bursts represented one of the top astronomical enigmas for a quarter of a century until the Italian/Dutch satellite BeppoSax (*4*), launched 10 years ago, showed that the bursts originated from enormous explosions in galaxies at cosmological distances, when galaxies were being born into a young Universe.

No one had observed stars being born before the development of satellite-based infrared astronomy, which yielded the first images of star "nurseries." These are "warm" (by interstellar standards, actually –200°C) dust cocoons, collapsing to form tens of new baby stars. Space infrared telescopes, such as ESA's Infrared Space Observatory (*5*), have also shown that water is abundant wherever stars are conceived and, in general, that water is everywhere in the sky. Water, we have learned, is the second most abundant molecule, after hydrogen, in the Universe. Think of it when you go swimming: You are floating in molecules that had probably been around for some time before raining on the newly formed Earth.

Where should we look in the next half-century? Europe has set for itself a long-term "Cosmic Vision" (*6*) to carry space science to 2025. Alas, we have discovered, like everyone else has, that choosing is hard. We want to study gravitational waves and we want to understand dark energy; we want to travel to Mars and we want to explore Jupiter. We need large interferometric telescopes in space to discover new planets (see the figure) and we need large orbiting collectors to catch more photons. To make a "concord out of this discord" is the challenge being faced by the new generation of European researchers.

References and Notes

1. Sounds of Sputnik are available at www.amsat.org/amsat/features/sounds/firstsat.html.
2. www.esa.int/esaSC/120375_index_0_m.html
3. R. Klebesadel *et al.*, *Astrophys. J.* **182**, L85 (1973).
4. www.asdc.asi.it/bepposax/
5. http://isowww.estec.esa.nl/
6. http://sci.esa.int/science-e/www/area/index.cfm?fareaid=100

10.1126/science.1149322

EVOLUTION

Feathers, Females, and Fathers

Sex linkage of genes involved in adaptation and speciation extends to birds, explaining why females prefer males of their own species.

Michael G. Ritchie

Alfred Wallace, Darwin's contemporary and rival, argued that when species hybridize, natural selection favors individuals who are more fussy about whom they mate with, which therefore increases female discrimination of males from different species (*1*). Modern evolutionary genetics has questioned the importance of the "Wallace effect" (also known as "reinforcement") because genetic recombination between female discrimination and male trait genes would scramble combinations of loci that favor speciation. Several solutions to this have been proposed, including close genetic linkage of such loci. A simpler possibility is sexual imprinting, which causes a female to prefer males that resemble her father. A study of flycatchers by Sæther *et al.* on page 95 of this issue (*2*) has taken advantage of natural hybridization that occurs between species of this bird, and demonstrates that female preference for father-like males is due to sex linkage of genes for female preferences rather than to sexual imprinting. The linkage of genes that influence speciation to sex chromosomes may turn out to be a common influence on the origin of species.

The evolutionary biologist J. Felsenstein (*3*) famously argued that because of genetic recombination, there might be fewer species of animals than we expect. In other words, if sexual species hybridize, recombination jumbles up their genes such that independent sets of loci coding for hybrid unfitness, male sexual traits, and female preferences are unlikely to crystallize out into new species. Exceptions may occur if the genes are all tightly genetically linked on one chromosome. Felsenstein also recognized that a "single-allele" solution could facilitate speciation. In this case, allelic replacement at one locus simultaneously causes selective mating between individuals

The author is at the University of St. Andrews, Fife KY16 9AJ, UK. E-mail: mgr@st-andrews.ac.uk

CREDIT: EUROPEAN SPACE AGENCY

that are genetically related or have similar characteristics (known as assortative mating), but it was difficult to imagine the mechanism for this. Sexual imprinting is one possibility (*4*, *5*); if a gene makes a female prefer males that are like her father, then the same allele could increase assortative mating between populations. It has been proposed that sexual imprinting may be involved in rapid speciation in the face of gene flow in birds (*6*) and fish, including the dramatic radiations of African cichlids (*7*).

Unlike most animals, female birds are the heterogametic sex, having the equivalent of a human Y chromosome, called the W chromosome (so females are ZW, males ZZ). Collared and pied flycatchers meet and occasionally hybridize along a contact zone in central and northern Europe. Hybrid females are sterile but hybrid males are fertile, an example of "Haldane's rule" in that the heterogametic sex (having two different sex chromosomes) shows greater dysfunction. It also indicates that fertility dysfunction probably involves genes on the sex chromosomes. In these hybrid zones of contact, male sexual plumage differences are accentuated and hybridization levels reduced, providing evidence that the Wallace effect has occurred (*8*). What accounts for this? Female sexual imprinting on paternal traits such as plumage differences, or genetic linkage between preference and trait loci?

Only up to 5% of mating pairs of flycatchers in the hybrid zone are between species, but Sæther *et al*. realized that the resulting offspring offered an excellent opportunity to test the mechanism underlying the inheritance of mate preferences. If preference genes are autosomal, hybrid females should have intermediate preferences, but if the preferences depend on the father, then hybrid females should prefer males that are like their father. This was unambiguously the case: Only 4 of 31 hybrid females mated with a male other than their paternal type (and hybrid males mated randomly). This pattern is consistent with Z linkage of mate preference loci (females receive their single Z chromosome from their father, whereas males get a copy from each parent), but it is also consistent with paternal sexual imprinting in females. Very neatly, Sæther *et al*. disentangled Z linkage and imprinting by examining the choice of females that had been cross-fostered. Offspring sometimes result from extra-pair copulations (females mating with males of another species, or heterospecific males), leading to females that are reared by heterospecific males. The authors also successfully cross-fostered some chicks between parents of either species. As adults, these females mated with males of their own species even if they had been reared by heterospecific males, ruling out sexual imprinting. Although sample sizes were understandably low (Sæther *et al*. must have been particularly anxious when awaiting the return of migratory females the season after the cross-fostering), the results strongly support Z linkage. There are perhaps alternative explanations (such as genomic imprinting, in which gene expression is influenced by which parent the allele comes from), but they seem much less likely.

CREDIT: JOHAN TRÄFF

Father-like traits preferred. A male collared flycatcher feeds its chicks. Collared and pied flycatchers occasionally hybridize in central and northern Europe. Females develop a sexual preference for males of their own species as a result of sex-linked genes, not sexual imprinting.

It has been argued that sexual imprinting is a widespread phenomenon that can increase speciation rates (*6*, *9*), particularly by reinforcement (*10*). However, some models give only ambiguous support for this (*11*, *12*), and another empirical study failed to demonstrate any role in speciation (*5*). Genetic linkage may be more straightforward (*13*). Previous studies of flycatchers implied that the Z chromosome also carries loci that influence male plumage and hybrid unfitness (*14*); therefore, all these loci will have reduced genetic recombination, facilitating the Wallace effect. Linkage may be a more common factor to promote this than "single-allele" solutions. One potential case of a single-allele system has recently been described in the fruit fly *Drosophila melanogaster* (*15*), but the locus is unidentified and very tight linkage cannot be unambiguously discounted. A series of hybridization studies in a variety of organisms suggest that chromosomal rearrangements such as inversions may be another means of reducing genetic recombination between favored gene arrangements (*16*). The fact that traits involved in sexual isolation (male traits and female preferences) are sex-limited may mean that sex linkage of loci is favored, as gene expression must be influenced by the sex chromosomes. Lepidoptera, the other major animal group in which females are heterogametic, are particularly likely to show sex linkage of genes involved in adaptation and speciation (*17*), so it is very interesting that Sæther *et al*. suggest that this phenomenon extends to birds.

More studies with the experimental ingenuity of Sæther *et al*. will be required to test whether this is a general phenomenon, but an intriguing hypothesis is that female heterogamety and strong sex linkage might mean that the Wallace effect is more common in birds and butterflies than in other groups.

References

1. A. R. Wallace, *Darwinism* (Macmillan, London, 1889).
2. S. A. Sæther *et al.*, *Science* **318**, 95 (2007).
3. J. Felsenstein, *Evolution* **35**, 124 (1981).
4. M. R. Servedio, M. A. F. Noor, *Annu. Rev. Ecol. Evol. Syst.* **34**, 339 (2003).
5. A. Y. K. Albert, *Evolution* **59**, 927 (2005).
6. D. E. Irwin, T. Price, *Heredity* **82**, 347 (1999).
7. M. N. Verzijden, C. ten Cate, *Biol. Lett.* **3**, 134 (2007).
8. G.-P. Sætre *et al.*, *Nature* **387**, 589 (1997).
9. I. P. F. Owens, C. Rowe, A. L. R. Thomas, *Trends Ecol. Evol.* **14**, 131 (1999).
10. M. R. Servedio, S. A. Sæther, G.-P. Sætre, *Evol. Ecol.*, 10.1007/s10682-007-9188-2 (2007).
11. M. N. Verzijden, R. F. Lachlan, M. R. Servedio, *Evolution* **59**, 2097 (2005).
12. K. Aoki, M. W. Feldman, B. Kerr, *Evolution* **55**, 25 (2001).
13. D. W. Hall, M. Kirkpatrick, *Evolution* **60**, 908 (2006).
14. G.-P. Sætre *et al.*, *Proc. R. Soc. London Ser. B* **270**, 53 (2003).
15. D. Ortiz-Barrientos, M. A. F. Noor, *Science* **310**, 1467 (2005).
16. L. H. Rieseberg, *Trends Ecol. Evol.* **16**, 351 (2001).
17. M. G. Ritchie, S. D. F. Phillips, in *Endless Forms: Species and Speciation*, D. A. Howard, S. Berlocher, Eds. (Oxford Univ. Press, Oxford, 1998), pp. 291–308.

10.1126/science.1149597

MEDICINE

Testing Hypotheses About Autism

A challenging, but potentially fruitful approach to evaluate proposed candidate genes for autism is to study analogous behaviors in mouse models.

Jacqueline N. Crawley

The Beatles' insight, that something in the way you move attracts me like no other, aptly describes how neurons connect with each other. Specific forms of cell adhesion molecules expressed in neuronal processes—a neurexin in axons and a neuroligin in dendrites—attract and bind in mid-synaptic space with exquisite selectivity (*1*, *2*). The resulting synaptic connections regulate excitatory and inhibitory transmission of information in neural circuits (see the figure). On page 71 of this issue, Tabuchi *et al.* (*3*) report that mice with a mutation in neuroligin-3 display increased activity of inhibitory synapses in the brain. This specific mutation was identified previously in the genomes of two brothers with autism (*4*), raising interest in the role of neurexin-neuroligin complexes in autism spectrum disorders.

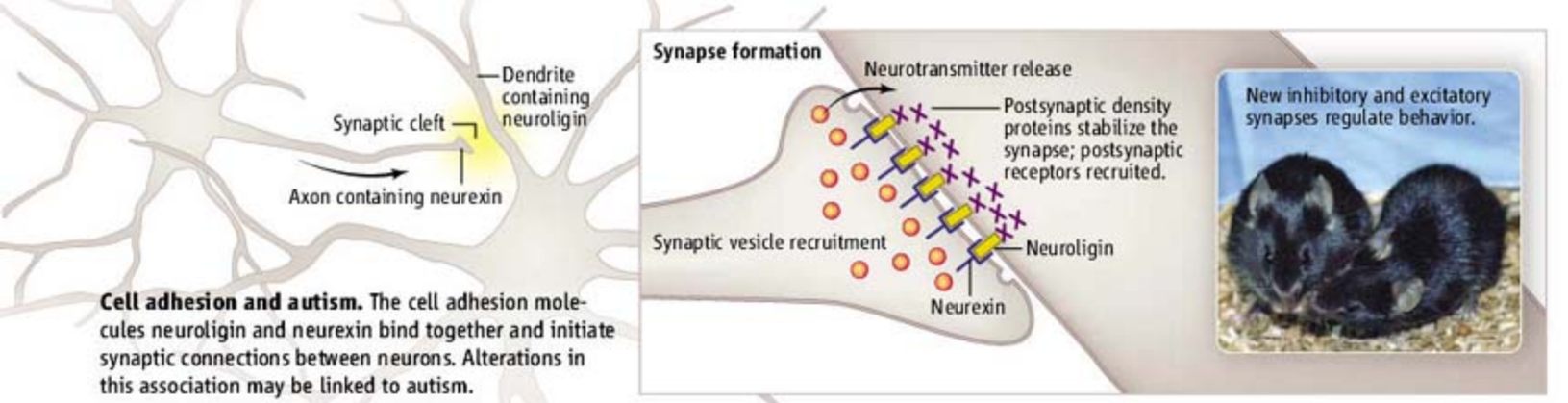

Cell adhesion and autism. The cell adhesion molecules neuroligin and neurexin bind together and initiate synaptic connections between neurons. Alterations in this association may be linked to autism.

The search is on for genes that underlie autism, a neurodevelopmental disorder of unknown cause that is diagnosed by abnormal social interactions, impaired communication, and repetitive behavior (*5*). Concordance for autism spectrum disorders reaches >90% for identical twins, compared to <10% for fraternal twins and siblings (*6*, *7*), indicating a strong genetic component. Like the mutation studied by Tabuchi *et al.*—R451C, in which arginine at position 451 in neuroligin-3 is substituted with cysteine—many genetic polymorphisms have been associated with autism, but each was found in only a few individuals, and seldom replicated across studies (*6*, *7*). No ubiquitous single-gene mutation linked to the disorder has yet been detected. Because multiple genes, each accounting for a small percentage of the variance, typify many neuropsychiatric disorders (*8*), focus is now shifting to alternate genetic strategies to reveal the genetic basis for autism (*7*). The true significance of so many unreplicated candidate genes for autism remains a fascinating conundrum. A logical working hypothesis is that many factors can disrupt developing brain pathways necessary for sociability, interactive communication, and flexible executive function (*9*).

Targeted mutations in mice offer a rational strategy to systematically test hypotheses about each candidate gene for autism. If the mutation results in a phenotype analogous to the symptoms of autism, then that gene may play a critical role. Because no biochemical or neuroanatomical markers for autism are known, the mouse phenotype is defined by behavioral criteria relevant to the three diagnostic symptoms of autism.

Why is it hard to develop good mouse models of autism, and why are model animals essential? The challenge is to design mouse behavioral tasks with sufficient analogies to the three diagnostic symptoms. Fortunately, mice are a social species, with high levels of social interaction. Behavioral neuroscientists are generating useful assays for autism-like social and communication deficits, and for motor stereotypies, repetitive behaviors, and perseverative habits (*10*–*19*). A caveat is the apparent circular logic in modeling symptoms (face validity) without knowing causes (construct validity). In fact, perfecting animal models as mechanistic hypotheses emerge, while investigating proposed genetic, biochemical, and environmental factors in model organisms, is a common iterative process at early stages of understanding a human disease. Altered neuronal connectivity and larger brain volume at early ages in autism (*20*) suggest exploring genes that control programmed cell death and/or dendritic pruning in rodent models. Poor attentional disengagement at very young ages, detected in the Baby Siblings project (*21*), may implicate inhibitory neurophysiological mechanisms similar to those described by the Sudhof team (*3*). Ultimately, robust mouse models provide translational tools for developing effective treatments.

Neuroligin-3 R451C mice displayed deficits in some, but not all, of the social tasks assessed by the authors, and not on the conventional parameters. These mice also showed faster acquisition and reversal in some components of a spatial learning and memory task, a finding counterintuitive to the resistance to change in routine that is a hallmark of autism. The authors are in good company. Mice with mutations in various candidate genes for autism, and proposed inbred strain models, display behavioral abnormalities relevant to only one or two diagnostic symptoms of autism, and some show confounding physical dysfunctions (*11*–*17*). Currently, only one strain, BTBR, appears to model all three symptoms without confounding abnormalities (*18*, *19*).

Faster learning of the Morris water maze by R451C mice is remarkable. The R451C mutation increased the frequency of inhibitory synaptic events in mouse brain structures without changing the total number of inhibitory synapses. It is intriguing to speculate how more inhibitory neurotransmission during early development could improve cognitive performance. As the authors state, cases

The author is in the Intramural Research Program, National Institute of Mental Health, Bethesda, MD 20892–3730, USA. E-mail: crawleyj@intra.nimh.nih.gov

CREDITS: PHOTO, VALERIE BOLIVAR/WADSWORTH CENTER, ALBANY, NY; P. HUEY/*SCIENCE*

of savant abilities are associated with autism, but exceedingly rarely, and not in the two brothers with the R451C polymorphism (*4*). Cognitive researchers may want to explore the appealing notion that alterations in neurexin-neuroligin complexes shift the balance of excitatory and inhibitory synapses to enhance learning and memory.

References

1. A. A. Chubykin *et al.*, *Neuron* **54**, 191 (2007).
2. H. Taniguchi *et al.*, *J. Neurosci.* **27**, 2815. (2007).
3. K. Tabuchi *et al.*, *Science* **318**, 71 (2007); published online 6 September 2007 (10.1126/science.1146221).
4. S. Jamain *et al.*, *Nat. Genet.* **34**, 27 (2003).
5. F. Volkmar, C. Lord, A. Bailey, R. T. Schultz, A. Klin, *J. Child Psychol. Psychiatry* **45**, 135 (2004).
6. D. H. Geschwind, P. Levitt, *Curr. Opin. Neurobiol.***17**, 103 (2007).
7. X. Zhao *et al.*, *Proc. Natl. Acad. Sci. U.S.A.* **104**, 12831 (2007).
8. K. S. Kendler, R. J. Greenspan, *Am. J. Psychiatry* **163**, 1683 (2006).
9. A. M. Persico, T. Bourgeron, *Trends. Neurosci.* **29**, 349 (2006).
10. T. R. Insel, *Mamm. Genome*, **12**, 755 (2001).
11. L. J. Young, L. J. Pitkow, J. N. Ferguson, *Mol. Psychiatry* **7**, S38 (2002).
12. P. Levitt *Epilepsia* **46** (suppl. 7), 22 (2005).
13. C. M. Spencer *et al.*, *Genes Brain Behav.* **4**, 420 (2005).
14. M. Cheh *et al.*, *Brain Res.* **1116**, 166 (2006).
15. C. H. Kwon *et al.*, *Neuron* **4**, 377 (2006).
16. J. B. Panksepp, G. P. Lahvis, *Genes Brain Behav.* 10.1111/j.1601-183X.2006.00295.x (2006).
17. E. S. Brodkin, *Behav. Brain Res.* **176**, 53 (2007).
18. S. S. Moy *et al.*, *Behav Brain Res.* **176**, 4 (2007).
19. H. G. McFarlane *et al.*, *Genes Brain Behav.* 10.1111/j.1601-183X.2007.00330.x (2007).
20. H. C. Hazlett *et al.*, *Biol. Psychiatry* **59**, 1 (2006).
21. L. Zwaigenbaum *et al.*, *Int. J. Dev. Neurosci.* **23**, 143 (2005).

10.1126/science.1149801

BIOPHYSICS

Going with the Flow

A growing synergy between rheology and biophysics is yielding insights into the flow properties of polymers and biomolecules.

Ronald G. Larson

The field of rheology—the study of the deformation and flow of polymers, colloids, or emulsions—long had to content itself with macroscopic experiments, because the microstructures that produce the rheological response were beyond the reach of experimental tools. But now, new tools borrowed from biophysics allow these microscopic substructures to be probed directly, as illustrated by a recent use of optical tweezers to study the dynamics of entangled polymers (*1*). Another recent study exemplifies borrowing in the reverse direction: the use of a microrheological tool to study the actin filament network of a cell (*2*). These examples are just a small sampling of a growing synergy between rheology and biophysics that is yielding deeper understanding of the dynamics of biopolymers such as DNA and actin filaments and of conventional synthetic polymers such as polyethylene.

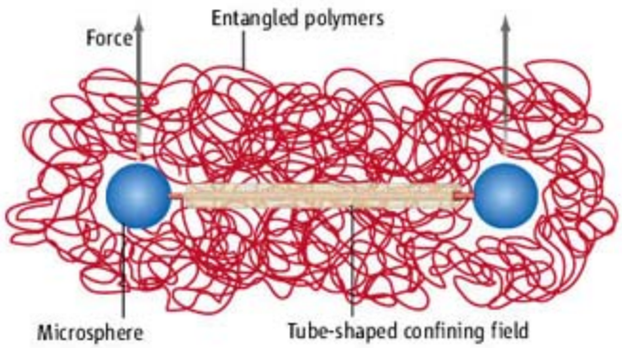

An insider view of entanglement. In (*9*), a probe DNA molecule was held stretched by two optically trapped microspheres in a solution of other DNA molecules. The confining tube potential (orange region) was explored by displacing the spheres perpendicular to the probe chain and measuring the resulting forces.

Since the mid-1990s, long double-stranded DNA molecules have been widely used to study the flow properties of polymers (*3*, *4*). Stained by intercalating dyes, double-stranded DNA molecules were visualized as they deformed, tumbled, stretched, and relaxed as a result of flow, yielding a thorough basis for understanding the flow behavior of dilute polymers (*5*–*8*).

However, dilute polymer solutions, in which the polymer molecules do not overlap, are rare in practical applications. Far more important are the higher-concentration regimes in which polymer molecules overlap and entangle with each other, as occurs, for example, when molten polyethylene is blown into plastic film or when silk solutions are spun by spiders into a thread.

Since the seminal work of de Gennes (*9*) and Doi and Edwards (*10*), theories for the rheology of densely entangled polymers have relied on the tube model. In this model, each polymer molecule is confined by entanglements with its neighboring molecules to a tubelike region that roughly follows the contorted, random-walk contour of the polymer molecule. Polymer motion is preferentially directed along this tube rather than perpendicular to it, with dramatic consequences for polymer dynamics and rheology. The tube model has remained largely phenomenological, with the properties of the confining tube determined only indirectly through observation of polymer motion and rheological properties. However, this may now be changing.

In a recent study, Robertson and Smith (*1*) attached small beads, which served as handles for optical traps, to both ends of a single long probe DNA molecule, which they mixed with a densely entangling solution of other, similar, DNA molecules (see the first figure). By stretching the probe molecule to nearly full extension using the traps and allowing surrounding molecules to relax, they created a straightened version of the tube. When both optical traps were displaced by the same

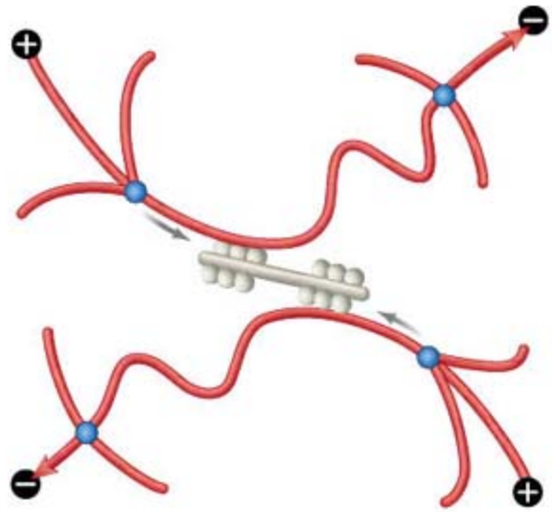

Motor-driven fluctuations. In (*12*), actin filaments (red) were pulled by ATP-powered myosin motors (gray) in the direction of the arrows. The resulting tensile forces are marked with (+); contractile forces are marked with (–). The cross-links (blue) link the mobile actin chains into a soft-solid network.

The author is in the Department of Chemical Engineering, University of Michigan, Ann Arbor, MI 48109, USA. E-mail: rlarson@umich.edu

CREDITS: (TOP) ADAPTED FROM (1); (BOTTOM) ADAPTED FROM (2)

amount perpendicular to the tube axis, the probe molecule was pressed into the entangling chains forming the "wall" of the tube (see the first figure).

By monitoring the slight deflections of the bead handles from the centers of their optical traps, the authors measured the forces exerted on the beads and hence on the probe molecule. The results indicate that the tube diameter slowly grows with time, as suggested by recent molecular dynamics simulations (*11*). Discoveries such as this are leading to a more refined understanding of entanglement interactions and should stimulate development of quantitative theories of entangled polymer dynamics and rheology.

While rheology has benefited from methods and tools borrowed from biophysical studies, microrheology tools developed for miniaturized rheological studies are used increasingly in biophysics. In conventional rheology, millimeter- or centimeter-size plates, cylinders, and other geometries are used to apply deformations and measure stress. In passive microrheology, these are replaced by thermal agitation, which spontaneously generates stress locally, with nanometer-scale deformation monitored by dynamic light scattering (*12*) or by laser interferometry (*2*). In active microrheology, optical traps are used to apply oscillatory forces onto probe particles, whose displacements then allow the frequency-dependent viscoelasticity of the micrometer-scale environment to be probed (*2*).

Originally applied to colloids, polymer solutions, and emulsions (*12*), versions of microrheology that use optical or atomic force microscopy are becoming prime tools for analyzing rheological behavior at the cellular and subcellular level in biology (*13*). For example, Mizuno *et al.* (*2*) recently used both active and passive microrheology to study networks of actin filaments interacting with myosin motors (see the second figure). At thermodynamic equilibrium, the frequency-dependent responses of active and passive methods were the same. However, in the presence of an energy source [in this case, adenosine 5′-triphosphate (ATP)], the active and passive methods yielded very different results at low frequency because of large nonequilibrium fluctuations driven by ATP hydrolysis. The motor-driven fluctuations also stiffened the actin network by a factor of 100. This finding may be of biological importance, because such networks form the "skeleton" of the cell, whose stiffness can be modulated through myosin motor activity, as demonstrated for a range of cells including stem cells (*14*).

Tools closely related to microrheology are likely to be used increasingly to manipulate single molecules of DNA and of the proteins that wrap, cleave, repair, unwind, copy, and transcribe the DNA (*15*, *16*). Likewise, new tools developed for studies of biopolymers and colloidal forces in the cell are likely to be applicable to a wide range of nonbiological fluids. Thus, the fruitful exchange of experimental and theoretical methods between the fields of biophysics and rheology is likely to continue.

References

1. R. M. Robertson, D. E. Smith, *Phys. Rev. Lett.* **99**, 126001 (2007).
2. D. Mizuno, C. Tardin, C. F. Schmidt, F. C. MacKintosh, *Science* **315**, 370 (2007).
3. T. T. Perkins, D. E. Smith, S. Chu, *Science* **276**, 2016 (1997).
4. C. Bustamante, J. F. Marko, E. D. Siggia, S. Smith, *Science* **265**, 1599 (1994).
5. E. S. G. Shaqfeh, *J. Non-Newt. Fluid Mech.* **130**, 1 (2005).
6. C. M. Schroeder, H. P. Babcock, E. S. G. Shaqfeh, S. Chu, *Science* **301**, 1515 (2003).
7. Y. L. Chen, M. D. Graham, J. J. de Pablo, K. Jo, D. C. Schwartz, *Macromolecules* **38**, 6680 (2005).
8. L. Fang, H. Hu, R. G. Larson, *J. Rheol.* **49**, 127 (2005).
9. P. G. de Gennes, *J. Chem. Phys.* **55**, 572 (1971).
10. M. Doi, S. F. Edwards, *Faraday Trans. II.* **74**, 1789 (1978).
11. Q. Zhou, R. G. Larson, *Macromolecules* **39**, 6737 (2006).
12. T. G. Mason, D. A. Weitz, *Phys. Rev. Lett.* **74**, 1250 (1995).
13. D. Weihs, T. G. Mason, M. A. Teitell, *Biophys. J.* **91**, 4296 (2006).
14. A. J. Engler, S. Sen, H. L. Sweeney, D. E. Discher, *Cell* **126**, 677 (2006).
15. N. R. Forde *et al.*, *Proc. Natl. Acad. Sci. U.S.A.* **99**, 11682 (2002).
16. P. C. Blainey, A. M. van Oijen, A. Banerjee, G. L. Verdine, X. S. Xie, *Proc. Natl. Acad. Sci. U.S.A.* **103**, 5752 (2006).

10.1126/science.1142441

MATERIALS SCIENCE

There's Room in the Middle

Dense inorganic-organic hybrid materials offer opportunities for creating unusual properties or combinations of properties.

Anthony K. Cheetham and C. N. R. Rao

Condensed matter researchers have traditionally focused either on inorganic materials or on organic and bio-materials. Much less effort has been devoted to hybrid materials that contain both inorganic and organic components. This has changed in the past decade with the discovery of crystalline hybrid materials—called metal-organic frameworks or MOFs—that contain cavities and channels akin to those found in zeolites. Other recent discoveries include hybrid framework structures that are dense rather than porous, and systems that are more similar to classical inorganic materials.

A. K. Cheetham is in the Department of Materials Science and Metallurgy, University of Cambridge, Cambridge CB2 3QZ, UK. C. N. R. Rao is at the Jawaharlal Nehru Centre for Advanced Scientific Research, Jakkur P.O., Bangalore 560 064, India. E-mail: akc30@cam.ac.uk; cnrrao@jncasr.ac.in

Hoskins and Robson were among the first to combine molecular inorganic and organic building blocks to create open networks. The resulting topologies were often analogous to known inorganic structures such as diamond (*1*). Many other highly porous MOFs have since been synthesized (*2*, *3*). The properties of porous hybrid frameworks often resemble those of classical zeolites; for example, they can absorb gases and allow shape-selective catalysis. However, hybrid frameworks offer a wider range of structures and properties. For example, they can display chirally selective heterogeneous catalysis (*4*). Their electronic properties have also attracted attention (*5*).

Yet, apart from porous hybrid frameworks, the field has other opportunities to offer. Two aspects of the enormous structural diversity of hybrid framework materials deserve greater emphasis.

First, an increasing number of hybrids are being discovered in which the inorganic structural elements form an infinite array in one, two, or three directions (see the figure, top panel) (*6*–*9*). (In contrast, in MOFs, isolated metal ions or clusters are connected via organic linkers.) Infinite inorganic connectivity—for example, metal-oxygen-metal—provides the structural basis for many key physical properties of inorganic materials, such as ferromagnetism, metallic conductivity, and even superconductivity. These properties are thus likely to be found in hybrids of the kind shown in the top panel of the figure. Furthermore, they may be found in combination with other properties that result from the presence of the organic components.

Second, given that the overwhelming majority of functional inorganic materials adopt dense structures, greater attention

should also be paid to dense hybrids. Dense hybrid systems can be much more thermally stable than their porous or molecular analogs, especially when they do not contain water and are thus not prone to dehydration. For example, the dense alkaline earth tartrate (see the figure, bottom panel) is stable to ~400°C in air (*10*), sufficiently robust for most applications.

Hybrids with dense or extended inorganic framework structures can exhibit a wide range of physical properties. The first example is iron(III) gallate (see the figure, top panel). Its structure comprises parallel chains of corner-sharing FeO_6 octahedra, which are cross-linked by the gallate linkers. There is no significant porosity, but the extended inorganic connectivity along the chains of octahedra leads to antiferromagnetic coupling, with an ordering temperature of 43 K in the cobalt analog of this phase. In the iron(III) phase, there is strong charge transfer from the gallate ion to iron, leading to a deep blue color. This unusual material has been used since Roman times as a dye and pigment in cosmetics and printing, but only recently have the origins of its properties been understood (*8*, *9*).

Examples of magnetically ordered hybrids are now quite common among both MOFs and extended inorganic systems, but most of these materials order at very low temperatures. Jain *et al.*, however, recently described a nickel tetracyanoethylene hybrid and related compounds that order ferromagnetically well above room temperature (*11*). The perovskite-like hybrid material $[(CH_3)_2NH_2]Ni(HCOO)_3$ (see the figure, middle panel) orders ferromagnetically at about 36 K, with magnetic exchange interactions that are mediated by formate bridges (*12*). There are also examples of ferroelectric hybrid framework compounds, including a three-dimensional cadmium coordination polymer, based on a chiral proline ligand, that exhibits a saturated spontaneous polarization higher than that in the classical ferroelectric, Rochelle's salt (potassium sodium tartrate) (*13*).

Hybrids with interesting optical properties are also beginning to attract attention, especially rare earth– and alkaline earth–containing photoluminescent materials that might be used as phosphors or sensors. Now that the synthetic procedures for forming anhydrous framework materials are better understood as a result of systematic studies as a function of temperature and composition (*6*), there is a much higher probability that phases with sufficient stability to be used as commercial phosphors (that is, up to 200°C in air) might be found.

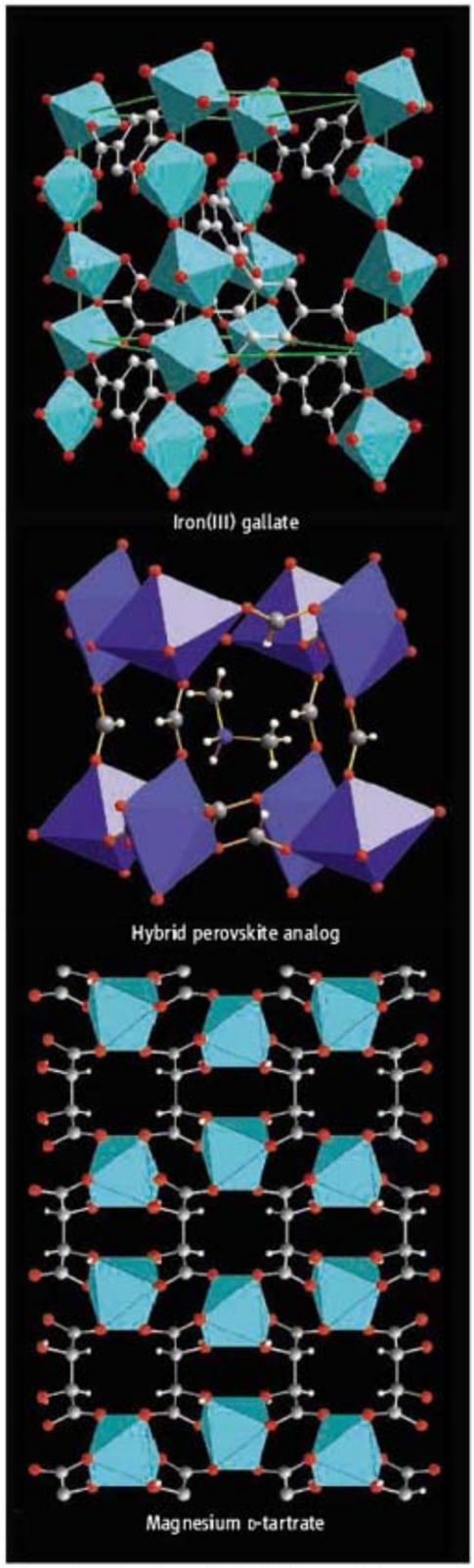

Examples of dense hybrid inorganic-organic framework structures. (Top) In iron(III) gallate, parallel chains of corner-sharing FeO_6 octahedra (in light blue) are cross-linked by organic ligands. The deep blue material has been used as a dye since Roman times. **(Middle)** This hybrid analog of the ubiquitous perovskite structure orders ferromagnetically. NiO_6 octahedra are shown in dark blue. **(Bottom)** The dense hybrid magnesium D-tartrate is stable in air to 400°C. MgO_6 octahedra are shown in blue.

Furthermore, in the case where the anhydrous materials are homochiral, as in some alkaline earth tartrates (see the figure, bottom panel) (*10*), it may be possible to achieve polarized light conversion.

In contrast to the magnetic and optical properties of hybrids, metallic and semiconducting behavior has been elusive, possibly because it has proven relatively difficult to introduce mixed valence into these systems. However, high conductivity (50 Scm^{-1} at 300 K, greater than that of most conducting polymers) has been observed in a Cu(I) coordination polymer containing an electron-accepting tetraazanaphthacene ligand (*14*), similar to some organic molecules found in conducting polymers. It may thus be possible to exploit the redox behavior of not only the metal ions but also the organic ligands.

Several aspects of hybrid framework materials have not yet been explored. Their mechanical properties could be of great utility, potentially offering hardness in some directions and softness in others. There has also been very little effort toward making nanoparticles of hybrids, although these could exhibit unique properties, as has been found for certain inorganic nanoparticles.

It may also be possible to make hybrids with properties that are rare in purely organic or inorganic systems. Future targets in this direction should include multiferroic behavior, such as the combination of ferroelectricity and ferromagnetism. This might be feasible, for example, in the hybrid perovskites described above. To adapt a famous quotation by Richard Feynman, there can be no doubt that "there is plenty of room in the middle."

References

1. B. F. Hoskins, R. Robson, *J. Am. Chem. Soc.* **112**, 1546 (1990).
2. H. Li, M. Eddaoudi, M. O'Keeffe, O. M. Yaghi, *Nature* **402**, 276 (1999).
3. G. Férey *et al.*, *Science* **309**, 2040 (2005).
4. J. S. Seo *et al.*, *Nature* **404**, 982 (2000).
5. G. J. Halder *et al.*, *Science* **298**, 1762 (2002).
6. A. K. Cheetham, C. N. R. Rao, R. K. Feller, *Chem. Commun.* **2006**, 4780 (2006).
7. C. N. R. Rao, S. Natarajan, R. Vaidhyanathan, *Angew. Chem. Int. Ed.* **43**, 1466 (2004).
8. C.-H. Wunderlich, R. Weber, G. Bergerhoff, *Z. Anorg. Allg. Chem.* **599**, 371 (1991).
9. R. K. Feller, A. K. Cheetham, *Solid State Sci.* **8**, 1121 (2006).
10. K. C. Kam, K. L. M. Young, A. K. Cheetham, *Cryst. Growth Des.* **7**, 1522 (2007).
11. R. Jain *et al.*, *Nature* **445**, 291 (2007).
12. X.-Y. Wang, L. Gan, S.-W. Zhang, S. Gao, *Inorg. Chem.* **43**, 4615 (2004).
13. Q. Ye *et al.*, *J. Am. Chem. Soc.* **128**, 6554 (2006).
14. M. Tadokoro *et al.*, *Angew. Chem. Int. Ed.* **45**, 5144 (2006).

10.1126/science.1147231

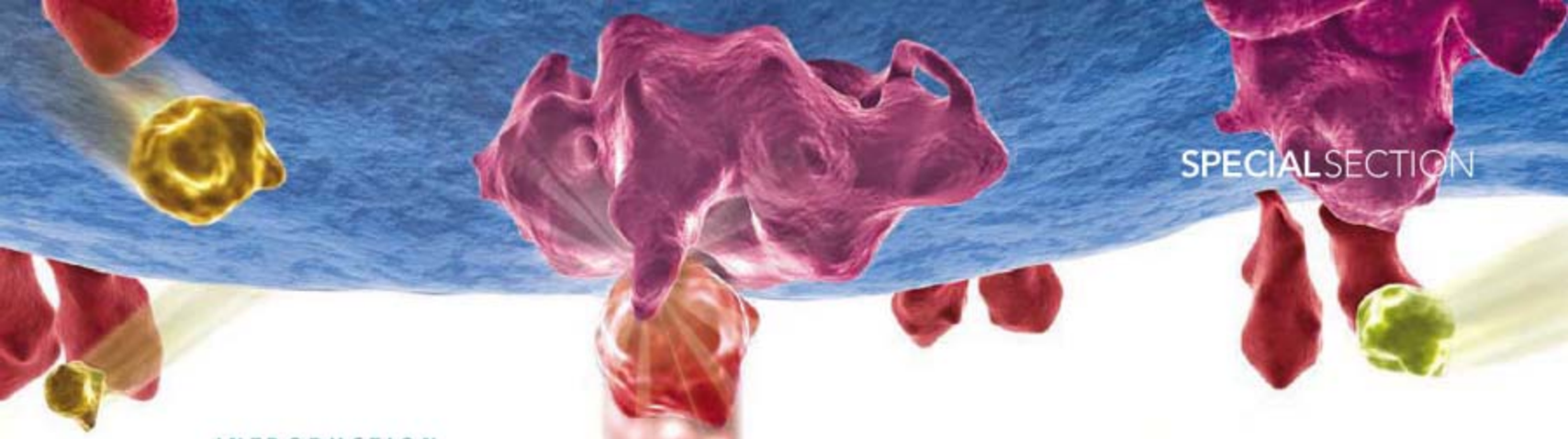

INTRODUCTION

An Insider's View

THE COVER OF THIS SPECIAL ISSUE DEPICTS A VANTAGE POINT NEAR THE surface of the cell as molecules carrying cellular signals veer down from the membrane and through the cytoplasm, some diving deep to the nucleus below. The image is apropos of the unusual and inspiring point of view of the field of cell signaling provided by an eclectic selection of topics chosen to reflect the nature of current signaling research and the viewpoints of authorities who have recently contributed detailed descriptions of cell regulatory pathways to the Database of Cell Signaling at *Science*'s STKE (see www.sciencemag.org/sciext/cellsignaling07/). These pathways describe mechanisms that underlie leading causes of life-threatening diseases (such as heart disease and cancer), control excessive stimulation of the immune system (like that in patients suffering from arthritis), and regulate development and a range of environmental responses in plants.

Oxygen is necessary for life as we know it, but either too much or too little oxygen can lead to trouble. Semenza (p. 62) describes how cells sense hypoxia through a mechanism that leads to activation of the transcription factor HIF-1α (hypoxia-inducible factor 1α), which in turn regulates the expression of hundreds of genes. Promoting such a signaling mechanism could provide a useful strategy to combat diseases such as atherosclerosis, in which circulation and resultant oxygenation are disrupted. Inhibition of HIF-1α–mediated acclimation of cancer cells might provide a strategy for combating invasion and metastasis.

Hedgehog is an unusual proteinaceous signaling molecule with key roles in developmental patterning. As Jacob and Lum explain (p. 66), not all the components of Hedgehog signaling are known. Nor do we fully understand why in mammalian cells Hedgehog signaling components are localized at the primary cilium. However, disruption of this pathway clearly leads to developmental defects in humans, and excessive Hedgehog signaling contributes to certain cancers.

Hawkins and Stephens (p. 64) describe signaling through the γ subtype of phosphoinositide 3-kinases, which link G protein–coupled receptors to the generation of phosphorylated lipid signaling molecules. The resistance of mice lacking functional PI3Kγ to inflammatory disease has focused efforts on exploiting PI3Kγ inhibitors to control diseases such as rheumatoid arthritis. Other indications suggest roles for this pathway in cardiovascular disease.

Müller and Sheen (p. 68) describe how plants use a two-component signaling mechanism, well known from prokaryotic organisms, to respond to cytokinin, a hormone derived from adenine. Examples of cytokinin-regulated processes include development and growth, stress tolerance, and leaf senescence, and the list continues to grow.

The new Connections Maps in the Database of Cell Signaling provide expertly curated information on these complex signaling mechanisms and may enable new insights into the pathways and help decipher the clues they offer to advance new therapies. A participating authority recently proclaimed, "I am excited just thinking about what might be possible in a few years' time." We hope you will be, too, and that you'll share your "wish list" with us at sigtrans-feedback@highwire.stanford.edu.

–L. BRYAN RAY, NANCY R. GOUGH, ELIZABETH M. ADLER, JOHN F. FOLEY

CREDIT: CHRIS BICKEL/SCIENCE

Cell Signaling

CONTENTS

Perspectives

62 Life with Oxygen
G. L. Semenza

64 PI3Kγ Is a Key Regulator of Inflammatory Responses and Cardiovascular Homeostasis
P. T. Hawkins and L. R. Stephens

66 Deconstructing the Hedgehog Pathway in Development and Disease
L. Jacob and L. Lum

68 Advances in Cytokinin Signaling
B. Müller and J. Sheen

Connections Maps

Hypoxia-Inducible Factor 1 (HIF-1) Pathway
G. L. Semenza, Sci. STKE,
http://stke.sciencemag.org/cgi/cm/stkecm;CMP_19178

PI3K Class IB Pathway
S. Andrews, L. Stephens, P. Hawkins, Sci. STKE,
http://stke.sciencemag.org/cgi/cm/stkecm;CMP_19912

PI3K Class IB Pathway in Neutrophils
S. Andrews, L. Stephens, P. Hawkins, Sci. STKE,
http://stke.sciencemag.org/cgi/cm/stkecm;CMP_20127

Hedgehog Signaling Pathway
L. Jacob and L. Lum, Sci. STKE,
http://stke.sciencemag.org/cgi/cm/stkecm;CMP_19889

Hedgehog Signaling Pathway in *Drosophila*
L. Jacob and L. Lum, Sci. STKE,
http://stke.sciencemag.org/cgi/cm/stkecm;CMP_20386

Cytokinin Signaling Pathway
B. Müller and J. Sheen, Sci. STKE,
http://stke.sciencemag.org/cgi/cm/stkecm;CMP_9724

***Arabidopsis* Cytokinin Signaling Pathway**
B. Müller and J. Sheen, Sci. STKE,
http://stke.sciencemag.org/cgi/cm/stkecm;CMP_10021

See also related STKE material on page 11 or at www.sciencemag.org/sciext/cellsignaling07/

Science

PERSPECTIVE

Life with Oxygen

Gregg L. Semenza

The survival of all metazoan organisms is dependent on the regulation of O_2 delivery and utilization to maintain a balance between the generation of energy and production of potentially toxic oxidants. Hypoxia-inducible factor 1 (HIF-1) is a transcription factor that functions as a master regulator of oxygen homeostasis and has essential roles in metazoan development, physiology, and disease pathogenesis. Remarkable progress has been made in delineating the molecular mechanisms whereby changes in cellular oxygenation are transduced to the nucleus as changes in gene transcription through the activity of HIF-1. Pharmacologic agents that activate or inhibit the hypoxia signal transduction pathway may be useful therapies for ischemic and neoplastic disorders, respectively, which are the major causes of mortality in industrialized societies.

Life with oxygen began some 2.5 billion years ago with the evolution of organisms capable of transducing solar energy into the chemical energy of carbon bonds. In this process of photosynthesis, carbon dioxide and water are converted into glucose, with O_2 generated as a side product of the reaction. Photosynthetic organisms prospered and multiplied, leading to a progressive increase in atmospheric O_2 concentrations. About 1.5 billion years ago eukaryotic organisms appeared containing mitochondria, subcellular organelles in which glucose is oxidized to carbon dioxide and water, thereby completing the energy cycle. Reducing equivalents are generated that pass through the mitochondrial respiratory complex, which results in the formation of a proton gradient that is used to drive the synthesis of adenosine 5′-triphosphate (ATP). A third landmark, the appearance of the first metazoan organisms, was attained ~0.5 billion years ago. Just as the evolution of eukaryotes was dependent on the prior establishment of photosynthesis, metazoan evolution was dependent on the highly efficient recovery of energy contained within the chemical bonds of glucose through the process of oxidative phosphorylation, which, compared with glycolysis, produces 18 times as much ATP per mole of glucose and thus provides the energy necessary for developing and maintaining complex multicellular organisms.

The utilization of O_2 as a substrate for energy production is not without risk. The electrons transferred through the mitochondrial respiratory chain ultimately react with O_2 to form H_2O, a process that is catalyzed by cytochrome c oxidase (complex IV). However, a fraction of electrons escape the respiratory chain and combine with O_2 prematurely, resulting in the generation of superoxide anion, which is converted to hydrogen peroxide by the action of superoxide dismutase. The oxidation of lipids, nucleic acids, and proteins by these reactive oxygen species (ROS) can result in cellular dysfunction or death. Acute increases or decreases in the cellular O_2 concentration (hyperoxia and hypoxia, respectively) result in generation of excess ROS (*1*). This finding implies that efficient respiratory chain function occurs within a narrow range of O_2 concentrations (*2*). Hypoxia may also result in deficient ATP production due to substrate limitation. All eukaryotic organisms must maintain oxygen homeostasis, and this requirement is a critical organizing principle of metazoan evolution and biology, as described in detail below.

The transcription factor HIF-1 (hypoxia-inducible factor 1) has an essential role in the maintenance of oxygen homeostasis in metazoan organisms. Within any given cell type, HIF-1 controls the expression of hundreds of genes (*2*), and because the battery of target genes varies considerably from one cell type to another, the complete HIF-1 transcriptome is likely to include thousands of genes. HIF-1 is a heterodimer composed of an O_2-regulated HIF-1α subunit and a constitutively expressed HIF-1β subunit (*2*). HIF-1α is continuously synthesized and degraded under normoxic conditions, whereas under hypoxic conditions, HIF-1α degradation is inhibited, the protein accumulates, dimerizes with HIF-1β, binds to cis-acting hypoxia-response elements in target genes, and recruits coactivator proteins, all of which leads to increased transcription (Fig. 1A). An important element of complexity derives from the HIF-1α paralogue HIF-2α, which is also O_2-regulated, dimerizes with HIF-1β, and activates transcription of an overlapping but distinct set of target genes (*3*). Another paralogue, HIF-3α, appears to function as an inhibitor of HIF-1α (*4*). Establishing the specific roles of HIF-1α, HIF-2α, and HIF-3α in oxygen homeostasis is a major challenge of current research.

O_2-dependent degradation of HIF-1α is triggered by binding of the von Hippel–Lindau tumor-suppressor protein (VHL), which interacts with the protein Elongin C, thereby recruiting an E3 ubiquitin–protein ligase complex that ubiquitinates HIF-1α and targets it for degradation by the 26*S* proteasome. VHL binding is dependent on the hydroxylation of proline residue 402 or 564, or of both residues, by the prolyl hydroxylase PHD2, which is a dioxygenase that uses O_2 and α-ketoglutarate as substrates and generates CO_2 and succinate as by-products (*5*–*8*). PHD1 and PHD3 also hydroxylate HIF-1α when overexpressed, but their physiological functions have not been established. PHD2 activity is reduced under hypoxic conditions either as a result of substrate limitation (*7*) or as a result of inhibition of the catalytic center [which contains Fe (II)] by ROS generated at complex III of the mitochondrial respiratory chain (*1*). ROS levels increase in response to hyperoxia, but HIF-1α levels do not, which suggests that the site of ROS generation may be different in hyperoxic cells or that ROS generation by complex III is necessary, but not sufficient, to induce HIF-1α under hypoxic conditions. FIH-1 (factor inhibiting HIF-1) is another dioxygenase that hydroxylates asparagine residue 803 of HIF-1α and, thereby, blocks its interaction with the coactivator p300 (*9*). The half-life of HIF-1α is also regulated in an O_2-independent manner by the competitive binding of either heat shock protein HSP90, which stabilizes the protein, or RACK1, which interacts with Elongin C and, thereby, promotes HIF-1α ubiquitination and degradation that is independent of PHD2 and VHL (*10*). A second major O_2-independent regulatory mechanism is the stimulation of HIF-1α protein synthesis by signal transduction via phosphatidylinositol 3-kinase, protein kinase B (AKT), and mammalian target of rapamycin (*11*).

HIF-1 is present in the roundworm *Caenorhabditis elegans* (*7*), which consists of fewer than one thousand cells and is so small and simple that all cells obtain O_2 by direct diffusion from the atmosphere. However, O_2 becomes limiting when the worms burrow into the soil in search of nutrients. The resulting hypoxia induces the HIF-1–mediated expression of genes encoding glucose transporters and glycolytic enzymes, which catalyze the anaerobic production of ATP through the fermentation of glucose to lactic acid (Fig. 1B). In mammalian cells, HIF-1 also regulates synthesis of mitochondrial acetyl coenzyme A (acetyl CoA), subunit composition of cytochrome c oxidase, and mitochondrial biogenesis (*2*, *12*). The evolution of larger and more complex metazoans required the concomitant evolution of anatomic structures and physiological mechanisms designed to ensure the delivery of optimal concentrations of O_2 to every cell. In the fruit fly *Drosophila melanogaster*, this is accomplished by tracheal tubules through which O_2 is transported to the interior of the organism. In mammals, such as the laboratory mouse *Mus musculus*, complex respiratory and circulatory

Vascular Program, Institute for Cell Engineering; Departments of Pediatrics, Medicine, Oncology, Radiation Oncology; and McKusick-Nathans Institute of Genetic Medicine; The Johns Hopkins University School of Medicine, Broadway Research Building, Suite 671, 733 North Broadway, Baltimore, MD 21205, USA. E-mail: gsemenza@jhmi.edu

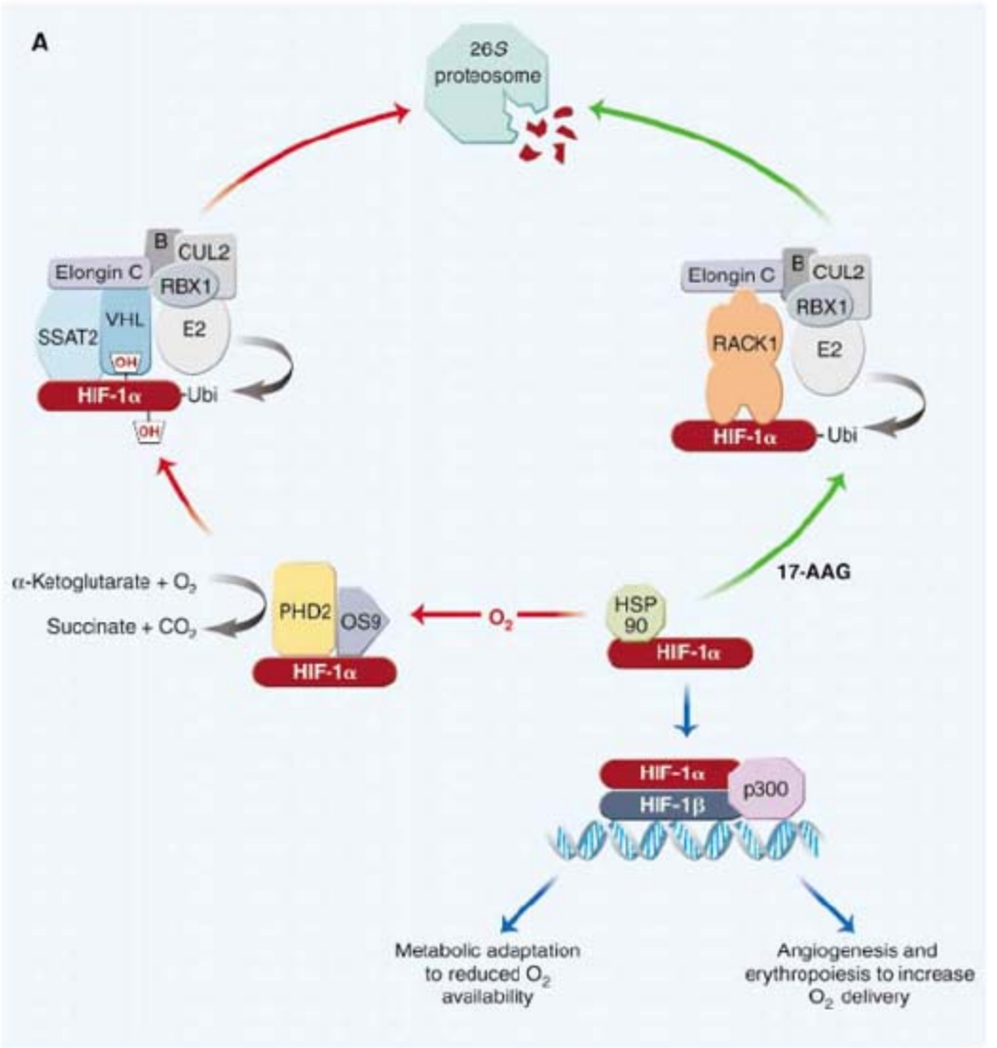

Fig. 1. Molecular mechanisms of oxygen homeostasis. **(A)** O_2-dependent posttranslational modifications of the HIF-1α subunit by PHD2 and FIH-1 (not shown) serve as molecular switches that regulate the interaction of HIF-1α with VHL and p300, which, in turn, determine the half-life and transcriptional activity of HIF-1, respectively. Two additional proteins form multivalent complexes that increase the efficiency of these reactions: OS-9 (a protein that was originally identified in osteosarcomas) interacts with HIF-1α and PHD2 and promotes hydroxylation, whereas SSAT2 (a paralog of spermidine/spermidine acetyltransferase-1) interacts with HIF-1α, VHL, and Elongin C and promotes ubiquitination. Finally, pharmacological inhibitors of HSP90, such as 17-allylaminogeldanamycin (17-AAG), promote the binding of HIF-1α to RACK1, which recruits the Elongin C ubiquitin-ligase complex in an O_2-independent manner. Blue, red, and green arrows denote processes that occur under hypoxic, normoxic, or O_2-independent conditions, respectively. Additional factors regulating HIF-1 are described in the STKE Connections Map (*17*). **(B)** Under hypoxic conditions, HIF-1 induces the expression of genes encoding the following proteins: (1) glucose transporters GLUT1 and GLUT3, which increase intracellular glucose uptake; (2) glycolytic enzymes, which convert glucose into pyruvate; (3) lactate dehydrogenase A, which converts pyruvate into lactate; (4) pyruvate dehydrogenase (PDH) kinase 1, which phosphorylates and inactivates PDH, the enzyme that converts pyruvate into acetyl CoA for entry into the mitochondrial tricarboxylic acid (TCA) cycle, which generates reducing equivalents that are passed on to the electron transport chain (ETC); and (5) cytochrome c oxidase subunit COX4-2, which replaces COX4-1 and, thereby, increases the efficiency of mitochondrial respiration under hypoxic conditions.

(heart, blood, and vasculature) systems evolved to deliver O_2 to each of the trillions of cells that compose the adult organism. The development of these systems before birth and their use after birth are controlled by HIF-1. Thus, HIF-1 mediates developmental and physiological pathways that either promote O_2 delivery to cells or allow cells to survive O_2 deprivation (Fig. 1).

In the case of *Homo sapiens*, the ability of the species to prosper and multiply over the last 0.0001 billion years has been associated with an increase in life span. Humans in industrialized societies are less likely to die of infection, predation, or starvation and more likely to die of cardiovascular and neoplastic disorders in which aging, dietary excess, and physical inactivity play important etiological roles. Atherosclerotic stenosis of large arteries in the coronary and femoral circulations results in myocardial and limb ischemia, respectively, conditions in which cells are deprived of O_2 and glucose and accumulate toxic metabolites. The deprivation of O_2 in ischemic cells induces adaptive homeostatic responses in young healthy experimental animals, such as the increased production of vascular endothelial growth factor and other angiogenic cytokines, which promote tissue perfusion. These processes appear to be blunted in humans as a result of aging, atherosclerosis, cigarette smoking, diabetes, and hypertension (*13*). A major challenge of current research in this field is to understand the mechanisms underlying the impairment of O_2 homeostasis and to devise therapeutic strategies to counteract them. In contrast, cancer cells co-opt adaptive mechanisms mediated by HIF-1 to promote their survival, proliferation, perfusion,

and invasion of body tissues (*14*, *15*), and clinical trials of therapeutic strategies designed to block these pathways are ongoing.

The last landmark on our timeline, a mere 0.0000002 billion years ago, is the discovery of oxygen, which has been called the most important discovery in the history of science (*16*). Life, after all, depends on it.

References and Notes

1. R. D. Guzy, P. T. Schumacker, *Exp. Physiol.* **91**, 807 (2006).
2. G. L. Semenza, *Biochem. J.* **406**, 317 (2007).
3. C. J. Hu *et al.*, *Mol. Cell. Biol.* **26**, 3514 (2006).
4. Y. Makino *et al.*, *J. Biol. Chem.* **282**, 14073 (2007).
5. M. Ivan *et al.*, *Science* **292**, 464 (2001).
6. R. K. Bruick, S. L. McKnight, *Science* **294**, 1337 (2001).
7. A. C. Epstein *et al.*, *Cell* **107**, 43 (2001).
8. E. Berra *et al.*, *EMBO J.* **22**, 4082 (2003).
9. D. Peet, S. Linke, *Novartis Found. Symp.* **272**, 37 (2006).
10. Y. V. Liu *et al.*, *Mol. Cell* **25**, 207 (2007).
11. E. Laughner *et al.*, *Mol. Cell. Biol.* **21**, 3995 (2001).
12. H. Zhang *et al.*, *Cancer Cell* **11**, 407 (2007).
13. M. J. Reed, J. M. Edelberg, *Sci. Ageing Knowledge Environ.* **2004**, pe7 (2004).
14. D. A. Chan, A. J. Giaccia, *Cancer Metastasis Rev.* **26**, 333 (2007).
15. D. Liao, R. S. Johnson, *Cancer Metastasis Rev.* **26**, 281 (2007).
16. J. W. Severinghaus, *Adv. Exp. Med. Biol.* **543**, 7 (2003).
17. G. L. Semenza, Hypoxia-inducible factor 1 (HIF-1) pathway. *Sci. STKE* (Connections Map, as seen October 2007), http://stke.sciencemag.org/cgi/cm/stkecm;CMP_19178.

18. I thank N. Prabhakar for presubmission review of the manuscript. Work in the author's laboratory is supported by funds from the American Diabetes Association, the Flight Attendant Medical Research Institute, the National Cancer Institute, National Heart, Lung, and Blood Institute, National Institute on Aging, and National Institute of General Medical Sciences, NIH, and the Johns Hopkins Institute for Cell Engineering.

10.1126/science.1147949

PERSPECTIVE

PI3Kγ Is a Key Regulator of Inflammatory Responses and Cardiovascular Homeostasis

Phillip T. Hawkins and Len R. Stephens

Class I phosphoinositide 3-kinase (PI3K) signaling pathways regulate several important cellular functions, including cellular growth, division, survival, and movement. Class IB PI3K (also known as PI3Kγ) links heterotrimeric GTP-binding protein–coupled receptors to these pathways. Activation of class IB PI3K results in the rapid synthesis of phosphatidylinositol-3,4,5-trisphosphate [PtdIns(3,4,5)P_3] and its dephosphorylation product PtdIns(3,4)P_2 in the plasma membrane. These two lipid messengers bind to pleckstrin homology domain–containing effectors that regulate a complex signaling web downstream of receptor activation. Characteristic features of this pathway are the regulation of protein kinases and the regulation of small guanosine triphosphatases that control cellular movement, adhesion, contraction, and secretion. Most of the ligands that activate class IB PI3K are involved in coordinating the body's response to injury and infection, and recent studies suggest that small molecule inhibitors of this enzyme may represent a novel class of anti-inflammatory therapeutic agents.

Class I PI3Ks are well-established signal transduction enzymes that drive extensive signaling networks downstream of cell surface receptor activation (*1*). Most of the interest in these enzymes has focused on the important roles of class IA PI3Ks (PI3Kα, β, and δ) in coordinating cell growth, division, and survival in response to activation of protein tyrosine kinase–coupled growth factor receptors. In contrast, class IB PI3K (PI3Kγ) allows fast-acting, heterotrimeric G protein–coupled receptors to access PI3K signaling networks. Most of the ligands that have been established to activate PI3Kγ are involved in the regulation of multiple cell types in the immune system and vascular lining, and mice lacking the catalytic subunit of PI3Kγ are generally healthy but remarkably resistant to the development of several inflammatory pathologies in mouse models of human inflammatory disease (*2*, *3*).

PI3Kγ was originally characterized as a heterodimer of p101 regulatory and p110γ catalytic subunits (*4*, *5*). A homolog of p101, called p84 or p87^{PIKAP}, has recently been discovered that also forms dimers with p110γ, but the relative tissue expression and relevance of p101 versus p84 to the activation of PI3Kγ in different cellular contexts has yet to be established (*6*, *7*). PI3Kγ is a lipid kinase that catalyzes the conversion of phosphatidylinositol-4,5-bisphosphate [PtdIns(4,5)P_2] to phosphatidylinositol-3,4,5-trisphosphate [PtdIns(3,4,5)P_3] in the inner leaflet of the plasma membrane. This lipid kinase activity is stimulated by the combined actions of p101- or p84-dependent interaction with Gβγ subunits and p110γ-dependent interaction with guanosine triphosphate (GTP)–bound Ras (*8*). Gβγ subunits are liberated during the direct interaction of receptors with the G, family of heterotrimeric GTP-binding proteins, but the origin of GTP-bound Ras in this pathway has yet to be established.

PtdIns(3,4,5)P_3, and its dephosphorylation product PtdIns(3,4)P_2, are signaling lipids whose increases in concentration coordinate the plasma membrane localization and regulation of several direct protein effectors. The magnitude and timing of these lipid signals is also controlled by phosphatases that remove the 5- [such as Src homology 2 (SH2) domain–containing inositol polyphosphate 5-phosphatase (SHIP) and other inositol polyphosphate 5-phosphatases], 3- (such as PTEN), and 4- (such as inositol polyphosphate 4-phosphatases) monoesterified phosphates from these lipids. As with other phosphoinositides [for example, PtdIns3P, PtdIns4P, PtdIns(3,5)P_2, and PtdIns(4,5)P_2], PtdIns(3,4,5)P_3 and PtdIns(3,4)P_2 recognize their protein effectors by binding to conserved families of small, lipid binding domains. PtdIns(3,4,5)P_3 and PtdIns(3,4)P_2 are thought to bind predominantly to a subfamily of pleckstrin homology (PH) domains, which bind the headgroup of either or both of these lipids with high affinity and specificity (*1*). A characteristic feature of PI3K signaling pathways is the large number of direct, PH domain–containing effectors and the complex signaling networks in which they are involved, usually in partnership with other signaling pathways that are activated in parallel (Fig. 1). The relative abundance of these effectors and their targets define the nature of the regulatory experience delivered in a particular cellular context; however, the activation of the serine/threonine kinase PKB (protein kinase B, also known as Akt) appears to be a universal response to activation of this pathway and plays a key role in regulating metabolic, secretory, and transcriptional responses [see the canonical PI3K class IB pathway in *Science*'s STKE database (*9*)].

PI3Kγ is activated by several chemokines [for example, interleukin-8, macrophage inflammatory protein (MIP)–1α, MIP-2, MCP-1, Gro-α, and RANTES], pro-inflammatory lipids (for example, PAF and LTB_4), bacterial products [for example, *N*-formyl-Met-Leu-Phe (fMLP)], and other vaso-active stimuli [for example, C5a, adenosine diphosphate (ADP), and angiotensin

The Babraham Institute, Cambridge CB22 3AT, UK. E-mail: phillip.hawkins@bbsrc.ac.uk (P.T.H.); len.stephens@bbsrc.ac.uk (L.R.S.)

II], acting predominantly through G_i-coupled receptors (*2*, *3*). Thus, this pathway is involved in the regulation of several cell types that are classically considered to be part of the innate and adaptive immune system (neutrophils, macrophages, monocytes, endothelial cells, mast cells, dendritic cells, and T cells) and also cell types additionally involved in the regulation of blood pressure (smooth muscle cells) and blood clotting (platelets). Most of these cell act together in coordinated responses to injury and infection that involve multiple ligands, receptors, and intracellular signaling cascades. Where sufficient detail is known concerning the regulation of a particular cell type, it invariably seems that activation of PI3Kγ by G_i-coupled receptors acts cooperatively with ligands working through other receptor types. Often these other receptors transduce their signals through protein tyrosine kinases, which in turn activate class IA PI3Ks (PI3Kα, PI3Kβ, and PI3Kδ) (*1*). Further, sustained activation of G_i-coupled receptors often stimulates Src family protein tyrosine kinases and subsequently activates class IA PI3Ks in parallel to PI3Kγ. Thus, in many contexts of cellular activation, multiple class I PI3Ks are involved. Because a major class IA PI3K in the hematopoietic system is PI3Kδ, PI3Kγ and PI3Kδ are often found working together to deliver physiological regulation of a particular response. Despite the apparent opportunity for redundancy that these complex signaling systems represent, work with p110γ knockout (KO) mice indicates that PI3Kγ plays a nonredundant role in several important physiological responses (*2*, *3*), probably because of its partial contribution to so many of the relevant cell-activation pathways.

PI3Kγ was discovered in neutrophils, and initially its expression was thought to be restricted to cells of the hematopoietic lineage; hence, most of our knowledge of this enzyme comes from the study of neutrophils and related cell types [see the specific PI3K class IB pathway in *Science's* STKE database (*10*)]. Activation of neutrophil PI3Kγ by chemoattractants present on the surface of inflamed endothelium regulates the efficiency with which these cells are captured and exit the vasculature. Activation of PI3Kγ also contributes to the efficiency with which neutrophils chemotax toward higher concentrations of chemoattractants released at sites of infection and inflammation and also to the efficiency with which they secrete proteases, reactive oxygen species (ROS), and other antimicrobial products at their final destination (usually in response to high concentrations of end-point chemoattractants and priming cytokines). The cooperation between chemoattractants and cytokines in the delivery of maximal ROS production appears to involve the sequential activation of PI3Kγ and PI3Kδ. The molecular details of how PtdIns(3,4,5)P_3 and PtdIns(3,4)P_2 coordinate the regulation of these neutrophil responses are still incompletely understood, but it is clear that there is a central role for the regulation of small gunosine triphosphatases (GTPases) of the Rac and Rho family and the Arf family and that this is likely to be a general feature of this pathway in different cell types. There also appears to be a small role for PI3Kγ in the development of the inflamed endothelium itself. The net result of all of these effects probably explains why several laboratories have reported a substantial reduction in the speed and sometimes extent to which neutrophils arrive at sites of inflammation in p110γ KO mice (*2*).

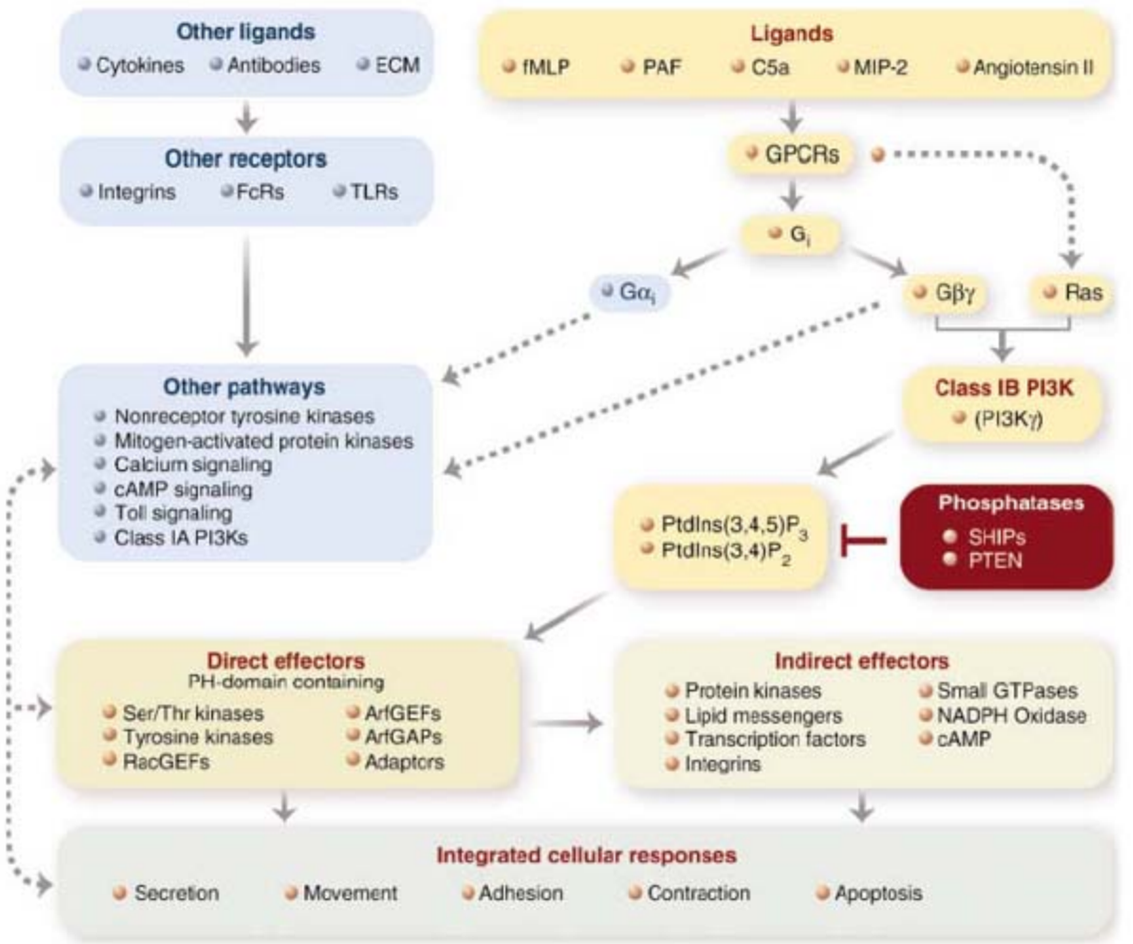

Fig. 1. This schematic diagram places the class IB signaling pathway into perspective, with respect to the other signaling pathways that usually operate in parallel to deliver physiological regulation in any particular context of cellular regulation. Some examples of the various categories of signaling elements are shown to illustrate different levels of signaling organization, but the lists are not meant to be exhaustive. Additional abbreviations are as follows: ECM, extracellular matrix; FcRs, Fc receptors; TLRs, Toll-like receptors; GPCRs, G protein–coupled receptors; GEFs, guanine nucleotide exchange factors; GAP, GTPase-activating protein; and NADPH, reduced form of nicotinamide adenine dinucleotide phosphate.

PI3Kγ also plays an important role in other immune cells and their functions, for example, in the chemotaxis of cells in the monocyte or macrophage lineage to sites of inflammation, in the homing of dendritic cells to lymph nodes, and in the development and activation of T lymphocytes (this last is a partially redundant role with PI3Kδ) (*2*, *3*). PI3Kγ also contributes to the activation of mast cell secretion by adenosine, in concert with immunoglobulin E (IgE)–dependent activation of PI3Kδ, and to the activation of platelet aggregation by ADP, in concert with PI3Kβ (*2*, *3*). It seems likely that PI3Kγ is involved in purinergic stimulation of autocrine and paracrine regulatory loops in other cell types as well.

Although PI3Kγ was initially thought to be restricted to cells of the hematopoietic lineage, it is now clear that this isoform also plays key roles in additional cell types. There is good evidence that PI3Kγ participates in angiotensin II regulation of smooth muscle con-

traction (*11*), and there is a fascinating story emerging on the role of PI3Kγ in the regulation of myocyte contractility (*12*). In particular, a comparison between the differential effects of p110γ deletion and a p110γ kinase–dead knockin mutation suggests that p110γ contributes a nonlipid kinase or scaffolding function to the reduction of cyclic adenosine monophosphate (cAMP) concentration in myocytes, delivering decreased contractile force in response to β-adrenergic stimulation. The mechanism for this effect may involve direct binding of PI3Kγ to a cAMP phosphodiesterase (PDE3B).

Because PI3Kγ is involved in the mechanisms that direct several types of immune cells to sites of inflammation in the joints, lungs, and other organs, several laboratories have investigated the susceptibility of p110γ KO mice to various models of inflammatory disease, particularly those with an autoimmune component. Descriptions of PI3Kγ involvement in the regulation of blood vessel contraction, clot formation, and the heart are also starting to prompt the analysis of these mice in models of cardiovascular disease (*13*). This work is driven by the knowledge that the adenosine triphosphate–binding site of the catalytic subunit of PI3Ks is a druggable target, with PI3K isoform-selective inhibitors in development in several pharmaceutical companies (*2*). The first PI3Kγ-selective inhibitors are now starting to appear, with efficacy so far in the treatment of mouse models of rheumatoid arthritis (*14*) and systemic lupus (*15*).

There is clearly still much to be discovered about the regulation of PI3Kγ individual receptors, the relative contributions of Gβγ subunits and Ras, the importance of p101 versus p84, and also the potential new scaffolding functions for both regulatory and catalytic subunits. There is also still more to learn about how the lipid products of PI3Kγ regulate complex cellular responses in different cell types. Perhaps of greatest general interest, however, is just how effective the first p110γ-specific inhibitors will prove to be in clinical trials of human inflammatory disease.

References and Notes

1. P. T. Hawkins, K. E. Anderson, K. Davidson, L. R. Stephens, *Biochem. Soc. Trans.* **34**, 647 (2006).
2. T. Ruckle, M. K. Schwarz, C. Rommel, *Nat. Rev. Drug Discov.* **5**, 903 (2006).
3. E. Hirsch *et al.*, *Thromb. Haemostasis* **95**, 29 (2006).
4. L. R. Stephens *et al.*, *Cell* **89**, 105 (1997).
5. B. Stoyanov *et al.*, *Science* **269**, 690 (1995).
6. P. Voigt, M. B. Dorner, M. Schaefer, *J. Biol. Chem.* **281**, 9977 (2006).
7. S. Suire *et al.*, *Curr. Biol.* **15**, 566 (2005).
8. S. Suire *et al.*, *Nat. Cell Biol.* **8**, 1303 (2006).
9. S. Andrews, L. Stephens, P. Hawkins, PI3K class IB pathway. *Sci. STKE* (Connections Map, as seen October 2007), http://stke.sciencemag.org/cgi/cm/stkecm;CMP_19912.
10. S. Andrews, L. Stephens, P. Hawkins, PI3K class IB pathway in neutrophils. *Sci. STKE* (Connections Map, as seen October 2007), http://stke.sciencemag.org/cgi/cm/stkecm;CMP_20127.
11. C. Vecchione *et al.*, *J. Exp. Med.* **201**, 1217 (2005).
12. E. Patrucco *et al.*, *Cell* **118**, 375 (2004).
13. J. D. Chang *et al.*, *Proc. Natl. Acad. Sci. U.S.A.* **104**, 8077 (2007).
14. M. Camps *et al.*, *Nat. Med.* **11**, 936 (2005).
15. D. F. Barber *et al.*, *Nat. Med.* **11**, 933 (2005).

16. We thank members of the Inositide Laboratory at the Babraham Institute for help and advice in the preparation of this article. Work in the author's laboratory is currently supported by grants from the Biotechnology and Biological Science Research Council, the Medical Research Council, and the British Lung Foundation.

10.1126/science.1145420

PERSPECTIVE

Deconstructing the Hedgehog Pathway in Development and Disease

Leni Jacob and Lawrence Lum*

The Hedgehog (Hh) family of secreted signaling proteins is a master regulator of cell fate determination in metazoans, contributing to both pattern formation during embryonic development and postembryonic tissue homeostasis. In a universally used mode of action, graded distribution of Hh protein induces differential cell fate in a dose-dependent manner in cells that receive Hh. Though much of this pathway has been elucidated from genetically based studies in model organisms, such as *Drosophila* and mice, the importance of Hh-mediated signaling in humans is clearly evident from malformations and a broad range of cancers that arise when the pathway is corrupted.

The goal of this Perspective and the two Connections Maps (*1*, *2*) is to highlight recent insights into the unconventional methods by which Hh proteins normally function and how this pathway is implicated in pathological contexts such as cancer. Production of active Hh protein begins with autocatalytic cleavage of a precursor molecule to yield a cholesterol-modified amino-terminal signaling domain (HhN). Subsequent palmitoylation of HhN results in a dually lipidated molecule that is restricted to the cell membrane. Release of HhN from the cell membrane is mediated by Dispatched (Disp/Disp1, hereafter Disp), a 12-transmembrane protein that is structurally similar to the Hh receptor, Patched (Ptc/Ptch1, hereafter Ptc) (Fig. 1A). Both proteins belong to the Resistance Nodulation Division (RND) superfamily of proteins that in prokaryotes function to transport small molecules across membranes. Disp and Ptc likely act as small-molecule transporters, as their activity in the Hh pathway is dependent on residues important to the function of RND protein family members. In *Drosophila*, HhN released by Disp appears to be incorporated into particles scaffolded by the lipid-transporting lipophorin proteins (*3*). This previously unknown role for lipoprotein complexes in Hh signaling may represent a universal mechanism for distributing other lipophilic signaling molecules in animals, such as the Wnt proteins (*3*).

Initiation of the pathway response entails Hh proteins binding to Ptc, which in turn derepresses the seven-transmembrane protein Smoothened (Smo). This process may be transduced through a small molecular intermediary because Ptc substoichiometrically inhibits Smo (*4*). Several candidate small molecules have emerged, including cholesterol biosynthesis metabolites, such as oxysterols, that promote Smo function when exogenously added to cultured cells (*5*). Considering that the potent Smo antagonist cyclopamine, a naturally occurring teratogen, is structurally similar to sterols, there is growing evidence that Ptc gates interactions between Smo and specific sterols to regulate Smo function.

A number of receptors facilitate Hh binding to Ptc (*1*, *2*), including members of the cell adhesion molecule–related/down-regulated by oncogenes (Cdo) family. Cdo and its *Drosophila* homolog Interference hog (Ihog) associate with Hh through a fibronectin type III (FnIII) repeat (*6*, *7*), a motif with potential for binding sulfate ions (*8*). Indeed, dimerization of Ihog and its conversion from a weak to a high-affinity Hh-binding molecule can be induced by heparin, a protein with sulfated polysaccharide modifications. How Ihog and Cdo proteins promote Hh-mediated responses in coordination with Ptc and other Hh receptors, particularly the heparan sulfate–modified Dally-like protein (Dlp), which also contributes to the Hh response (*1*), remains to be addressed.

Department of Cell Biology, University of Texas Southwestern Medical Center, Dallas, TX 75390, USA.

*To whom correspondence should be addressed. E-mail: lawrence.lum@utsouthwestern.edu

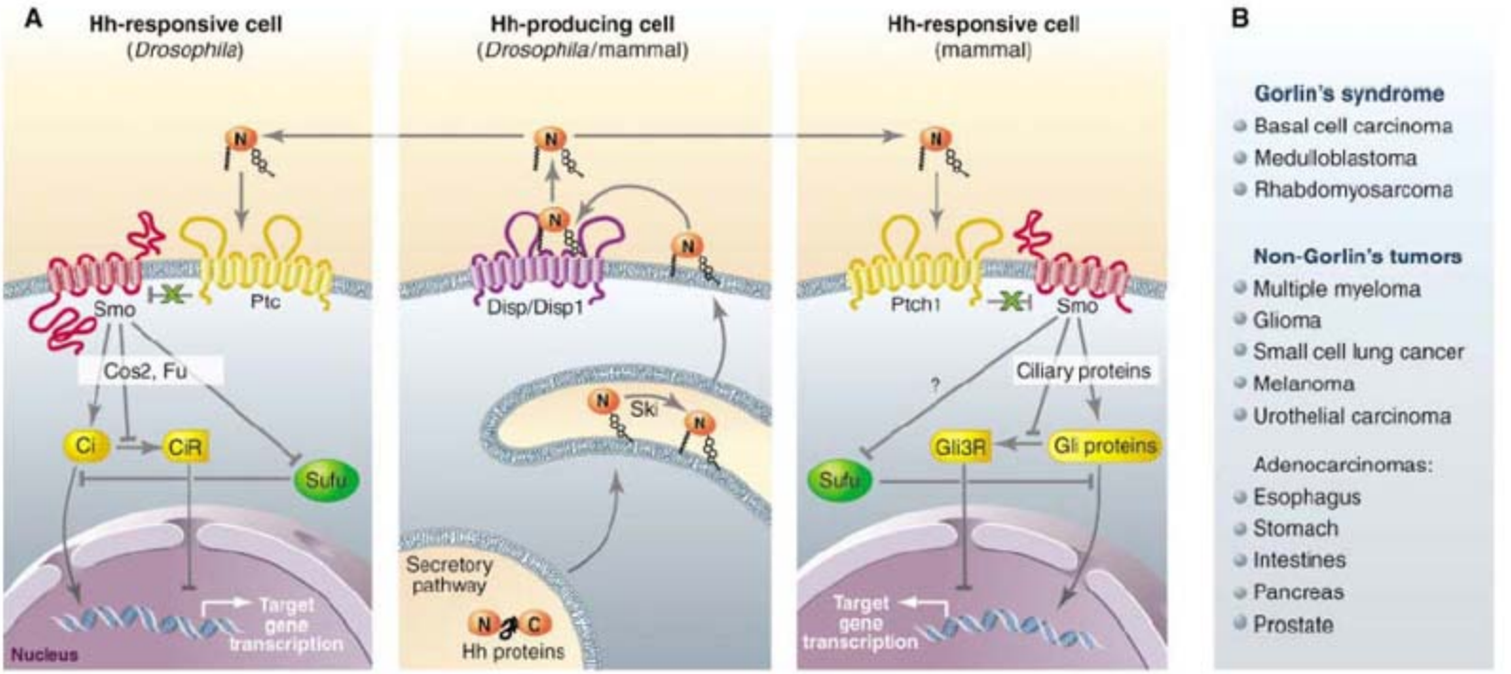

Fig. 1. Hh signaling in animals. **(A)** Hh production is highly conserved between *Drosophila* and mammals (middle). Autocatalytic cleavage of the Hh precursor protein yields a cholesterol-modified signaling peptide (HhN), which is further palmitoylated by Skinny Hedgehog (Ski), then released from the cell by Disp (*Drosophila*) or Disp1 (mammals). In *Drosophila* (left), the released lipophilic HhN is incorporated into lipophorin complexes (not shown) and distributed to other cells with the help of heparan sulfate proteoglycans (Dally and Dlp; also not shown). The suppressive action of Ptc or Ptch1 on Smo is conserved in Hh-responsive cells from *Drosophila* (left) and mammals (right). Members of the CDO receptor family (not shown), including Ihog, facilitate Hh binding and inhibition of Ptc or Ptch1, allowing activation of Smo. In *Drosophila*, Dlp also appears to facilitate Hh response. Smo-mediated regulation of Ci (*Drosophila*) or Gli (mammals) nuclear localization and proteolytic processing into a repressor (CiR or Gli3R) depends on Cos2, Fu, and Su(fu) in *Drosophila*, and proteins that function in the primary cilium in mammals. The mechanism by which Smo inhibits the pathway suppressor Su(fu) in mammals is unknown. **(B)** Tumors with aberrant Hh pathway activity in Gorlin's syndrome, as well as their sporadic counterparts, frequently harbor mutations in Ptch1. Other tumors for which molecular lesions have not been defined also exhibit aberrant Hh pathway response. References for most of the tumors described here can be found in (*16*).

Ultimately, the concerted action of these receptors activates Smo by promoting Hh interaction with Ptc. Smo activation is best understood in *Drosophila* (*9*). Initial phosphorylation of cytosolic tail sequences in Smo corresponds with protein accumulation at the plasma membrane, thus favoring interactions with a cytoplasmic regulatory complex scaffolded by the kinesin-like molecule Costal-2 (Cos2). This complex also contains the serine/threonine kinase Fused (Fu) and the transcriptional effector Cubitus interruptus (Ci) (Fig. 1A). The mechanism by which Smo stimulates the transcriptional activity of Ci and inhibits proteolytic processing of Ci to a repressor (CiR) through Cos2, Fu, and another cytoplasmic regulator, Suppressor of Fu [Su(fu)], was previously reviewed (*9*).

The ultimate target of Smo action in mammals is the Gli zinc finger family of proteins composed of three mammalian homologs of Ci (Gli1 to Gli3), with proteolytically processed Gli3 (Gli3R) predominantly functioning as a transcriptional repressor (Fig. 1A). Many studies support the hypothesis that Smo in *Drosophila* and mammals uses different mechanisms of action to activate Ci or Gli proteins, respectively (*10*). The inability to identify mammalian Cos2 and Fu homologs also likely exemplifies differences in Hh signaling between flies and mammals (*2*, *10*).

Insight into the mammalian Hh pathway has come from forward genetic screens in mice with chemically induced mutations that have revealed genes essential to neural tube formation, a Hh-dependent process (*11*). Surprisingly, the majority of these genes are involved in the formation of the primary cilium, a microtubule-scaffolded organelle found in most cells (*2*). Subsequent studies revealed that components of the cilia, such as intraflagellar transport proteins, participate not only in the activation of Gli proteins but also in the processing of Gli3 (*11*). In this capacity, ciliary proteins appear to be the functional equivalent of Cos2 (Fig. 1A). Furthermore, almost all the known mammalian Hh components, including Ptch1, Smo, Su(fu), and Gli proteins, localize to primary cilia (*11*, *12*). Ptch1 apparently inhibits the localization of Smo to cilia in a Hh-dependent manner, suggesting that this compartment is essential to Smo activation (*12*). Though it is conceivable that the cilium may simply represent an assembly point for pathway components, its requirement for both Hh pathway activation and suppression implicates a more direct role.

More complete understanding of cilia and their role in the Hh response awaits the identification of the immediate downstream effector of Smo and its subcellular localization. In *Drosophila*, the kinase Fu appears to contribute to most downstream events controlled by Smo, including suppression of Cos2 and Su(fu) (*13*, *14*). The central role of Fu to Hh response in insects implies that a functional equivalent of Fu remains to be found in mammals. Whether or not a mammalian Fu exists, the mechanism of Smo action will likely have to account for Hh-dependent regulation of Su(fu), which appears to function as a major pathway suppressor in both insects and mammals (Fig. 1A) (*15*).

The role of the Hh pathway in tumorigenesis likely exemplifies its nearly universal participation in cell fate decision-making (*16*). Hh-related tumors can be broadly categorized based on whether or not they present as part of Gorlin's (also called basal cell nevus) syndrome. Patients with this syndrome often harbor an inactivating mutation in Ptch1, which, independently of Hh ligand, promotes a broad range of tumors, most frequently basal cell carcinoma (Fig. 1B). Conversely, the oncogenic events that drive the Hh-dependent aberrant response often observed in non-Gorlin's tumors have not been defined, despite the greater number of cancers that fall into this category (Fig. 1B). These tumors likely are sustained by Hh-dependent cell-autonomous signaling in populations of cancer stem cells (*17*), suggesting that therapeutics that attack the Hh pathway may offer specificity over strategies that generally block cell proliferation.

The wealth of mechanistic insight into how the Hh pathway functions has revealed both the sophistication of this signal transduction network and the challenges that remain in the treatment of Hh-related diseases. Of urgency is the development of rational therapeutic approaches using knowledge of the pathway to specifically target the events underlying aberrant pathway response. Success in this endeavor will require an understanding of how primary cilia, lipoproteins, and sterol biosynthesis contribute to Hh-related diseases.

References and Notes

1. L. Jacob, L. Lum, Hedgehog signaling pathway. *Sci. STKE* (Connections Map, as seen October 2007), http://stke.sciencemag.org/cgi/cm/stkecm;CMP_19889.
2. L. Jacob, L. Lum, Hedgehog signaling pathway in *Drosophila*. *Sci. STKE* (Connections Map, as seen October 2007), http://stke.sciencemag.org/cgi/cm/stkecm;CMP_20386.
3. D. Panakova, H. Sprong, E. Marois, C. Thiele, S. Eaton, *Nature* **435**, 58 (2005).
4. J. Taipale, M. K. Cooper, T. Maiti, P. A. Beachy, *Nature* **418**, 892 (2002).
5. R. B. Corcoran, M. P. Scott, *Proc. Natl. Acad. Sci. U.S.A.* **103**, 8408 (2006).
6. T. Tenzen *et al.*, *Dev. Cell* **10**, 647 (2006).
7. S. Yao, L. Lum, P. Beachy, *Cell* **125**, 343 (2006).
8. J. S. McLellan *et al.*, *Proc. Natl. Acad. Sci. U.S.A.* **103**, 17208 (2006).
9. L. Lum, P. A. Beachy, *Science* **304**, 1755 (2004).
10. M. Varjosalo, S. P. Li, J. Taipale, *Dev. Cell* **10**, 177 (2006).
11. D. Huangfu, K. V. Anderson, *Development* **133**, 3 (2006).
12. R. Rohatgi, L. Milenkovic, M. P. Scott, *Science* **317**, 372 (2007).
13. S. Claret, M. Sanial, A. Plessis, *Curr. Biol.* **17**, 1326 (2007).
14. Y. Liu, X. Cao, J. Jiang, J. Jia, *Genes Dev.* **21**, 1949 (2007).
15. J. Svard *et al.*, *Dev. Cell* **10**, 187 (2006).
16. P. A. Beachy, S. S. Karhadkar, D. M. Berman, *Nature* **432**, 324 (2004).
17. C. D. Peacock *et al.*, *Proc. Natl. Acad. Sci. U.S.A.* **104**, 4048 (2007).

18. Our research is supported by an endowment from Virginia Murchison Linthicum, the NIH, the American Cancer Society, and the Welch Foundation. We thank M. Dodge and other members of the Lum laboratory for useful discussions.

10.1126/science.1147314

PERSPECTIVE

Advances in Cytokinin Signaling

Bruno Müller and Jen Sheen*

Cytokinins are essential plant hormones that control various processes in plants' development and response to external stimuli. The *Arabidopsis* cytokinin signal transduction pathway involves hybrid histidine protein kinase sensors, phosphotransfer proteins, and regulators as transcription activators and repressors in a phosphorelay system. Each step is executed by components encoded by multigene families. Recent findings have revealed new functions, new feedback loops, and connections to other signaling pathways.

The plant hormone cytokinin comprises a class of adenine-derived signaling molecules involved in diverse processes throughout a plant's life, such as stem-cell control in root and shoot; vascular differentiation; chloroplast biogenesis; root, shoot, and inflorescence growth and branching; nutrient balance; leaf senescence; stress tolerance; and seed development (*1*–*6*). More than 50 years ago, Skoog, Miller, and collaborators purified the first cytokinin crystal from autoclaved herring sperm DNA extracts and demonstrated its ability to strongly stimulate proliferation in tobacco tissue culture (*7*). It then took some 40 years to identify the first genes involved in cytokinin signaling. Kakimoto and colleagues pioneered in performing large screens based on the effects of cytokinin on cultured *Arabidopsis* tissues and uncovered a role for histidine kinases (HKs) in cytokinin signal transduction (*8*, *9*). HKs are prevailing sensors in prokaryotes that initiate a signaling system in which phosphoryl groups are transferred between histidines and aspartates (phosphorelay signaling system) to activate or inhibit cognate downstream partners called response regulators (RRs). Completion of the *Arabidopsis* genome sequence facilitated the identification of all potential components of phosphorelay signaling: There are eight transmembrane HKs, six histidine phosphotransfer proteins (HPTs), and more than 20 RRs (*1*, *2*, *10*, *11*). Isolated leaf cells were systematically transfected with putative tagged phosphorelay components to test how these components affected the responsiveness of a cytokinin reporter. This analysis resulted in a model (Fig. 1) that distinguishes four major steps of the cytokinin phosphorelay from the plasma membrane to the nucleus: (i) cytokinin sensing and initiation of signaling by receptor HKs; (ii) phosphoryl group transfer to HPTs and their nuclear translocation; (iii) phosphotransfer to nuclear B-type RRs, which activate transcription; and (iv) negative feedback through cytokinin-inducible A-type RRs, which are products of the early cytokinin target genes (*11*). Identification of the orthologs for cytokinin signaling components in other plant species suggests evolutionary conservation of this pathway.

Careful and extensive analyses of plants harboring loss-of-function mutations in signaling components have corroborated the core logic of the cell-based model. Mutant phenotypes became apparent only after multiple family members were knocked out, which suggests extensive functional redundancy at each signaling step (*2*). However, individual components seem to accomplish specific tasks as well, as illustrated by the following findings. Receptors exhibit differential affinities for different cytokinins (*1*, *5*, *12*). One out of three well-characterized cytokinin receptors specifically mediates a delay of senescence in *Arabidopsis* leaves (*2*, *13*). Plants mutated in some RR gene pairs (out of the large RR family) display subtle differences in phenotypes (*2*). In addition, overexpressing different A- or B-type RR family members results in plants with different phenotypes (*1*, *2*, *11*). A comprehensive protein interaction map for all potential components involved in signaling shows distinct patterns of interaction between protein family members (*10*). The molecular basis and biological importance of these observations will need further studies.

To understand the pathway mechanism in more detail, several questions need to be addressed. Not all eight HKs found in the *Arabidopsis* genome encode cytokinin receptors. For example, two HKs encode ethylene receptors, one encodes a putative osmosensor, and another one shows constitutive HK activity when overexpressed (*1*–*4*, *8*, *10*). Their precise roles with respect to cytokinin signaling remain unclear. B-type RRs bind similar cis elements in vitro and induce transcription (*14*). How are they involved in generating tissue- and cell-specific signaling outputs? Do they interact with specific but unknown partners? And what is the molecular mechanism by which A-type RRs attenuate signaling?

Recent findings have added some twists to the pathway. Aside from its kinase function, a cytokinin receptor was found to exhibit phosphatase activity that removes phosphoryl groups from interacting *Arabidopsis* histidine phosphotransfer proteins (AHPs) when no cytokinin is bound. Many prokaryote HKs have such phosphatase activity, and they are associated with phosphorelay systems that need to be shut off quickly. In *Arabidopsis*, the phosphatase activity of this HK may help to ensure that, in the absence of cytokinin, the pathway is quickly and completely inactivated (*15*). One of the six *Arabidopsis* HPTs, AHP6, was identified as a "pseudo-HPT" because of a mutation in the conserved histidine residue required to accept the incoming phosphoryl group from the recep-

Department of Molecular Biology, Massachusetts General Hospital, and Department of Genetics, Harvard Medical School, Boston, MA 02114, USA.

*To whom correspondence should be addressed. E-mail: sheen@molbio.mgh.harvard.edu

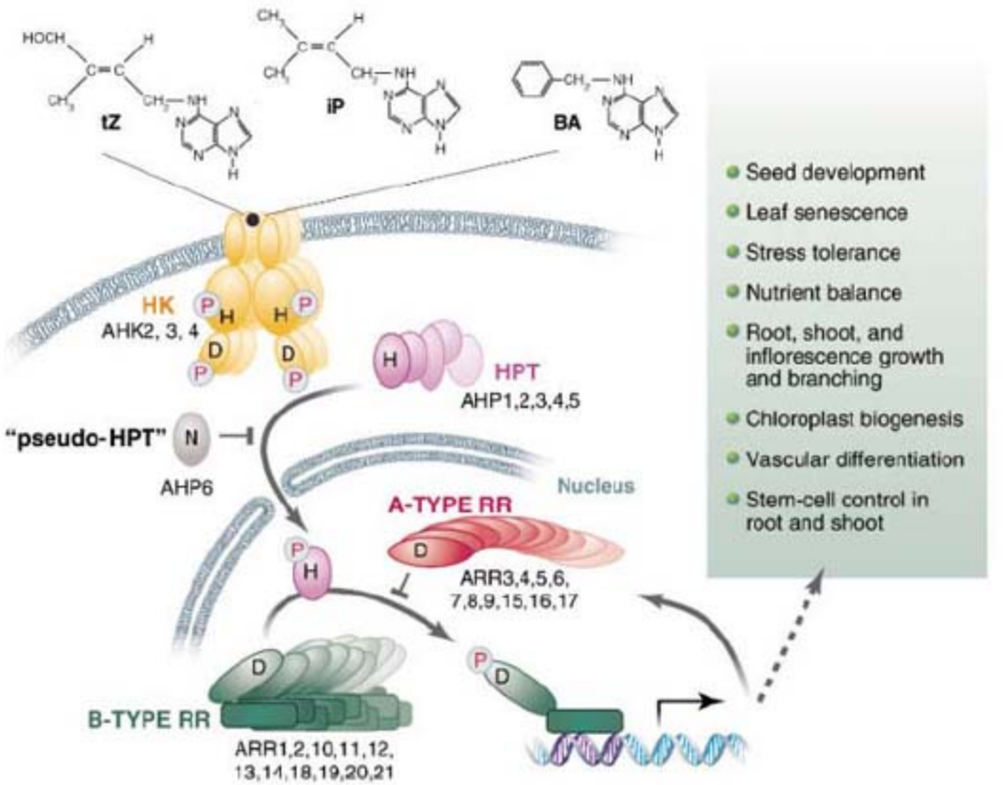

Fig. 1. Model for the cytokinin multistep two-component circuitry through histidine (H), and aspartate (D) phosphorelay, involving histidine-kinase receptors (HK), phosphotransfer proteins (HPT), a "pseudo–HPT" with an asparagine (N) instead of the D, and A-type and B-type RRs. Each signaling step is executed by a family of genes that largely act redundantly, as illustrated. *Arabidopsis* genes implicated in signaling are listed as abbreviations (AHK, *Arabidopsis* histidine kinases; AHP, *Arabidopsis* histidine phosphotransfer proteins; ARR, *Arabidopsis* response regulator). Different effects of cytokinin signaling are indicated on the right. The chemical structure of three cytokinins is shown on top: trans-zeatin (tZ), N^6-(Δ^2-isopentenyl)adenine (iP), and 6-benzylamino purine (BA).

tors. AHP6 inhibits cytokinin signaling, probably by competing with other AHPs for interaction with activated receptors or RRs in *Arabidopsis*. Cytokinin signaling, in turn, represses transcription of *AHP6*. Lack of AHP6 function causes ectopic cytokinin signaling, leading to pattern defects in vascular tissue (*16*). Thus, the presence of AHP6 may limit the number of cells responding to cytokinin and, thereby, may help sharpen and define cell differentiation boundaries.

Plants not only use feedback loops to control cytokinin signaling but selectively allow other factors to influence pathway activity. WUSCHEL, a homeodomain transcription factor required for shoot-stem cell function, directly attenuates transcription of some A-type RR genes, which likely increases cytokinin signaling activity in the shoot-stem cell pool and extends its size (*17*). New transcriptional regulators involved in mediating cytokinin signaling other than the conserved B-type RRs have emerged. Studies of a subset of cytokinin responsive factors (CRFs) have revealed their cytokinin-dependent nuclear translocation. CRFs and B-type RRs share some cytokinin target genes but do not control the most prominent cytokinin-inducible A-type RR genes. The phenotypes of *crf* mutants appear to be complex with both cytokinin-dependent and independent features (*18*).

Is there a common denominator in the seemingly diverse cytokinin responses? Ectopic cytokinin causes cell proliferation and shoot growth in tissue culture. The cell cycle regulator cyclin D3 seems to be an important mediator of this effect. Consistently, cytokinin receptor triple mutants (*2*) or B-type RR triple mutants (*19*) have retarded growth in roots and shoots. However, plants with partially reduced endogenous cytokinin signaling or concentrations display an increase in the size of the root system (*2*, *6*, *20*). A detailed analysis of cytokinin's function in the root supports a role of cytokinin to promote differentiation, which counteracts proliferation (*6*, *20*). One explanation for the opposite effects depending on signaling activity might be that plants with a strong reduction in cytokinin reception and signaling have an impaired vascular system that might limit the potential to grow. It is also possible that different cytokinin threshold levels are required for cell proliferation, elongation, and differentiation (*2*). In fully differentiated leaves, cytokinin's role in inhibiting senescence is unlikely to depend on cell proliferation. Thus, the functions of cytokinin seem to be more diverse and context-dependent than previously anticipated. In accordance with this view, data sets from different microarray experiments aimed at identifying transcriptional targets of cytokinin appear to vary considerably except for their inclusion of the common targets, A-type RR genes. The future challenge is to analyze cytokinin functions at cellular resolution to understand how signaling integrates with the context.

The genetic and molecular characterization of cytokinin signaling began about 10 years ago, and the core signaling circuitry has now been established and verified. However, most functional studies have been based on whole-plant responses to exogenously applied cytokinins. Given the multiple roles and redundancy of the pathway, tailored approaches will be required to study the individual functions of cytokinin in different tissues and cell types at various developmental stages. For example, sensitive cytokinin reporters will facilitate in vivo analyses of the cells that transduce cytokinin signaling. To circumvent redundancy and lethality of classical genetic approaches, inducible transgenes expressing RNA interference constructs, or constitutively active or dominant-negative signaling components, can be used to manipulate the pathway activity in a targeted manner. Understanding how cytokinin signaling integrates with other interacting signals and elucidating its complex biosynthesis pathways and little-known transport systems will bring additional exciting discoveries (*5*). With the increased availability of plant genome sequences and functional analysis systems, it will be interesting to compare the role of phosphorelay signaling among different plant species exhibiting diverse architecture and life cycles and various growth patterns.

References and Notes

1. T. Mizuno, *Curr. Opin. Plant Biol.* **7**, 499 (2004).
2. F. J. Ferreira, J. J. Kieber, *Curr. Opin. Plant Biol.* **8**, 518 (2005).
3. B. Müller, J. Sheen, *Arabidopsis* cytokinin signaling pathway. *Sci. STKE* (Connections Map, as seen October 2007), http://stke.sciencemag.org/cgi/cm/stkecm;CMP_10021.
4. B. Müller, J. Sheen, Cytokinin signaling pathway. *Sci. STKE* (Connections Map, as seen October 2007), http://stke.sciencemag.org/cgi/cm/stkecm;CMP_9724.
5. H. Sakakibara, *Annu. Rev. Plant Biol.* **57**, 431 (2006).
6. T. Werner *et al.*, *Plant Cell* **15**, 2532 (2003).
7. R. Amasino, *Plant Physiol.* **138**, 1177 (2005).
8. T. Kakimoto, *Science* **274**, 982 (1996).
9. T. Inoue *et al.*, *Nature* **409**, 1060 (2001).
10. H. Dortay *et al.*, *FEBS J.* **273**, 4631 (2006).
11. I. Hwang, J. Sheen, *Nature* **413**, 383 (2001).
12. G. A. Romanov, S. N. Lomin, T. Schmülling, *J. Exp. Bot.* **57**, 4051 (2006).
13. H. J. Kim *et al.*, *Proc. Natl. Acad. Sci. U.S.A.* **103**, 814 (2006).
14. H. Sakai, T. Aoyama, A. Oka, *Plant J.* **24**, 703 (2000).
15. A. P. Mähönen *et al.*, *Curr. Biol.* **16**, 1116 (2006).
16. A. P. Mähönen *et al.*, *Science* **311**, 94 (2006).
17. A. Leibfried *et al.*, *Nature* **438**, 1172 (2005).
18. A. M. Rashotte *et al.*, *Proc. Natl. Acad. Sci. U.S.A.* **103**, 11081 (2006).
19. A. Yokoyama *et al.*, *Plant Cell Physiol.* **48**, 84 (2007).
20. R. D. Dello Ioio *et al.*, *Curr. Biol.* **17**, 678 (2007).

10.1126/science.1145461

Odor-Mediated Push-Pull Pollination in Cycads

Irene Terry,[1]* Gimme H. Walter,[2] Chris Moore,[2] Robert Roemer,[3] Craig Hull[2]

Cycads are dioecious gymnosperms, with male and female individuals, of Permian origin. Cycads share obligate mutualisms with specialist insect pollinators, almost universally beetles (*1*). The known exception involves thrips of the genus *Cycadothrips* (*1*, *2*), which participate in obligate pollination mutualisms with endemic Australian *Macrozamia* cycads. *Cycadothrips* are in a basal thysanopteran family, proposed as arising by at least the Cretaceous (*3*). Thrips are primarily found on male cones, which provide food (pollen) for adults and larvae (*2*, *4*). During pollination, male and female *Macrozamia lucida* cones self-heat daily, up to 12°C above ambient temperatures between the hours of ~1100 and 1500, when nearly a million-fold increase in male volatile emissions occurs [females reach ~one-fifth that amount (*4*)]. In concert, adult *Cycadothrips chadwicki* leave male and female cones en masse (movie S1) (*4*), and larvae move to the exterior of their male cone habitat. Pollination is mediated by pollen-laden thrips that enter female cones.

We tested thrips' electrophysiological and behavioral responses to cone volatiles. A two-way choice between male sporophyll volatiles or air in a Y-tube olfactometer (*5*) demonstrated that thrips are attracted (or neutral) to sporophylls early in the day, repelled at midday, and attracted at later times (Fig. 1A). These phases parallel field results; cones retain (morning, low volatile emissions), repel (midday high emissions), and later attract (low emissions) thrips (*4*).

Electrophysiological tests (*5*) with volatiles from cones and their specific chemical components revealed that *Cycadothrips* respond to three components (Fig. 1, B and C): β-myrcene (>90% of total emissions during thermogenesis) and (*E*)-β-ocimene (2%), which change postthermogenesis (*4*, *5*), and allo-ocimene (~2%) (*5*). Y-tube tests at ecological concentrations of these chemicals (*5*) showed that ocimenes attract thrips (fig. S1), whereas β-myrcene attracts thrips at low concentrations but repels them at higher levels (Fig. 1D). When control and high-concentration β-myrcene vessels (*5*) were switched after thrips had entered the control arm, 77% moved directly into the new control arm. Most that remained died within 10 min, suggesting that by leaving cones thrips avoid toxic β-myrcene levels.

These cone volatile changes sufficiently explain the diel thrips behavior observed in situ (*4*), although temperature and light may modulate their effects. We characterize this as a "push-pull" pollination strategy. Flowers are generally portrayed as only "pulling" pollinators via visual or odor cues. Some orchids, though, chemically repel pollinators after pollination (*6*). Driving thrips from male cones increases pollen-laden thrips attendance at female cones, which presumably attract by deceit because their volatile components match those of males (*4*). Parallel attraction to male cones allows thrips to accrue pollen for the next day's cycle. This obligate pollination mutualism stands out for its push-pull behavior and because it involves an ancient gymnosperm lineage and a basal thrips clade (*2*). Floral scent may have originally evolved to deter herbivores (*7*), and this system may represent a conserved early intermediary in the evolution of seed plant pollination.

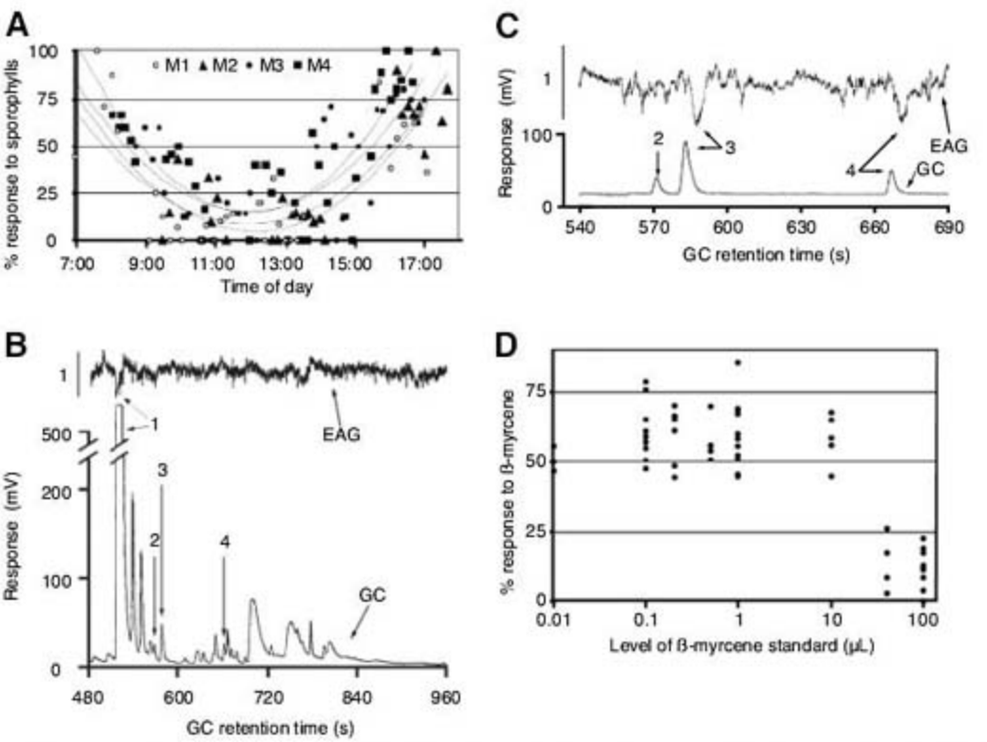

Fig. 1. *Cycadothrips* responses to *M. lucida* volatiles. (**A**) The % of insects going to sporophylls of four mid-pollination-stage male cones (M1 to M4) versus controls (Y-tube tests). Lines are quadratic fits to data from separate cones; fit parameters are not statistically different (*5*). (**B** and **C**) Male thrips physiologically respond [gas chromatography electroantennographic (EAG) detection, GC-EAD] (B) to β-myrcene (peak 1) from male cone volatiles and (C) to (*E*)-β-ocimene (peak 3) and allo-ocimene (peak 4) but not to (*Z*)-β-ocimene (peak 2) from ocimene standard. (**D**) The % of insects attracted to different concentrations of β-myrcene standard versus controls (Y-tube tests).

References and Notes

1. W. Tang, in *Vistas in Palaeobotany and Plant Morphology*, P. Srivastava, Ed. (UP Offset, Lucknow, India, 2004), pp. 383–394.
2. I. Terry *et al.*, *Am. J. Bot.* **92**, 931 (2005).
3. D. Grimaldi, A. Shmakov, N. Fraser, *J. Paleontol.* **78**, 941 (2004).
4. I. Terry *et al.*, *Plant Syst. Evol.* **243**, 233 (2004).
5. Materials and methods are available at *Science* Online.
6. F. Schiestl, M. Ayasse, *Oecologia* **126**, 531 (2001).
7. O. Pellmyr, L. Thien, *Taxon* **35**, 76 (1986).
8. Studies partially supported by National Geographic Society. Thanks to R. Raguso, A. Najar, F. Adler, and anonymous reviewers.

Supporting Online Material

www.science.org/cgi/content/full/318/5847/70/DC1
Materials and Methods
Fig. S1
Movie S1

15 May 2007; accepted 27 August 2007
10.1126/science.1145147

[1]Department of Biology, University of Utah, Salt Lake City, UT 84112, USA. [2]The School of Integrative Biology, University of Queensland, Brisbane, QLD 4072, Australia. [3]Department of Mechanical Engineering, University of Utah, Salt Lake City, UT 84112, USA.

*To whom correspondence should be addressed. E-mail: terry@biology.utah.edu

A Neuroligin-3 Mutation Implicated in Autism Increases Inhibitory Synaptic Transmission in Mice

Katsuhiko Tabuchi,[1] Jacqueline Blundell,[2] Mark R. Etherton,[1] Robert E. Hammer,[3] Xinran Liu,[1] Craig M. Powell,[2,4] Thomas C. Südhof[1,5,6]*

Autism spectrum disorders (ASDs) are characterized by impairments in social behaviors that are sometimes coupled to specialized cognitive abilities. A small percentage of ASD patients carry mutations in genes encoding neuroligins, which are postsynaptic cell-adhesion molecules. We introduced one of these mutations into mice: the Arg^{451}→Cys^{451} (R451C) substitution in neuroligin-3. R451C mutant mice showed impaired social interactions but enhanced spatial learning abilities. Unexpectedly, these behavioral changes were accompanied by an increase in inhibitory synaptic transmission with no apparent effect on excitatory synapses. Deletion of neuroligin-3, in contrast, did not cause such changes, indicating that the R451C substitution represents a gain-of-function mutation. These data suggest that increased inhibitory synaptic transmission may contribute to human ASDs and that the R451C knockin mice may be a useful model for studying autism-related behaviors.

Autism is a widespread cognitive disorder characterized by impairments in social interactions, including verbal communication and social play, and can be accompanied by stereotyped patterns of behavior (*1–3*). Autism is a heterogeneous condition, prompting the designation of ASDs. Individuals with ASDs occasionally show enhanced cognitive abilities [autistic savant syndrome (*4*)]. At the other end of the spectrum, ASDs are often associated with mental retardation, and the symptoms of ASDs are part of several neurological diseases, such as fragile X and Rett syndromes (*5–7*). Genetics strongly contributes to ASDs (*1*, *2*), and a small number of cases with idiopathic ASD are associated with mutations in a single gene, including genes encoding neuroligins and their associated proteins (*8*).

Neuroligins are a family of postsynaptic cell-adhesion molecules that are ligands (or receptors, depending on the perspective) for neurexins, another class of synaptic cell-adhesion molecules (*9*, *10*). Humans express five neuroligins, including neuroligin-3, an X-chromosomal gene that undergoes regular X inactivation, and neuroligin-4 and -5, which are encoded by a pair of pseudoautosomal genes on the X and Y chromosomes (*11*). Mice express close homologs to human neuroligin-1, -2, and -3 (*9*) and a fourth isoform that appears to be more distantly related to other neuroligins (GenBank accession number EF692521) (*11*). Neuroligin-1 and -2 are differentially localized to excitatory or inhibitory synapses (*12–14*). Overexpression of neuroligins in transfected neurons increases synapse numbers and the frequency of spontaneous synaptic events (*15–20*). Consistent with their localizations, overexpression of neuroligin-1 enhances only excitatory synaptic transmission, whereas overexpression of neuroligin-2 enhances only inhibitory synaptic transmission

[1]Department of Neuroscience, University of Texas Southwestern Medical Center, Dallas, TX 75390, USA. [2]Department of Neurology, University of Texas Southwestern Medical Center, Dallas, TX 75390, USA. [3]Department of Biochemistry, University of Texas Southwestern Medical Center, Dallas, TX 75390, USA. [4]Department of Psychiatry, University of Texas Southwestern Medical Center, Dallas, TX 75390, USA. [5]Department of Molecular Genetics, University of Texas Southwestern Medical Center, Dallas, TX 75390, USA. [6]Howard Hughes Medical Institute, University of Texas Southwestern Medical Center, Dallas, TX 75390, USA.

*To whom correspondence should be addressed. E-mail: thomas.sudhof@utsouthwestern.edu

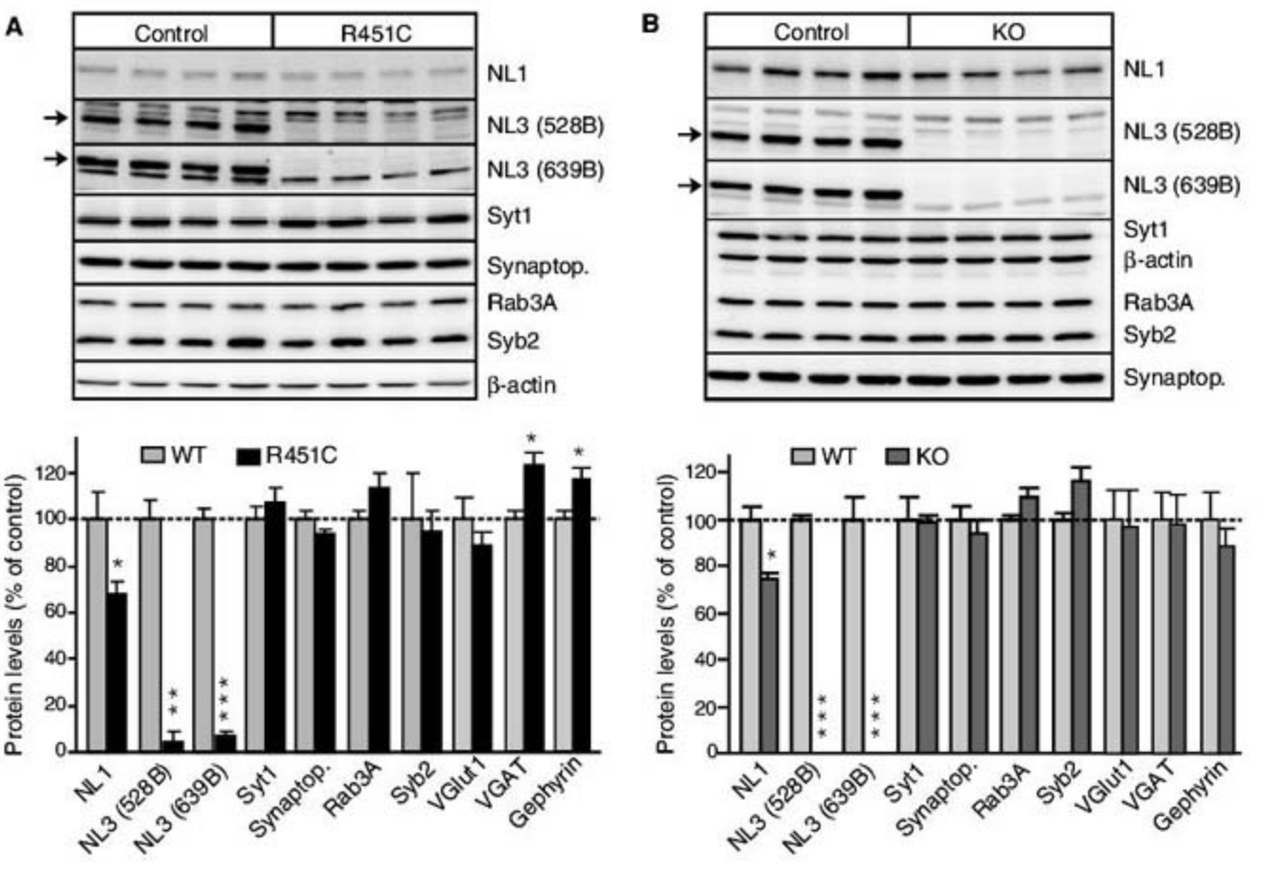

Fig. 1. Generation and characterization of neuroligin-3 R451C KI and neuroligin-3 KO mice. (**A** and **B**) Representative immunoblots and summary graphs of protein levels in the brains of neuroligin-3 R451C KI mice (A) and neuroligin-3 KO mice (B). Selected synaptic proteins (NL1, neuroligin-1; NL3, neuroligin-3; Synaptop., synaptophysin; Syt1, synaptotagmin-1; and Syb2, synaptobrevin-2) were analyzed by quantitative immunoblotting; two different neuroligin-3 antibodies were used (528B and 639B; arrows point to neuroligin-3 band; data shown are means ± SEMs; $n = 4$ littermate pairs; $^*P < 0.05$; $^{**}P < 0.01$; $^{***}P < 0.005$ by Student's t test).

(*20*). Deletion of neuroligin-1 or -2 in mice causes corresponding selective decreases in excitatory or inhibitory synaptic transmission, respectively, but no significant synapse loss, whereas neuroligin-3 has not been examined (*11*, *21*).

Missense and nonsense mutations in neuroligin-3 and -4 have been identified in a subset of human patients with ASDs (*22*–*24*). One of these mutations, the Arg^{451}→Cys^{451} (R451C) substitution in neuroligin-3, alters a conserved residue in the extracellular esterase-homology domain of neuroligin-3 (*22*). In transfected neurons, the R451C substitution causes partial retention of neuroligin-3 in the endoplasmic reticulum but does not abolish its ability to promote synapse formation (*20*, *25*, *26*). In addition, an internal deletion in the gene encoding neurexin-1 that interacts with neuroligins was connected to ASDs (*27*), and three different nonsense mutations in Shank3, an intracellular binding partner for neuroligins, were also found in patients with ASDs (*28*). Thus, in rare instances mutations in three gene families that encode neuroligins or their interacting proteins are associated with familial idiopathic ASDs.

An increase in inhibitory synapse markers in R451C mutant mice. Autism is thought to arise from functional changes in neural circuitry and to be associated with an imbalance between excitatory and inhibitory synaptic transmission, but the mechanisms involved are unknown (*29*). To investigate possible mechanisms, we introduced the R451C substitution into the endogenous neuroligin-3 gene in mice by gene targeting, generating R451C knockin (KI) mice (fig. S1) (*30*). Moreover, to test whether the R451C substitution represents a gain- or a loss-of-function change, we also analyzed neuroligin-3 knockout (KO) mice (fig. S1). Because the neuroligin-3 gene is X-chromosomal, we performed analyses on male offspring derived from matings of a heterozygous female with a wild-type (WT) male mouse. Neuroligin-3 R451C KI and neuroligin-3 KO mice were viable and fertile and exhibited no obvious abnormalities or premature mortality (fig. S2) (*11*).

We first analyzed the amounts of neuroligin-3 and of other synaptic proteins in neuroligin-3 R451C KI and KO mice. The R451C substitution caused a decrease in neuroligin-3 of ~90% in forebrain as measured by quantitative immunoblotting with two different antibodies, whereas the KO caused a complete loss of neuroligin-3 (Fig. 1). In addition, we observed a small decrease in neuroligin-1 in both the KI and the KO mice and a significant increase in the levels of two markers for inhibitory synapses [the vesicular γ-aminobutyric acid (GABA) transporter VGAT and the postsynaptic protein gephyrin] in the KI mice, whereas no increases in VGAT or gephyrin levels were detected in the KO mice (Fig. 1). No significant change in the levels of other proteins examined were observed, in par-

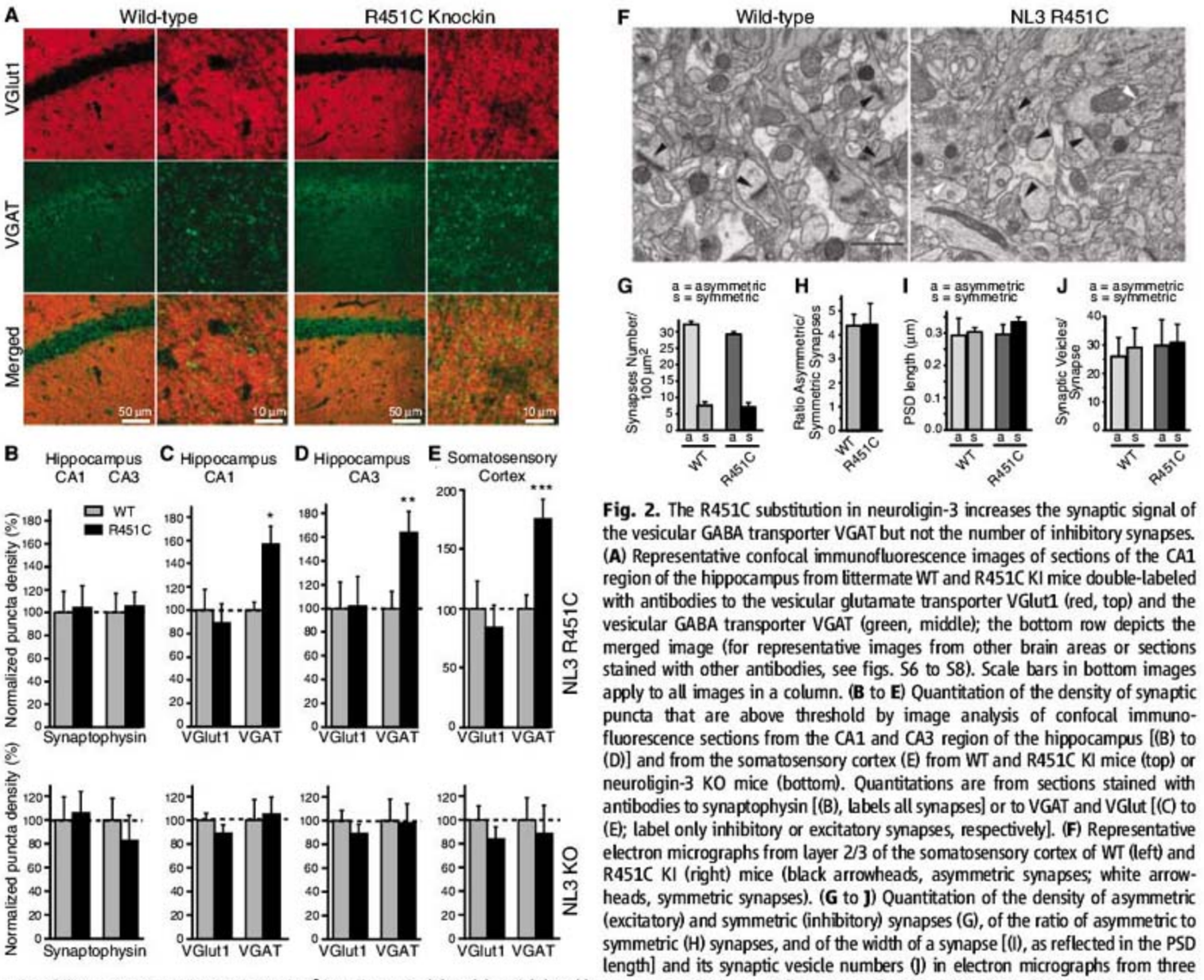

Fig. 2. The R451C substitution in neuroligin-3 increases the synaptic signal of the vesicular GABA transporter VGAT but not the number of inhibitory synapses. (**A**) Representative confocal immunofluorescence images of sections of the CA1 region of the hippocampus from littermate WT and R451C KI mice double-labeled with antibodies to the vesicular glutamate transporter VGlut1 (red, top) and the vesicular GABA transporter VGAT (green, middle); the bottom row depicts the merged image (for representative images from other brain areas or sections stained with other antibodies, see figs. S6 to S8). Scale bars in bottom images apply to all images in a column. (**B** to **E**) Quantitation of the density of synaptic puncta that are above threshold by image analysis of confocal immunofluorescence sections from the CA1 and CA3 region of the hippocampus [(B) to (D)] and from the somatosensory cortex (E) from WT and R451C KI mice (top) or neuroligin-3 KO mice (bottom). Quantitations are from sections stained with antibodies to synaptophysin [(B), labels all synapses] or to VGAT and VGlut [(C) to (E); label only inhibitory or excitatory synapses, respectively]. (**F**) Representative electron micrographs from layer 2/3 of the somatosensory cortex of WT (left) and R451C KI (right) mice (black arrowheads, asymmetric synapses; white arrowheads, symmetric synapses). (**G** to **J**) Quantitation of the density of asymmetric (excitatory) and symmetric (inhibitory) synapses (G), of the ratio of asymmetric to symmetric (H) synapses, and of the width of a synapse [(I), as reflected in the PSD length] and its synaptic vesicle numbers (J) in electron micrographs from three pairs of littermate WT and R451C KI mice [data shown in (B) to (E) and (G) to (J) are means ± SEMs; $n = 3$ littermate pairs; $^*P < 0.05$; $^{**}P < 0.01$; $^{***}P < 0.005$ by Student's t test]. PSD, postsynaptic density.

ticular no change in the levels of the vesicular glutamate transporter or other proteins characteristic of excitatory synapses (Fig. 1 and figs. S3 and S4) (*30*). These data suggest that the neuroligin-3 R451C KI and KO did not cause a global change in the molecular composition of the brain, except for a small increase in inhibitory markers in the KI but not the KO mice.

The decreased concentrations of R451C mutant neuroligin-3 could be due to a destabilization of the mutant protein. Alternatively, because the construction of the R451C KI mice involved the introduction of loxP and frt recombination sites into the neuroligin-3 gene intron, it is possible that the genetic manipulation may have impaired expression of neuroligin-3. To differentiate between these two possibilities, we measured the messenger RNA (mRNA) levels of neuroligin-3 in WT and R451C KI mice by using quantitative reverse transcription polymerase chain reaction (RT-PCR) but detected no decrease of the neuroligin-3 mRNA in the mutant mice (fig. S5). These data indicate that the R451C substitution destabilizes neuroligin-3, consistent with the retention of R451C mutant neuroligin-3 in the endoplasmic reticulum observed in transfection studies (*20*, *25*).

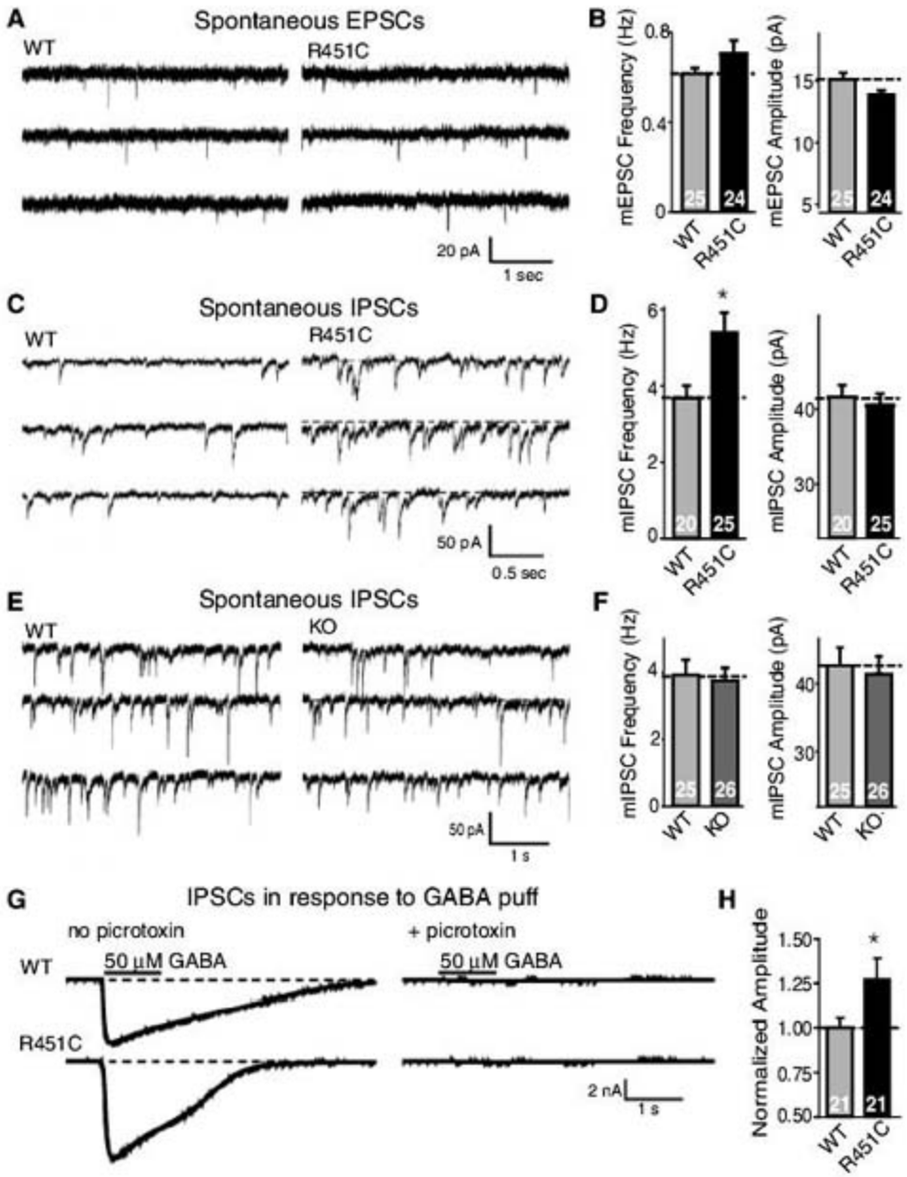

Fig. 3. Neuroligin-3 R451C KI but not neuroligin-3 KO mice exhibit increased spontaneous inhibitory synaptic transmission. Recordings were performed in whole-cell patch-clamp mode in pyramidal neurons in layer 2/3 of the somatosensory cortex in acute slices. Representative traces (**A**, **C**, and **E**) and summary graphs of the amplitudes and frequency (**B**, **D**, and **F**) of spontaneous miniature excitatory postsynaptic currents [mEPSCs; (A) and (B)] and inhibitory postsynaptic currents [mIPSCs; (C) and (D)] from R451C KI [(A) to (D)] or KO mice [(E) and (F)]. (**G** and **H**) Representative traces (G) and summary graph for response to a locally applied GABA puff (50 μM injected at 5 psi for 1 s) in layer 2/3 of the somatosensory cortex. In (G), responses are also shown in the presence of 50 μM picrotoxin to document their inhibitory nature (data shown are means ± SEMs; $n = 3$ littermate pairs; total number of cells recorded are indicated within bars; $^{*}P < 0.05$; $^{**}P < 0.01$; $^{***}P < 0.005$ by Student's t test; all electrophysiological parameters are listed in table S1).

We next examined the R451C mutant brains morphologically but failed to detect a major change in brain architecture (fig. S6). We then measured the intensity of synapse staining by using antibodies to synaptic vesicle proteins. We stained cryostat sections from the somatosensory cortex and from the CA1 and CA3 regions of the hippocampus with antibodies to synaptophysin, a general marker of all synapses, and to the vesicular glutamate transporter VGlut1 and the vesicular GABA transporter VGAT, markers of excitatory and inhibitory synapses, respectively. The staining patterns observed were characteristic for the excitatory and inhibitory synapses in these brain regions, but the intensity for VGAT staining appeared to be brighter in R451C KI mice than in control or in KO mice (Fig. 2A and figs. S7 and S8). To test this, we used an image analysis that estimates the number and size of puncta labeled with the various antibodies above a defined threshold value applied to all images (Fig. 2, B to E, and figs. S7 and S8). We observed a dramatic increase in the number of VGAT-positive puncta in the R451C KI mice in all three brain regions analyzed (50 to 80% increase). In contrast, the number of VGlut1- or synaptophysin-positive puncta above threshold was unchanged, and the average size of the puncta was also not altered for any of the three antibodies (Fig. 2, B to E, and figs. S7 and S8) (*30*). Moreover, no increase in the density of VGAT-positive puncta was detected in the neuroligin-3 KO mice (Fig. 2, B to E).

The increased number of VGAT-positive puncta above threshold in the R451C KI mice could be due to an increase in inhibitory synapse numbers or a shift in the distribution of VGAT, such that more synapses contain a high concentration of the transporter. To differentiate between these two possibilities, we examined the number and structure of synapses in layer 2/3 of the somatosensory cortex by electron microscopy but detected no major change in synapse number of structure (Fig. 2, F to J). Thus, the R451C substitution does not increase synapse formation but appears to act at a step downstream of synapse formation to increase the average VGAT signal per synapse. This conclusion is also consistent with the fact that neuroligin deletions in general have not been found to alter synapse numbers but instead selectively impair synaptic strength (*11*, *21*).

Inhibitory synaptic strength is increased in neuroligin-3 R451C KI but not KO mice. We measured synaptic function in the R451C KI mice with whole-cell recordings in layer 2/3 of the somatosensory (barrel) cortex in acute slices. Examination of spontaneous synaptic "mini" events (Fig. 3, A to D) uncovered no significant change in the frequency or size of excitatory events but detected a ~50% increase in the frequency of spontaneous inhibitory events. No change in the amplitude of spontaneous inhibitory events was detected. To determine whether the increased frequency of spontaneous

inhibitory synaptic events is due to the loss of neuroligin-3 induced by the R451C substitution (Fig. 1) or reflects a specific action of the mutant protein, we measured the frequency and size of spontaneous inhibitory mini events in neuroligin-3 KO mice (Fig. 3E). Neuroligin-3 KO mice exhibited no increase in the frequency of spontaneous inhibitory mini events (Fig. 3F).

The selective increase of spontaneous inhibitory events in R451C KI mice agrees with the increase in the levels of inhibitory synaptic proteins (Fig. 1) and the number of inhibitory synapses with VGAT signals above threshold (Fig. 2), suggesting that inhibitory synaptic transmission may be enhanced by the R451C substitution. Consistent with this hypothesis, the amplitude of the response to exogenous GABA puffed onto neurons in layer 2/3 of the somatosensory cortex significantly increased (Fig. 3, G and H).

We next investigated synaptic strength by measuring input/output curves of evoked synaptic responses. We detected no difference in excitatory responses between WT and R451C KI mice but observed a significant increase in inhibitory responses (~50%) (Fig. 4, A, B, D, and E). Measurements in neuroligin-3 KO mice, by contrast, uncovered no change in inhibitory responses but detected a small, although insignificant, decrease in excitatory responses (Fig. 4, C and F, and fig. S9). This result confirms the finding made in the spontaneous synaptic measurements that the neuroligin-3 R451C KI but not the KO causes a selective increase in inhibitory synaptic transmission. Consistent with the postsynaptic localization of neuroligins (*12*), we found that the short-term synaptic plasticity properties of inhibitory synapses in neuroligin-3 R451C KI or KO brains did not exhibit a major change (figs. S10 to S12).

Neuroligin-3 R451C KI mice exhibit impaired social behaviors but enhanced spatial learning abilities. To determine whether the changes in synaptic transmission in R451C KI mice produce behavioral impairments, we first tested the mice for global behavioral changes and detected no changes in locomotor activity, motor coordination, and anxiety-related behaviors in R451C KI mice with a series of tests [dark/light box, open field, novel home cage activity, rotarod, open field arena, and elevated plus maze (fig. S13)].

We next investigated whether R451C KI mice display abnormal social behaviors. R451C KI mice showed no change in the time of interaction with a novel inanimate object. However, the KI mice exhibited a small but significant decrease in interaction with a novel caged adult target mouse compared with interactions of WT littermate controls, indicating a social interaction deficit (Fig. 5, A and B). Similarly, in a test for social versus inanimate preference, R451C KI mice spent significantly less time interacting with a social target than did the WT littermate controls (Fig. 5C). In agreement with a selective effect on social behavior, R451C KI mice spent the same amount of time interacting with an inanimate target as controls during this task. However, when placed into a neutral home cage with a freely moving conspecific juvenile target mouse

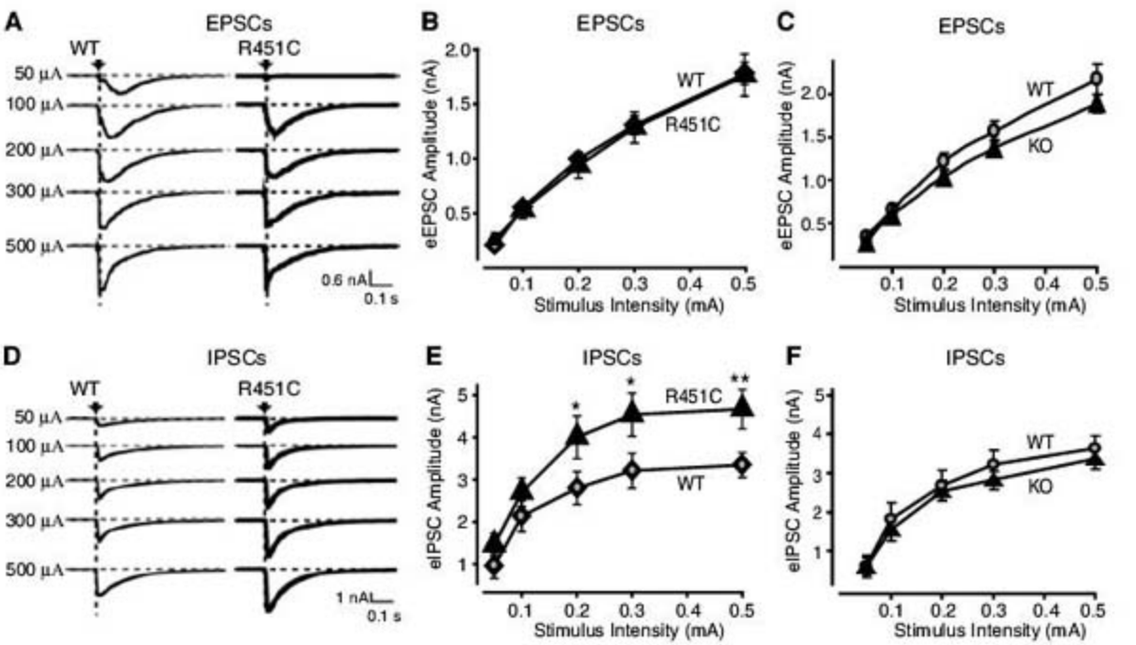

Fig. 4. Selective increase in inhibitory synaptic strength in neuroligin-3 R451C KI but not in neuroligin-3 KO mice. Representative traces (**A** and **D**) and summary graphs (**B**, **C**, **E**, and **F**) of synaptic responses induced with increasing stimulus intensities applied with a local microelectrode in acute slices of the somatosensory cortex from littermate pairs of R451C KI mice [(A), (B), (D), and (E)] or KO mice [(C) and (F)]. Recordings were obtained in the whole-cell mode in layer 2/3. EPSCs [(A) to (C)] and IPSCs [(D) to (F)] were analyzed separately after pharmacological isolation. In (A) and (D), arrows and vertical dashed lines indicate peaks measured for determining evoked response amplitude. Dotted horizontal lines represent baselines. All data were recorded in acute slices from littermate R451C mutant and WT mice [data shown are means ± SEMs; $n = 4$ or 3 littermate pairs for EPSCs (KI or KO) and 5 or 3 littermate pairs for IPSCs (KI or KO); $^{*}P < 0.05$; $^{**}P < 0.01$ by t test]. For representative traces from the KO mice, see fig. S9; for short-term plasticity measurements in KI and KO mice, see figs. S10 to S13.

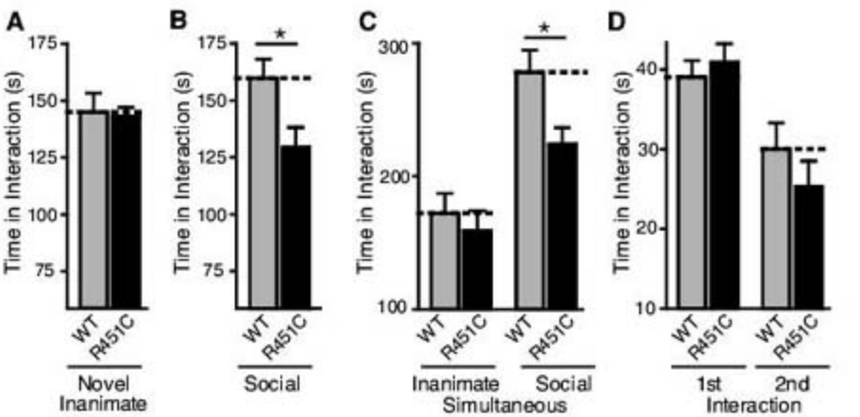

Fig. 5. Impaired social interaction behaviors in neuroligin-3 R451C KI mice. (**A**) Interacting time of individual WT and R451C KI mice exposed to a novel inanimate object in an unfamiliar cage (5 min). (**B**) Interacting times of mice that are exposed to an unfamiliar immobilized target mouse in a now-familiar cage [5 min; procedure immediately follows (A)]. (**C**) Interacting times of mice that are exposed simultaneously to a novel inanimate object and a novel, caged target mouse. (**D**) Social learning measured by monitoring the times of direct interactions of WT and R451C KI mice with the same freely moving juvenile target mouse on day 1 (first interaction) and day 4 (second interaction for social learning). All data shown are means ± SEMs; $n = 19$ male littermate pairs; only statistically significant differences between WT and R451C KI mice are specifically identified in the figure ($^{*}P < 0.05$; $^{**}P < 0.01$; $^{***}P < 0.001$ by t test or two-way analysis of variance); a detailed statistical analysis for all parameters is provided in table S2 (*30*).

for 2 min, R451C mutant and WT littermate control mice interacted similarly with the target mouse, presumably because in this test the target mouse initiates the interaction as much as the test mouse, potentially masking social interaction deficits of the test mouse (Fig. 5D). When re-exposed to the same juvenile 3 days later, both the control and the R451C KI mice exhibited a significant decrease in social interaction compared with the initial interaction, demonstrating that the mutant mice recognize the familiar juvenile mouse and are capable of social learning.

Individuals with ASDs exhibit impaired social abilities but can display normal or, rarely, even enhanced cognitive abilities (*1*–*4*). To examine whether the selective decrease in social interactions in R451C KI mice is associated with a gain or a loss of other cognitive abilities, we tested spatial learning and memory in R451C KI mice by using the Morris water maze. R451C KI mice learned to locate and mount a visible platform as well as WT littermate control mice did, indicating that basic neurological functions required for swimming, vision, etc. were intact. When the platform was hidden, the R451C KI mice exhibited a significantly enhanced ability to locate the platform (Fig. 6A) and required fewer days of training to learn the location of the platform (Fig. 6B). During the probe trial 24 hours after the seventh day of training, both WT and R451C KI mice displayed a significant preference for the target versus the opposite quadrant, but the R451C KI mice crossed the precise former location of the target platform almost twice as often as their WT littermate controls (Fig. 6B and fig. S14).

To ensure that the increase in number of target location crossings in the R451C KI mice during the probe trial was due to enhanced spatial memory rather than perseveration, we reversed the location of the platform and retrained the same cohort of mice (so-called reversal training). Again, R451C KI mice exhibited a significantly enhanced learning curve during (Fig. 6D) and required fewer days of training to learn the location of the platform (Fig. 6E). Twenty-four hours after the final reversal training day, R451C KI mice displayed enhanced spatial memory during the probe trial. R451C KI mice showed a significant preference for the new target quadrant and spent significantly more time in the target quadrant than did WT littermate control mice (Fig. 6F). Similarly, R451C KI mice crossed the new target location more often than control mice did and exhibited a significant preference for the target location over all other locations, unlike WT mice (Fig. 6F and fig. S14), suggesting that they have an increased ability for spatial learning and memory.

Summary. The phenotype of neuroligin-3 R451C KI mice suggests that this mouse may facilitate for a mechanistic analysis of the pathogenesis of idiopathic ASDs and provide a possible model system to search for more effective treatments for ASDs. We found that the R451C substitution increases inhibitory synaptic transmission without affecting excitatory synaptic transmission and simultaneously impairs social behaviors while selectively enhancing spatial learning abilities. These findings are surprising because ASDs were thought to be associated with a loss of inhibitory drive (*29*, *31*), although a Rett syndrome mouse model also exhibits an increase in synaptic inhibitory drive (*32*). The R451C substitution increases inhibitory synapse markers, spontaneous inhibitory event frequency, and the size of inhibitory synaptic responses but does not change short-term synaptic plasticity of inhibitory synapses (Figs. 1 to 3 and figs. S7 and S8), suggesting that the mutation enhances inhibitory synaptic transmission without changing the release probability of these synapses. Thus, our results not only validate the hypothesis that neuroligins act at synapses to specify synaptic properties (*20*, *33*) but also indicate that interfering with the function of a neuroligin alters the excitatory/inhibitory balance in vivo. Moreover, if the mouse model mimics the situation in humans with ASDs, it may be possible to ameliorate autism-related behavioral abnormalities by using attenuation of inhibitory synaptic transmission.

How does the R451C mutation increase inhibitory synaptic transmission? A facile explanation would have been that the destabilization of neuroligin-3 by the R451C substitution (*25*) and the resulting loss of neuroligin-3 protein produces a loss-of-function of neuroligin-3, which then causes the phenotype. However, our analysis of the neuroligin-3 KO mice rules out this explanation. Although only ~10% of the neuroligin-3 protein remains in the R451C KI mice, this remaining neuroligin-3 protein produces increased inhibitory synaptic transmission, whereas the complete neuroligin-3 KO exerts no such effect. Thus, the R451C substitution likely acts as a gain-of-function mutation, a hypothesis that also explains why no loss-of-function neuroligin-3 mutation was found in humans with ASDs, whereas several loss-

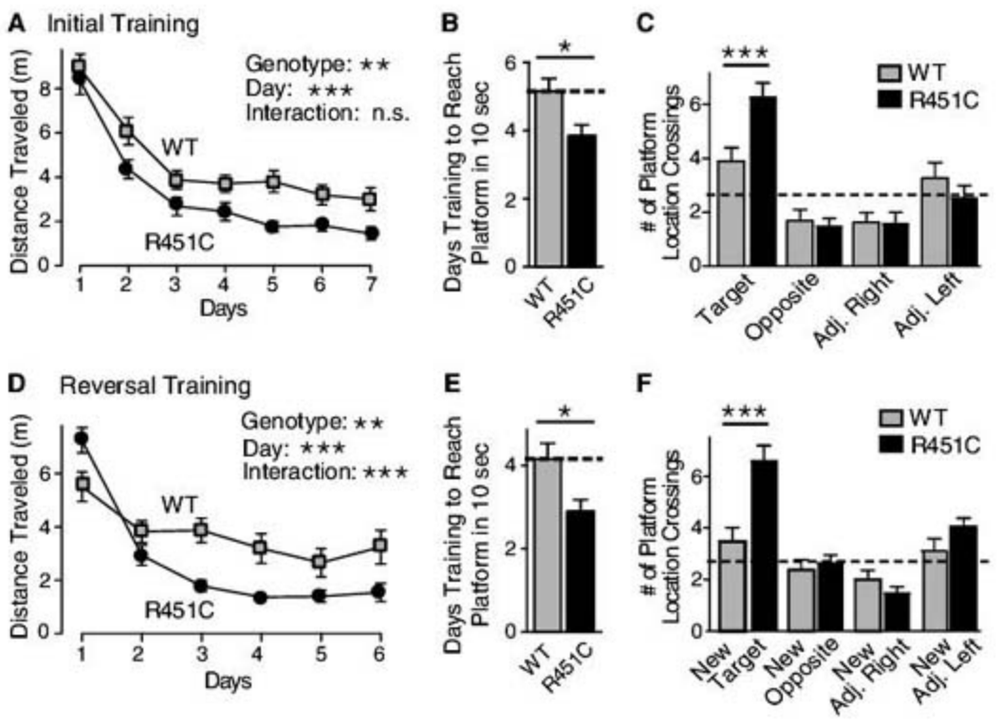

Fig. 6. Neuroligin-3 R451C KI mice exhibit enhanced spatial learning. **(A)** Morris water maze analysis of spatial learning in R451C KI and littermate WT control mice during the initial 7 days of training as measured by the distance traveled to reach a submerged platform [n. s., not significant; $*P < 0.05$; $**P < 0.01$; $***P < 0.001$; in (A) and (D), Genotype indicates main effect of genotype; Day, main effect of day of training; and Interaction, interaction between genotype and day.] **(B)** Number of days of initial training required to reach the submerged platform in an average of 10 s or less. **(C)** Number of crossings over the previous location of the target platform and over corresponding locations in the other three quadrants measured on day 8 after removal of the platform (probe trial). **(D)** Reversal learning experiment, in which on day 9 after the probe trial the platform was moved to the opposite quadrant and the learning of the new location of the platform by the mice was monitored. Learning is measured as distance traveled before mounting the newly localized target platform as a function of days of training. **(E)** Number of days of reversal training required to reach the submerged platform in an average of 10 s or less. **(F)** Probe trial after reversal learning uncovers a large increase in spatial learning abilities of the R451C KI mice [dashed lines in (C) and (F) are the mean overall numbers of platform crossings for WT mice]. Only statistically significant differences between WT and R451C KI mice are identified. All data shown are means ± SEMs; $n = 19$ male littermate pairs; see fig. S14 and table S2 for all statistical comparisons.

of-function mutations were found in neuroligin-4 in such individuals (*22*–*24*).

Our data strongly support the notion that a change in the inhibitory/excitatory balance contributes to the pathogenesis of ASDs. Such a change may alter oscillatory rhythms in brain (*34*, *35*). Given the relatively focused nature of behavioral abnormalities in the R451C KI mice and in some humans with idiopathic ASDs, it is likely that this change is not global but selectively affects only a subset of the many classes of inhibitory interneurons in the forebrain [reviewed in (*36*, *37*)], a question that can now be addressed with the R451C KI mice.

References and Notes

1. D. H. Geschwind, P. Levitt, *Curr. Opin. Neurobiol.* **17**, 103 (2007).
2. A. M. Persico, T. Bourgeron, *Trends Neurosci.* **29**, 349 (2006).
3. American Psychiatric Association, *Diagnostic and Statistical Manual of Mental Disorders: DSM IV* (American Psychiatric Publishing, Arlington, VA, ed. 4, 2002).
4. N. O'Connor, B. Hermelin, *Br. J. Psychol.* **80**, 97 (1989).
5. P. Moretti, H. Y. Zoghbi, *Curr. Opin. Genet. Dev.* **16**, 276 (2006).
6. M. K. Belmonte, T. Bourgeron, *Nat. Neurosci.* **9**, 1221 (2006).
7. S. O. Moldin, J. L. Rubenstein, S. E. Hyman, *J. Neurosci.* **26**, 6893 (2006).
8. K. Garber, *Science* **317**, 190 (2007).
9. K. Ichtchenko, T. Nguyen, T. C. Südhof, *J. Biol. Chem.* **271**, 2676 (1996).
10. Y. A. Ushkaryov, A. G. Petrenko, M. Geppert, T. C. Südhof, *Science* **257**, 50 (1992).
11. F. Varoqueaux *et al.*, *Neuron* **51**, 741 (2006).
12. J.-Y. Song, K. Ichtchenko, T. C. Südhof, N. Brose, *Proc. Natl. Acad. Sci. U.S.A.* **96**, 1100 (1999).
13. E. R. Graf, X. Zhang, S. X. Jin, M. W. Linhoff, A. M. Craig, *Cell* **119**, 1013 (2004).
14. F. Varoqueaux, S. Jamain, N. Brose, *Eur. J. Cell Biol.* **83**, 449 (2004).
15. O. Prange, T. P. Wong, K. Gerrow, Y. T. Wang, A. El-Husseini, *Proc. Natl. Acad. Sci. U.S.A.* **101**, 13915 (2004).
16. A. Boucard, A. A. Chubykin, D. Comoletti, P. Taylor, T. C. Südhof, *Neuron* **48**, 229 (2005).
17. C. I. Nam, L. Chen, *Proc. Natl. Acad. Sci. U.S.A.* **102**, 6137 (2005).
18. K. Futai *et al.*, *Nat. Neurosci.* **10**, 186 (2007).
19. B. Chih, S. K. Afridi, L. Clark, P. Scheiffele, *Hum. Mol. Genet.* **13**, 1471 (2004).
20. J. N. Levinson *et al.*, *J. Biol. Chem.* **280**, 17312 (2005).
21. A. A. Chubykin *et al.*, *Neuron* **54**, 919 (2007).
22. S. Jamain *et al.*, *Nat. Genet.* **34**, 27 (2003).
23. F. Laumonnier *et al.*, *Am. J. Hum. Genet.* **74**, 552 (2004).
24. J. Yan *et al.*, *Mol. Psychiatry* **10**, 329 (2005).
25. D. Comoletti *et al.*, *J. Neurosci.* **24**, 4889 (2004).
26. A. A. Chubykin *et al.*, *J. Biol. Chem.* **280**, 22365 (2005).
27. P. Szatmari *et al.*, *Nat. Genet.* **39**, 319 (2007).
28. C. M. Durand *et al.*, *Nat. Genet.* **39**, 25 (2007).
29. J. L. Rubenstein, M. M. Merzenich, *Genes Brain Behav.* **2**, 255 (2003).
30. Materials and methods are available on *Science* Online.
31. J. P. Hussman, *J. Autism Dev. Disord.* **31**, 247 (2001).
32. V. S. Dani *et al.*, *Proc. Natl. Acad. Sci. U.S.A.* **102**, 12560 (2005).
33. K. Ichtchenko *et al.*, *Cell* **81**, 435 (1995).
34. P. J. Uhlhaas, W. Singer, *Neuron* **52**, 155 (2006).
35. G. Buzsáki, A. Draguhn, *Science* **304**, 1926 (2004).
36. G. Silberberg, S. Grillner, F. E. LeBeau, R. Maex, H. Markram, *Trends Neurosci.* **28**, 541 (2005).
37. P. Somogyi, T. Klausberger, *J. Physiol.* **562**, 9 (2005).

38. We thank I. Kornblum, J. Mitchell, L. Fan, J. Cormier, and A. Roth for technical support. Supported by grants from the National Institute of Mental Health (R37 MH52804-08 to T.C.S. and K08 MH065975-04 to C.M.P.) and from Autism Speaks (to C.M.P.).

Supporting Online Material

www.sciencemag.org/cgi/content/full/1146221/DC1
Materials and Methods
Figs. S1 to S14
Tables S1 and S2
References

7 June 2007; accepted 23 August 2007
Published online 6 September 2007;
10.1126/science.1146221
Include this information when citing this paper.

REPORTS

Polymer Gate Dielectric Surface Viscoelasticity Modulates Pentacene Transistor Performance

Choongik Kim, Antonio Facchetti,* Tobin J. Marks*

Nanoscopically confined polymer films are known to exhibit substantially depressed glass transition temperatures (T_g's) as compared to the corresponding bulk materials. We report here that pentacene thin films grown on polymer gate dielectrics at temperatures well below their bulk T_g's exhibit distinctive and abrupt morphological and microstructural transitions and thin-film transistor (TFT) performance discontinuities at well-defined growth temperatures. The changes reflect the higher chain mobility of the dielectric in its rubbery state and are independent of dielectric film thickness. Optimization of organic TFT performance must recognize this fundamental buried interface viscoelasticity effect, which is detectable in the current-voltage response.

Organic thin-film transistors (OTFTs) have attracted considerable attention as the central components of "printed" electronics (*1*–*3*). Moreover, OTFT performance can be substantially enhanced by manipulating the semiconductor/dielectric interfacial properties via optimizing the gate dielectric (*4*–*7*). To this end, polymer dielectrics are ideal because of their diverse properties, favorable film-forming characteristics, and tunable surface chemistry for the control of device-critical interfacial trap state densities (*8*–*10*). However, whether polymer dielectric chain dynamics affect organic semiconductor growth and OTFT current-voltage (*I-V*) response has remained unclear.

The glass transition temperature (T_g) of amorphous polymers provides a qualitative measure of chain motion (*11*–*13*). At temperatures below T_g, polymers are in a glassy state with little cooperative chain motion, whereas above T_g, polymers enter a rubbery state having substantial chain motion. Relative to bulk materials, T_g is depressed in ultrathin films (*14*) and in nanoscale pores (*15*). The extent of T_g depression depends on the polymer film thickness and substrate/polymer interactions, as characterized by ellipsometry (*16*), dielectric relaxation spectroscopy (*17*), Brillouin scattering (*18*), and fluorescence spectroscopy (*19*). For extensively studied polystyrene (PS) films on Si or SiO_2 substrates, the empirical Eq. 1 applies (*14*, *20*)

$$T_g(h) = T_g(b)\,[1 - (A/h)^{\delta}] \qquad (1)$$

where $T_g(h)$ is T_g for a film of thickness h, $T_g(b)$ is the bulk polystyrene T_g (both in degrees kelvin), A is a characteristic length (3.2 nm), and $\delta = 1.8$. The experimental results from which empirical Eq. 1 was derived confer on $T_g(h)$ the meaning of an "average" T_g across the nanoscopic film that is strongly thickness-dependent. For example, a 20-nm-thick PS film with $T_g(b) \sim 100°C$ exhibits a T_g depression [$\Delta T_g(h,b) = T_g(b) - T_g(h)$] of ~14°C, but this effect vanishes ($\Delta T_g(h,b) < 1°C$) when $h > 100$ nm. Thus, for PS films of thickness >100 nm, the polymer gate dielectric viscoelastic properties should play little role in OTFT interfacial effects when $T < T_g(b)$. Relations similar to Eq. 1 are applicable to other polymer classes, although parameters A and δ differ and may depend on the substrate [for example, for poly(methylmethacrylate) (PMMA), A = 0.35 nm and $\delta = 0.8$ (*21*); for poly(*t*-butylstyrene) (PTBS), $A = 3.0$ nm and $\delta = 1.05$ (*22*)]. We show here that when glassy polymeric materials are used as OTFT gate dielectrics, polymer viscoelastic properties strongly influence organic semiconductor film growth, microstructure, and OTFT *I-V*

Department of Chemistry and the Materials Research Center, Northwestern University, 2145 Sheridan Road, Evanston, IL 60208, USA.

*To whom correspondence should be addressed. E-mail: a-facchetti@northwestern.edu (A.F.); t-marks@northwestern.edu (T.J.M.)

performance. This effect is independent of polymer film thickness; the film need not be nanoscopically confined, so this effect can be used to probe the surface viscoelastic properties in buried interfaces via the OTFT response.

The top-contact, bottom-gate OTFT structure used in this study (Fig. 1) consisted of a thin pentacene semiconducting layer grown on top of the gate dielectric, together with an underlying p^+-Si gate electrode and top Au charge-injecting and -extracting source and drain electrodes. Pentacene was selected as the model organic semiconductor because of the large pentacene TFT database and the importance of this semiconductor in organic electronics (*23*–*26*). The dielectric was either a 300-nm-thick SiO_2 film [dielectric c-SiO_2, T_g(b) = 1175°C] or a polymer (10 to 800 nm, top)/SiO_2 (300 nm, bottom) bilayer, with the polymer layer selected to span commonly used OTFT gate dielectrics having a range of T_g(b)'s and surface chemical characteristics, such as PS [dielectric PS1, T_g(b) = 103°C; dielectric PS2, T_g(b) = 94°C; dielectric PS3 T_g(b) = 83°C], PTBS [dielectric PTBS, T_g(b) = 137°C], and PMMA [dielectric PMMA, T_g(b) = 86°C] (table S1). We used PS specimens of different molecular weights, and hence different T_g(b)'s, which should differentiate dielectric viscoelasticity effects from local buried interfacial chemical effects. The relatively low T_g(b) values of the polymers used in this study are due to relatively low molecular weights. The bilayer SiO_2/polymer dielectric (Fig. 1) allowed us to vary the polymer surface in contact with the semiconductor and the polymer film thickness and still maintain gate leakage current densities (J_{leak}) below levels that affect OTFT response. For all bilayer dielectrics, $J_{leak} < 10^{-8}$ A/cm^2 at a gate field of ~3 MV/cm, as established in metal/insulator/semiconductor capacitor structures, and is identical to that of the control c-SiO_2 substrates (*10*); hence, the leakage current densities at the maximum OTFT gate fields used here (~3 MV/cm) were dominated by the bottom SiO_2 layer. Tapping-mode atomic force microscopy (AFM) images of the bilayers reveal that all of the dielectric films exhibit similar topologies, characterized by root mean square roughnesses of ~0.3 nm.

After establishing the dielectric properties, pentacene films were next vapor-deposited on the gate insulator substrates maintained at preset deposition temperatures (T_D's) and were then characterized by tapping-mode AFM and wide-angle x-ray diffraction (WAXRD). OTFTs were then fabricated at room temperature on the bilayer dielectrics and on the c-SiO_2 control, and response parameters were extracted from *I-V* data using standard methodologies (*27*).

The saturation field-effect mobility (μ) and other relevant OTFT performance data for the present pentacene TFTs as a function of polymer dielectric and T_D are summarized in table S1. *I-V* transfer and output plots exhibit classical linear/saturation behavior in all cases (figs. S1 and S2). As also shown in Fig. 2A for PS2- and c-SiO_2-based devices, pentacene carrier mobility depends on T_D for the polymeric gate insulator-based devices. As expected, absolute μ values vary somewhat for different pentacene/dielectric combinations because of differing interfacial chemical interactions and charge trap densities (*10*, *28*, *29*). Hence, pentacene TFT maximum carrier mobilities (μ_{max}) vary from ~0.50 to 0.65 cm^2/V·s on hydrophobic PS1 and PS2 and PTBS to ~0.20 to 0.30 cm^2/V·s on polar/hydrophilic PMMA and c-SiO_2.

The dependence of OTFT response characteristics on pentacene growth temperature is even more marked when the normalized carrier mobility ($N_\mu = \mu/\mu_{max}$) is plotted versus T_D (Fig. 2B). This plot also compares N_μ to experimental T_g(b) values measured for the polymer insulators by temperature-modulated differential scanning calorimetry (DSC). Over a narrow and well-defined T_D range, pentacene carrier mobility drops precipitously (by more than 10 times), and this transition is characteristic of the specific polymeric gate dielectric. The N_μ transition temperatures are substantially below the corresponding polymer bulk transition temperatures and are substantially below the T_g(h)'s estimated for these polymers from Eq. 1. To quantify OTFT performance suppression caused by thermal and viscoelastic properties of the polymer dielectric, we define T_g(s) as the temperature where $N_\mu = 0.5$, or the surface T_g. From these results, as well as additional experiments reported below, we infer that T_g(s) has broad importance and correlates with surface viscoelastic properties. This correlation is reasonable only if the measured T_g(s) is always lower than T_g(h) and is also independent of the polymer film thickness.

In the plots of Fig. 2B, the T_g(s)'s of the PS-based samples [59°C for PS1, 51°C for PS2, and <34°C for PS3] track the corresponding polymer T_g(b)'s [103°C for PS1, 94°C for PS2, and 83°C for PS3). Thus, T_g(b) – T_g(s) [ΔT_g(s,b)] remains in a narrow range (~43° to 49°C) for these PSs. That ΔT_g(s,b) is only marginally sensitive to the absolute T_g(b) is expected considering that the chain microstructures of these PS samples differ only in molecular weight. In contrast, ΔT_g(s,b) absolute values for PMMA [T_g(b) = 86°C] and PTBS [T_g(b) = 137°C] are smaller (11°C) and larger (61°C), respectively, than that of PS1, PS2, and PS3. Previous studies have shown that nanoscopic PMMA and PTBS films exhibit smaller and greater T_g depressions, respectively, versus PS (*19*, *21*). Also, the ΔT_g(s,b) values are far larger than the corresponding ΔT_g(b,h)'s derived from Eq. 1 for similar polymer thicknesses. The PS film thickness used here (~25 nm) should have ΔT_g(b,h) ~ 9°C, but the experimental OTFT-derived ΔT_g(b,s)'s are >40°C. That T_g(s) is a surface and not a film/bulk polymer property is demonstrated in Fig. 2C, where the pentacene

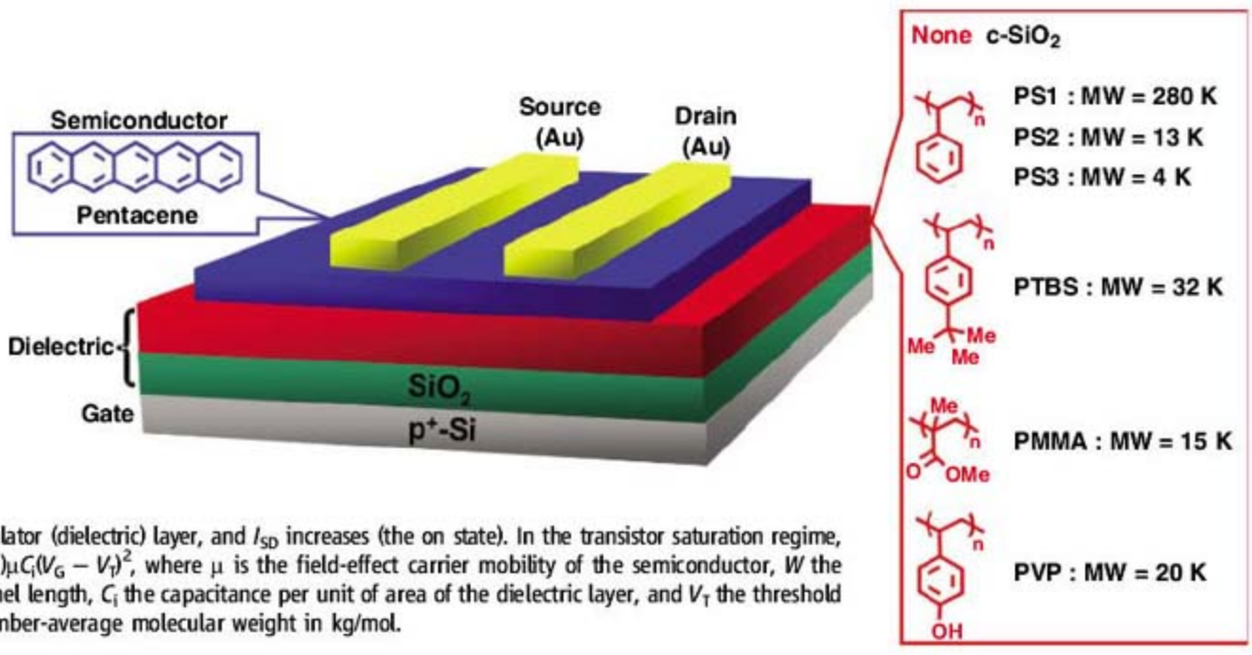

Fig. 1. Schematic representation of the top-contact, bottom-gate OTFT structure and the materials components used in this study. In a TFT device, the current between source and drain electrodes (I_{SD}) is minimal when no voltage (V_G) is applied between the source and gate electrodes (the off state). When a positive or negative V_G is applied, electrons or holes, respectively, are induced in the semiconductor at the interface with the insulator (dielectric) layer, and I_{SD} increases (the on state). In the transistor saturation regime, I_{SD} is given by $I_{SD} = (W/2L)\mu C_i(V_G - V_T)^2$, where μ is the field-effect carrier mobility of the semiconductor, W the channel width, L the channel length, C_i the capacitance per unit of area of the dielectric layer, and V_T the threshold voltage. MW, polymer number-average molecular weight in kg/mol.

carrier mobility is plotted versus T_D for the PS1-based OTFTs over a wide range of PS film thickness (20 to 800 nm). The mobility transition occurs at the same T_g(s) of 59°C independent of the dielectric polymer film thickness. Similar results are observed for the other polymer dielectrics used here, supporting the broad generality of this effect (Fig. 2C).

The origin of the precipitous mobility drop at $T_D = T_g$(s) could in principle result from the microstructural changes within the pentacene films. Thus, we examined the pentacene films by XRD and AFM. Figure 3 shows θ to 2θ XRD scans of 50-nm-thick pentacene films deposited at different T_Ds on the bilayer insulators and on c-SiO_2. All of the pentacene films exhibit the exclusive presence of the thin-film phase, consistent with the small film thicknesses (*30*), and the intensity of the (001) Bragg reflection (2θ = 5.74°) strongly depends on T_D. Pentacene films (50 nm) deposited at temperatures below T_g(s) exhibit far more intense reflections (by a factor of 10 to 100) as compared to films grown at higher substrate temperatures. The XRD data for 50-nm pentacene films grown on c-SiO_2 exhibit negligible T_D dependence. These results indicate a direct correlation between deposition temperature–dependent discontinuities in pentacene film microstructure and those in field-effect mobility. In contrast to growth on inorganic c-SiO_2, increasing polymer chain segmental mobility at the free dielectric surface with increasing T_D strongly disrupts the growth of highly textured pentacene grains.

AFM images of pentacene films show similar transitions near T_g(s) in pentacene film grain size distributions versus T_D, with the bilayer dielectric substrates behaving very differently from c-SiO_2. Detailed AFM data analysis for ~100 devices indicates that pentacene carrier mobility is substantially less affected by grain size variations and gate dielectric chemical characteristics than previously thought; rather, there appear to be two size regimes for mobility. Figure 4A shows AFM images for 50-nm-thick pentacene films grown on PS1 and c-SiO_2, as well as pentacene average grain size versus T_D data for representative dielectrics. Similar growth morphologies as a function of T_D are observed for pentacene monolayers (~5 nm thick) on the same insulators (fig. S3); hence, microstructural differences in the initial film growth stages are preserved in thicker films.

The plot in Fig. 4A shows that on the c-SiO_2 control substrate, pentacene film grain size increases monotonically from ~0.8 to ~2.5 μm when T_D is increased from 25° to 80°C, which is typical growth behavior for pentacene films (*31*). In marked contrast, for the films grown on PS1, the grain size increases slightly from ~1.2 μm at T_D = 25°C to ~1.4 μm at T_D = 60°C, then abruptly decreases to <0.5 μm for $T_D \geq$ 70°C. Similar behavior is observed for PS2 [~1.3 μm (25°C) → ~0.3 μm (60°C) (fig. S4A)], PS3 [~0.7 μm (25°C) → ~0.2 μm (50°C) (fig. S4B)], and polar PMMA [~1.8 μm (25°C) → ~3.3 μm (60°C) → ~0.5 μm (80°C) (Fig. 4A)]. Pentacene films on very high T_g(b) PTBS behave somewhat differently. For $T_D < T_g$(s), exceptionally large grains (>5.0 μm) are observed. However, for $T_D > T_g$(s), the pentacene film growth mode deviates from typical layer-by-layer and island growth modes (*32*), with formation of large circular polycrystalline aggregates separated by large gaps (fig. S4C).

These morphology variations as a function of T_D correlate with the diffraction-derived film microstructural variations at T_g(s) for the bilayer insulators. For the c-SiO_2 substrates, increased T_D correlates with increased grain size caused by increased diffusion of the pentacene molecules on the surface (*31*, *33*). However, the effect of temperature on diffusion for the bilayer dielectrics differs greatly, because diffusion of the pentacene molecules and grain size should both scale with temperature, which is indeed observed when T_D increases, but only for $T_D < T_g$(s). For $T_D > T_g$(s), the grain size abruptly falls, probably because molecular diffusion is disturbed because of enhanced polymer dielectric surface roughness and/or friction at higher temperatures (*34*, *35*). Rough gate dielectric surfaces are known to impede lateral pentacene molecular diffusion, affording smaller grain sizes versus growth on very smooth substrates (*36*, *37*), and in the present case drastically suppress pentacene ordered molecular nucleation. Clearly, insulating polymer viscoelastic dynamics at $T_D > T_g$(s) disrupt the growth of large textured grains. Furthermore, as illustrated in Fig. 4B, this study reveals two grain

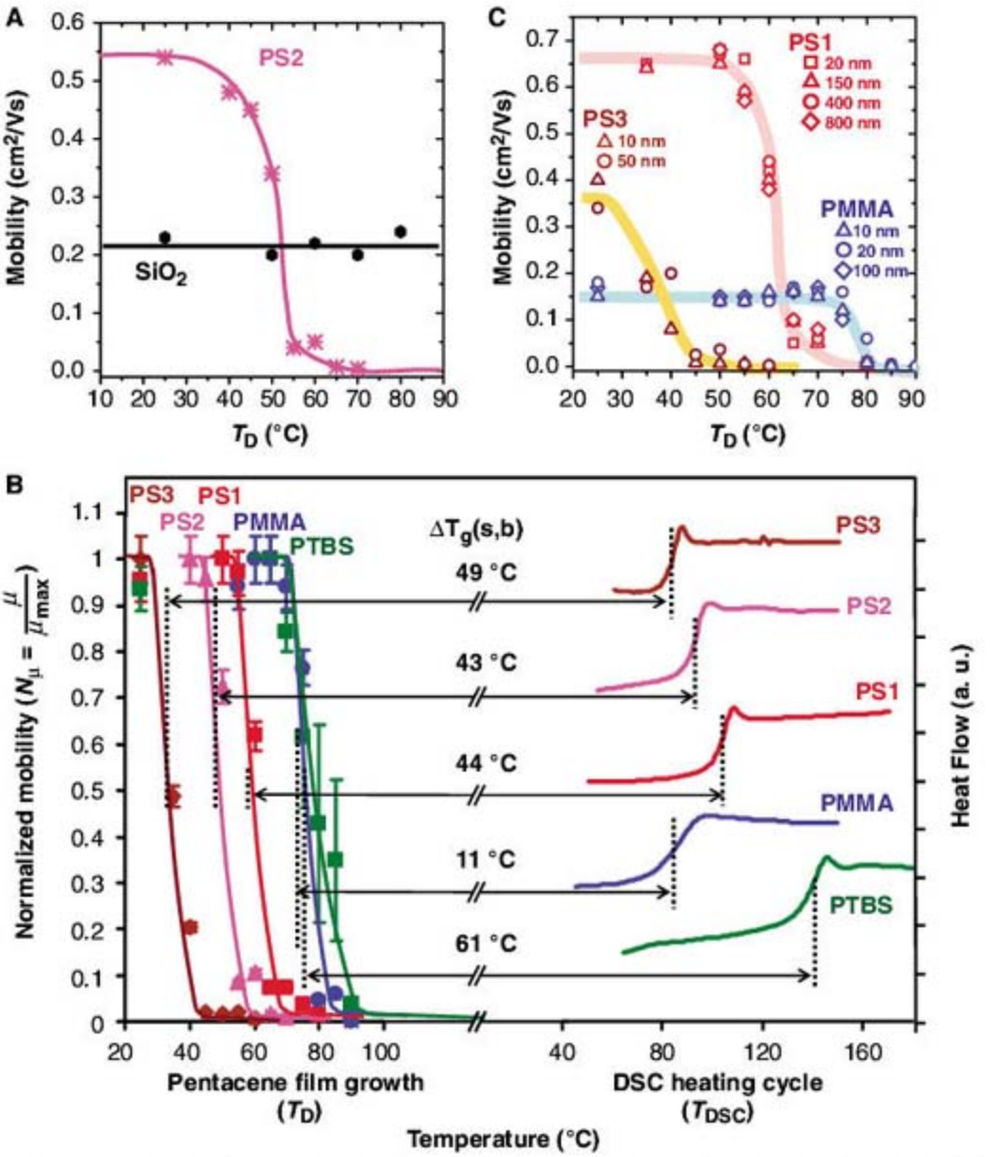

Fig. 2. (**A**) Carrier field-effect mobility μ for pentacene OTFTs fabricated at different pentacene film T_D's on polymer bilayer dielectric PS2 (24 nm) and on c-SiO_2. (**B**) (Left) Normalized charge carrier mobility $N_\mu = \mu/\mu_{max}$ [μ_{max} (cm^2/V·s) = 0.68 (PS1); 0.54 (PS2); 0.34 (PS3); 0.18 (PMMA); and 0.63 (PTBS)] at different T_D's for pentacene OTFTs on various bilayer dielectrics. (Right) DSC scans for the polymers investigated in this study. The polymer T_g(s) is defined as the temperature where $N_\mu = 0.5$, and $\Delta T_g(s,b) = T_g(b) - T_g(s)$ [T_g(s) = 59°C (PS1); 51°C (PS2); <34°C (PS3); 75°C (PMMA); and 76°C (PTBS)]. (**C**) Carrier field-effect mobility of pentacene TFTs as a function of T_D for different PS1, PS3, and PMMA gate dielectric thicknesses. Except for the DSC plots, all the remaining lines are drawn as guides for the eye.

size/mobility dependence regimes for pentacene. When the pentacene grain size is above a critical value, identified here as ~0.8 μm, the carrier mobility is large (>0.15 $cm^2/V{\cdot}s$) and independent of the crystallite size (for each dielectric type) and depends marginally on dielectric chemical structure. Below ~0.8 μm, pentacene carrier mobility becomes very sensitive to the grain size distribution, varying from 0.1 $cm^2/V{\cdot}s$ to ~10^{-7} $cm^2/V{\cdot}s$.

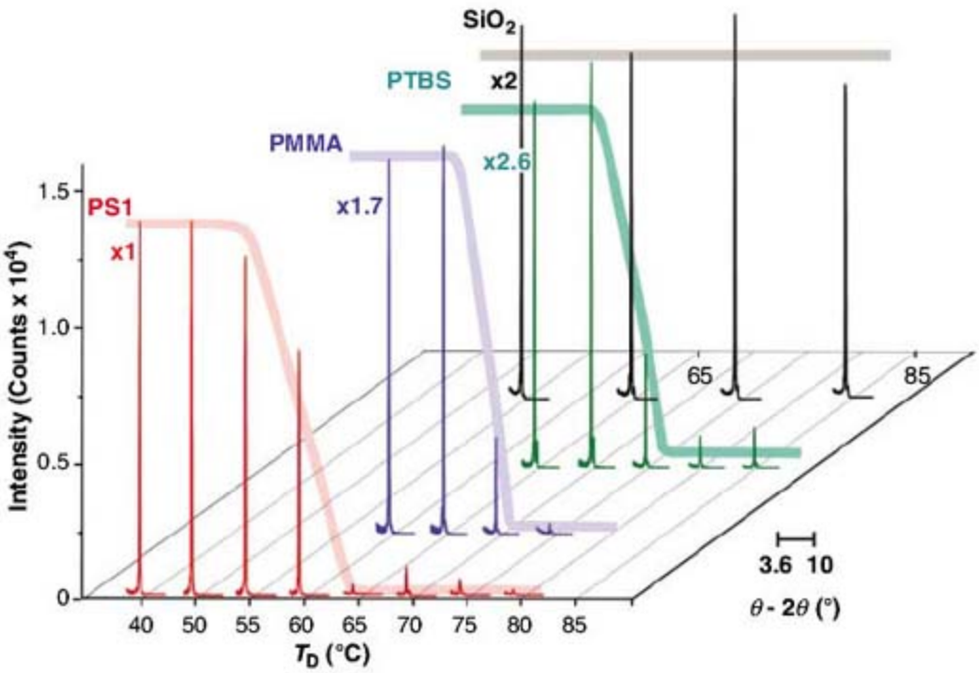

Fig. 3. XRD data (*001* reflection of the thin-film phase) for 50-nm-thick pentacene films grown on PS1, PMMA, PTBS, and c-SiO_2 gate dielectrics at the indicated substrate temperatures (T_D). The lines are drawn as guides for the eye. The scale bar indicates the θ to 2θ XRD scan angle ranges from 3.6° to 10.0°.

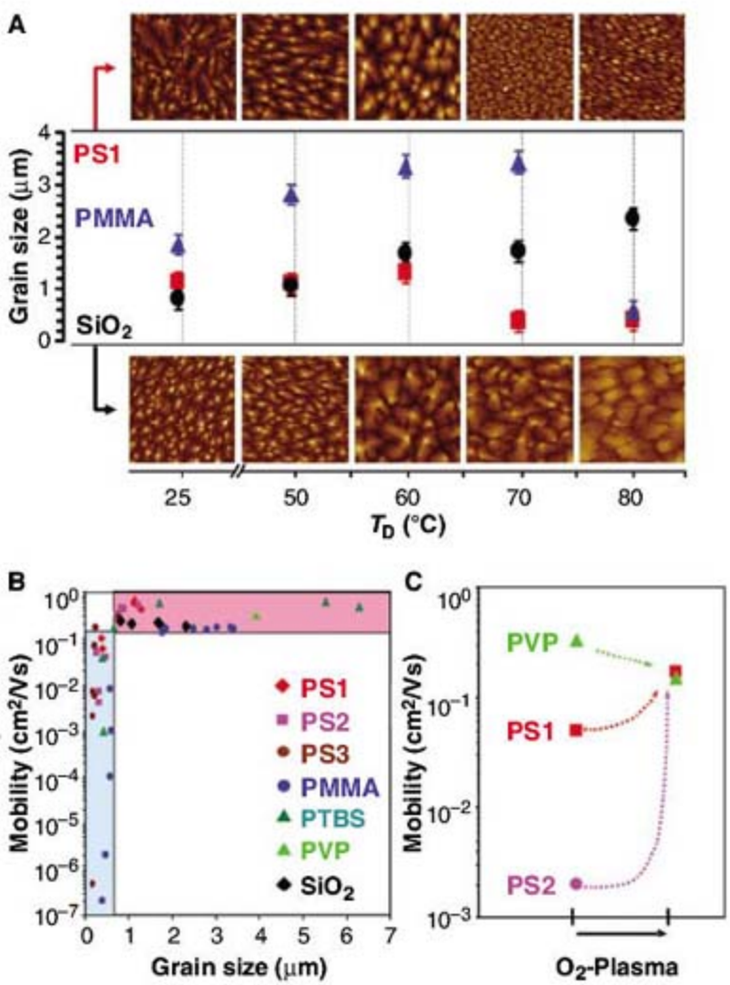

Fig. 4. (**A**) AFM images (5.0 × 5.0 μm^2) of 50-nm-thick pentacene films grown on dielectrics PS1 (top) and c-SiO_2 (bottom) at different T_D's and the corresponding average grain size versus T_D plots for PS1 (red), PMMA (blue), and c-SiO_2 (black). (**B**) Mobility versus average grain size plot for pentacene TFTs on all dielectrics. The blue- and red-shaded areas represent the low- and high-carrier-mobility regions, respectively. (**C**) Mobility of pentacene TFTs before (left) and after (right) O_2 plasma treatment of the polymer dielectric surface (T_D = 70°C).

Finally, to demonstrate that the present large pentacene microstructure-OTFT *I-V* correlations result from polymer chain surface segmental mobility, the T_g(s)'s of representative low-T_g(b) polymers were increased via surface chemical modification. Treatment of PS films with an O_2 plasma forms oxygenated species (mainly hydroxyl groups) penetrating only ~2 nm into the film (*38*, *39*). This process should convert the surface properties of the PS-coated substrates to those approaching polyvinylphenol (PVP), a polymer with a far larger T_g(b) (~170°C) than PS. We fabricated TFTs based on PS1and PS2 (as a control), on PS substrates treated with an O_2 plasma (PS1/2-OXY), and on PVP-based bilayer insulators (PVP and PVP-OXY as a control), on which pentacene films were then deposited at T_D = 70°C (for details, see the supporting online material). The field-effect transistor mobilities of PS1/2-OXY-based devices for $T_D > T_g$(s) using PS1 and PS2 increase dramatically despite the low T_g(b)'s of these polymers and approach those of the PVP-based devices (Fig. 4C). This result strongly supports the surface polymer chain viscoelastic origin of the dramatic mobility and microstructure variations observed here. A practical implication is that the surfaces of low-T_g(b)/T_g(s) polymer insulators (usually more processable) can be modified after deposition to tolerate higher-temperature fabrication processes, readily affording higher-performance OTFTs.

The present results illuminate new polymer surface thermal and viscoelasticity phenomena of general importance and demonstrate their crucial consequences for pentacene TFT response when polymers are used as gate dielectrics. First, there is an unprecedented and general effect of the dielectric T_g on the charge transport properties of overlying thin-film organic semiconductors. General and abrupt mobility transitions occur at well-defined pentacene film growth temperatures characteristic of each underlying polymer dielectric. This temperature, associated with a surface T_g, is substantially lower than the bulk T_g and is independent of film thickness. Second, the transition from high to low pentacene TFT field-effect mobility is closely correlated with large microstructural and morphological alterations of pentacene film growth occurring at the same surface T_g. Third, pentacene grain size–TFT carrier mobility analysis reveals two mobility states for pentacene TFTs, well separated by a critical grain size (~0.8 μm). Fourth, observing and quantifying surface T_g via field-effect mobility measurements suggests a useful new probe of polymer interfacial viscoelastic properties versus those in thin films and the bulk. The observation of the effect of polymer surface chain dynamics of organic transistor response should also contribute to the more rational fabrication of advanced organic electronics.

References and Notes

1. J. A. Rogers, Z. Bao, H. E. Katz, A. Dodabalapur, in *Thin-Film Transistors*, C. R. Kagan, P. Andry, Eds. (Marcel Dekker, New York, 2003), pp. 377–425.
2. R. Brown, A. Pomp, C. M. Hart, D. M. de Leeuw, *Science* **270**, 972 (1995).
3. V. C. Sundar *et al.*, *Science* **303**, 1644 (2004).
4. L.-L. Chua *et al.*, *Nature* **434**, 194 (2005).
5. M. J. Panzer, C. D. Frisbie, *J. Am. Chem. Soc.* **127**, 6960 (2005).
6. A. Facchetti, M.-H. Yoon, T. J. Marks, *Adv. Mater.* **17**, 1705 (2005).
7. A. Salleo, M. L. Chabinyc, M. S. Yang, R. A. Street, *Appl. Phys. Lett.* **81**, 4383 (2002).
8. T. Takahashi, T. Takenobu, J. Takeya, Y. Iwasa, *Appl. Phys. Lett.* **88**, 033505 (2006).
9. N. Stutzmann, R. H. Friend, H. Sirringhaus, *Science* **299**, 1881 (2003).
10. M.-H. Yoon, C. Kim, A. Facchetti, T. J. Marks, *J. Am. Chem. Soc.* **128**, 12851 (2006).
11. L. Berthier *et al.*, *Science* **310**, 1797 (2005).
12. L. A. Deschenes, D. A. Vanden Bout, *Science* **292**, 255 (2001).
13. P. G. Debenedetti, F. H. Stillinger, *Nature* **410**, 259 (2001).
14. J. A. Forrest, K. Dalnoki-Veress, J. R. Dutcher, *Phys. Rev. E Stat. Phys. Plasmas Fluids Relat. Interdiscip. Top.* **56**, 5705 (1997).
15. C. L. Jackson, G. B. McKenna, *J. Non-Cryst. Solids* **131-133**, 221 (1991).
16. S. Kawana, R. A. L. Jones, *Phys. Rev. E Stat. Phys. Nonlin. Soft Matter Phys.* **63**, 021501 (2001).
17. K. Fukao, Y. Miyamoto, *Phys. Rev. E Stat. Phys. Plasmas Fluids Relat. Interdiscip. Top.* **61**, 1743 (2000).
18. J. A. Forrest, K. Dalnoki-Veress, J. R. Stevens, J. R. Dutcher, *Phys. Rev. Lett.* **77**, 2002 (1996).
19. C. J. Ellison, M. K. Mundra, J. M. Torkelson, *Macromolecules* **38**, 1767 (2005).
20. J. A. Forrest, K. Dalnoki-Veress, *Adv. Coll. Interf. Sci.* **94**, 167 (2001).
21. O. Prucker *et al.*, *Macromol. Chem. Phys.* **199**, 1435 (1998).
22. These coefficients were estimated from the data provided by (*19*).
23. H. Klauk, U. Zschieschang, J. Pflaum, M. Halik, *Nature* **445**, 745 (2007).
24. R. Ruiz, A. Papadimitratos, A. C. Mayer, G. G. Malliaras, *Adv. Mater.* **17**, 1795 (2005).
25. C. D. Dimitrakopoulos *et al.*, *Science* **283**, 822 (1999).
26. A. L. Briseno *et al.*, *Nature* **444**, 913 (2006).
27. Materials and methods are available as supporting material on *Science* Online.
28. K. Puntambekar, J. Dong, G. Haugstad, C. D. Frisbie, *Adv. Funct. Mater.* **16**, 879 (2006).
29. K. N. N. Unni, S. Dabos-Seignon, J.-M. Nunzi, *J. Mater. Sci.* **41**, 317 (2006).
30. C. D. Dimitrakopoulos, A. R. Brown, A. Pomp, *J. Appl. Phys.* **80**, 2501 (1996).
31. H. Yanagisawa, T. Tamaki, M. Nakamura, K. Kudo, *Thin Solid Films* **464-465**, 398 (2004).
32. D. L. Smith, *Thin-Film Deposition: Principles and Practice* (McGraw Hill, New York, 1995).
33. Z. Zhang, M. G. Lagally, *Science* **276**, 377 (1997).
34. K. Tanaka, A. Takahara, T. Kajiyama, *Macromolecules* **33**, 7588 (2000).
35. S. Ge *et al.*, *Phys. Rev. Lett.* **85**, 2340 (2000).
36. S. Steudel *et al.*, *Appl. Phys. Lett.* **85**, 4400 (2004).
37. D. Knipp, R. A. Street, A. R. Volkel, A. Ho, *J. Appl. Phys.* **93**, 347 (2003).
38. S. Guruvenket, G. M. Rao, M. Komath, A. M. Raichur, *Appl. Surf. Sci.* **236**, 278 (2004).
39. R. W. Paynter, *Surf. Interface Anal.* **33**, 862 (2002).

40. We thank J. M. Torkelson and J. Kim for helpful discussion. This work was supported by the Air Force Office of Scientific Research (grant STTRFA 9550-04-0080), Polyera Corp., and the NSF Materials Research Science and Engineering Centers program through the Northwestern Materials Research Center (grant DMR-0520513). This contribution is dedicated to Prof. G. A. Pagani on the occasion of his 70th birthday.

Supporting Online Material

www.sciencemag.org/cgi/content/full/318/5847/76/DC1
Materials and Methods
Figs. S1 to S4
Table S1
Reference

13 June 2007; accepted 7 September 2007
10.1126/science.1146458

Ultrastrong and Stiff Layered Polymer Nanocomposites

Paul Podsiadlo,[1] Amit K. Kaushik,[2] Ellen M. Arruda,[2,3] Anthony M. Waas,[2,4] Bong Sup Shim,[1] Jiadi Xu,[5] Himabindu Nandivada,[1] Benjamin G. Pumplin,[2] Joerg Lahann,[1,3,6] Ayyalusamy Ramamoorthy,[5] Nicholas A. Kotov[1,6,7]*

Nanoscale building blocks are individually exceptionally strong because they are close to ideal, defect-free materials. It is, however, difficult to retain the ideal properties in macroscale composites. Bottom-up assembly of a clay/polymer nanocomposite allowed for the preparation of a homogeneous, optically transparent material with planar orientation of the alumosilicate nanosheets. The stiffness and tensile strength of these multilayer composites are one order of magnitude greater than those of analogous nanocomposites at a processing temperature that is much lower than those of ceramic or polymer materials with similar characteristics. A high level of ordering of the nanoscale building blocks, combined with dense covalent and hydrogen bonding and stiffening of the polymer chains, leads to highly effective load transfer between nanosheets and the polymer.

A critical challenge in nanocomposite fabrication is the ability to realize materials that allow the transfer of the exceptional mechanical properties (i.e., tensile strength, σ_{UTS}, and Young's modulus, E) of the nanoscale materials to the macroscale properties of the bulk materials. Nanoparticle-filled polymer composites based on these structural elements have mechanical properties that fall far below the expected theoretical and experimentally determined values of the individual building blocks, except at low volume fractions of the reinforcement (*1*–*9*). The deficiency in the properties of the composite is largely related to the difficulty of obtaining well-dispersed large volume fractions of the reinforcing nanomaterials and a lack of structural control. The difficulty is also associated with realizing an effective load transfer from the polymeric matrix to the nanoscale components and the insufficiently understood mechanical interactions of the two constituents at the nanoscale. We demonstrate that it is possible to produce composites with properties that approach the theoretical maxima using spatial and orientational control of clay platelets in a polymer matrix at the nanoscale and retaining this order at the macroscale.

Hybrid organic-inorganic nanocomposites of polymer and clay nanoplatelets have received special attention because of the very low cost of the inorganic component, relatively simple preparation, and fairly predictable stiffening behavior when introduced into polymers (*9*, *10*). Montmorillonite (MTM) clay (~1–nm–thick-by-100– to 1000–nm–diameter sheets) has been extensively used for this purpose because it is readily available and has exceptional mechanical properties. The in-plane modulus of elasticity has been estimated by Monte Carlo simulations to be ~270 GPa (*6*). Although composites incorporating 50 volume % of MTM should theoretically have stiffness values on the order of 100 GPa, values achieved to date with MTM platelets are at least one order of magnitude lower. This is because, in general, less than ~10 weight % (wt %) of the clay can be incorporated homogeneously as completely dispersed silicates rather than intercalated structures into the polymer because of the strong tendency of the clay to aggregate and phase separate. Further increases in the volume of the clay content have either marginally increased or even reduced both the strength and stiffness (*9*, *11*).

We approached preparation of the clay nanocomposite by using a bottom-up assembly process called layer-by-layer (LBL) assembly (*12*). The LBL process is based on sequential adsorption of nanometer-thick monolayers of oppositely charged compounds (such as polyelectrolytes, charged nanoparticles, and biological macromolecules) to form a multilayered structure with nanometer-level control over the architecture. In the past, we have used the LBL technique to prepare nanocomposites from carbon nanotubes (CNTs) that have $\sigma_{UTS} \sim 220$ MPa (*13*, *14*). We have also shown that the organization of LBL composites has many analogies with the structure

[1]Department of Chemical Engineering, University of Michigan, Ann Arbor, MI 48109–2136, USA. [2]Department of Mechanical Engineering, University of Michigan, Ann Arbor, MI 48109–2125, USA. [3]Program in Macromolecular Science and Engineering, University of Michigan, Ann Arbor, MI 48109–2140, USA. [4]Department of Aerospace Engineering, University of Michigan, Ann Arbor, MI 48109–2140, USA. [5]Biophysics Research Division and Department of Chemistry, University of Michigan, Ann Arbor, MI 48109–1055, USA. [6]Department of Biomedical Engineering, University of Michigan, Ann Arbor, MI 48109–2099, USA. [7]Department of Materials Science and Engineering, University of Michigan, Ann Arbor, MI 48109–2136, USA.

*To whom correspondence should be addressed. E-mail: kotov@umich.edu

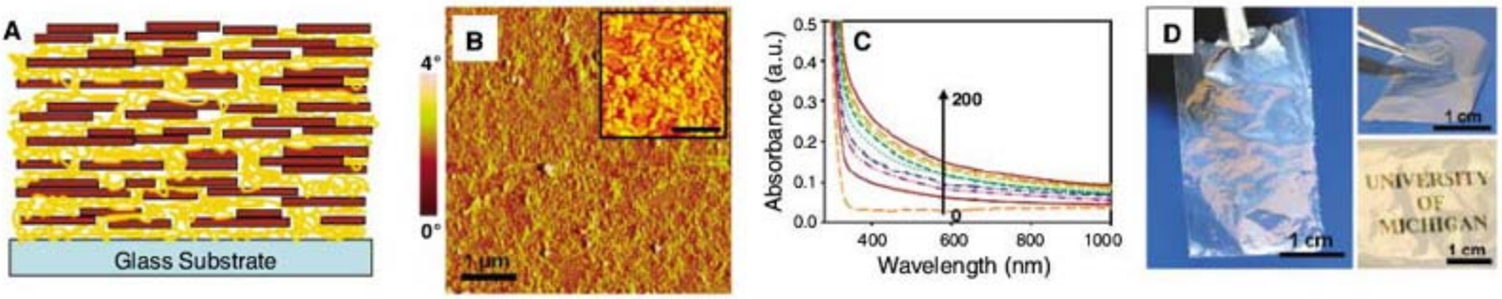

Fig. 1. Preparation of PVA/MTM nanocomposites. **(A)** Schematic representation of the internal architecture of the PVA/MTM nanocomposite (picture shows 8 bilayers). **(B)** ATM phase image of a single PVA/MTM bilayer adsorbed on top of a silicon wafer. (Inset) Close up of the main image showing individual MTM platelets more clearly. Scale bar in inset, 400 nm. **(C)** Compilation of UV/VIS absorbance spectra collected after multiples of 25 bilayers of PVA/MTM composite deposited on both sides of a microscope glass slide up to 200 bilayers. a.u., arbitrary units. **(D)** Free-standing, 300-bilayer PVA/MTM composite film showing high flexibility and transparency. The lower image was taken at an angle to show diffraction colors.

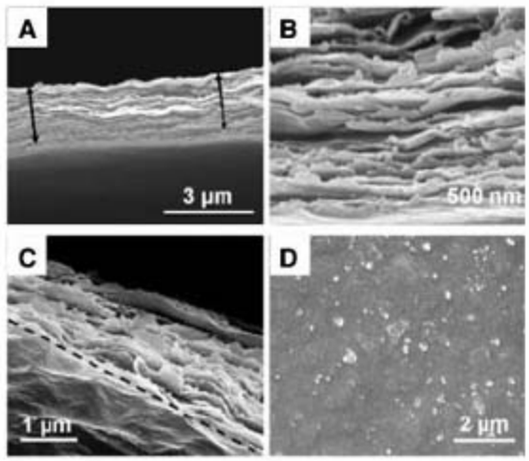

Fig. 2. Scanning electron microscopy characterization of a 300-bilayer, free-standing PVA/MTM nanocomposite. **(A)** Cross section of the film. Arrows indicate the span of the cross section. **(B)** Close-up of the cross section showing the separation of layers. **(C)** Top-down view of a fracture edge of the composite after tensile testing. Dashed line indicates edge of the sample. **(D)** Top-down view of the composite's surface. The slight separation of the layers seen in (A) and (B) is due to a shearing force resulting from cutting the sample with a razor blade during scanning electron microscopy sample preparation.

of one of the toughest natural mineral-based materials, nacre (*15*). In this respect, LBL assembly of negatively charged nanosheets of hectorite or MTM clays with a poly(diallyldimethylammonium chloride) (PDDA) polycation led to the formation of a material with σ_{UTS} ~100 MPa and a tangent stiffness after strain stiffening of ~11 GPa (*15*, *16*). Although fairly high, these values are still below the theoretical limits for these materials, based on the mechanical properties of individual nanotubes and/or clay sheets.

A traditional LBL process of sequentially coating a surface with nanometer-thick layers of poly(vinyl alcohol) (PVA) and MTM by immersing a glass substrate in dilute solutions of the components was used in this study (*17*–*19*). Ellipsometry and ultraviolet/visible (UV/VIS) spectroscopy (Fig. 1 and fig. S1) revealed linear and uniform growth.

Characterization of the assembly with the use of atomic force microscopy (AFM) (Fig. 1) and scanning electron microscopy (Fig. 2) verified dense coverage of the nanoplatelets and their strictly planar orientation. The electron microscopy characterization provided thickness measurements of 1.0 ± 0.1 μm (SEM) and 1.5 ± 0.1 μm (SEM) for 200- and 300-bilayer films, respectively, indicating an average of ~5 nm of thickness per bilayer (Fig. 2A). Nearly identical thickness was obtained from ellipsometry for a 300-bilayer film grown on a silicon wafer: 1.480 ± 0.004 μm (SEM). The cross section also revealed a well-defined layered architecture.

We note that PVA is uncharged, unlike many other polymeric materials used in LBL. Nevertheless, it produces a stronger composite than do other polymers that undergo electrostatic attraction to the clay sheets (*19*–*21*). The PVA/MTM pair has two unique properties. The first is the high efficiency of hydrogen bonding. Atomic modeling revealed that the geometry of SiO_4 tetrahedrons on the surface of the alumosilicates is conducive to cooperative hydrogen bonding (the Velcro effect). The distances between the O atoms of clay and H atoms of PVA are 2.75 and 2.65 Å, respectively, which makes hydrogen bonding epitaxial (fig. S3). Second, a substantial part of the efficient load transfer between the polymer and the inorganic building block is attributed to the cyclic cross-linking to Al substitution present on the surface of MTM sheets and to Al atoms located along the edges of the MTM platelets (*22*). These Al atoms are easily accessible (Fig. 3A) to the macromolecules, unlike similar groups in the middle of the sheets. An atom of Al, two atoms of O, and three atoms of C from PVA participating in this bond form a six-membered ring structure, which is known to be particularly stable (Fig. 3A). Experimental data from Fourier transform infrared (FTIR) spectroscopy, nuclear magnetic resonance (NMR), and x-ray photoelectron scattering (XPS) spectroscopy, point to the formation of the Al–PVA covalent linkages. As such, we see a characteristic shift in the XPS spectra of Al from 74.4 to 74.9 eV (1 and 2 in Fig. 3B); concomitantly, a change in the ratio of carbon XPS peaks at 284.8 eV (–C–H_2) and 286.2 eV (–C–O–H) was observed (Fig. 3C). The formation of Al–PVA bonds can be further confirmed by the appearance of the characteristic FTIR vibration of Al–O–C (Fig. 3D, inset) at 848 cm^{-1} (*22*) and the strong suppression of the C–O–H band at 3290 cm^{-1} (Fig. 3E), which correlate well with the condensation of hydroxyls at Al sites with those from PVA groups. The NMR spectra of ^{27}Al (fig. S4) remain the same as expected because the coordination environment of Al (octahedral) did not change. The nanometer-scale organization and the layered structure of the composite provide the necessary conditions for the formation of multiples of such cyclic linkages.

Films were treated with glutaraldehyde (GA) after LBL assembly to further the bonding and load transfer between the –OH groups and the clay surface. GA is a highly efficient cross-linking agent for PVA (*23*, *24*) that forms covalent acetal bridges between –OH groups of the polymer chains (fig. S5), as well as the hydroxyl groups present on the MTM sheets and particularly on their edges. Solid-state NMR techniques revealed dramatic changes in the spectra before and after GA treatment (fig. S4). We can also see clear evidence of a reaction between GA and clay from NMR (fig. S5) and FTIR spectra (fig. S6), which indicates that this type of cross-linking further increases connectivity between PVA and clay sheets as well as the clay particles themselves.

Cross-linked free-standing films showed high uniformity, strength, flexibility, and remarkable transparency (Fig. 1D). UV/VIS spectra of the 300-bilayer free-standing films showed 80 to 90% transparency across the visible light spectrum, whereas pure PVA showed 90 to 95% transparency (fig. S7). Thermogravimetric analysis showed that the same films were composed in ~70 wt % (~50 volume %) of the MTM (fig. S8). This can be explained by the nanoscale dimensions of the inorganic phase and the nearly perfect orientation and fine dispersion of the nanoplatelets. UV/VIS spectroscopy also showed Fabry-Perot patterns (*25*, *26*), which are a further indication of high uniformity in the film.

Evaluation of mechanical properties by microtensile tests yielded remarkable results even

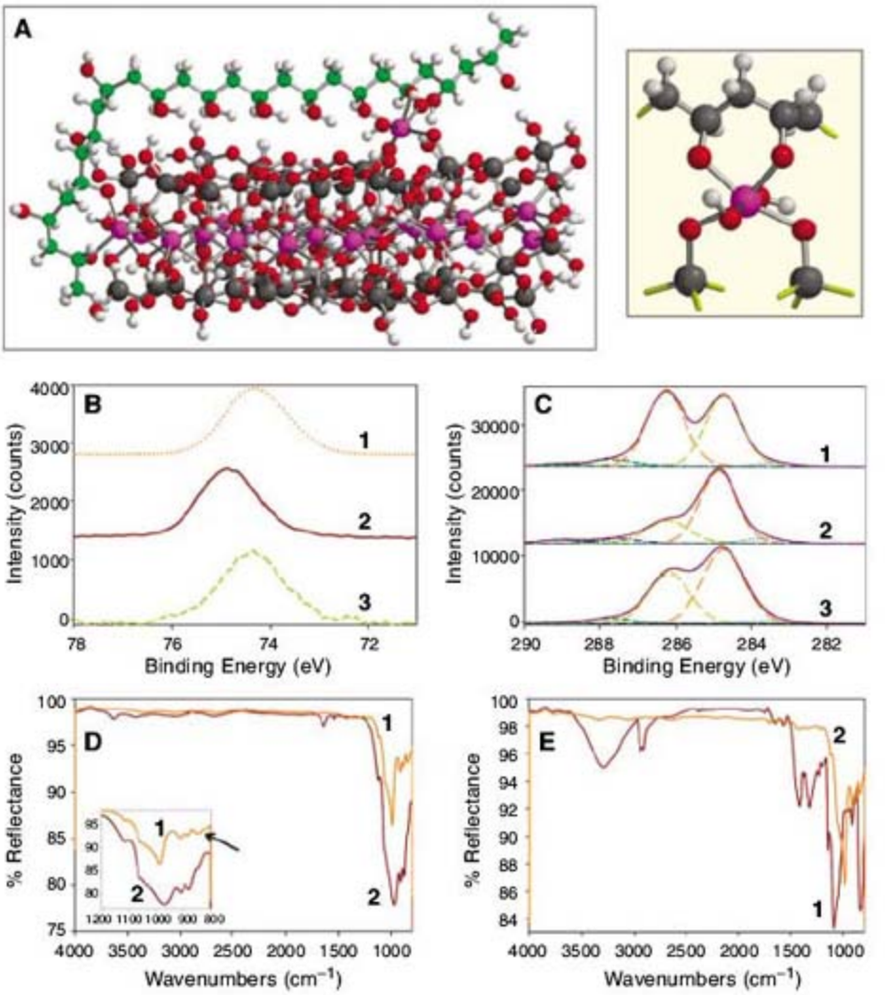

Fig. 3. Characterization of PVA and MTM molecular interactions. **(A)** Energy-optimized geometry of bonding between PVA and MTM via Al substitution sites obtained by computer calculations with the AM1 semi-empirical algorithm. (Right) Enlarged portion of the six-membered cycle formed between PVA and MTM. Al, purple; O, red; H, light gray; Si, dark gray; C, green. **(B)** Al 2p orbital XPS spectra for (1) MTM, (2) PVA/MTM nanocomposite, and (3) PVA/MTM nanocomposite with GA cross-linking. A positive energy shift is indicative of the increased oxidation state of the Al. **(C)** C 1s orbital XPS spectra for (1) PVA, (2) PVA/MTM composite, and (3) PVA/MTM composite with GA cross-linking. XPS spectra were deconvoluted in component peaks corresponding to the different oxidation states of C. The major peaks at 284.8 and 286.2 eV correspond to $-C-H_2$ and $-C-O-H$ carbons, respectively. **(D)** Comparison of FTIR spectra for (1) PVA/MTM composite and (2) MTM. (Inset) Close-up of the major peaks. Arrow points to the characteristic vibration peak at 848 cm^{-1}. **(E)** Comparison of FTIR spectra for pure (1) PVA and (2) PVA/MTM composite. The spectrum of PVA/MTM shows suppression of the C–O–H vibrations because of covalent binding with the MTM surface.

without GA cross-linking (Fig. 4, Table 1, and fig. S2). The nanocomposite displayed ~four times higher strength and nearly one order of magnitude higher modulus when compared with pure PVA polymer. GA cross-linking increased the strength, stiffness, and brittleness of both pure PVA and the PVA/MTM composite. (Fig. 4, A and B) The ultimate tensile strength increased by nearly a factor of 3 over the uncross-linked PVA/MTM strength and 10 times in comparison with that of pure PVA, to values as high as 480 MPa. The modulus of the PVA/MTM with GA exceeded that of uncross-linked PVA/MTM by one order of magnitude and that of pure PVA by two orders of magnitude, with the highest values reaching 125 GPa. The modulus of PVA/MTM with GA is comparable to that of various grades of Kevlar (*27*–*29*), $E \sim 80$ to 220 GPa, and exceeds the stiffness of the strongest CNT-based fibers (*30*). Additionally, unlike PDDA-MTM composites, the PVA/MTM films with GA cross-linking showed exceptional stability under humid conditions (fig. S9), which is consistent with the covalent character of the bonds responsible for load transfer.

Theoretical estimates for nanocomposite properties with nanometer-scale spacing of constituents in a polymer and such a large volume fraction of the filler are not available, and the currently recognized theories from the filled-rubber literature are not entirely applicable (*31*).

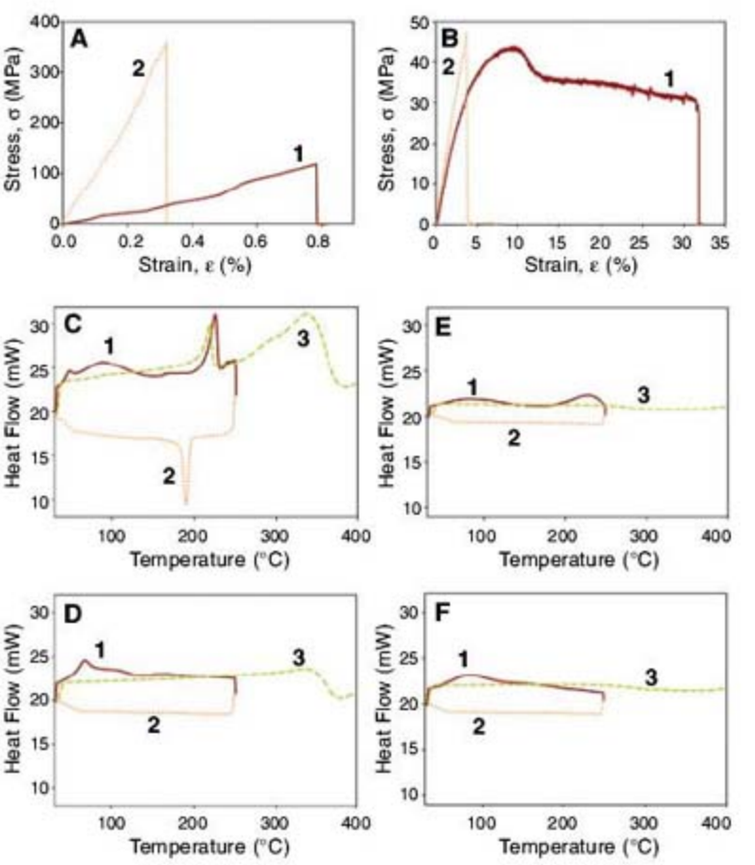

Fig. 4. Mechanical and thermal properties of PVA and PVA/MTM nanocomposites. **(A)** Stress-strain curves for 300-bilayer PVA/MTM composites (1) without and (2) with GA cross-linking. **(B)** Stress-strain curves for pure PVA polymer (1) without and (2) with GA cross-linking. The stress-strain curves were obtained from a home-built tensiometer (see supporting online material). **(C to F)** Differential scanning calorimetric analyses results for PVA polymer (C) without and (D) with GA cross-linking and for PVA/MTM (E) without and (F) with GA cross-linking. The DSC scans follow (1) heat, (2) cool, (3) heat cycles, as indicated by the numbering on the graphs.

Table 1. Summary of mechanical properties for PVA and its nanocomposites. The data are mean ± SD. The tensile strengths reported were obtained using both a commercially available servohydraulic test system and a custom in-house–built tensiometer (fig. S2). The moduli were obtained using the custom-built tensiometer. *N* indicates the minimum number of experimental data points that we used in the statistical calculations.

Sample type (*N*)	Tensile strength σ_{UTS} (MPa)	Modulus E' (GPa)	Ultimate strain ε (%)
PVA (5)	40 ± 4	1.7 ± 0.2	35 ± 4
PVA with GA (5)	40 ± 10	2.0 ± 0.5	3.3 ± 1.3
PDDA (5)	12 ± 4	0.2 ± 0.03	48 ± 9
PDDA-MTM (*)	100 ± 10	11 ± 2	10 ± 2
PVA/MTM (5)	150 ± 40	13 ± 2	0.7 ± 0.2
PVA/MTM with GA (5)	400 ± 40	106 ± 11	0.33 ± 0.04

*Data are the previously published results by Tang *et al.* (15) for 1.2-to-4.9–μm–thick (50 to 200 bilayers) samples tested at relative humidity of 32%.

We believe that the explanation of these results lies in the effective stiffening of the PVA matrix (due to constrained motion of the polymer chains) because of its close proximity to and many interactions with the MTM platelets. The evidence of this reinforcement mechanism comes from differential scanning calorimetry (DSC) analysis (Fig. 3, C to F), which shows suppression of the thermal motion of the PVA when it is constrained between dispersed nanoplatelets. This effect should result in a shift in glass transition temperature (T_g) toward the higher values. However, the overall suppression of motion makes the actual T_g of the polymer not very well defined for such systems, as can be seen in the width of the corresponding DSC peaks. A similar effect can be seen from a comparison of polymer melting temperatures (T_m) between pure PVA (Fig. 4C) and PVA/MTM (Fig. 4E). Whereas the T_m in PVA is sharp and very well defined, PVA/MTM shows strong suppression and broadening of the peak. An additional consequence of such stiffening is that traditional theories of composite mechanics using the bulk properties of pure polymers are difficult to apply to composites with high contents of a uniformly distributed inorganic phase. Mechanical-property enhancement in the GA cross-linked PVA/MTM is a result of an increase in the likelihood that a polymer chain in the PVA/MTM with GA system interacts strongly with two or more clay platelets, thereby improving the particle-to-matrix-to-particle load-transfer process over that in the PVA/MTM system.

In conclusion, reinforcement in polymer-nanoplatelet systems such as PVA/MTM is the result of several mechanisms operating at the nanoscale. The degree of structural organization (afforded by the LBL process) of the clay platelets in the composite maximizes the number of polymer/MTM interactions and constrains the polymer-chain motion, which results in a highly efficient load transfer between the polymer phase and the stiff MTM platelets.

References and Notes

1. M. M. J. Treacy, T. W. Ebbesen, J. M. Gibson, *Nature* **381**, 678 (1996).
2. M.-F. Yu *et al.*, *Science* **287**, 637 (2000).
3. O. Breuer, U. Sundararaj, *Polym. Compos.* **25**, 630 (2004).
4. G. Van Lier, C. Van Alsenoy, V. Van Doren, P. Geerlings, *Chem. Phys. Lett.* **326**, 181 (2000).
5. A. Sturcova, G. R. Davies, S. J. Eichhorn, *Biomacromolecules* **6**, 1055 (2005).
6. O. L. Manevitch, G. C. Rutledge, *J. Phys. Chem. B* **108**, 1428 (2004).
7. J. J. Mack *et al.*, *Adv. Mater.* **17**, 77 (2005).
8. M. A. S. A. Samir, F. Alloin, A. Dufresne, *Biomacromolecules* **6**, 612 (2005).
9. S. S. Ray, M. Okamoto, *Prog. Polym. Sci.* **28**, 1539 (2003).
10. E. P. Giannelis, *Adv. Mater.* **8**, 29 (1996).
11. G. Lagaly, *Appl. Clay Sci.* **15**, 1 (1999).
12. G. Decher, *Science* **277**, 1232 (1997).
13. A. A. Mamedov *et al.*, *Nat. Mater.* **1**, 190 (2002).
14. M. Olek *et al.*, *Nano Lett.* **4**, 1889 (2004).
15. Z. Tang, N. A. Kotov, S. Magonov, B. Ozturk, *Nat. Mater.* **2**, 413 (2003).
16. E. R. Kleinfeld, G. S. Ferguson, *Science* **265**, 370 (1994).
17. P. T. Hammond, *Adv. Mater.* **16**, 1271 (2004).
18. C. Jiang, V. V. Tsukruk, *Adv. Mater.* **18**, 829 (2006).
19. Z. Tang, Y. Wang, P. Podsiadlo, N. A. Kotov, *Adv. Mater.* **18**, 3203 (2006).
20. P. Podsiadlo, Z. Tang, B. S. Shim, N. A. Kotov, *Nano Lett.* **7**, 1224 (2007).
21. P. Podsiadlo, Z. Liu, D. Paterson, P. B. Messersmith, N. A. Kotov, *Adv. Mater.* **19**, 949 (2007).
22. A. A. Bonapasta, F. Buda, P. Colombet, *Chem. Mater.* **12**, 738 (2000).
23. M. Nagy, E. Wolfram, T. Varadi, *Prog. Colloid Polym. Sci.* **60**, 138 (1976).
24. D. Braun, E. Walter, *Colloid Polym. Sci.* **258**, 795 (1980).
25. Y. Guan *et al.*, *J. Phys. Chem. B* **110**, 13484 (2006).
26. A. Mamedov, J. Ostrander, F. Aliev, N. A. Kotov, *Langmuir* **16**, 3941 (2000).
27. M. Cheng, W. Chen, T. Weerasooriya, *J. Eng. Mater. Technol.* **127**, 197 (2005).
28. C. Y. Yue, G. X. Sui, H. C. Looi, *Compos. Sci. Technol.* **60**, 421 (2000).
29. A. M. Hindeleh, S. Abdo, *Polym. Commun.* **30**, 184 (1989).
30. A. B. Dalton *et al.*, *Nature* **423**, 703 (2003).
31. J. S. Bergstrom, M. C. Boyce, *Rubber Chem. Technol.* **72**, 633 (1999).

32. P.P. thanks the Fannie and John Hertz Foundation for support of his work through graduate fellowship. The authors thank Y. Elkasabi for help with FTIR spectroscopy and ellipsometry measurements; the staff of the Electron Microscopy Analysis Laboratory (Univ. of Michigan) and NSF (grant DMR-0320740); the Air Force Office of Scientific Research program on multifunctional materials (grant FA9550-05-1-043), and the U.S. Office of Naval Research (grant N00014-06-1-0473) for financial support.

Supporting Online Material

www.sciencemag.org/cgi/content/full/318/5847/80/DC1
Materials and Methods
Figs. S1 to S10
References

28 March 2007; accepted 4 September 2007
10.1126/science.1143176

Major Australian-Antarctic Plate Reorganization at Hawaiian-Emperor Bend Time

J. M. Whittaker,[1]* R. D. Müller,[1] G. Leitchenkov,[2] H. Stagg,[3] M. Sdrolias,[1] C. Gaina,[4] A. Goncharov[3]

A marked bend in the Hawaiian-Emperor seamount chain supposedly resulted from a recent major reorganization of the plate-mantle system there 50 million years ago. Although alternative mantle-driven and plate-shifting hypotheses have been proposed, no contemporaneous circum-Pacific plate events have been identified. We report reconstructions for Australia and Antarctica that reveal a major plate reorganization between 50 and 53 million years ago. Revised Pacific Ocean sea-floor reconstructions suggest that subduction of the Pacific-Izanagi spreading ridge and subsequent Marianas/Tonga-Kermadec subduction initiation may have been the ultimate causes of these events. Thus, these plate reconstructions solve long-standing continental fit problems and improve constraints on the motion between East and West Antarctica and global plate circuit closure.

A long-standing controversy in global tectonics concerns the ultimate driving forces that episodically cause major plate tectonic reorganizations. Proponents of "top-down" mechanisms [e.g., (*1*, *2*)] argue that plates themselves drive instabilities of the plate-mantle system, whereas others [e.g., (*3*)] have argued that major mantle overturns drive plate tectonic punctuations. The most prominent manifestation of this controversy is the Hawaiian-Emperor sea-

mount chain bend (HEB) (*4*). Whereas there is ample evidence from hotspot trails (*5*), paleomagnetism (*4*), geodynamic models (*6*), and intraplate volcanism (*7*) to support a mantle flow mechanism, there has been a lack of evidence for a plate reorganization at the original age of 43 million years ago (Ma) (*8*) proposed for the HEB (*9*). However, Wessel *et al.* (*10*) recognized that the recent redating of bend initiation to ~50 Ma (*11*) correlates the HEB with major tectonic events from around the Pacific, such as South Pacific triple-junction reorganization at magnetic anomaly chron 22-21 (49.7 to 47.9 Ma) (*12*), Farallon-Pacific fracture zone bends at magnetic anomaly chron 24-21 (53.3 to 47.9 Ma) (*13*), and the direction change and proposed halt of Pacific–Kula plate spreading at magnetic anomaly chron 24-20/19 (53.3 to 43.8/41.5 Ma) (*14*).

The southeast Indian Ocean is a region where a plate event contemporaneous with a major Pacific plate reorganization might be expected, but a historical paucity of magnetic anomaly data close to the Australian and Antarctic margins, combined with slow initial spreading rates, has resulted in poorly constrained plate fits before 50 Ma (*15*). Published reconstructions that assume a north-south spreading direction between Australia and Antarctica result in large overlaps between the South Tasman Rise and Cape Adare (*15*), and offsets in matching Australia-Antarctic geological terranes (*16*). Magnetic anomaly identifications, related to India-Antarctica spreading at 126 to 130 Ma (*17*), have been identified north of the Bruce Rise, Antarctica (Fig. 1), which results in the tectonically problematic juxtaposition of India-Antarctica–related magnetic anomalies between Australia and Antarctica when the Naturaliste Plateau is reconstructed to the north of the Bruce Rise (*15*). These problems indicate that Australia has been placed too far west with respect to a fixed Antarctica and that it is incorrect that the Perth and Vincennes fracture zones are conjugates (*15*). Two Australian-Antarctic fracture zone fabrics can be clearly identified from gravity anomaly data (Fig. 1): a northwest-southeast fabric on ocean floor older than chron 34 (83 Ma) and a north-south fabric on ocean crust younger than chron 21 (47.9 Ma). The model by Tikku and Cande (*15*) implies that the change in spreading direction resulting in these different fabrics occurred before chron 34 (83 Ma). Instead, we test the hypothesis that the Perth Fracture Zone is conjugate to a fracture zone, here named the Perth South Fracture Zone (Fig. 1), resulting in reconstruction of the Bruce Rise to the west of the Naturaliste Plateau. For our revised model, we investigate whether gravity

[1]EarthByte Group, School of Geosciences, University of Sydney, Sydney 2006, Australia. [2]VNII Okeangeologia (Antarctic Branch), St. Petersburg 190121, Russia. [3]Geoscience Australia, Canberra 2601, Australia. [4]Center for Geodynamics, Norwegian Geological Survey, Trondheim 7491, Norway.

*To whom correspondence should be addressed: E-mail: j.whittaker@geosci.usyd.edu.au

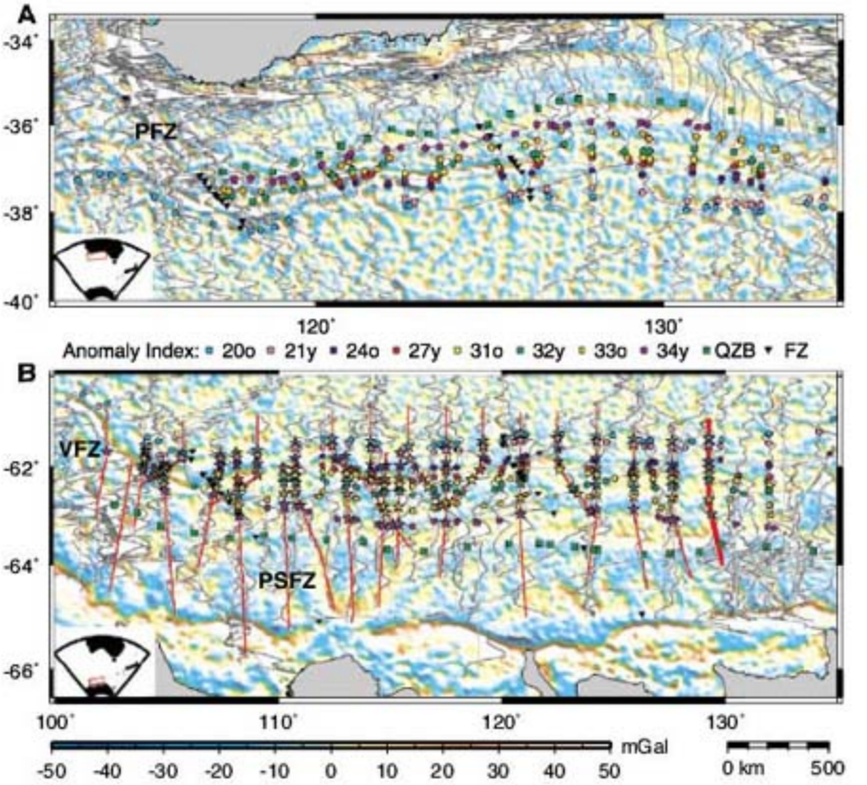

Fig. 1. Low-pass filtered (downward continued to the sea floor) 2-min gravity anomaly grid (*18*, *28*) for (**A**) Southern Australia and (**B**) East Antarctica (inset shows locations). Overlaid are ship tracks (gray lines), magnetic anomaly wiggles (black lines filled with white), gravity anomaly picks [squares, QZB (Quiet Zone Boundary)], fracture zone picks (inverted triangles, FZ), and magnetic anomaly picks [stars, this study; circles, Tikku and Cande (*15*)] used in this paper. Red lines in (B) are Geoscience Australia and Russian shiptracks (see main text), and bold red is shiptrack GA-22825 (fig. S1). PFZ, Perth Fracture Zone; PSFZ, Perth South Fracture Zone; and VFZ, Vincennes Fracture Zone.

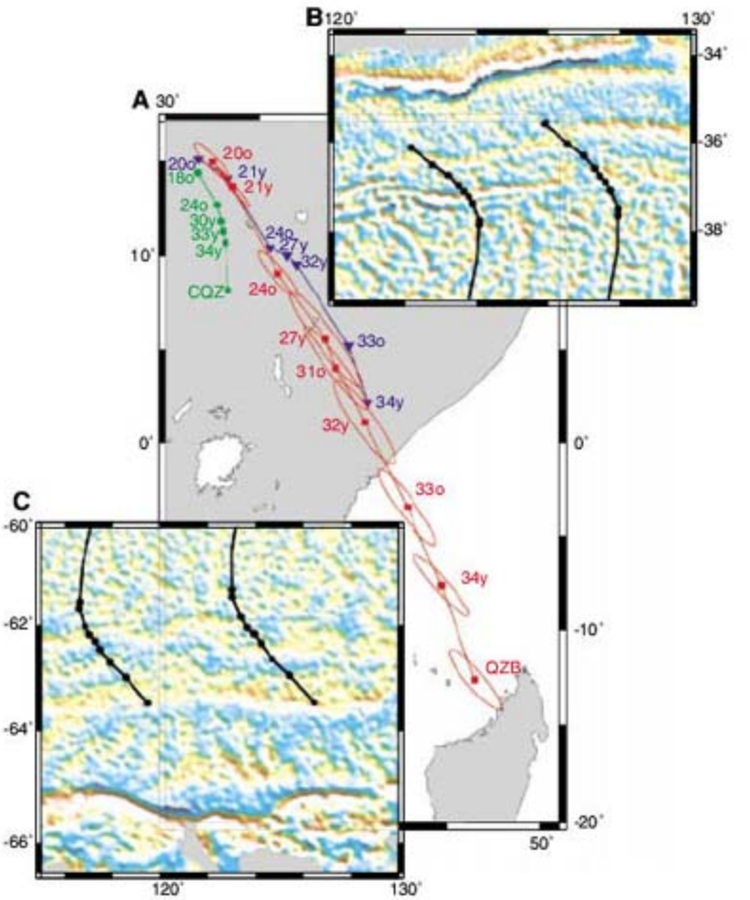

Fig. 2. (**A**) Poles about which Australia is restored to Antarctica based on calculated angles of rotation (finite poles of rotation) with 95% confidence interval ellipses. Red squares and red error ellipses represent our new rotation poles, inverted triangles are Tikku and Cande's (*15*) rotation poles, and green circles are Royer and Rollet's (*29*) rotation poles. (**B**) South Australian margin and (**C**) East Antarctic margin, downward continued gravity anomaly with fit of tectonic flowlines resulting from our new model. Tectonic flowlines are constructed for stage rotations between magnetic chrons shown in Fig. 1.

anomalies (*18*) permit a change in spreading direction at a younger time, resulting in a longer period of oblique relative motion than previously assumed.

New magnetic anomaly identifications made with recently acquired high-quality magnetic data in the Bruce Rise area (90° to 115°E) and along the Terre Adelie and Wilkes Land margins (115° to 132°E) were integrated with earlier identifications (*15*) (Fig. 1 and table S2). The motion of a tectonic plate can be described by a rotation angle about a virtual axis that passes through the center of the Earth and intersects its surface (finite pole of rotation). We used the combined fracture zone and magnetic anomaly identifications (Fig. 1) to define a new set of plate boundaries and compute well-constrained finite rotations and 95% uncertainty intervals (Fig. 2 and tables S3 and S4) that describe our new plate motion history for Australia and East Antarctica.

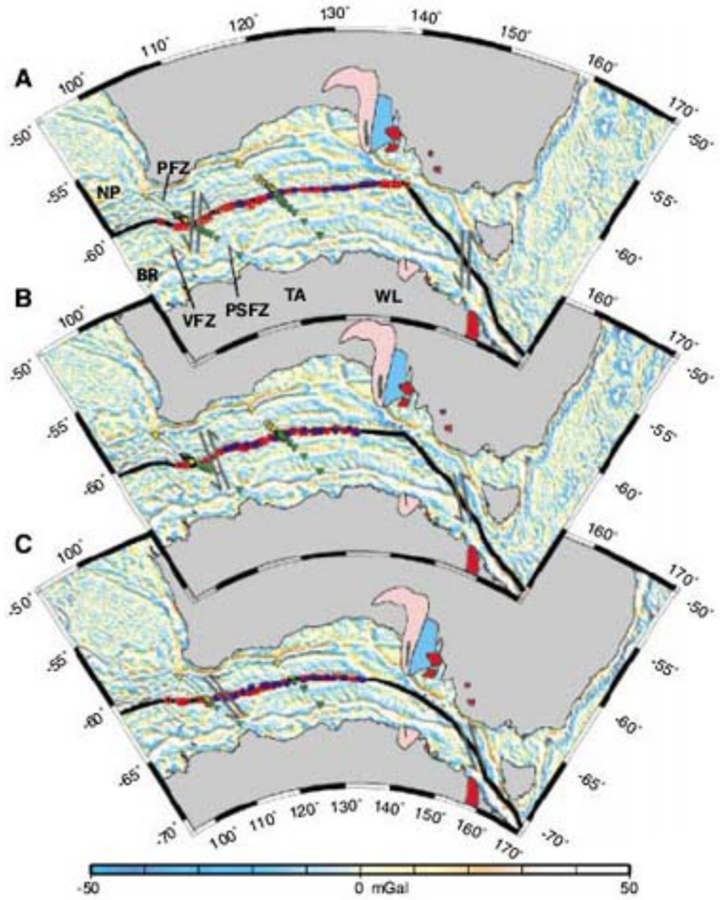

Fig. 3. Australia-Antarctica reconstructions based on our rotations at three stage boundaries: **(A)** 47.9 Ma, chron 21; **(B)** 61 Ma, chron 27; and **(C)** 83 Ma, chron 34. All magnetic chron ages are based on the time scale of Cande and Kent (*30*). Underlying image shows downward continued gravity anomalies. At 83 Ma, the Naturaliste Plateau (NP) is located to the east of the Bruce Rise (BR), there is no overlap between southeast Australia and Antarctica, and the Australian/Antarctic geological provinces align. Dark gray arrows show direction of motion of Australia and Antarctica for stages chron 21 to chron 18, chron 27 to chron 21, and chron 34 to chron 27 in (A), (B), and (C), respectively. Magnetic anomaly identifications for Australia and Antarctica for each reconstruction time are shown as red circles and black squares, respectively. Inverted triangles are fracture zone identifications for each chron older than the time of reconstruction. Geological provinces are as follows: pink, Neoarchean basement [~2.5 billion years ago (Ga)]; green, Paleoproterozoic basin (~1.69 Ga); light blue, metasediments (~2 Ga); and red, plutonic belt (~500 Ma) (*16*, *31*, *32*). WL, Wilkesland; TA, Terra Adelie; PFZ, Perth Fracture Zone; PSFZ, Perth South Fracture Zone; and VFZ, Vincennes Fracture Zone.

Our new plate reconstructions resolve long-standing continental and geological terrane fit problems with Australia, relative to Antarctica, positioned ~500 km east of previous reconstructions at 83 Ma (Fig. 3), and provide improved constraints on the motion between East and West Antarctica and global plate circuit closure.

When combined with geological evidence for relative plate motion changes around the Pacific, our reconstructions provide strong evidence for a major plate reorganization, which we argue was initiated by the subduction of the Izanagi-Pacific (I-P) ridge—a "top-down" mechanism. Circum-Pacific fracture zone bends document relative plate motion changes precipitated by the I-P ridge subduction, whereas the prominent HEB formed through a combination of altered Pacific plate motion and the well-documented deceleration of Pacific mantle (*4*, *6*).

We present a new plate reconstruction for the western Pacific (Fig. 4) based on matching isochrons and a set of simple assumptions (table S5). In our plate model, mid-ocean ridge subduction beneath southern Japan occurs at 60 to 55 Ma, 20 million years later than proposed for Kula-Pacific (*19*) or Farallon-Izanagi (*20*) ridge subduction. The difference arises because I-P spreading ceases in previous models after 110 Ma, whereas our model incorporates continued spreading until the I-P ridge subducts beneath eastern Asia at 60 to 55 Ma. Cessation of spreading at the I-P ridge between 110 and 80 Ma is unlikely because the Izanagi plate was undergoing rapid motion, driven by net slab-pull force, from the north-northwest (*21*), immediately before the proposed spreading cessation.

Metamorphism of the Ryoke Belt in southern Japan has previously been attributed to Kula–Pacific ridge subduction at 85 Ma (*19*), but the high-temperature/low-pressure Ryoke Belt cannot be uniquely linked to a ridge subduction event (*22*). Unreasonably high spreading rates of 35 to 40 cm/year during the Cretaceous Normal Superchron between the Pacific and Izanagi plates would be necessary to subduct the I-P ridge at 85 Ma, which is more than double the fastest current spreading rate globally [~15 cm/

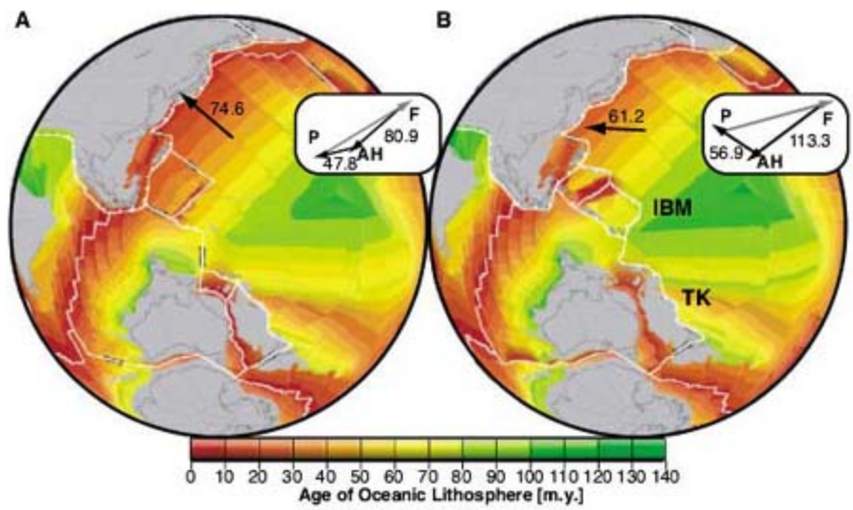

Fig. 4. Reconstructed oceanic crustal age grids at two time slices **(A)** 55 Ma and **(B)** 45 Ma. Black arrows (in mm/year) show western Pacific (30°N, 150°E) plate motion over the stages 60 to 50 Ma and 50 to 40 Ma, respectively. (Inset) Vectors (in mm/year) (same 10-Ma stages) show motion of the eastern Pacific (30°N, 240°E) (P) and Farallon (F) plates relative to fixed African hotspots (AH) over the period 60 to 50 Ma and 50 to 40 Ma. Eastern and western Pacific directions and changes in plate motion are substantially different. Geographical location of poles (latitude, longitude) about which rotations (angle) describing Pacific plate motion relative to an African hotspot reference frame are 55.0°N, –118.4°W, –7.90° and 59.4°N, –19.3°W, –5.52° at 60 to 50 Ma and 50 to 40 Ma, respectively. The resultant relative plate motions between the Pacific and Farallon plates show that our model explains the shape of the Pacific-Farallon fracture zone bend as well as the HEB. TK, Tonga-Kermadec subduction zone; IBM, Izu-Bonin-Marianas subduction zone. m.y., millions of years.

year between the Pacific and Nazca plates (*23*)]. We propose that subparallel subduction of the I-P mid-ocean ridge beneath Japan at 60 to 55 Ma resulted in nearly simultaneous slab break-off along the length of the Japanese trench (~2700 km). Geological observations from southern Japan support subduction of the I-P ridge and subsequent slab break-off at 60 to 55 Ma. Evidence includes cessation of a major accretion phase in the Late Cretaceous (*24*), emplacement of the Okitsu Melange due to subduction of hot, buoyant material at 55 Ma (*24*), and cross-cutting fault fabrics that indicate a counterclockwise rotation in relative plate motions between Eurasia and the I-P plate, which are also consistent with paleothermal and paleopressure data, between 55 and 34 Ma (*25*).

Rapid subduction of the I-P ridge, over a vast distance, triggered a chain reaction of tectonic plate reorganizations. With complete subduction of the I-P ridge at 55 Ma, forces acting on the Pacific changed from ridge-push to slab-pull, which changed Pacific absolute plate motions from northwest to west (Fig. 4). The change in Pacific plate motion caused cessation of Tasman Sea spreading at ~52 Ma (*26*). Increased slab pull north of Australia, due to a westerly progression of the subducting Wharton Basin mid-ocean ridge (Fig. 4), changed Australian absolute plate motion from northwest to north. A combination of Australian and Pacific plate motion changes between 53 and 50 Ma initiated both the Tonga-Kermadec (*2*) subduction system and the Izu-Bonin-Marianas subduction systems, which initiated likely before 50 Ma, due to convergence across a fracture zone caused by the Pacific plate motion change (*27*). We suggest that the observed slowdown of sub-Pacific mantle flow at 47 Ma (*4*) was due to progressive impediment of lateral sub-Pacific mantle flow by the descending slabs of the Izu-Bonin-Marianas and Tonga-Kermadec subduction zones.

The observed opposite bend geometries of the Emperor-Hawaii seamount chain and the Pacific-Farallon fracture zones can be explained with combined absolute (relative to a fixed reference frame) and relative plate motions. Clockwise rotation of eastern Pacific absolute plate motion, combined with stable Farallon plate motion (Fig. 4), results in a clockwise bend in Pacific-Farallon fracture zones at 53 to 49 Ma (*16*). In the western Pacific, a counterclockwise change in absolute plate motion, from northwest to west due to Izanagi Ridge subduction (Fig. 4), combined with a sub-Pacific mantle flow slowdown, results in the HEB. This conceptual model is testable via three-dimensional fully dynamic mantle flow simulations.

References and Notes

1. D. L. Anderson, *Science* **293**, 2016 (2001).
2. M. Gurnis, C. Hall, L. Lavier, *Geochem. Geophys. Geosyst.* **5**, Q07001 (2004).
3. S. D. King, J. P. Lowman, C. W. Gable, *Earth Planet. Sci. Lett.* **203**, 83 (2002).
4. J. A. Tarduno *et al.*, *Science* **301**, 1064 (2003).
5. P. Molnar, J. Stock, *Nature* **327**, 587 (1987).
6. B. Steinberger, R. Sutherland, R. J. O'Connell, *Nature* **430**, 167 (2004).
7. C. A. Finn, R. D. Müller, K. S. Panter, *Geochem. Geophys. Geosyst.* **6**, Q02005 (2005).
8. D. A. Clague, G. B. Dalrymple, *U.S. Geol. Surv. Prof. Paper* **1350** (1987).
9. I. O. Norton, *Tectonics* **14**, 1080 (1995).
10. P. Wessel, Y. Harada, L. W. Kroenke, *Geochem. Geophys. Geosyst.* **7**, Q03L12 (2006).
11. W. D. Sharp, D. A. Clague, *Science* **313**, 1281 (2006).
12. S. C. Cande, E. M. Herron, B. R. Hall, *Earth Planet. Sci. Lett.* **57**, 63 (1982).
13. D. W. Caress, H. W. Menard, R. N. Hey, *J. Geophys. Res.* **93**, 2813 (1988).
14. P. F. Lonsdale, *Bull. Geol. Soc. Am.* **100**, 733 (1988).
15. A. A. Tikku, S. C. Cande, *J. Geophys. Res.* **104**, 661 (1999).
16. C. A. Finn, D. Moore, D. Damaske, T. Mackey, *Geology* **27**, 1087 (1999).
17. C. Gaina, R. D. Müller, B. Brown, T. Ishihara, S. Ivanov, *Geophys. J. Int.* **170**, 151 (2007).
18. D. T. Sandwell, W. H. F. Smith, *Geophys. J. Int.* **163**, 79 (2005).
19. D. C. Engebretson, A. Cox, R. G. Gordon, *Geol. Soc. Am. Spec. Pap.* **206**, 1 (1985).
20. C. T. Onishi, G. Kimura, *Tectonics* **14**, 1273 (1995).
21. K. Otsuki, *Island Arc* **1**, 51 (1992).
22. M. Brown, *J. Metamorphic Geol.* **16**, 3 (1998).
23. W. P. Schellart, J. Freeman, D. R. Stegman, L. Moresi, D. May, *Nature* **446**, 308 (2007).
24. S. M. Agar, R. A. Cliff, I. R. Duddy, D. C. Rex, *J. Geol. Soc.* **146**, 893 (1989).
25. J. C. Lewis, T. B. Byrne, *Tectonics* **20**, 548 (2001).
26. C. Gaina *et al.*, *J. Geophys. Res.* **103**, 12413 (1998).
27. C. E. Hall, M. Gurnis, M. Sdrolias, L. L. Lavier, R. D. Müller, *Earth Planet. Sci. Lett.* **212**, 15 (2003).
28. W. H. F. Smith, D. T. Sandwell, *J. Geophys. Res.* **99**, 21803 (1994).
29. J.-Y. Royer, N. Rollet, *Aust. J. Earth Sci.* **44**, 543 (1997).
30. S. C. Cande, D. V. Kent, *J. Geophys. Res.* **100**, 6093 (1995).
31. G. Duclaux, P. Rey, S. Guillot, R. P. Ménot, *Geology* **35**, 715 (2007).
32. R. P. Ménot *et al.*, in *Antarctica: A Keystone in a Changing World—Online Proceedings of the 10th ISAES*, A. K. Cooper et al., Eds. (USGS Open-File Rep. 2007-1047, Short Research Paper 048, 2007).

33. We thank W. Smith for providing the downward continued gravity grid. Reviews by M. Gurnis and S. Cande, as well as detailed comments on early versions of the manuscript by P. Wessel, A. Dutkiewicz, and J. Stock, improved the manuscript considerably. We acknowledge the Ministry of Natural Resources of the Russian Federation and Geoscience Australia, who funded collection of some of the new marine magnetic data used in this work.

Supporting Online Material

www.sciencemag.org/cgi/content/full/318/5847/83/DC1
Fig. S1
Tables S1 to S5
References

13 April 2007; accepted 3 September 2007
10.1126/science.1143769

Absence of Cooling in New Zealand and the Adjacent Ocean During the Younger Dryas Chronozone

Timothy T. Barrows,[1]* Scott J. Lehman,[2] L. Keith Fifield,[1] Patrick De Deckker[3]

As the climate warmed at the end of the last glacial period, a rapid reversal in temperature, the Younger Dryas (YD) event, briefly returned much of the North Atlantic region to near full-glacial conditions. The event was associated with climate reversals in many other areas of the Northern Hemisphere and also with warming over and near Antarctica. However, the expression of the YD in the mid- to low latitudes of the Southern Hemisphere (and the southwest Pacific region in particular) is much more controversial. Here we show that the Waiho Loop advance of the Franz Josef Glacier in New Zealand was not a YD event, as previously thought, and that the adjacent ocean warmed throughout the YD.

The Younger Dryas (YD) event was originally recognized in Northern Europe and the adjacent North Atlantic Ocean as an abrupt return to near full-glacial conditions between 11,000 and 10,000 radiocarbon (^{14}C) years ago, an interval defined as the YD chronozone (*1*). Layer counting of Greenland ice cores (*2*), tree ring counts (*3*), and calibration of the ^{14}C time scale (*4*) now place the event between ~12,900 and ~11,600 calendar years before the present (cal yr B.P.). Evidence for teleconnected reversals of climate at this time occurs widely in the Northern Hemisphere (*5*), whereas the transfer of the Greenland climate stratigraphy to Antarctic ice cores via measurements of globally well-mixed atmospheric CH_4 trapped within the ice show clearly that a deglacial reversal of climate warming in Antarctica [the Antarctic Cold Reversal (ACR)] ended just as the Northern Hemisphere YD began (*6*). The latter is consistent with an antiphased relation of climate between Greenland and Antarctica seen earlier

[1]Department of Nuclear Physics, Research School of Physical Sciences and Engineering, The Australian National University, Canberra, ACT 0200, Australia. [2]Institute of Arctic and Alpine Research and Department of Geological Sciences, University of Colorado, Boulder, CO 80309, USA. [3]Department of Earth and Marine Sciences, The Australian National University, Canberra, ACT 0200, Australia.

*To whom correspondence should be addressed. E-mail: Tim.Barrows@anu.edu.au

in the glacial period (*6*, *7*), most likely due to altered interhemispheric heat transport by the ocean and/or alternation of deep-water formation between hemispheres (*8*). What remains both uncertain and very controversial is the nature of the YD climate signal, if any, in the mid- to low latitudes of the Southern Hemisphere (*9*–*12*).

The strongest case for cooling in the mid-latitude Southern Hemisphere during the YD is made on the basis of the Waiho Loop advance of the Franz Josef Glacier on the west coast of South Island, New Zealand (*9*). Twenty-five pieces of wood found buried beneath till at Canavans Knob, 1.6 km behind the moraine and ranging in age from ~12,800 to ~13,400 cal yr B.P. (10,750 to 11,520 ^{14}C yr B.P.) (*9*) suggest that the Waiho Loop formed immediately after this period during the YD chronozone. Higher in the Southern Alps, a mean ^{10}Be exposure age of 11,720 ± 320 years on boulders from the Lake Misery moraines in Arthur's Pass (*13*) also appears to support the claim for a glacier advance during the YD. These ages have prompted widespread debate, both because other climate proxies such as pollen do not indicate substantial YD cooling (*10*) and because marine records in the southwest Pacific Ocean display very different deglacial climate signals (*12*, *14*, *15*).

We chose a twofold approach to reassess the status of the YD interval in the region. First, we exposure dated the Waiho Loop moraine using the cosmogenic isotopes ^{10}Be and ^{36}Cl. This method has an advantage over ^{14}C dating in that it directly dates the moraine itself. Two nuclides provide internal-age control because each nuclide is produced from different targets and is analyzed and standardized independently. We collected samples from 10 boulders spatially distributed along the moraine crest. In two cases [WH-06 and WH-07 (Table 1)], we collected samples from both ends of large boulders, and in six cases it was possible to sample for both ^{10}Be and ^{36}Cl from the same boulder. Samples were prepared with the use of established methods (*16*). In total, we determined 24 ages, including 6 independently prepared duplicates for ^{36}Cl.

The choice of production rates for calculating exposure age is critical because systematic calibration errors directly propagate into the exposure-age uncertainty. We chose production rates calibrated with the retreat of ice at the conclusion of the YD in Scotland (*17*). This ties the exposure age of the Waiho Loop with a location of known YD age, making a direct age comparison possible. Uncertainties in production-rate scaling factors due to the geomagnetic field and atmospheric thickness are small because our site is similar to the YD calibration sites in terms of age, latitude, and altitude.

Exposure-age results are presented in Table 1 and tables S1 to S4. There is a high degree of coherence between the ages, and only one boulder age falls within the YD chronozone. Statistical dispersion between the ages of duplicates, ages derived from different isotopes analyzed from the same sample, and ages of different samples from the same boulder is similar to the dispersion between the ages of the boulders themselves. One exception is boulder WH-09, where all three ages are significantly younger than the main grouping. This was the only boulder sampled with smaller blocks resting on top of it, perhaps indicating a former till cover. The ages from the other nine boulders form a population ($\chi^2/\nu = 2.55$, where ν is the number of degrees of freedom) with a weighted mean age of 10,480 ± 240 years (*18*). Therefore, ice retreated from the Waiho Loop moraine ~1100 years after the end of the YD, meaning that it cannot be a YD-associated event. The moraine is ~2300 years younger than the youngest wood recovered beneath till correlated with the moraine (*9*). Those dates may record the initial advance of the Franz Josef Glacier just before the YD and during the ACR (~14,450 to 12,900 cal yr B.P.), a possibility raised earlier by Broecker (*5*) on the basis of the older ^{14}C dates at Canavans Knob. If these dates record a full advance of ice to the Waiho Loop, then the moraine must have formed over a period of ~2300 years, explaining its large size.

To compare our exposure ages directly with those from the putative YD moraines at Arthur's Pass (*13*), we recalculated the latter using the YD ^{10}Be production rate (*19*). Four out of the five samples form a population ($\chi^2/\nu = 0.28$) with a weighted mean age of 13,420 ± 630 years (*20*). Therefore, ice retreated from the Lake Misery moraines at the end of the ACR, ~1800 years before the conclusion of the YD and ~3000 years before the Waiho Loop moraine was abandoned by ice. To validate our production-rate methodology, we recalculated the age of the Egesen moraines in Julier Pass, Switzerland, that are believed to have formed during the YD (*13*). The new weighted mean ages for the outer and inner Egesen moraines are 13,020 ± 670 and 11,410 ± 440 years (versus the originally calculated ages of 11,750 ± 240 and 10,470 ± 260 years), indicating that the glacier occupied Julier Pass during the YD. Consequently, our method confirms the age of known YD moraines in the Northern Hemisphere. Even if we applied other commonly used ^{10}Be production rates (*21*, *22*), these rates would decrease the age of the Waiho Loop boulders and increase the mismatch with the YD.

The second approach we used to detect possible cooling during the YD was to construct a new high-resolution deep-sea record of sea surface temperature (SST) 180 km west of the Waiho Loop in the Tasman Sea. Core SO136-GC11 was collected during a *Sonne* cruise on the Challenger Plateau (43° 26.40′S, 167° 51.04′E, water depth of 1556 m), north of the present-day Subtropical Front and in the same meteorological area as the glacier (*23*). We estimated SST using the alkenone-unsaturation paleotemperature technique [see supporting online material (SOM)] and the empirical temperature calibration from sediments of Müller *et al.* (*24*), which is statistically identical to the laboratory-based calibration of Prahl *et al.* (*25*). Although the absolute temperature calculated from alkenone measurements depends on the choice of calibration, the relative precision of individual measurements is high (typically 0.5°C) and sufficient to detect small relative changes in SST. The age model was constructed with the use of 13 accelerator mass spectrometry (AMS) ^{14}C dates on the planktonic foraminifera *Globorotalia inflata* back to 23,830 cal yr B.P. (Fig. 1, table S5, and SOM). Because of the proximity to outwash from coastal glaciers, sedimentation rates peaked at ~18,400 and ~27,000 to 28,000 cal yr B.P., during maximum glaciation (*26*). The alkenone-sample interval during the YD chronozone is 200 to 300 years and as little as ~20 years during the last glacial maximum (LGM).

The SST reconstruction is shown in Fig. 1, along with δ^{18}O of the planktonic foraminifera *Globigerina bulloides* from SO136-GC11, Greenland and Antarctic oxygen isotope records

Table 1. Exposure ages for boulders on the Waiho Loop. Boulder ages are error-weighted means with standard deviation of the ages. The second "^{36}Cl age" column represents a duplicate analysis. Ages are in thousands of years. ND, not done.

Sample	^{36}Cl age	^{36}Cl age	^{10}Be age	Boulder age
WH-01	11.43 ± 0.60	10.70 ± 0.91	11.29 ± 0.90	11.23 ± 0.39
WH-02	11.31 ± 0.59	ND	10.39 ± 1.01	11.08 ± 0.65
WH-03	ND	ND	10.75 ± 0.85	10.75 ± 0.85
WH-04	9.57 ± 0.52	8.52 ± 1.11	9.69 ± 0.83	9.46 ± 0.64
WH-05	ND	ND	9.12 ± 0.76	9.12 ± 0.76
WH-06*	11.11 ± 0.55	ND	ND	9.24 ± 2.14†
WH-06*	8.09 ± 0.44	ND	ND	See above†
WH-07*	8.58 ± 0.47	11.62 ± 1.33	ND	9.40 ± 1.52‡
WH-07*	10.23 ± 0.58	ND	ND	See above‡
WH-08	8.28 ± 0.47	8.90 ± 0.83	6.87 ± 1.03	8.22 ± 1.04
WH-09	5.16 ± 0.30	5.03 ± 0.55	5.32 ± 0.50	5.17 ± 0.15
WH-10	12.79 ± 0.67	10.37 ± 0.81	11.37 ± 1.76	11.77 ± 1.22

*Samples from either end of large boulders. †The above value is an average age for both WH-06 samples. ‡The above value is an average age for both WH-07 samples.

(*7*, *27*), and a nearby pollen record (*28*). The timing of full-glacial cooling and subsequent deglacial warming is very similar to that seen in the South Island pollen record, consistent with a strong influence of the adjacent ocean on the local climate (*29*). Although not yet directly dated, a rapidly fluctuating SST decline and planktonic $\delta^{18}O$ increase (cooling) began ~29,000 cal yr B.P. and reached near full-glacial temperatures ~27,000 cal yr B.P., consistent with an early glacial cooling seen in the pollen series (*28*) and the longer record of New Zealand glaciation (*30*). Similar high-amplitude SST fluctuations are seen to the east of New Zealand and in the Southern Ocean (*29*).

Despite the documented presence of high-amplitude SST variability in the early (pre-LGM) part of the record, the warming after the abrupt increase in SST at ~19,000 cal yr B.P. is monotonic. There is no discernible decrease in SST during the deglacial period, only gradual warming that peaks at ~11,400 cal yr B.P. at the conclusion of the YD. There are no short-term fluctuations late in the Pleistocene that could potentially be a YD cooling event, even allowing for generous errors in the age model. Consistent with warming in the SST series, the YD interval appears to be associated locally with a period of maximum forest growth (increasing abundance of podocarps and hardwoods, Fig. 1), not cooling. The Holocene is characterized by a continuous SST decline to the present, seen also in the tropical western Pacific Ocean (*31*). This is consistent with late Holocene neoglaciation in New Zealand, including in the valley behind the Waiho Loop moraine (*32*).

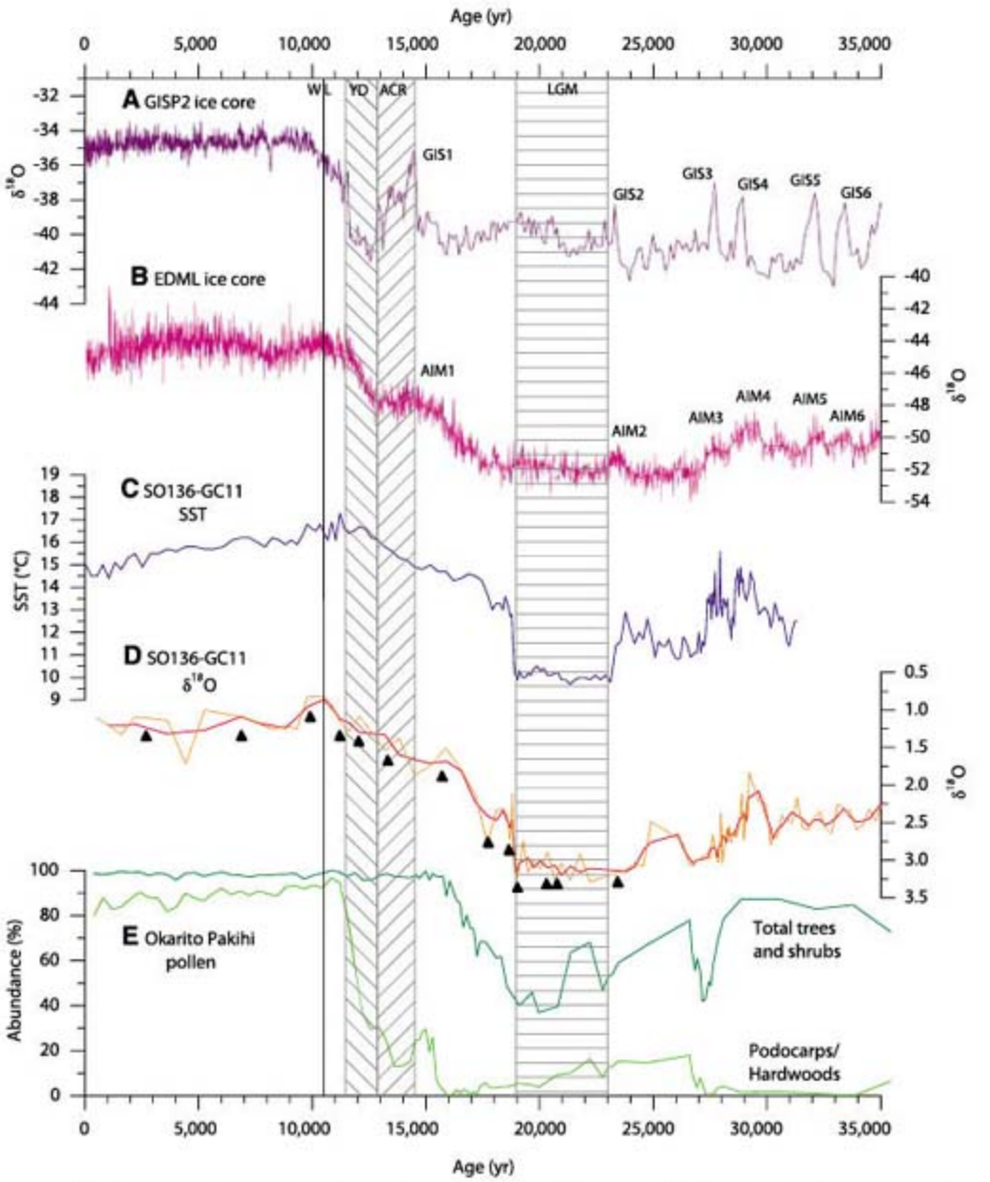

Fig. 1. (**A**) Greenland Ice Sheet Project 2 (GISP2) ice core $\delta^{18}O$ record (*27*). GIS, Greenland Interstadial. (**B**) Antarctic European Project for Ice Coring in Antarctica (EPICA) Dronning Maud Land (EDML) ice core $\delta^{18}O$ record (*7*) (solid line is a spline fit). AIM, Antarctic isotope maximum. (**C**) Alkenone-derived SST record of SO136-GC11. (**D**) Planktonic oxygen isotope record of SO136-GC11 (solid line is a three-point running mean). Triangles show the position of ^{14}C dates. (**E**) Pollen abundance of podocarps and hardwoods together with that of total trees and shrubs from Okarito Pakihi (*28*), located about 12 km from the Waiho Loop. YD, Younger Dryas chronozone; WL, age of the Waiho Loop.

The new and revised exposure ages presented here overturn evidence for glacier advance in New Zealand during the YD chronozone, previously considered to be the strongest basis for cooling in the Southern Hemisphere at this time (*5*). The possibility of glacier advance of the Franz Josef Glacier during the ACR cannot be ruled out, but we show that retreat from the Waiho Loop occurred several millennia later. Glacier retreat from the moraines at Arthur's Pass occurred much earlier. The upwind SST record indicating progressive warming during both the ACR and the YD is not readily consistent with regional forcing of coordinated glacier advance at either time and probably points to more local controls on glacier mass balance, especially for the Franz Josef Glacier (*33*). The absence of YD cooling in New Zealand increasingly calls into question its presence within the Southern Hemisphere, especially in mid-latitudes where there is little or no physical basis for climate teleconnection with the North Atlantic region.

References and Notes

1. J. Mangerud, S. T. Andersen, B. E. Berglund, J. J. Donner, *Boreas* **3**, 109 (1974).
2. S. O. Rasmussen *et al.*, *J. Geophys. Res.* **111**, D06102 (2006).
3. B. Becker, B. Kromer, *Radiocarbon* **28**, 961 (1986).
4. K. A. Hughen, J. R. Southon, S. J. Lehman, J. T. Overpeck, *Science* **290**, 1951 (2000).
5. W. S. Broecker, *Science* **300**, 1519 (2003).
6. T. Blunier, E. J. Brook, *Science* **291**, 109 (2001).
7. EPICA Community Members, *Nature* **444**, 195 (2006).
8. T. M. Marchitto, S. J. Lehman, J. D. Ortiz, J. Flückiger, A. van Geen, *Science* **316**, 1456 (2007); published online 10 May 2007 (10.1126/science.1138679).
9. G. H. Denton, C. H. Hendy, *Science* **264**, 1434 (1994).
10. C. Singer, J. Shulmeister, B. McLea, *Science* **281**, 812 (1998).
11. F. Lamy *et al.*, *Science* **304**, 1959 (2004).
12. T. Correge *et al.*, *Nature* **428**, 927 (2004).
13. S. Ivy-Ochs, C. Schlüchter, P. W. Kubik, G. H. Denton, *Geogr. Ann. Ser. A Phys. Geogr.* **81**, 313 (1999).
14. K. Pahnke, J. P. Sachs, *Paleoceanography* **21**, PA2003 (2006).
15. K. Pahnke, R. Zahn, H. Elderfield, M. Schulz, *Science* **301**, 948 (2003).
16. T. T. Barrows, J. O. Stone, L. K. Fifield, R. G. Cresswell, *Quat. Sci. Rev.* **21**, 159 (2002).
17. Materials and methods are available as supporting material online.
18. The χ^2/ν statistic > 1 suggests that there may be former shielding on some of the younger boulders or earlier exposure on some of the older boulders, increasing the overall scatter in the data. Eliminating some of the younger ages would increase the age of the moraine but would not affect the conclusion that the moraine is younger than 11,600 years.
19. J. O. Stone, C. K. Ballantyne, L. K. Fifield, *Geology* **26**, 587 (1998).
20. The inclusion of the fifth younger age increases the χ^2/ν statistic to 1.5 and does not change the conclusion (weighted mean age for the moraine becomes 12,720 ± 550 years).
21. K. Nishiizumi *et al.*, *J. Geophys. Res.* **94**, 17907 (1989).
22. P. W. Kubik, S. Ivy-Ochs, *Nucl. Instrum. Methods* **B223–B224**, 618 (2004).
23. B. Anderson, W. Lawson, I. Owens, B. Goodsell, *J. Glaciol.* **52**, 597 (2006).
24. P. J. Müller, G. Kirst, G. Ruhland, I. von Storch, A. Rosell-Melé, *Geochim. Cosmochim. Acta* **62**, 1757 (1998).

25. F. G. Prahl, L. A. Muehlhausen, D. L. Zahnle, *Geochim. Cosmochim. Acta* **52**, 2303 (1988).
26. R. P. Suggate, P. C. Almond, *Quat. Sci. Rev.* **24**, 1923 (2005).
27. P. M. Grootes, M. Stuiver, J. W. C. White, S. Johnsen, J. Jouzel, *Nature* **366**, 552 (1993).
28. M. J. Vandergoes *et al.*, *Nature* **436**, 242 (2005).
29. T. T. Barrows, S. Juggins, P. De Deckker, E. Calvo, C. Pelejero, *Paleoceanography* **22**, PA2215 (2007).
30. S. C. Porter, *Quat. Res.* **5**, 27 (1975).
31. L. Stott *et al.*, *Nature* **431**, 56 (2004).
32. S. C. Porter, *J. Quat. Sci.* **15**, 395 (2000).
33. Moraines similar to the Waiho Loop are absent from adjacent glacier-occupied valleys. Nonetheless, circulation patterns are closely linked to glacier advance and retreat in New Zealand (*34*), so it is likely that persistent southwesterly circulation occurred at the time of the deposition of the Waiho Loop.
34. P. D. Tyson, A. P. Sturman, B. B. Fitzharris, S. J. Mason, I. F. Owens, *Int. J. Climatol.* **17**, 1499 (1997).
35. We thank H. Scott-Gagan, J. Cali, and M. Gagan (Research School of Earth Sciences, Australian National Univ.) for helping to prepare the oxygen isotope data; A. Crotwell [Institute of Arctic and Alpine Research (INSTAAR), Univ. of Colorado] for helping to prepare alkenone samples; J. Turnbull (INSTAAR Laboratory for AMS Radiocarbon Preparation and Research, Univ. of Colorado) for the preparation of ^{14}C samples for AMS; J. Thiede, S. Nees, and K. Swanson, who were instrumental in obtaining core SO136-GC11; and S. Tims for helping to collect the AMS data. This work was supported by Australian Research Council grants [to T.T.B. (DP0557143) and P.D.D.] and NSF grant OCE 0081257 (to S.J.L.).

Supporting Online Material
www.sciencemag.org/cgi/content/full/318/5847/86/DC1
Materials and Methods
Fig. S1
Tables S1 to S5
References

30 May 2007; accepted 30 August 2007
10.1126/science.1145873

Toward Direct Measurement of Atmospheric Nucleation

Markku Kulmala,[1]* Ilona Riipinen,[1] Mikko Sipilä,[1] Hanna E. Manninen,[1] Tuukka Petäjä,[1] Heikki Junninen,[1] Miikka Dal Maso,[1] Genrik Mordas,[1] Aadu Mirme,[2] Marko Vana,[1,2] Anne Hirsikko,[1] Lauri Laakso,[1] Roy M. Harrison,[3] Ian Hanson,[3] Carl Leung,[3] Kari E. J. Lehtinen,[4] Veli-Matti Kerminen[5]

Atmospheric aerosol formation is known to occur almost all over the world, and the importance of these particles to climate and air quality has been recognized. Although almost all of the processes driving aerosol formation take place below a particle diameter of 3 nanometers, observations cover only larger particles. We introduce an instrumental setup to measure atmospheric concentrations of both neutral and charged nanometer-sized clusters. By applying the instruments in the field, we come to three important conclusions: (i) A pool of numerous neutral clusters in the sub–3 nanometer size range is continuously present; (ii) the processes initiating atmospheric aerosol formation start from particle sizes of ~1.5 nanometers; and (iii) neutral nucleation dominates over the ion-induced mechanism, at least in boreal forest conditions.

Formation of new atmospheric aerosol particles (diameter of 3 to 10 nm) by nucleation and subsequent growth has been observed in a wide variety of low- and high-altitude locations (*1*). Once the formed particles grow further in size, they may participate in cloud formation and influence the regional or even global radiation balance and ultimately climate. On more local scales, these particles may be deleterious to human health and impair visibility.

Despite the growing list of locations where frequent aerosol formation has been observed, the overall magnitude of this source is still very poorly understood compared with that of any other major source generating particles into the atmosphere. There are at least two reasons for this. First, atmospheric aerosol formation is driven by processes taking place below a 3-nm particle diameter, which is outside the range of most measuring devices in use. Second, the nucleation mechanism initiating aerosol formation is likely to vary with location and atmospheric conditions. Proposed atmospheric nucleation mechanisms include kinetic (or barrierless), binary, ternary, and ion-induced (or ion-mediated) nucleation (*1*–*3*), some of which might further be affected by meteorological processes such as turbulent fluctuations, atmospheric waves, and mixing (*4*, *5*). Most nucleation mechanisms have been thought to involve gaseous sulfuric acid, even though nucleation taking place in association with clouds and in coastal areas could be induced by water-insoluble (*6*) and iodine compounds (*7*), respectively.

Recently it was suggested that the formation of new atmospheric aerosol particles is connected with the existence of thermodynamically stable 1- to 2-nm clusters (*8*), formed in the atmosphere by some nucleation mechanism. From a physical standpoint, two very different cluster types in the sub–3 nm size range can be distinguished: charged (air ions or ion clusters) and neutral species. The existence of atmospheric ion clusters as small as 0.5 to 1 nm in diameter has been known for decades, and measurements with ion spectrometers, such as the Air Ion Spectrometer (AIS) and Balanced Scanning Mobility Analyzer (BSMA), have demonstrated that such clusters are present almost all the time (*9*). The production rates of ion clusters are, however, generally too low to explain the observed aerosol-formation rates (*10*).

In view of the insufficient numbers of ion clusters, the key to understanding atmospheric aerosol formation is clearly the presence of neutral clusters. Theoretical arguments predict the existence of such clusters (*8*, *11*) and suggest that

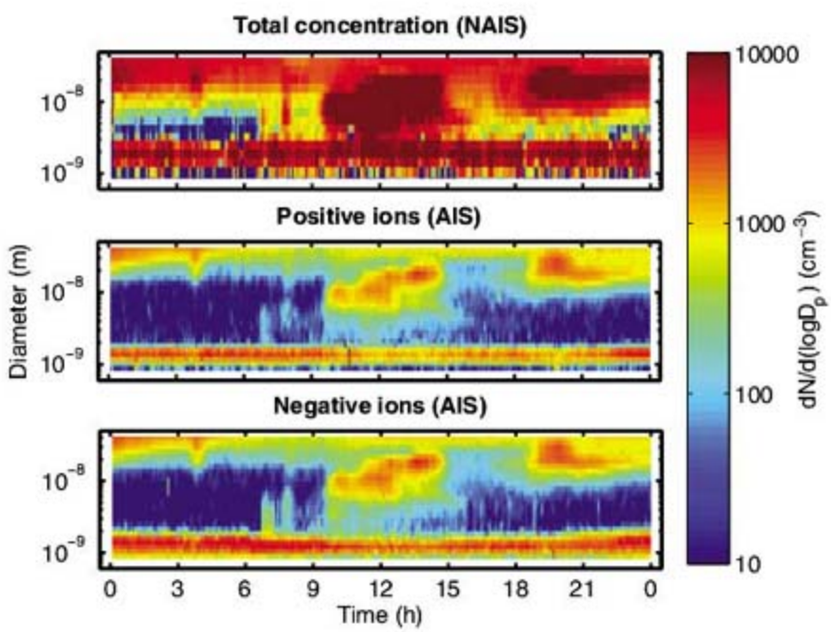

Fig. 1. Evolution of particle number size distribution measured with the NAIS on a particle formation event day (23 April 2006) in Hyytiälä, Finland.

[1]Department of Physical Sciences, University of Helsinki, Post Office Box 64, FI-00014, Helsinki, Finland. [2]Institute of Environmental Physics, University of Tartu, Ülikooli 18, EE-50090, Tartu, Estonia. [3]Division of Environmental Health and Risk Management, School of Geography, Earth and Environmental Sciences, University of Birmingham, Edgbaston, Birmingham B15 2TT, UK. [4]Department of Physics, University of Kuopio and Finnish Meteorological Institute, Kuopio Unit, Post Office Box 1627, 70211 Kuopio, Finland. [5]Finnish Meteorological Institute, Post Office Box 503, FI-00101, Helsinki, Finland.

*To whom correspondence should be addressed. E-mail: kulmala@pcu.helsinki.fi

they should play an important role in aerosol formation processes via their activation (*12*). Proposed candidates for neutral clusters include ammonium bisulfate clusters (*12*, *13*) and clusters formed by ion-ion recombination (*14*). The presence of neutral atmospheric clusters has not been experimentally verified so far, because the commercially available instruments cannot reliably detect neutral aerosol particles smaller than about 3 nm in diameter.

Here we provide experimental evidence for the existence of neutral clusters in the atmosphere and demonstrate that the processes initiating atmospheric aerosol formation include clusters with sizes close to 2 nm in diameter. The investigation is based on three very recently developed instruments: the Neutral Cluster–Air Ion Spectrometer (NAIS), the UF-02proto Condensation Particle Counter (UF-02proto CPC), and a Grimm nanoDMA and Faraday Cup Electrometer preceded by a unipolar charger (*15*, *16*). Measured total (air ion plus neutral) cluster concentrations are compared with corresponding air ion concentrations obtained from BSMA and AIS measurements, as well as with cluster concentrations calculated theoretically (*16*, *17*).

The data collected in this work were measured in Hyytiälä, southern Finland, during 10 weeks and during 3 weeks in Birmingham, UK, in spring 2006 (*16*). The most compelling evidence for the existence of neutral clusters is given by the NAIS measurements. Figure 1 shows the evolution of the cluster size distribution, both neutral and charged clusters, on one particle-formation event day in Hyytiälä. Similarly to ion measurements (see also figs. S7 to S9), there seems to be a cluster mode present all the time, with a median size of ~1.5 to 1.8 nm and extending to slightly below 1 nm at the lower end and to ~2.5 nm at the upper end. The total number concentration of this cluster mode is on the order of 1000 cm^{-3}. Owing to continuous scavenging of the clusters by coagulation, the presence of a continuous cluster mode suggests also continuous nucleation. If the particles do not grow above 3 nm before they are scavenged, they cannot be detected with traditional aerosol sizing instruments (such as Differential Mobility Particle Sizer, DMPS; fig. S6). This is the case for our example day before ~9 a.m.

At ~10 a.m. a fraction of the clusters activate, i.e., start growing to larger sizes. This can be caused by a sudden lowering of the coagulation sink and/or an increase of condensable vapor concentrations. The particle formation is also observable with DMPS (fig. S6).

The air ion and total cluster concentrations in Hyytiälä, in the size range of 1.8 to 3.0 nm, are shown in Fig. 2 for a period of 70 days. Typical concentrations of air ions were between about 10 and 100 cm^{-3} in the daytime and <10 cm^{-3} during the night. The total cluster concentrations were much higher, on the order of 1000 cm^{-3}. Therefore, there must have been a large number (~1000 to 10000 cm^{-3}) of neutral clusters present almost all the time. The observed order of magnitude can be predicted by using simple balance equations for neutral and charged particle concentrations (*16*), but only if a substantial neutral nucleation rate is assumed. Consequently, ion-induced nucleation, activation of ion clusters, or ion-ion recombination cannot produce sufficient number of neutral clusters, and thus the majority of nucleation (at least in Hyytiälä) has to be neutral.

For a more detailed analysis, we selected two aerosol formation event days in Hyytiälä, during which simultaneous data from the NAIS, UF-02proto CPCs, AIS, BSMA, and DMPS were available. On the first day (23 April), we observed an aerosol formation event between about 09:00 and 15:00 (*16*). The time evolution of the total cluster concentration in the size range of 1.8 to 3.0 nm, as measured by the UF-02proto CPC pair, followed closely that measured by the NAIS (Fig. 3A). On the next day (24 April) there was less agreement between these two measurement systems, yet both showed similar overall cluster concentrations (Fig. 3B). Compared with the total cluster numbers, which reached concentrations of up to 1500 to 3000 cm^{-3}, the concentrations of air ions in the same range were much lower, on the order of 10 to 100 cm^{-3} (Fig. 3, C and D).

Figure 4 compares theoretically calculated cluster concentrations with those measured by the NAIS on 23 April during the active period of 3-nm particle formation. Outside the actual particle formation and growth time frame, our calculation procedure is not valid (*16*). Excluding the few short periods when momentary decreases in particle formation rate drive down calculated

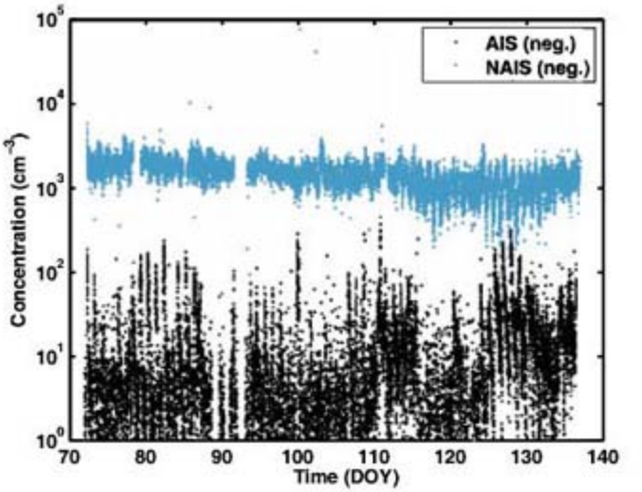

Fig. 2. Time series of cluster concentrations. Number concentrations of 1.8- to 3-nm aerosol particles and negative air ions measured with the NAIS (blue) and AIS (black) between 13 March and 16 May 2006.

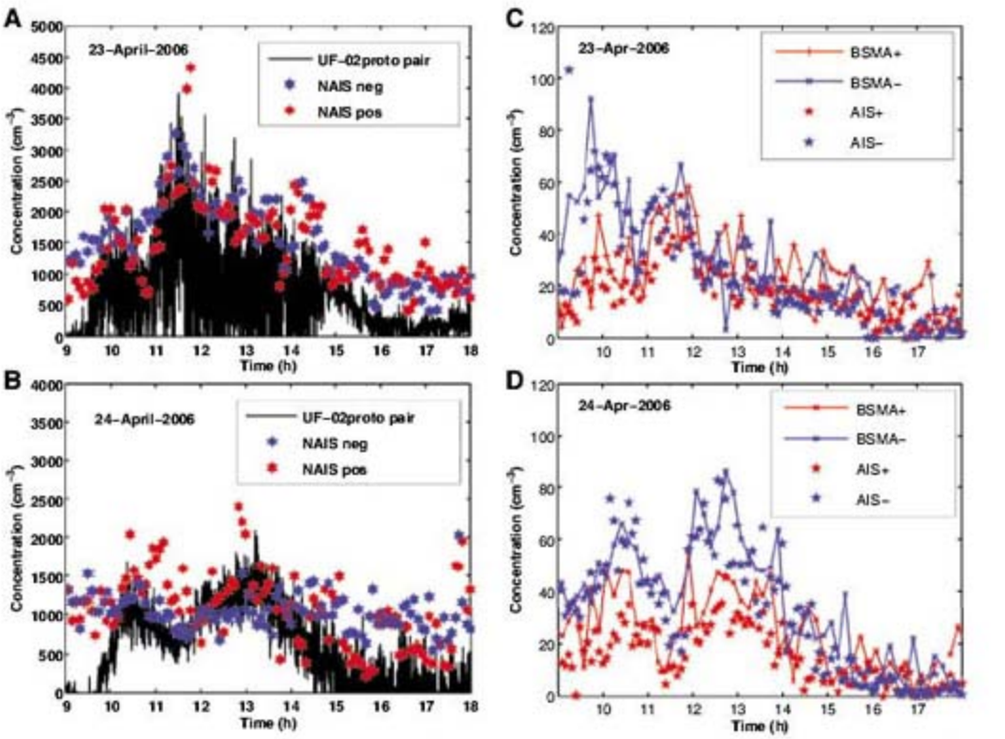

Fig. 3. Cluster concentrations on 2 days with new particle formation. (**A** and **B**) Total cluster-number concentrations between 1.8 and 3.0 nm observed by the NAIS (blue and red) and UF-02proto CPC pair (black) during 23 and 24 April 2006. (**C** and **D**) Negative (blue) and positive (red) air ion number concentrations measured with the AIS and BSMA during 23 and 24 April 2006.

cluster concentrations, a close agreement between calculated and measured cluster concentrations is seen. The data measured in Birmingham (*16*) show also a strong diurnal cycle in particles of 1.8- to 3-nm diameter (fig. S10)

Thus, the three different approaches applied here give total cluster concentrations that are usually within a factor of 2 of each other and roughly two orders of magnitude larger than air ion concentrations of similar size. These findings demonstrate unambiguously that sub–3 nm neutral clusters exist in the atmosphere and that they dominate over corresponding charged clusters at least down to 1.8 nm in size.

Hints about the existence of neutral clusters can be found in the scientific literature. In their laboratory measurements of prenucleation molecular clusters in a ternary $NH_3/H_2SO_4/H_2O$ system, Hanson and Eisele (*18*) observed large amounts of neutral clusters, using a transverse chemical ionization apparatus. The composition of their clusters might be comparable to that of atmospheric clusters observed in the present study. In another laboratory study, Kim *et al.* (*19*) analyzed homogeneous and ion-induced nucleation in the ternary $NH_3/SO_2/H_2O$/air mixture. They proposed homogeneous nucleation of $(NH_4)_2SO_4$ molecules produced by the H_2SO_4-NH_3 reaction as the main nucleation mechanism. Regardless of the details of the nucleation mechanism, e.g., ammonium bisulfate clusters can be considered proper candidates for neutral clusters in the atmosphere. Our CPC is probably not the only such instrument capable of observing the neutral clusters: Gamero-Castaño and de la Mora (*20*) proposed clusters as "impurities in the gas phase." However, their study focused on the activation of ions and charged nanoclusters under laboratory conditions.

Our observations can be used to test different hypotheses related to atmospheric nucleation and initial growth of nucleated clusters. For example, we have calculated the formation rate of 1.8-nm clusters in Hyytiälä, denoted here as J_2 (*16*). On 23 April, the value of J_2 for all clusters together was in the range of 1.5 to 1.6 cm^{-3} s^{-1}, as calculated from the NAIS data, and 1.1 cm^{-3} s^{-1}, as calculated from the UF-02proto CPC pair data. For negative and positive ions, values of J_2 calculated from the AIS data were 0.02 and 0.04 cm^{-3} s^{-1}, respectively. On the basis of our ion-DMPS method (*21*), no appreciable ion-nucleation was observed on this day. On 24 April, the values of J_2 for total clusters and positive ions were similar to those observed on the previous day, whereas the average J_2 for negative ions was roughly three times as high. These features are reflected in the ratio between total cluster and air ion concentrations in the 1.8- to 3-nm size range (Fig. 5). On both days, the relative fractions of neutral clusters tracked each other, except during the new particle formation from 12:00 to 15:00 on 24 April. In this time period, the fraction of neutral clusters decreased from 0.97 to 0.93, indicating a larger (but less than 10%) contribution of ion-induced nucleation to J_2. The dominance of neutral over ion-induced nucleation is consistent with the findings of Eisele *et al.* (*22*) at another continental location.

Cluster size distributions (*16*) measured by the NAIS revealed that, similar to cluster ions, there appears to be a large pool of neutral clusters in the atmosphere all the time. These clusters have a larger mean size than ion clusters, and their distribution has a tail extending slightly above 2 nm. The presence of such a tail even in the absence of 3-nm aerosol formation, and the ~2-nm upper size of the continuous ion cluster and neutral cluster band, indicate strongly that dynamic processes initiating atmospheric aerosol formation take place at a particle diameter of ~2 nm, not 1 nm as previously thought. If true, this finding is important for at least two reasons. First, it suggests that with the latest instrumental developments, we can probe the size range in which atmospheric aerosol formation begins. Second, it makes atmospheric aerosol formation much less sensitive to nucleating vapor concentrations than if the aerosol formation were driven by traditional thermodynamic nucleation. The second point is consistent with the reported interdependencies of the atmospheric aerosol formation rate and gaseous sulfuric acid concentration (*23*, *24*). The obtained values of J_2 are in agreement with the nucleation rates predicted by the recent cluster activation theory (*12*), which further supports our experimental findings.

The observed nearly global occurrence of atmospheric aerosol formation provides compelling justification to include this phenomenon in large-scale atmospheric models, such as regional air-quality models and global climate models. Attempts to realize this objective have already been made (*25*–*29*). These pilot studies have demonstrated the need for more reliable nucleation parameterizations than are currently available. The instrumental developments described here, by observing neutral clusters about a nanometer smaller than previously measured, offer the opportunity to test existing nucleation theories against real atmospheric data. By conducting measurements similar to those reported here in a few carefully selected locations, it should be possible to develop simple yet sufficiently accurate nucleation parameterizations for large-scale modeling.

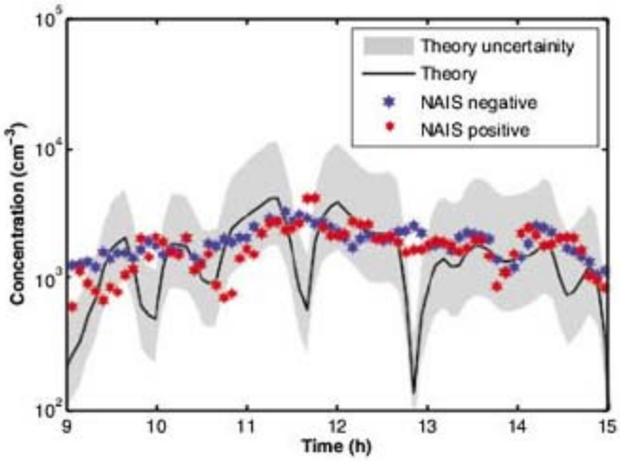

Fig. 4. Comparison with theory. Theoretically calculated total cluster concentrations (black) during the aerosol formation event on 23 April, along with the corresponding concentrations measured by the NAIS (blue and red). The shaded area gives an uncertainty range for theoretically calculated values (*16*, *17*), obtained by assuming that the real growth rate of 1.8- to 3.0-nm clusters might be a factor of 2 lower or higher than the growth rate estimated from the BSMA data (2.1 nm/hour).

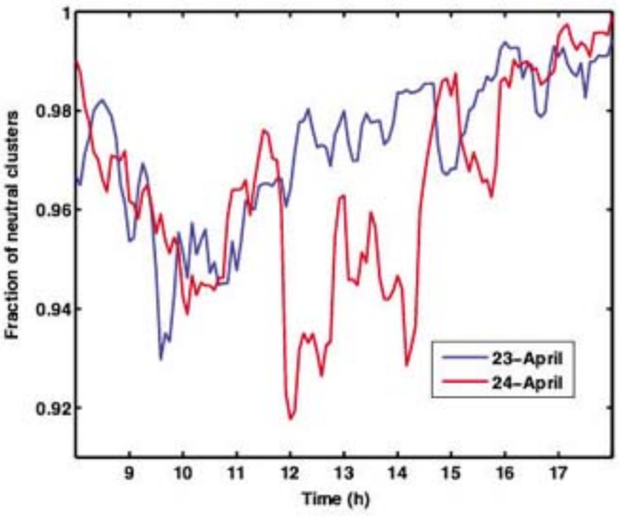

Fig. 5. Neutral cluster fraction. The neutral fraction of the total cluster concentration (1.8 to 3.0 nm) during 23 April 2006 (blue curve) and 24 April 2006 (red curve). During the latter day, the formed particles are negatively overcharged compared to the steady-state charge distribution based on observations obtained with the ion-DMPS (*21*).

References and Notes

1. M. Kulmala *et al.*, *J. Aerosol Sci.* **35**, 143 (2004).
2. F. Yu, R. P. Turco, *J. Geophys. Res.* **106**, 4797 (2001).
3. S. H. Lee *et al.*, *Science* **301**, 1886 (2003).
4. R. C. Easter, L. K. Peters, *J. Appl. Meteorol.* **33**, 775 (1994).
5. E. D. Nilsson, M. Kulmala, *J. Geophys. Res.* **103**, 1381 (1998).
6. M. Kulmala *et al.*, *J. Geophys. Res.* **111**, D17202 (2006).
7. C. D. O'Dowd *et al.*, *Nature* **417**, 632 (2002).

8. M. Kulmala, L. Pirjola, J. M. Mäkelä, *Nature* **404**, 66 (2000).
9. U. Hõrrak, J. Salm, H. Tammet, *J. Geophys. Res.* **103**, 13909 (1998).
10. L. Laakso, J. M. Mäkelä, L. Pirjola, M. Kulmala, *J. Geophys. Res.* **107**, 4427 (2002).
11. M. Kulmala, K. E. J. Lehtinen, L. Laakso, G. Mordas, K. Hämeri, *Boreal. Environ. Res.* **10**, 79 (2005).
12. M. Kulmala, K. E. J. Lehtinen, A. Laaksonen, *Atmos. Chem. Phys.* **6**, 787 (2006).
13. H. Vehkamäki, I. Napari, M. Kulmala, M. Noppel, *Phys. Rev. Lett.* **93**, 148501 (2004).
14. R. P. Turco, J.-X. Zhao, F. Yu, *Geophys. Res. Lett.* **25**, 635 (1998).
15. A. Alam, J.-P. Shi, R. M. Harrison, *J. Geophys. Res.* **108**, 4093 (2003).
16. Materials and methods are available as supporting material on *Science* Online.
17. V.-M. Kerminen, M. Kulmala, *J. Aerosol Sci.* **33**, 609 (2002).
18. D. R. Hanson, F. L. Eisele, *J. Geophys. Res.* **107**, 4158 (2002).
19. T. O. Kim, T. Ishida, M. Adachi, K. Okuyama, J. H. Seinfeld, *Aerosol Sci. Technol.* **29**, 111 (1998).
20. M. Gamero-Castaño, J. F. de la Mora, *J. Aerosol Sci.* **31**, 757 (2000).
21. L. Laakso *et al.*, *Atmos. Chem. Phys.* **7**, 1333 (2007).
22. F. L. Eisele *et al.*, *J. Geophys. Res.* **111**, D04305 (2006).
23. R. J. Weber *et al.*, *Chem. Eng. Commun.* **151**, 53 (1996).
24. S.-L. Sihto *et al.*, *Atmos. Chem. Phys.* **6**, 4079 (2006).
25. P. Stier *et al.*, *Atmos. Chem. Phys.* **5**, 1125 (2005).
26. D. V. Spracklen, K. J. Pringle, K. Carslaw, M. P. Chipperfield, G. W. Mann, *Atmos. Chem. Phys.* **5**, 3233 (2005).
27. D. V. Spracklen *et al.*, *Atmos. Chem. Phys.* **6**, 5631 (2006).
28. D. D. Lucas, H. Akimoto, *Geophys. Res. Lett.* **33**, L10808 (2006).
29. R. E. P. Sotiropoulou, E. Tagaris, C. Pilinis, T. Anttila, M. Kulmala, *Aerosol Sci. Technol.* **40**, 557 (2006).

30. Financial support by The Academy of Finland and the UK Natural Environment Research Council is gratefully acknowledged.

Supporting Online Material

www.sciencemag.org/cgi/content/full/1144124/DC1
Materials and Methods
Figs. S1 to S10
Tables S1 to S3
References

23 April 2007; accepted 13 August 2007
Published online 30 August 2007;
10.1126/science.1144124
Include this information when citing this paper.

A Cretaceous Scleractinian Coral with a Calcitic Skeleton

Jarosław Stolarski,[1]* Anders Meibom,[2] Radosław Przeniosło,[3] Maciej Mazur[4]

It has been generally thought that scleractinian corals form purely aragonitic skeletons. We show that a well-preserved fossil coral, *Coelosmilia* sp. from the Upper Cretaceous (about 70 million years ago), has preserved skeletal structural features identical to those observed in present-day scleractinians. However, the skeleton of *Coelosmilia* sp. is entirely calcitic. Its fine-scale structure and chemistry indicate that the calcite is primary and did not form from the diagenetic alteration of aragonite. This result implies that corals, like other groups of marine, calcium carbonate–producing organisms, can form skeletons of different carbonate polymorphs.

Scleractinian corals belong to the taxonomic class of anthozoans and are among the most prolific biomineralizing organisms in nature (*1*). Their calcium carbonate skeletons form shallow- and deep-water reefs and are prominent in the fossil record as far back as 240 million years ago (Ma) (*2*). Living scleractinians produce entirely aragonitic skeletons (*3*, *4*). An identification of calcite in calcification centers of the shallow-water scleractinian *Mussa* sp. (*5*) was not confirmed by subsequent analysis (*6*). Aragonite is metastable at ambient temperatures and pressures and is susceptible to diagenetic transformation to calcite, the stable form of calcium carbonate under ambient conditions. Most fossil scleractinians have therefore been dissolved or transformed to calcite, preserving only their macroscopic morphology. In these cases, the original mineralogy can be inferred on the basis of their Sr content and by analogy with living scleractinians (*7*). Although some studies have left open the possibility that the original mineralogy of some fossil Scleractinia was calcitic (*8*–*10*), it has been generally accepted that the aragonitic skeletal mineralogy of scleractinians was highly conserved throughout their evolution (*11*).

Here we show that a fossil scleractinian coral formed a calcitic skeleton. We studied a suite of fossil corals attributed to the caryophylliid genus *Coelosmilia*. Our specimens are from the Upper Cretaceous (Maastrichtian) deposits of Poland (fig. S1) and are similar, but not identical, to the fossils studied in (*12*) in which the calcite in the corals was inferred to have formed diagenetically. We have now used a variety of microanalytical methods to show that the calcite is instead primary. The overall skeletal architecture of *Coelosmilia* is similar to that of modern deep-sea corals, such as *Desmophyllum* (Fig. 1) and *Javania* (fig. S2). *Coelosmilia* sp. has a conical calice with septa arranged into five full cycles forming a hexameral pattern. Our specimens are complete skeletons and well preserved. External

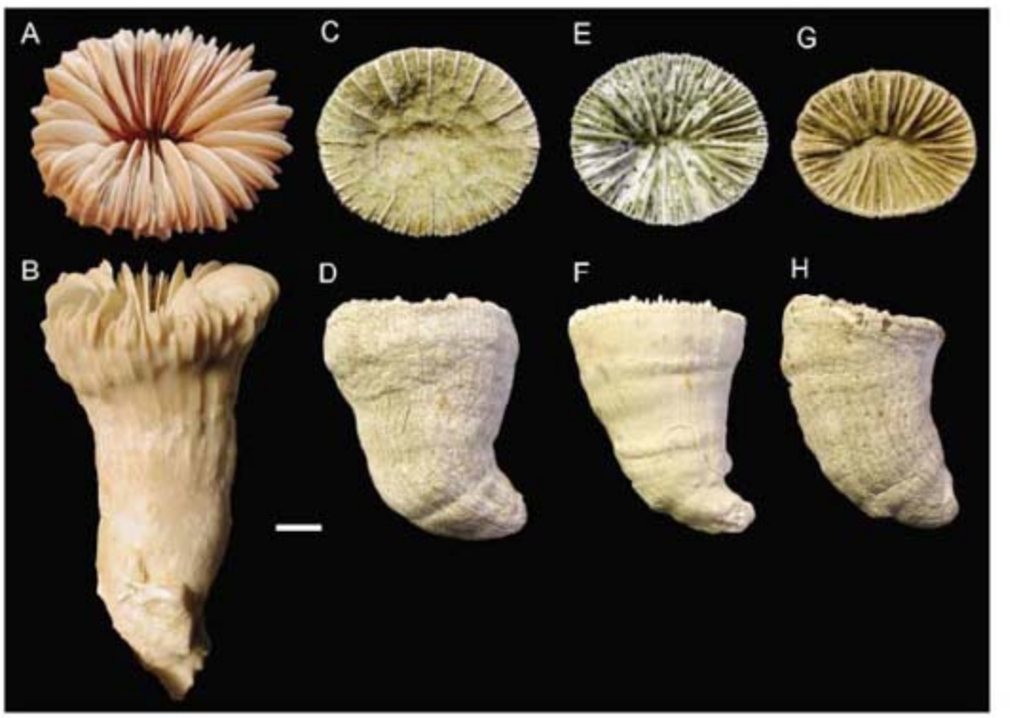

Fig. 1. Morphology of the modern aragonite *Desmophyllum* sp. and the Late Cretaceous calcitic *Coelosmilia* sp. (**A** and **B**) *Desmophyllum* sp. Relatively smooth septa, a thick septothecal wall, and a lack of pali are typical features of this solitary, azooxanthellate scleractinian coral. (**C** to **H**) *Coelosmilia* sp. resembles *Desmophyllum* sp. in all morphological aspects. Distal [(A), (C), (E), and (G)] and lateral [(B), (D), (F), and (H)] views are shown. Scale bar, 10 mm.

[1]Institute of Paleobiology, Polish Academy of Sciences, Twarda 51/55, PL-00-818 Warsaw, Poland. [2]Muséum National d'Histoire Naturelle, Laboratoire d'Etude de la Matière Extraterrestre, USM 0205 (LEME), Case Postale 52, 61 rue Buffon, 75005 Paris, France. [3]Institute of Experimental Physics, University of Warsaw, Hoża 69, PL-00-681 Warsaw, Poland. [4]Department of Chemistry, Laboratory of Electrochemistry, University of Warsaw, Pasteura 1, PL-02-093 Warsaw, Poland.

*To whom correspondence should be addressed. E-mail: stolacy@twarda.pan.pl

microarchitectural details, such as fine granulations on septal surfaces and, in some specimens, desmocyte attachment scars are still visible (fig. S2). In contrast, shells of gastropods, phragmocones of cephalopods, and other scleractinian coral species (*13*), which occur with *Coelosmilia* sp. in the same deposits, are dissolved and preserved only as molds and casts.

The skeleton of the specimen *Coelosmilia* sp., which we present in detail here, preserves all the structural details intact throughout its ontogeny (Fig. 2, A to C). The septal ultrastructure is characterized by a central line of well-organized calcification centers and radiating fiber bundles, constructed by the sequential addition of micrometer-sized growth layers (*14*, *15*). Longitudinal sections through the mid-septal zone reveal discrete vertical rods, similar to trabeculae in modern Scleractinia (Fig. 2D). Individual half-moon–shaped growth segments in the thecal region correspond to the position of former growth fronts in the wall (Fig. 2E). In polarized light, bundles of fibers show simultaneous and complete light extinction, indicating a parallel arrangement of crystallographic axes. All of these features are identical to those of living scleractinians (*14*, *15*). The structural similarity between *Coelosmilia* sp. and modern Scleractinia is strong, especially with the azooxanthellate members of the traditional suborder Caryophylliina, here represented by *Desmophyllum* sp. (Fig. 2, H to L).

Synchrotron radiation diffraction studies demonstrate that the *Coelosmilia* sp. skeleton is composed of calcite, without any trace of aragonite (Fig. 3A and fig. S6). In comparison to synthetic and geological calcite reference materials, the *Coelosmilia* sp. skeleton has broader Bragg peaks, indicating smaller crystallite sizes and/or larger microstrain fluctuations in the *Coelosmilia* sp. calcite. The inferred crystallite grain size is consistent with the size of individual calcite domains observed by atomic force microscopy (Fig. 2, F and G) and shows that, in analogy with modern corals, the *Coelosmilia* sp. skeleton is composed of crystallites typically 30 to 100 nm in linear dimension (*15*, *16*). Slight shifts in the *Coelosmilia* sp. Bragg peaks relative to the reference calcite spectrum are consistent with the lattice parameter differences between biogenic and synthetic Mg-containing calcite (*17*, *18*) (fig. S7).

The trace element composition of the *Coelosmilia* sp. skeleton is also consistent with a calcitic mineralogy. The fibrous (bulk) part of the skeleton has Mg/Ca and Sr/Ca ratios averaging about 15 and 0.7 mmol/mol, respectively (Fig. 3B). Typical Mg/Ca and Sr/Ca concentrations of modern aragonitic scleractinian corals are 1 to 5 and 7 to 10 mmol/mol, respectively. High-spatial-resolution (~200 nm) secondary ion mass spectrometry analyses (*19*) show that the Mg/Ca and Sr/Ca ratios oscillate in the *Coelosmilia* sp. skeleton across scales of a few micrometers, in a pattern similar to those observed in modern scleractinians (*20*).

We rule out the possibility that the calcite formed from the transformation of an originally aragonitic skeleton. The diagenetic transformation of aragonitic skeletons to calcite in fossil corals invariably involves complete reorganization of the skeletal ultrastructure. During diagenetic recrystallization, growing calcite cuts across septa and walls, leaving behind an irregular mosaic of calcite crystals, which eventually completely replaces the original ultrastructural organization of the skeleton (*7*). In contrast, in the *Coelosmilia* sp. skeleton, all ultrastructural elements are preserved and the crystals in the fiber bundles are well aligned, as demonstrated by the simultaneous and complete extinction of polarized light.

Cathodoluminescence observations of the fibrous part of the skeleton show no evidence of the cloudiness that is typically associated with recrystallization (fig. S3). The trace element chemistry also rules out a hypothetical aragonite-to-calcite transformation in which the crystal structure simply "flips" from aragonite to calcite, leaving all micrometer-scale features intact. During such a hypothetical transformation, the bulk chemistry of the skeleton would not change, because mass transfer (the dissolution and reprecipitation of carbonate) would not take place. However, the Mg/Ca and Sr/Ca ratios of the skeleton are different from typical aragonitic ratios, both by a factor of approximately 10, and the oscillatory pattern is inconsistent with simple equilibrium precipitation of carbonate from a supersaturated solution. In modern scleractinians, such trace element variations are driven by biological mechanisms involved in the biomineralization process (*19*, *20*). We therefore conclude that *Coelosmilia* sp. is a scleractinian coral with a primary calcitic skeleton.

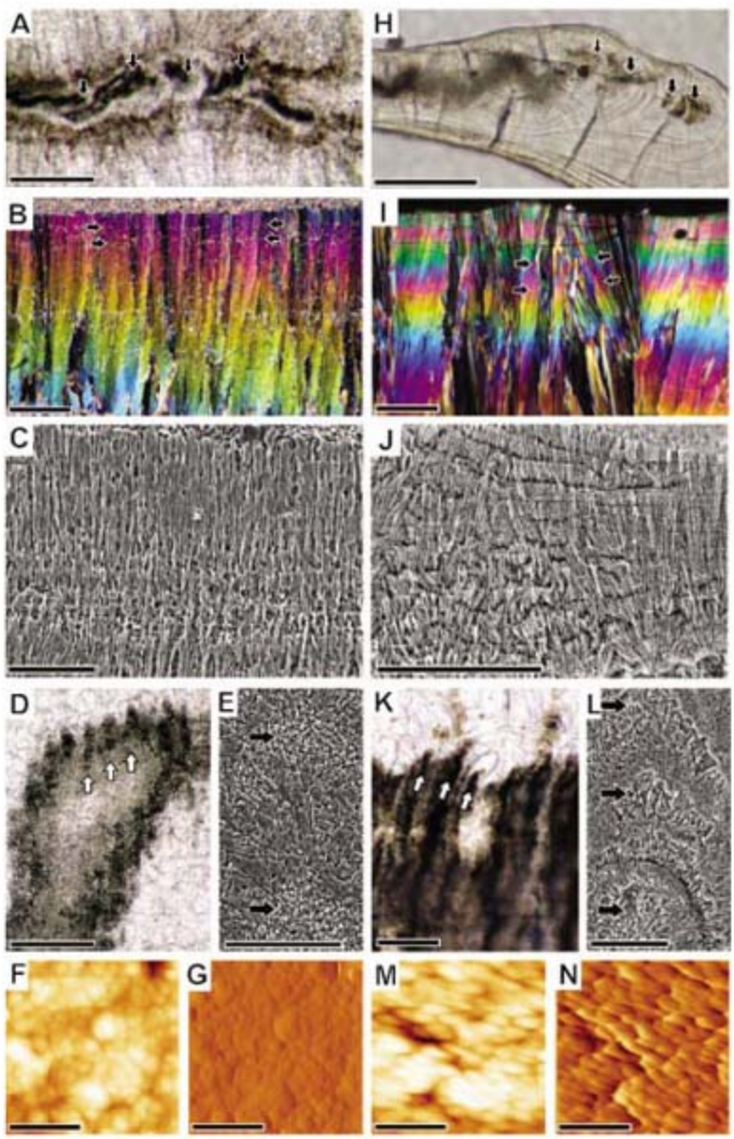

Fig. 2. Structural characteristics of the *Coelosmilia* sp. skeleton (left column) in direct comparison with the skeleton of *Desmophyllum* sp. (right column). (**A** and **H**) Optical microscopy transmitted-light images of a thin section through a septum perpendicular to the growth direction. Black arrows indicate successive growth steps in the zone of centers of calcification (COC), which appear darker than the surrounding fibrous skeleton. (**B** and **I**) Optical microscopy polarized transmitted-light images of a thin section through a septum perpendicular to the growth direction. The individual growth layers of the fibrous skeleton are clearly visible in both corals as optical layering (indicated by black arrows). (**C** and **J**) Scanning electron microscopy (SEM) images of the polished and etched surface of a septum perpendicular to the growth direction. Fiber bundles with individual growth layers are visible. (**D** and **K**) Optical microscopy transmitted-light images of a thin section through the midplane of a septum parallel to the growth direction and through the central axis of the COC. Successive COCs are organized as rods, or trabeculae, in the direction of growth, as indicated by white arrows. A slight undulating of the mid-septal zone trabecular centers make them appear and disappear from the plane of the cut section. (**E** and **L**) SEM images of the polished and etched surface of a cut through the thecal region parallel to the growth direction. Half-moon–shaped segments correspond to the position of organic enriched growth fronts in the wall. (**F**, **G**, **M**, and **N**) Atomic force microscopy images of skeletal fibers in height mode [(F) and (M)] and deflection mode [(G) and (N)], showing nanogranular structure. Scale bars in (A) to (E) and (H) to (L), 100 μm; in (F), (G), (M), and (N), 200 nm.

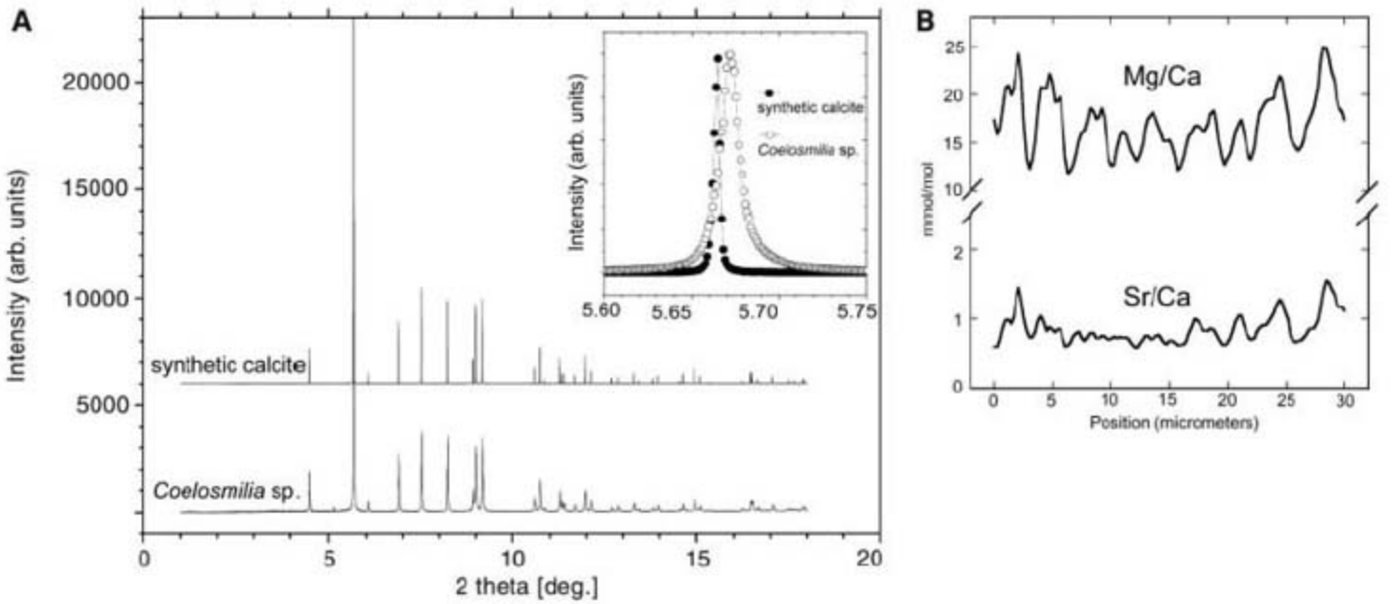

Fig. 3. Crystal structure and chemical composition of the *Coelosmilia* sp. calcitic skeleton. **(A)** High-resolution synchrotron radiation powder diffraction patterns of *Coelosmilia* sp. skeleton (lower trace) and synthetic calcite (upper trace). The most intense (104) Bragg peak is shown in the inset. The Bragg peaks of *Coelosmilia* sp. are broader than those of synthetic calcite. **(B)** Typical NanoSIMS ion microprobe transect across the layered fibrous part of the *Coelosmilia* sp. skeleton. The observed variations in Mg/Ca and Sr/Ca ratios are similar in wavelength and amplitude to those observed in modern scleractinians.

It has been suggested that hypercalcifying organisms, including corals, are sensitive to the Mg/Ca ratio of seawater, which has changed through geologic history in response to variations in the plate tectonic cycle (*21*). According to this model, hypercalcifying aragonite-producing organisms (including corals) flourish during periods in which seawater has a Mg/Ca ratio greater than 2, whereas hypercalcifying calcite-producing organisms flourish when the Mg/Ca ratio is less than 2 (in the modern ocean Mg/Ca = 5.2). The *Coelosmilia* sp. lived in the Late Cretaceous when the inferred Mg/Ca ratio of seawater was below 2. Our findings may thus appear to support the recently proposed idea that seawater composition can even change the skeletal mineralogy of scleractinians (*22*). However, other aragonitic scleractinians lived at about the same time as the *Coelosmilia* sp. specimens studied here (*16*, *23*), and other studies have shown that the chemical and isotopic composition of scleractinian skeletons is under strong biological control (*15*, *19*, *20*, *24*–*26*). Therefore, it seems more likely that the capability of scleractinians to produce either aragonitic or calcitic skeletons is genetically determined. In any case, skeletal mineralogy can no longer be considered a conservative feature among scleractinians throughout their evolution.

Scleractinians first appear in the fossil record in the Middle Triassic (~240 Ma), 12 to 14 million years after the Permian mass extinction, which exterminated an already weakened population of Paleozoic rugosan (calcitic) corals. The Permian mass extinction possibly resulted from the synergistic effects of environmentally linked stresses on marine organisms, perhaps including hypercapnia: the direct physiological effects of an increased partial pressure of CO_2 (*27*). The scleractinians represent the first corals in the fossil record after the extinction (*2*). Increased atmospheric CO_2 levels may increase the acidity of seawater, leading to the decalcification of carbonate skeletons and the formation of naked corals that can survive and resume calcification when atmospheric CO_2 levels decrease again (*28*). Our result, although from a much younger fossil, is consistent with the idea that scleractinians derive from naked corals or anemonelike ancestors, which survived the Permian mass extinction (*29*). When the scleractinians appeared in the Triassic, they abruptly formed a taxonomically robust and diverse group (*30*), consistent with having a substantial evolution and origin in the Paleozoic before the Permian mass extinction (*31*). Previously, the notion of a deeper evolutionary origin and a potential link between rugosans and some Mesozoic "scleractiniamorphs" ["aberrant scleractinians" (*11*)] was weakened by the presumed difference in skeletal mineralogy, but as we have shown here, this is no longer the case.

References and Notes

1. D. J. Barnes, M. J. Devereux, *J. Exp. Mar. Biol. Ecol.* **79**, 213 (1984).
2. G. D. Stanley, *Earth Sci. Rev.* **60**, 195 (2003).
3. M. Enders, *Arch. Naturgesch.* **1**, 646 (1932).
4. S. D. Cairns, *N.Z. Ocean. Instit. Mem.* **103**, 1 (1995).
5. B. R. Constantz, A. Meike, in *Origin, Evolution, and Modern Aspects of Biomineralization in Plants and Animals*, R. E. Crick, Ed. (Plenum, New York, 1990), pp. 201–207.
6. J. P. Cuif, Y. Dauphin, *Paläontol. Zeit* **72**, 257 (1998).
7. P. A. Sandberg, *Palaeontograph. Am.* **54**, 272 (1984).
8. V. Cornish, P. F. Kendall, *Geol. Mag.* **5**, 66 (1888).
9. O. B. Bøggild, *D. Kgl. Danske Vidensk. Selsk. Skrifter. Naturvidensk. Mathem.* **2**, 232 (1930).
10. J. Wendt, in *Skeletal Biomineralization: Patterns, Processes and Evolutionary Trends*, J. G. Carter, Ed. (Van Nostrand Reinhold, New York, 1990), pp. 45–66.
11. W. A. Oliver, *Paleobiology* **6**, 146 (1980).
12. P. Gautret, J. P. Cuif, J. Stolarski, *Acta Palaeontol. Pol.* **45**, 107 (2000).
13. J. Stolarski, A. Vertino, *Facies* **53**, 67 (2007).
14. J. Stolarski, *Acta Palaeontol. Pol.* **48**, 497 (2003).
15. J. P. Cuif, Y. Dauphin, *J. Struct. Biol.* **150**, 319 (2005).
16. J. Stolarski, M. Mazur, *Acta Palaeontol. Pol.* **50**, 847 (2005).
17. B. Pokroy, J. P. Quintana, E. N. Caspi, A. Berner, E. Zolotoyabko, *Nat. Mater.* **3**, 900 (2004).
18. B. Pokroy *et al.*, *J. Struct. Biol.* **155**, 96 (2006).
19. A. Meibom *et al.*, *Geophys. Res. Lett.* **34**, L02601 (2007).
20. A. Meibom *et al.*, *Geophys. Res. Lett.* **33**, L11608 (2006).
21. S. M. Stanley, L. A. Hardie, *Palaeogeogr. Palaeoclimatol. Palaeoecol.* **144**, 3 (1998).
22. J. B. Ries, S. M. Stanley, L. A. Hardie, *Geology* **34**, 525 (2006).
23. J. Sorauf, *J. Paleontol.* **73**, 1029 (1999).
24. D. J. Sinclair, B. Williams, M. Risk, *Geophys. Res. Lett.* **33**, 10.1029/2006GL027183 (2006).
25. C. Rollion-Bard, M. Chaussidon, C. France-Lanord, *Earth Planet. Sci. Lett.* **215**, 275 (2003).
26. N. Allison, A. A. Finch, M. Newville, S. R. Sutton, *Geochim. Cosmochim. Acta* **69**, 3801 (2005).
27. A. H. Knoll, R. K. Bambach, J. L. Payne, S. Pruss, W. Fischer, *Earth Planet. Sci. Lett.* **256**, 295 (2007).
28. M. Fine, D. Tchernov, *Science* **315**, 1811 (2007).
29. G. Stanley, D. Fautin, *Science* **291**, 1913 (2001).
30. E. Roniewicz, E. Morycowa, *Cour. Forsch. Inst. Senckenberg* **164**, 233 (1993).
31. S. L. Romano, S. R. Palumbi, *Science* **271**, 640 (1996).

32. We thank the European Synchrotron Radiation Facility (Grenoble, France) for access to synchrotron radiation facilities and M. Brunelli for technical support. Funding for this work was provided by the Polish Ministry of Science and Higher Education (projects N307-015733 and 155/ESR/2006/03), the French Agence Nationale de la Recherche, and by the Muséum National d'Histoire Naturelle.

Supporting Online Material

www.sciencemag.org/cgi/content/full/318/5847/92/DC1
Materials and Methods
Figs. S1 to S7
References

5 August 2007; accepted 5 September 2007
10.1126/science.1149237

Sex Chromosome–Linked Species Recognition and Evolution of Reproductive Isolation in Flycatchers

Stein A. Sæther,[1,2,3]* Glenn-Peter Sætre,[3] Thomas Borge,[2,3] Chris Wiley,[4,5] Nina Svedin,[4] Gunilla Andersson,[3] Thor Veen,[6] Jon Haavie,[2,3] Maria R. Servedio,[7] Stanislav Bureš,[8] Miroslav Král,[9] Mårten B. Hjernquist,[4] Lars Gustafsson,[4] Johan Träff,[10] Anna Qvarnström[4]

Interbreeding between species (hybridization) typically produces unfit offspring. Reduced hybridization should therefore be favored by natural selection. However, this is difficult to accomplish because hybridization also sets the stage for genetic recombination to dissociate species-specific traits from the preferences for them. Here we show that this association is maintained by physical linkage (on the same chromosome) in two hybridizing *Ficedula* flycatchers. By analyzing the mating patterns of female hybrids and cross-fostered offspring, we demonstrate that species recognition is inherited on the Z chromosome, which is also the known location of species-specific male plumage traits and genes causing low hybrid fitness. Limited recombination on the Z chromosome maintains associations of Z-linked genes despite hybridization, suggesting that the sex chromosomes may be a hotspot for adaptive speciation.

Reproductive isolation is traditionally viewed as an incidental by-product of genetic divergence during geographic isolation. However, many diverged populations come into contact before complete reproductive isolation has evolved. In such cases, natural selection against maladaptive interbreeding (hybridization) may complete speciation by reinforcing a tendency to mate with one's own kind (assortative mating) (*1*–*3*). This process, termed reinforcement, is of potentially great evolutionary significance because it suggests that reproductive isolation itself can be an adaptive response to natural selection. However, the empirical support for reinforcement is limited, and the conditions under which it can theoretically occur are sometimes strict (*2*, *4*).

Selection for assortative mating favors the buildup of genetic associations between components of assortative mating (species-specific traits and the preferences for these traits) and between such pre-zygotic barriers and low hybrid fitness (post-zygotic barriers). However, DNA recombination during hybridization breaks these associations necessary for speciation (*5*). Using a combination of field experiments, molecular techniques, and long-term breeding data from hybrid zones of wild birds in the Czech Republic and Sweden, we tested this central problem of reinforcement: How can the traits involved in reproductive isolation remain associated in the face of gene flow?

Two solutions to this problem have been suggested. First, species recognition can occur through a "one-allele mechanism": a single allele, established in both incipient species, can cause assortative mating (*2*, *5*, *6*). For example, sexual imprinting is a widespread phenomenon in birds (*7*), whereby females learn the traits of their fathers and later prefer similar males as mates. An allele causing sexual imprinting would make recombination irrelevant, because it would result in opposite mate preferences in the two species (*7*–*9*). Second, recombination can be suppressed through, for example, physical linkage of genes (*2*, *5*, *10*–*13*). Recent theoretical studies have highlighted the idea that sex linkage (placement on a sex chromosome) of species-recognition genes may enhance reinforcement when, as is often the case, genes causing low hybrid fitness are also sex-linked (*9*, *13*–*15*). We tested whether species recognition is due to sex-linked preferences, sexual imprinting, or autosomally inherited preferences in an avian system with evidence for reinforcement (*16*).

Where the breeding distributions of pied flycatchers [*Ficedula hypoleuca* (pied)] and collared flycatchers [*F. albicollis* (collared)] overlap (sympatry), the populations mate assortatively with respect to species (*17*). However, some interbreeding occurs [2 to 5% of pairs (*17*)], and the resulting hybrids have reduced fitness, female hybrids being sterile (*17*). Despite gene flow through male hybrids (*18*), both male plumage and female mate preferences have diverged furthest in sympatric areas, presumably to facilitate avoiding hybridization (*16*).

Genes causing hybrid incompatibility and genes influencing the expression of diverged male plumage traits are both located on the Z sex chromosome in flycatchers (*18*). Genes on the Z chromosome are in general likely to recombine less than if they were on autosomes; for instance, because sex chromosome recombination can occur only in the homogametic sex (supporting online text). In fact, previous studies have failed to detect any interspecific recombination between the Z chromosomes of hybridizing flycatchers, whereas autosomes recombine between the species (*18*). If genes on the Z also determine species recognition by females, recombination between loci that are important for reinforcement would be greatly reduced.

In birds, females inherit half of their autosomal genes from either parent, but their single Z chromosome solely from their father. We used this fact to distinguish between whether species recognition is inherited on autosomes or is paternally determined (by Z linkage or learned by sexual imprinting on fathers). If mate preferences are paternally determined, the mate choice of female hybrids should vary according to the species of their father, corresponding to that of pure females of the paternal species. To determine the paternal and maternal species of female hybrids, as well as their status as F_1 hybrids, we used species-specific genetic markers at the Z chromosome (paternally inherited) and in the mitochondrial genome (maternally inherited) (*19*).

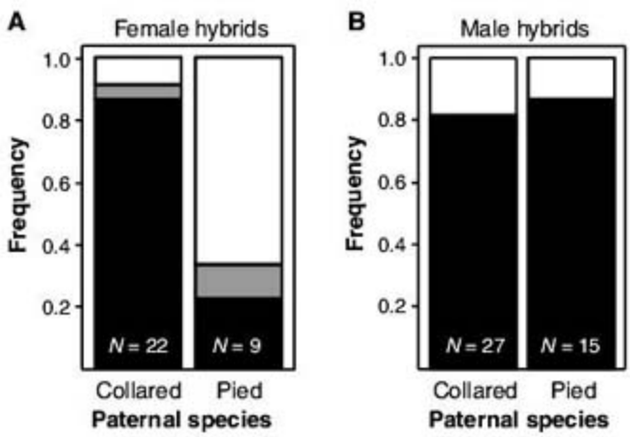

Fig. 1. Mating patterns of hybrid flycatchers. Female hybrids (**A**) predominately mated with males belonging to the same species as their father regardless of whether the father was a collared flycatcher or a pied flycatcher (black, collared partner; white, pied partner; gray, hybrid partner). In contrast, in male hybrids (**B**) no relationship was present between paternal species and the species of their mate.

[1]Department of Animal Population Biology, Netherlands Institute of Ecology, Post Office Box 40, 6666 ZG Heteren, Netherlands. [2]Department of Evolutionary Biology, Evolutionary Biology Centre (EBC), Uppsala University, Norbyvägen 18D, SE 75236 Uppsala, Sweden. [3]Centre for Ecological and Evolutionary Synthesis, Department of Biology, University of Oslo, Post Office Box 1050, Blindern, N 0316 Oslo, Norway. [4]Department of Animal Ecology, EBC, Uppsala University, Norbyvägen 18D, SE 75236 Uppsala, Sweden. [5]Department of Neurobiology and Behavior, Cornell University, Mudd Hall, Ithaca, NY 14853, USA. [6]Theoretical Biology Group, Centre for Ecological and Evolutionary Studies, University of Groningen, Kerklaan 30, 9751 NN Haren, Netherlands. [7]Department of Biology, University of North Carolina, CB 3280 Coker Hall, Chapel Hill, NC 27599, USA. [8]Laboratory of Ornithology, Palacký University, třída Svobody 26, 771 46 Olomouc, Czech Republic. [9]Forestry Commission, 783 86 Dlouhá Loučka, Czech Republic. [10]Visborgsgatan 28 A, SE 621 58 Visby, Sweden.

*To whom correspondence should be addressed. E-mail: s.a.sather@bio.uio.no

We found that female hybrids having a pied father predominately mated with a pied male, whereas female hybrids having a collared father predominately mated with a collared male (Fig. 1A). Only 4 out of 31 female hybrids mated with a male of the maternal species. Thus, there was a nonrandom association between the species of a female hybrid's father and the species of her mate [$x_2^2 = 12.37$, exact $P = 0.001$, $N = 31$ hybrids; excluding matings with male hybrids, Fisher's exact test, $P = 0.001$, $N = 29$]. This pattern was present in both Czech ($P = 0.048$, $N = 9$) and Swedish ($P = 0.062$, $N = 22$) sympatric areas.

Male hybrids, on the other hand, inherit a Z chromosome from both parental species and are unaffected by sexual imprinting because male flycatchers do not discriminate against heterospecific partners (*20*). As expected, there was no association between the paternal species of male hybrids and the species of their mate (Fisher's exact test, $N = 42$, $P = 1$, Fig. 1B). This implies that the pattern observed in female hybrids is not simply some artefact of hybrids but is consistent only with paternal inheritance (through Z linkage or sexual imprinting) of species recognition; this therefore eliminates autosomal inheritance as the mechanism behind species-assortative mating.

Flycatchers provide an ideal system in which to disentangle sexual imprinting from Z linkage, because hybridizing females often engage in extrapair copulations with conspecific males (*17*), resulting in purebred offspring being reared by cuckolded heterospecific males. We used multigenerational breeding data to analyze the mate choices of such pure female flycatchers that had been reared by a male of the other species. If assortative mating is due to sexual imprinting, these females should prefer heterospecific males as their mates. We also experimentally cross-fostered offspring between nests of the two species and recorded the mate choice of cross-fostered females that returned to breed. Under genetic inheritance of species recognition, cross-fostered females should mate as other females of their own species, whereas under sexual imprinting, they should mate as females of the foster father's species (*19*).

In contrast to prevailing views on the development of sexual preferences in birds (*7*), Fig. 2 shows that females did not become sexually imprinted on their social father. Instead, females with a heterospecific foster father mated with conspecific males to the same extent as other females of their own species did. This conclusion applies to females of both species, using both naturally (Fig. 2, A and B) and experimentally (Fig. 2, C and D) cross-fostered offspring and regardless of whether expected mating patterns were calculated from all breeding pairs or from recruits of known parents only. Although some of the sample sizes are small because of the rarity of these events, the evidence is overwhelming that species recognition does not develop by sexual imprinting in these birds. Instead, our results imply that species-assortative mating has a genetic basis.

Assuming Mendelian inheritance, the different mate preference of the two kinds of female hybrids is solely consistent with Z linkage. A non-Mendelian epigenetic possibility is that the preference genes are autosomally inherited, but only the paternal allele is expressed (maternal genomic imprinting). However, such parent-of-origin effects have not been found in birds (*21*).

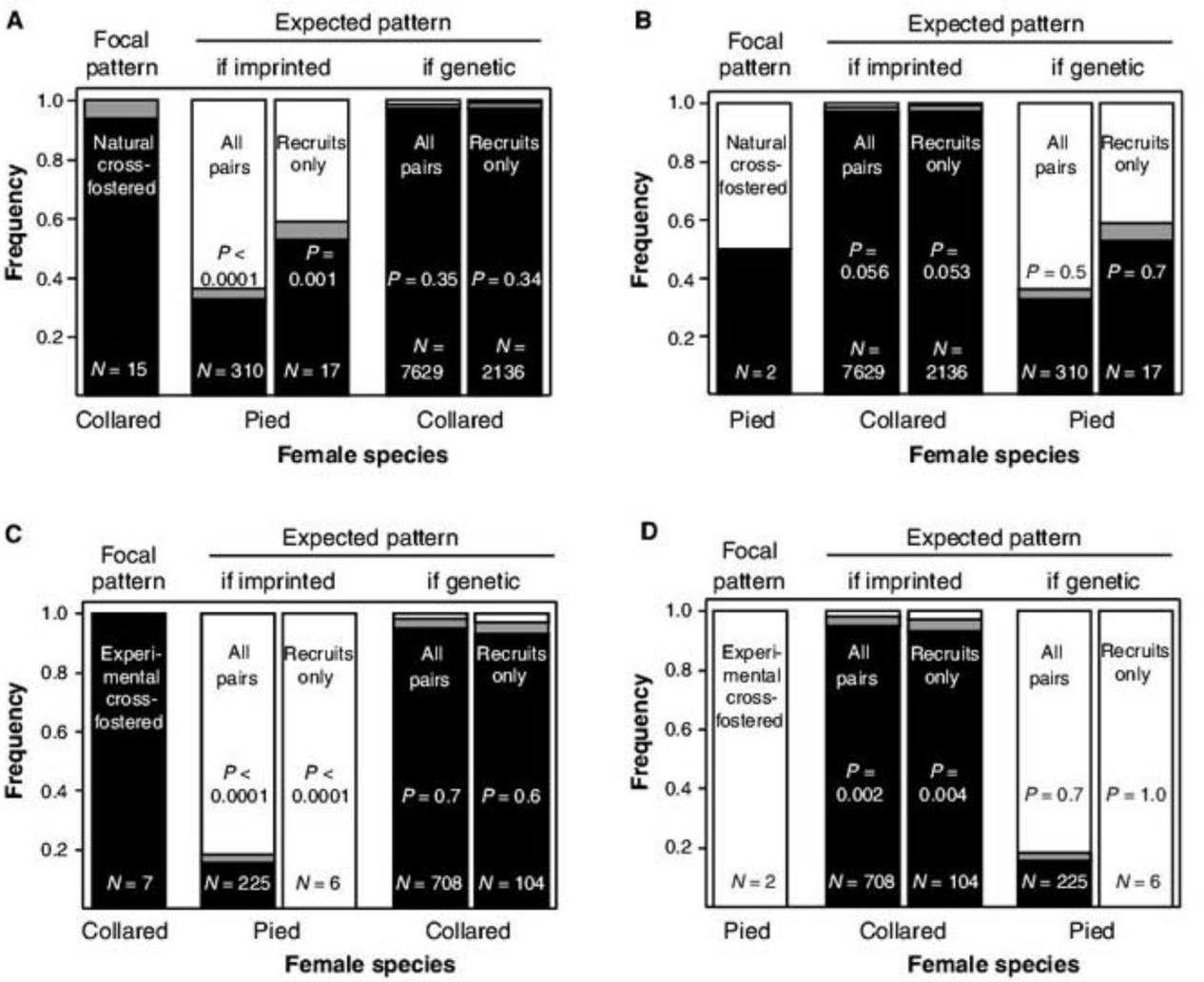

Fig. 2. Mating patterns of female flycatchers reared by heterospecific foster fathers compared to expectations based on sexual imprinting or genetic inheritance of species recognition. In each panel, the first bar shows the mating pattern of females reared by heterospecific foster fathers (focal pattern; black, collared flycatcher partner; white, pied flycatcher partner; gray, hybrid partner). The upper panels (**A** and **B**) show mating patterns of females naturally raised in mixed-species nests by cuckolded heterospecific stepfathers (natural cross-fostered), and the lower panels (**C** and **D**) show mating patterns of females experimentally transferred to heterospecific nests (experimental cross-fostered). The left panels [(A) and (C)] refer to collared flycatchers, whereas the right panels [(B) and (D)] present pied flycatchers. The expected mating patterns (specific to the population in which the focal patterns were obtained) were constructed in two ways, using either the mating pattern in the population (all pairs) or using only the mating pattern of females born in nests of known pure pairs (recruits only). *P* values indicate the exact binomial two-tailed probability of obtaining the observed focal mating pattern of females reared by heterospecific fathers (number of such females mating with conspecific males versus other males) under the different expected proportions. *N* indicates number of breeding pairs.

Moreover, they are not expected to occur in birds according to one predominant theory of the evolution of genomic imprinting, and genes that are imprinted in mammals show ordinary bi-allelic expression in birds (*21*). We therefore conclude that species-assortative mating preferences in flycatcher hybrid zones are mainly due to Z-linked genes.

All three major components of reproductive isolation (species recognition, species-specific male traits, and hybrid incompatibilities) being Z linked in flycatchers should facilitate an evolutionary response to natural selection against hybridization. This is because genetic associations between the male and the female components of pre-zygotic barriers to gene flow, as well as between pre-zygotic and post-zygotic barriers, can easily be maintained (see supporting online text for further discussion of the flycatcher system). Our results suggest that some organisms may be prone to speciation through reinforcement because of the mediating role of the sex chromosomes. Compared to autosomally inherited species recognition, both sex linkage and sexual imprinting may allow incipient species to avoid a collapse in assortative mating during secondary contact and be less likely to succumb to gene flow and fusion (*9*). However, paternal sexual imprinting requires that females be socially exposed to their father, which is not always true even in birds. Conversely, because reduced hybrid fitness is commonly caused by sex-linked incompatibilities (*3*), sex linkage of species recognition might provide a general connection between key components of reproductive isolation, which facilitates adaptive speciation in the face of gene flow.

Sex-chromosome linkage of species-assortative female mate preferences may be widespread, but few previous studies have explicitly investigated the mechanism of species recognition in hybrid zones. Even fewer studies have provided additional information on the genetics of hybrid fitness and the preferred traits, or evidence for reinforcement (*22*–*25*). Nevertheless, disproportionately many genes involved in reproductive isolation seem to be located on the sex chromosomes (*15*, *26*, *27*). In Lepidoptera, which also have heterogametic females, sex-linked traits seem to be more associated with reproductive isolation than in other insects (*28*), and it has been suggested that ornaments and preferences for these ornaments evolve more readily in organisms with ZW than with XY sex chromosomes (*26*, *29*). Although speciation would benefit from any kind of linkage (or other recombination-suppressing mechanism) that can maintain these genetic associations, traits involved in pre-zygotic isolation may simply be more likely to occur on sex chromosomes than on autosomes and possibly more likely on Z than on X chromosomes (*27*). Sex chromosomes in general, and the Z in particular, may therefore be hotspots for speciation genes.

References and Notes

1. T. Dobzhansky, *Am. Nat.* **74**, 312 (1940).
2. M. R. Servedio, M. A. F. Noor, *Annu. Rev. Ecol. Syst.* **34**, 339 (2003).
3. J. A. Coyne, H. A. Orr, *Speciation* (Sinauer, Sunderland, MA, 2004).
4. M. Kirkpatrick, V. Ravigné, *Am. Nat.* **159**, 865 (2000).
5. J. Felsenstein, *Evol. Int. J. Org. Evol.* **35**, 124 (1981).
6. D. Ortíz-Barrientos, M. A. F. Noor, *Science* **310**, 1467 (2005).
7. C. ten Cate, D. R. Vos, *Adv. Stud. Behav.* **28**, 1 (1999).
8. D. E. Irwin, T. Price, *Heredity* **82**, 347 (1999).
9. M. R. Servedio, S. A. Sæther, G.-P. Sætre, *Evol. Ecol.*, in press, available at www.springerlink.com/content/ut50156832448324/.
10. A. J. Trickett, R. K. Butlin, *Heredity* **73**, 339 (1994).
11. M. R. Servedio, *Evol. Int. J. Org. Evol.* **54**, 21 (2000).
12. D. Ortíz-Barrientos *et al.*, *Genetica* **116**, 167 (2002).
13. M. R. Servedio, G.-P. Sætre, *Proc. R. Soc. London Ser. B* **270**, 1473 (2003).
14. D. W. Hall, M. Kirkpatrick, *Evol. Int. J. Org. Evol.* **60**, 908 (2006).
15. A. R. Lemmon, M. Kirkpatrick, *Genetics* **173**, 1145 (2006).
16. G.-P. Sætre *et al.*, *Nature* **387**, 589 (1997).
17. T. Veen *et al.*, *Nature* **411**, 45 (2001).
18. G.-P. Sætre *et al.*, *Proc. R. Soc. London Ser. B* **270**, 53 (2003).
19. See methods in supporting material on *Science* Online.
20. G.-P. Sætre, M. Král, S. Bureš, *J. Avian Biol.* **28**, 259 (1997).
21. M. J. O'Neill *et al.*, *Dev. Gen. Evol.* **210**, 18 (2000).
22. J. W. Grula, O. R. J. Taylor, *Evol. Int. J. Org. Evol.* **34**, 688 (1980).
23. P. R. Grant, R. B. Grant, *Biol. J. Linn. Soc.* **60**, 317 (1997).
24. V. K. Iyengar, H. K. Reeve, T. Eisner, *Nature* **419**, 830 (2002).
25. M. A. F. Noor *et al.*, *Proc. Natl. Acad. Sci. U.S.A.* **98**, 12084 (2001).
26. M. Kirkpatrick, D. W. Hall, *Evol. Int. J. Org. Evol.* **58**, 683 (2004).
27. V. B. Kaiser, H. Ellegren, *Evol. Int. J. Org. Evol.* **60**, 1945 (2006).
28. M. G. Ritchie, S. D. F. Phillips, in *Endless Forms: Species and Speciation*, D. J. Howard, S. H. Berlocher, Eds. (Oxford Univ. Press, Oxford, 1998), pp. 291–308.
29. H. K. Reeve, D. F. Pfenning, *Proc. Natl. Acad. Sci. U.S.A.* **100**, 1089 (2003).

30. We thank T. F. Hansen, Ø. H. Holen, A. J. van Noordwijk, K. van Oers, F. Pulido, T. O. Svennungsen, and M. Visser for suggestions. The study was supported by grants from the Swedish Research Council, the Research Council of Norway, Formas, the Netherlands Organization for Scientific Research, NSF, the Czech Ministry of Education, and the Czech Science Foundation.

Supporting Online Material

www.sciencemag.org/cgi/content/full/318/5847/95/DC1
Materials and Methods
SOM Text
References

20 February 2007; accepted 15 August 2007
10.1126/science.1141506

Microbial Population Structures in the Deep Marine Biosphere

Julie A. Huber,[1]* David B. Mark Welch,[1] Hilary G. Morrison,[1] Susan M. Huse,[1] Phillip R. Neal,[1] David A. Butterfield,[2] Mitchell L. Sogin[1]

The analytical power of environmental DNA sequences for modeling microbial ecosystems depends on accurate assessments of population structure, including diversity (richness) and relative abundance (evenness). We investigated both aspects of population structure for microbial communities at two neighboring hydrothermal vents by examining the sequences of more than 900,000 microbial small-subunit ribosomal RNA amplicons. The two vent communities have different population structures that reflect local geochemical regimes. Descriptions of archaeal diversity were nearly exhaustive, but despite collecting an unparalleled number of sequences, statistical analyses indicated additional bacterial diversity at every taxonomic level. We predict that hundreds of thousands of sequences will be necessary to capture the vast diversity of microbial communities, and that different patterns of evenness for both high- and low-abundance taxa may be important in defining microbial ecosystem dynamics.

The interrogation of DNA from environmental samples has revealed new dimensions in microbial diversity and community-wide metabolic potential. The first analysis of a dozen polymerase chain reaction (PCR) amplicons of ribosomal RNA (rRNA) sequence from a mixed bacterioplankton population revealed the ubiquitous SAR11 cluster (*1*), and a recent environmental shotgun sequence survey of microbial communities in the surface ocean has identified 6.1 million predicted proteins (*2*, *3*). To realize the full potential of metagenomics for modeling energy and carbon flow, microbial biogeography, and the relationship between microbial diversity and ecosystem function, it is necessary to estimate both the richness and evenness of microbial population structures.

We used a tag sequencing strategy that combines the use of amplicons of the V6 hypervariable region of small-subunit (SSU) rRNA as proxies for the presence of individual phylotypes [operational taxonomic units (OTUs)] with massively parallel sequencing. Our goal was to provide assessments of microbial diversity, evenness, and community structure at a resolution two to three orders of magnitude greater than that afforded by cloning and capillary sequencing of longer SSU rRNA amplicons (*4*). We used this strategy to attempt an exhaustive characterization of the bacterial and archaeal diversity at two

low-temperature diffuse flow vents, Marker 52 and Bag City, from Axial Seamount, an active volcano at 1520 m depth in the northeast Pacific Ocean (*5*, *6*). These vents host archaeal and bacterial communities originating from the subseafloor, local microbial mats, symbionts of vent macrofauna, and microorganisms from the surrounding seawater (*7*–*9*). Although new production from hydrothermal vents may correspond to as much as 25% of the total imported carbon flow in the deep sea (*10*), these globally distributed habitats remain relatively unexplored, and there are few descriptions of diversity, evenness, and dispersal of their endemic microbial populations.

Marker 52 and Bag City are less than 3 km apart, but differ markedly in chemical composition and appearance. Marker 52 was sampled on bare rock; Bag City vent fluids were sampled within a clump of tube worms. Both sites had microbial mats growing on rock and tube worm surfaces (fig. S1). Relative to Bag City and most other diffuse vents at Axial, Marker 52 has a higher $H_2S/\Delta T$ ratio, lower pH, and elevated alkalinity and iron levels (Table 1), all of which indicate a higher carbon dioxide content; Marker 52 fluids were effervescent at 1 atm (*9*).

We sequenced more than 900,000 archaeal and bacterial V6 amplicons from these two sites. Tags that differed by no more than 3% [generally considered to define microbial species (*11*)] were clustered (*12*) into OTUs to calculate rarefaction and nonparametric estimators (*13*). Taxonomic and statistical analyses revealed differences in community membership with very little overlap between the two sites (Table 2), which is particularly evident when comparing the fine structure of the communities (Fig. 1). For example, although ε-proteobacteria often dominate 10° to 80°C vent habitats, where they orchestrate the cycling of carbon, nitrogen, and sulfur (*14*), the richness and evenness of ε-proteobacterial families and genera are different at each site (Fig. 1). Nearly 6600 distinct ε-proteobacterial tag sequences accounted for 39% of bacterial amplicons, raising the estimate for total ε-proteobacterial diversity by at least one order of magnitude. Sequences identified as *Arcobacter* spp., a group of microaerophilic sulfur and hydrogen sulfide–oxidizing bacteria, dominated the ε-proteobacterial phylotypes at Bag City (FS312, Fig. 1), whereas sequences identified as *Sulfurovum* spp., a group of mesophilic microaerobes that use sulfur species as electron donors with nitrate or oxygen as electron acceptors, dominated Marker 52 (FS396, Fig. 1).

We hypothesize that the geochemical regimes shape the ε-proteobacterial community structure (Table 1) (*11*). A few highly abundant, specific tag sequences dominated each genus at each site, but extensive sampling revealed the presence of many less common and rare variants (Fig. 1). Microdiversity within groups of bacteria and archaea has been noted previously in the marine environment (*15*, *16*). It is clear that in some cases, these closely related organisms are ecologically distinct (*15*, *17*).

Nearly 6000 unique sequences from a data set of more than 215,000 V6 amplicon tags identified as archaeal defined more than 1900 phylotypes. The slope of the rarefaction curve (*18*) for the archaea became nearly asymptotic, and nonparametric statistical analyses estimated an ultimate richness of ~2700 archaeal phylotypes (Fig. 2 and Table 2). In contrast, despite examining nearly 690,000 tags identified as bacterial, rarefaction curves (Fig. 2) indicated that our sampling of bacterial richness was far from complete. We observed more than 30,000 unique bacterial sequences forming ~18,500 phylotypes, and nonparametric estimates predicted the presence of ~37,000 phylotypes (*13*) (Table 2), with steeply sloping rarefaction curves for many diverse classes, orders, and families (fig. S2). Even the dominant genera *Arcobacter* and *Sulfurovum* were incompletely sampled (fig. S2). The lower diversity of archaeal phylotypes agreed with other molecular surveys indicating that marine archaeal diversity is relatively limited (*19*); hence, our approach does not result in inflated richness estimates due to spurious data. Furthermore, extensive quality control of tag sequences ensured that the total error from PCR and pyrosequencing was less than 0.0025 per base and that sequencing error misassigned fewer than 1% of tags to phylotypes (*20*).

Table 1. Chemical and SSU rRNA tag characteristics of the two sites.

	FS312	FS396
Vent name	Bag City	Marker 52
Sample year	2003	2004
Volume filtered (ml)	1003	2000
Cells ml^{-1} (range)	1.21×10^5 (9.77×10^4 to 1.26×10^5)	1.57×10^5 (1.02×10^5 to 2.12×10^5)
Culturable* hyper/thermophilic heterotrophs per liter	140 to 4200	20 to 720
DNA recovered (μg)	0.9	2.4
Total number of archaeal V6 tag sequences†	200,199	16,428
Total number of bacterial V6 tag sequences†	442,058	247,662
Total number of ε-proteobacterial V6 tag sequences†	122,823	147,515
Depth (m)	1,537	1,529
Latitude and longitude	45.92°N, 129.99°W	45.94°N, 129.99°W
Average temperature (°C)	31.2	24.4
Maximum temperature (°C)	31.4	24.9
$H_2S/\Delta T$ (μmol kg^{-1} $°C^{-1}$)	7.2	18.9
pH	6.26	5.08
Mg (mmol/kg)	48.3	50.8
Alkalinity (meq/liter)	2.4	3.7
Mn (μmol/kg)	19.8	4.8
Fe (μmol/kg)	0.8	7.9
Silica (mmol/kg)	1.46	1.07

*Cultured at 70° or 90°C in 0.3% yeast extract and peptone with elemental sulfur; Ar headspace. †Trimmed reads that passed quality control [as described in (*11*)].

Table 2. Sequencing information and diversity estimates for all bacteria and archaea.

	Bacteria	Archaea
Total number of V6 tag sequences*	689,720	216,627
Total unique V6 tag sequences	30,108	5,979
Total OTUs at 3% difference (phylotypes)	18,537	1,931
Chao1 estimator of richness at 3% difference (95% CI)	36,869 (36,108 to 37,663)	2,754 (2,594 to 2,952)
ACE estimator of richness at 3% difference (95% CI)	37,038 (36,613 to 37,473)	2,678 (2,616 to 2,745)
Bray-Curtis similarity index at 3% difference†	0.08	0.01
Jaccard similarity index at 3% difference†	0.12	0.08

*Trimmed reads that passed quality control [as described in (*11*)]. †Similarity between communities at sites FS312 and FS396 on a scale of 0 to 1 (where 1 represents identical communities).

[1]Josephine Bay Paul Center, Marine Biological Laboratory, 7 MBL Street, Woods Hole, MA 02543, USA. [2]Joint Institute for the Study of Atmosphere and Ocean, University of Washington, Post Office Box 354925, Seattle, WA 98105, USA.

*To whom correspondence should be addressed. E-mail: jhuber@mbl.edu

Comparing each unique sequence to our V6 reference database revealed well-characterized taxa, as well as many unknown microbial phylotypes. The 10 most abundant sequences occurred more than 10,000 times and were exact matches to sequences in our database, indicating that our sampling was representative. Of the 36,725 unique sequences found at the two sites, 36,180 were represented by fewer than 100 tags; of these, 13,385 were >10% different and ~4000 were >20% different from known SSU rRNA genes. Many rare, divergent taxa account for most of the observed novel microbial diversity (*4*, *21*).

Although this study only examined samples at two sites in the deep ocean, it has important im-

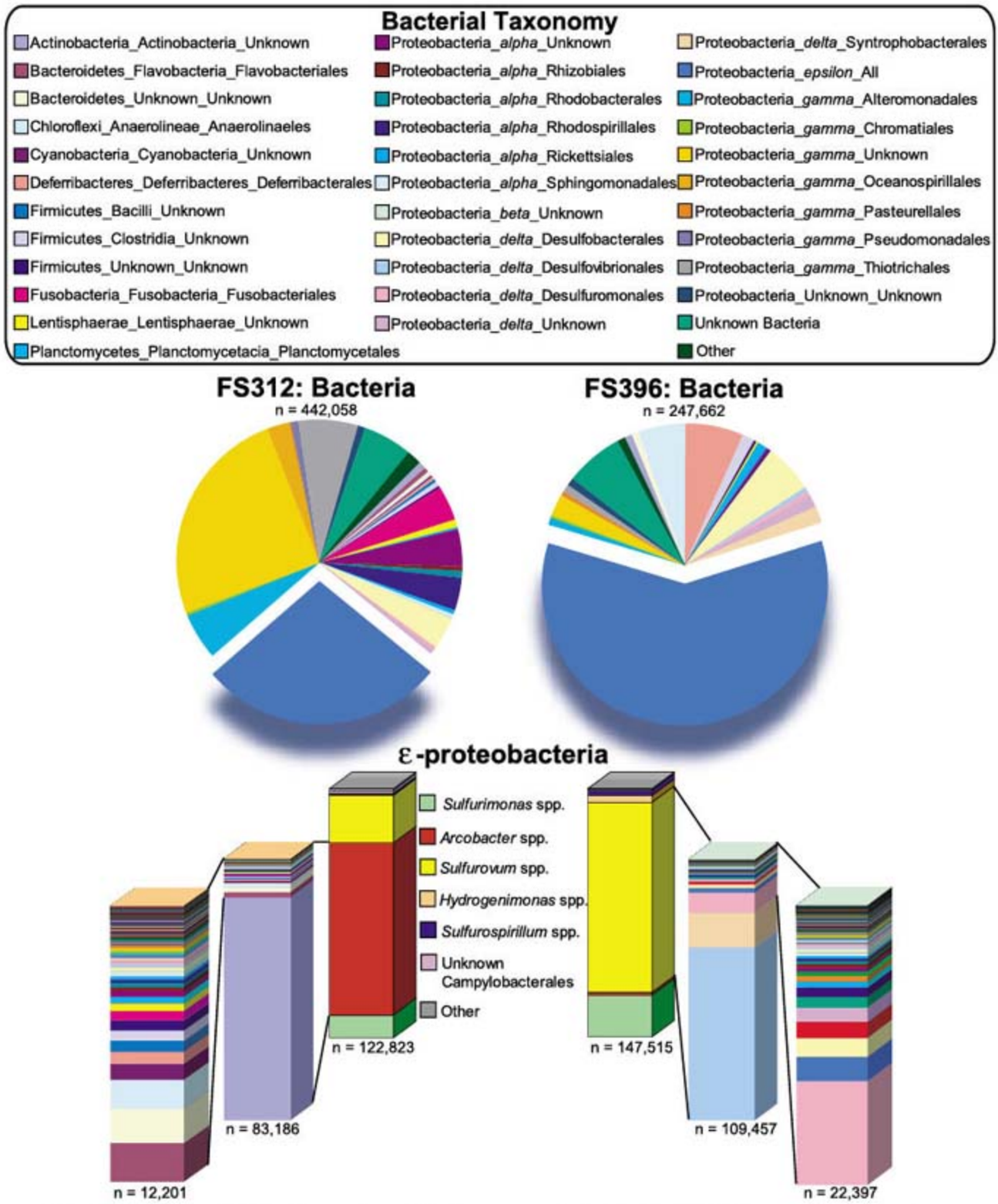

Fig. 1. Taxonomic breakdown of bacterial V6 tags from each vent. Pie charts show the Phylum_Class_Order distribution for taxonomically assigned tags that occurred more than 1000 times; the remaining tag sequences are grouped into "Other." The taxonomic distribution of ε-proteobacterial genera is shown in normalized histograms for each site, with further breakdown of the dominant ε-proteobacteria in additional histograms, with each color in the histograms representing a unique tag sequence. For FS312, the *Arcobacter* are expanded to the left with a histogram showing those tag sequences that occurred ≥10 times, followed by a histogram showing the diversity of tags that occurred 10 to 1800 times. For FS396, the *Sulfurovum* are expanded to the right, with a histogram showing those tag sequences that occurred ≥10 times, followed by a histogram showing the diversity of tags that occurred 10 to 8400 times. Nonparametric estimates suggested more than 900 phylotypes each of *Arcobacter* at FS312 and *Sulfurovum* at FS396.

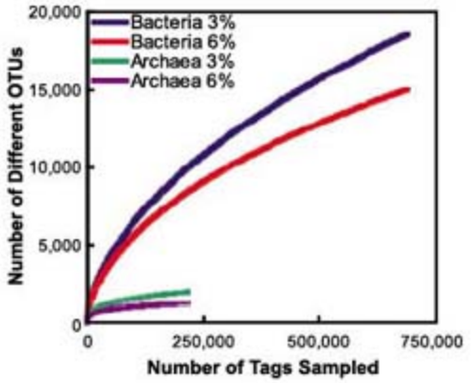

Fig. 2. Rarefaction curves for total bacterial and archaeal communities at the two sampling sites FS312 and FS396 at 3% and 6% difference levels.

plications for our ability to sample and identify all the ecologically relevant members of microbial communities in other high-diversity habitats, such as soils (*22*), microbial mats (*23*), and communities where low-abundance taxa may play crucial roles, such as the human microbiome. It provides a comparative population structure analysis with statistically significant descriptions of diversity and relative abundance of microbial populations. These large estimates of phylogenetic diversity at every taxonomic level present a challenge to large-scale microbial community genomic surveys. Metagenomic studies seek to inventory the full range of metabolic capabilities that define ecosystem function or to determine their context within assembled genomic scaffolds. Our results suggest that even the largest of published metagenomic investigations inadequately represent the full extent of microbial diversity, as they survey only the most highly abundant taxa (*11*).

In addition, the importance of microdiversity cannot be overlooked, and metagenomic community reconstructions from the two vents studied here would likely be largely chimeric assemblies of sequences from closely related phylotypes, which may mask important biological differences. Methods such as the massively parallel tag sequencing approach used here, combined with the multitude of other quantitative and descriptive tools now available to microbial ecologists, can serve as necessary accompaniments to metagenomic gene surveys as we strive to understand the impact of diversity on ecosystem function and long-term stability (*24*).

References and Notes

1. S. J. Giovannoni, T. B. Britschgi, C. L. Moyer, K. G. Field, *Nature* **345**, 60 (1990).
2. D. B. Rusch *et al.*, *PLoS Biol.* **5**, e77 (2007).
3. S. Yooseph *et al.*, *PLoS Biol.* **5**, e16 (2007).
4. M. L. Sogin *et al.*, *Proc. Natl. Acad. Sci. U.S.A.* **103**, 12115 (2006).
5. H. P. Johnson, R. W. Embley, *J. Geophys. Res.* **95**, 12689 (1990).
6. R. W. Embley, E. T. Baker, *Eos* **80**, 213 (1999).
7. J. A. Huber, D. A. Butterfield, J. A. Baross, *Appl. Environ. Microbiol.* **68**, 1585 (2002).
8. J. A. Huber, D. A. Butterfield, J. A. Baross, *FEMS Microbiol. Ecol.* **43**, 393 (2003).
9. D. A. Butterfield *et al.*, in *The Subseafloor Biosphere at Mid-Ocean Ridges*, W. S. D. Wilcock, E. F. DeLong, D. S. Kelley, J. A. Baross, S. C. Cary, Eds. (American Geophysical Union, Washington, DC, 2004), pp. 269–289.
10. A. Maruyama, T. Urabe, J. Ishibashi, R. A. Feely, E. T. Baker, *Cah. Biol. Mar.* **39**, 249 (1998).
11. See supporting material on *Science* Online.
12. P. D. Schloss, J. Handelsman, *Appl. Environ. Microbiol.* **71**, 1501 (2005).
13. A. Chao, *Scand. J. Stat.* **11**, 265 (1984).
14. B. J. Campbell, A. S. Engel, M. L. Porter, K. Takai, *Nat. Rev. Microbiol.* **4**, 458 (2006).
15. L. R. Moore, G. Rocap, S. W. Chisholm, *Nature* **393**, 464 (1998).
16. S. G. Acinas *et al.*, *Nature* **430**, 551 (2004).
17. G. Rocap, D. L. Distel, J. B. Waterbury, S. W. Chisholm, *Appl. Environ. Microbiol.* **68**, 1180 (2002).
18. D. M. Raup, *Paleobiology* **1**, 333 (1975).
19. R. Massana, E. F. DeLong, C. Pedros-Alio, *Appl. Environ. Microbiol.* **66**, 1777 (2000).
20. S. M. Huse, J. A. Huber, H. G. Morrison, M. L. Sogin, D. Mark Welch, *Genome Biol.* **8**, R143 (2007).
21. C. Pedros-Alio, *Trends Microbiol.* **14**, 257 (2006).
22. P. D. Schloss, J. Handelsman, *PLoS Comput. Biol.* **2**, e92 (2006).
23. R. E. Ley *et al.*, *Appl. Environ. Microbiol.* **72**, 3685 (2006).
24. E. F. DeLong, *Nat. Rev. Microbiol.* **5**, 326 (2007).
25. We thank the NOAA Pacific Marine Environmental Laboratory Vents Program, the ROPOS Remotely Operated Vehicle, and S. Bolton for field support, and P. Schloss and L. Amaral Zettler for assistance in data analysis and primer design. Supported by NASA Astrobiology Institute Cooperative Agreement NNA04CC04A (M.L.S.), a National Research Council Research Associateship Award and L'Oréal USA Fellowship (J.A.H.), the Alfred P. Sloan Foundation's ICoMM field project, the W. M. Keck Foundation, and the Joint Institute for the Study of the Atmosphere and Ocean under NOAA Cooperative Agreement NA17RJ1232, Contribution 1388. This is NOAA Pacific Marine Environmental Laboratory Contribution 3047. The new sequences reported in this paper have been deposited in the NCBI Short Read Archive under accession numbers SRA000195 and SRA000196. The zip file available for download via http from jbpc.mbl.edu/research_supplements/g454/20070822-private/supplemental.zip contains all the fasta-formatted trimmed reads used in the analyses.

Supporting Online Material

www.sciencemag.org/cgi/content/full/318/5847/97/DC1
Materials and Methods
SOM Text
Figs. S1 and S2
References

19 June 2007; accepted 28 August 2007
10.1126/science.1146689

Genetic Effects of Captive Breeding Cause a Rapid, Cumulative Fitness Decline in the Wild

Hitoshi Araki,* Becky Cooper, Michael S. Blouin

Captive breeding is used to supplement populations of many species that are declining in the wild. The suitability of and long-term species survival from such programs remain largely untested, however. We measured lifetime reproductive success of the first two generations of steelhead trout that were reared in captivity and bred in the wild after they were released. By reconstructing a three-generation pedigree with microsatellite markers, we show that genetic effects of domestication reduce subsequent reproductive capabilities by ~40% per captive-reared generation when fish are moved to natural environments. These results suggest that even a few generations of domestication may have negative effects on natural reproduction in the wild and that the repeated use of captive-reared parents to supplement wild populations should be carefully reconsidered.

Captive breeding was originally used as a form of conservation for the most critically endangered species, but is now widely used for the restoration of declining natural populations (*1–3*). In theory, captive-reared organisms may accumulate deleterious alleles that could hinder the recovery of natural populations (*3–6*). However, the extent to which captive-reared individuals contribute genetically to the restoration of natural populations is not known.

Hatchery programs for enhancing threatened populations of Pacific salmon and steelhead trout (*Oncorhynchus* spp.) release more than five billion juvenile hatchery fish into the North Pacific every year (*7*, *8*). Although most of these hatchery programs are meant to produce fish for harvest, an increasing number of captive breeding programs are releasing fish to restore declining natural populations (*8*, *9*). Hatchery fish breed in the wild, and many natural populations are affected by hatchery fish. The use of hatchery-reared fish as broodstock (parents of hatchery fish) for many generations has resulted in individuals that contribute less to the gene pool (are less fit), in comparison with wild fish, in natural environments (*10–12*). On the other hand, captive breeding programs that use local wild fish as broodstock are expected to produce hatchery fish having minimal differences in fitness from wild fish. Nevertheless, such captive-reared fish can be genetically distinct from wild fish for a variety of traits (*13–16*). Thus, it is a real concern that these fish will also have low fitness (reproductive success) in natural environments.

A two-generation pedigree of DNA-based parentage analyses of steelhead (*Oncorhynchus*

Department of Zoology, 3029 Cordley Hall, Oregon State University Corvallis, OR 97331, USA.

*To whom correspondence should be addressed. E-mail: arakih@science.oregonstate.edu

mykiss) in the Hood River in Oregon (U.S.A.) showed that the first generation of captive-reared fish had natural reproductive success indistinguishable from that of wild fish in two out of three run-years (*17*). (Each run-year begins when parents arrive at the river to spawn.) This comparison, however, neglected the fact that captive-reared and wild individuals experience different environments as juveniles, which might affect mating behaviors, fecundity, and/or fertility (*18*). Therefore, it is difficult to disentangle environmental effects from genetic effects of a difference or lack of difference in reproductive success (*17*).

In this study, we investigated the strength of genetic effects of domestication on the reproductive success of captive-reared individuals in the wild. Confounding environmental effects were avoided by comparing captive-reared individuals with different histories of captive breeding in the previous generation (Fig. 1). We reconstructed a three-generation pedigree of the winter-run steelhead in the Hood River (*19*) and compared adult-to-adult reproductive success (number of wild-born, adult offspring per parent) of two types of captive-reared fish (designated *C*): captive-reared fish from two wild-born parents (C[WxW]), and captive-reared fish from a wild-born parent and a first-generation captive-reared parent (C[**C**xW]). C[**C**xW] and C[WxW] were born in the same year, reared in the same hatchery without distinction, and released at the same time. Both fish originated from the same local population, so we can also exclude the influence of local origin. The only difference between them is half of the genome. The half genome in C[**C**xW] was inherited from the captive-reared parent and experienced captivity for two consecutive generations (during the egg-to-juvenile development). The other half in C[**C**xW] was from the wild parent and experienced captivity for one generation (C[**C**xW] itself). In contrast, the entire genome of the C[WxW] experienced captivity for one generation. Thus, by comparing C[**C**xW] with C[WxW], we were able to evaluate the effect of a single extra generation of captive rearing on subsequent reproductive success in the wild, while controlling for the effect of rearing environment (Fig. 1).

We estimated the reproductive success of 547 C[**C**xW] and 193 C[WxW] over three run-years (1998–2000) (*19*). On the basis of the parentage analysis, we assigned 355 wild-born, returning adult offspring to at least one of their C[**C**xW] or C[WxW] parents (Table 1). Our estimate of relative reproductive success (RRS) with an unbiased method (*20*) revealed that the overall reproductive success of C[**C**xW] is only 55% that of C[WxW] ($P = 0.009$ by one-tailed permutation tests). We also compared the reproductive success of C[**C**xW] and C[WxW] from single cohorts (i.e., using only 3-year-olds at the time of spawning) (Table 1). In this comparison, environmental differences were eliminated because both types of hatchery fish were born, returned, and spawned in the same environments in the same year. The smaller sample size resulted in lower power, but the overall estimate was very similar to the above result (single-cohort RRS of C[**C**xW] to C[WxW] = 0.609, $P = 0.042$).

In addition to comparing reproductive success between C[WxW] and C[**C**xW], we also compared the reproductive success of these captive-reared fish to that of wild-born fish (*W*) returning in the same run-years (1998–2000). Overall RRS of C[WxW] to *W* was 0.595 and that of C[**C**xW] to *W* was 0.310 [both $P < 0.001$, (table S1)]. Our estimates of RRS for C[WxW] can be compared with those from our previous study of run years 1995–1997 (*17*) (table S1). Interestingly, the estimate from run years 1998–2000 was significantly lower than the average RRS ~ 1 estimated from run-years 1995–1997 (*17*) (Fig. 2A). One possible explanation for this difference is presence of C[**C**xW] on the spawning grounds in 1998–2000. For example, reproductive interaction between C[**C**xW] and C[WxW] might reduce the average reproductive success of C[WxW] if C[WxW] tend to mate more with C[**C**xW] than with *W*. Another possibility is nonadditive fitness effects such that mating between hatchery fish results in lower fitness than expected. In our data, nonrandom mating was supported by a test of independence [$P < 0.001$ for all three run-years (table S2)]. However, an excess of observed mating was found between wild parents, not between captive-reared parents. This might indicate both nonrandom mating (*W*x*W* and *C*x*C* mating preferences) and nonadditive fitness effects (i.e.,

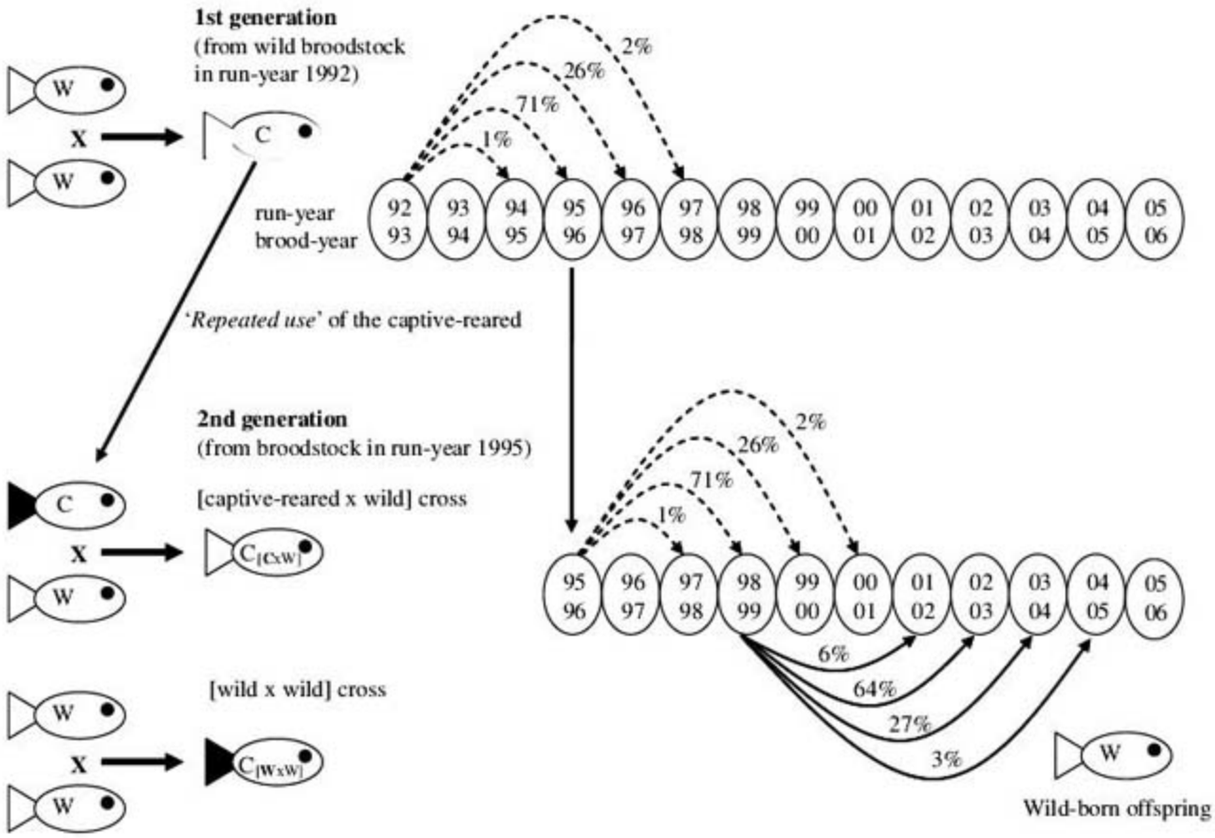

Fig. 1. Distribution of run-years in which captive-reared fish and their wild-born offspring returned. Numbers in a circle represent a run-year of parents (**top**) and a brood-year of their offspring (**bottom**). The percentage on each arrow represents the proportion of adults that return in each subsequent year, which differs between captive-reared fish (dotted line) and wild fish (solid line). C[**C**xW] were iteratively created from wild individuals and the first generation of captive-reared individuals that returned in run-year 1995; subsequent C[**C**xW] individuals were created from those individuals returning in 1996 and so forth. These first-year C[**C**xW] fish returned to spawn mostly in run-year 1998, and we estimated their reproductive success by matching them to the wild-born offspring that returned in run-year 2001–2004.

low fitness of *CxC*), although analyses of reproductive success between crosses did not show the presence of nonadditive genetic effects {RRS of [C[**C**xW] × C[WxW]] to [*W* × C[WxW]] = 1.1 in run-year 2000, $P = 0.878$ (table S3)}. Over six run-years of data (1995–2000), four of six years showed lower fitness of C[WxW] (overall RRS of C[WxW] to $W = 0.848$, $P < 0.001$).

Table 1. RRS (relative number of adult offspring per parent) of two types of captive-reared fish, $C_{[CxW]}$ versus $C_{[WxW]}$. RRS is given as an unbiased estimate (*19*, *20*). *P* values were calculated by a one-tailed permutation test. Statistical power represents the minimum effect size (displayed as RRS) detectable with 80% and 95% power. [See (*19*) and footnote of table S1 for details.] When all parents were compared, overall RRS was estimated using weighted geometric means. The *P* values were calculated on the basis of Fisher's combined probability (*19*). For single cohorts, only 3-year-old C[**C**xW] and C[WxW] were compared. *$P < 0.05$, **$P < 0.01$

Run-year	*N* [offspring assigned]	RRS	*P* value	Statistical power (80%/95%)
		From all parents		
[Male]				
1998	79	0.341	0.035*	0.626/0.341
1999	26	0.577	0.239	0.462/0.296
2000	79	0.856	0.381	0.701/0.540
Overall male		0.545	0.074	
[Female]				
1998	74	0.504	0.238	0.384/0.156
1999	25	0.212	0.007**	0.468/0.321
2000	72	0.828	0.319	0.706/0.567
Overall female		0.547	0.020*	
Overall both sexes		0.546	0.009**	
		From single cohorts		
[Male]				
1998	48	0.361	0.044*	0.582/0.361
1999	25	0.502	0.171	0.502/0.324
2000	77	0.862	0.390	0.705/0.543
Overall male		0.596	0.070	
[Female]				
1998	22	0.985	0.591	0.257/0.075
1999	15	0.137	0.036*	0.351/0.137
2000	56	0.798	0.319	0.641/0.480
Overall female		0.631	0.125	
Overall both sexes		0.609	0.042*	

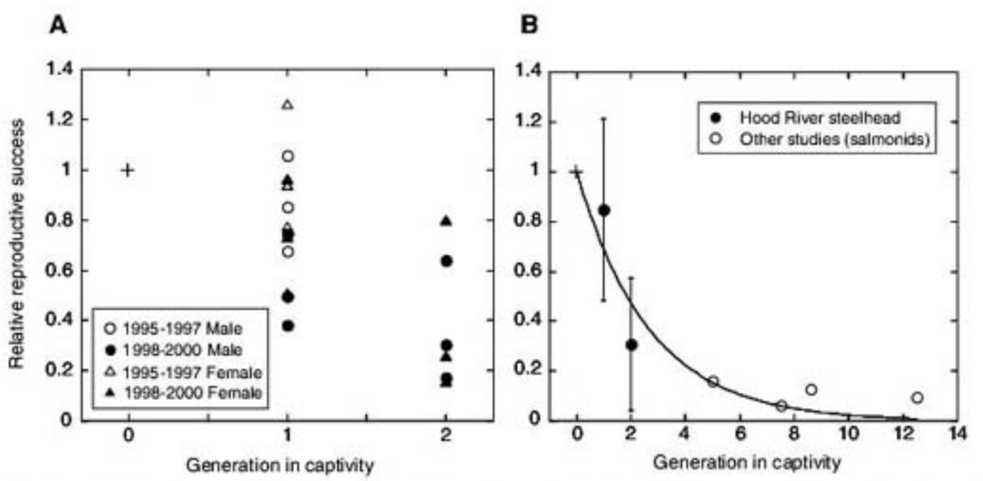

Fig. 2. (**A**) Estimated RRS of captive-reared fish relative to wild fish, plotted against generation time in captivity. Each point represents an estimate from a run-year and sex. The point at generation 0 represents wild fish as a control (marked as a cross). Estimates of the RRS of C[WxW] are plotted at generation 1 and C[**C**xW] at generation 2. Three years of data at generation 1 (open plots) are from (*17*). (**B**) Meta-analysis of the RRS of captive-reared versus wild fish plotted against generation time in captivity of other salmonid species. Solid circles are the estimates from our data (weighted geometric means from Fig. 2A). The bar represents 1 SD. The other four points are from two studies on steelhead, one on brown trout, and one on Atlantic salmon (table S4) from (*25*). The exponential regressions were obtained as $y = e^{-0.375x}$ (correlation coefficient = 0.962), which suggest that fitness in the wild is reduced 37.5% per generation of captive breeding.

One factor we cannot completely exclude in these comparisons is nongenetic grandparental effects, which have been demonstrated in various organisms, including fish (*21*–*24*). However, known grandparental effects are mostly female-specific (i.e., grandmaternal egg effects). The reproductive success of C[**C**xW] did not depend on the sex of the captive-reared parent (overall RRS of C[**C**xW] with a captive-reared mother to C[**C**xW] with a captive-reared father = 1.009, $P = 0.81$). Similarly, there were no noticeable maternal effects on the reproductive success when hatchery and wild fish mated in the wild, either in this study or in our previous study [i.e., number of resulting offspring did not depend on which type of fish was the mother (table S1) (*17*)]. Thus, the grandparental effect is less likely in this case, and the most likely explanation for the fitness decline is a genetic disadvantage of C[**C**xW] resulting from the half genome exposed to artificial environments for an additional generation.

Our data suggest a sharp decline in reproductive success follows a very short time in captivity (Fig. 2A). We also conducted a meta-analysis to compare our data with those available for four hatchery stocks for which we know the number of generations in hatcheries (*19*, *25*). These data fit very well on an exponentially declining curve (Fig. 2B), despite the fact that the previous data include RRS estimates using different species and methods and that they are subject to confounding environmental effects (*19*, *25*). It shows 37.5% fitness decline per captive-reared generation, suggesting that the fitness decline of captive-reared fish can be remarkably fast. Because any purely environmental effects should not accumulate over time, the continued decline with generations in captivity (Fig. 2) further supports genetic effects as the cause.

The evolutionary mechanism causing the fitness decline remains unknown. We suspect that unintentional domestication selection and relaxation of natural selection, due to artificially modified and well-protected rearing environments for hatchery fish, are probably occurring (SOM text). Considering the mating scheme for C[**C**xW] and the generation time for the fitness decline, however, inbreeding depression and accumulation of new mutations should not affect these results. Regardless, our data demonstrate how strong the effects can be and how quickly they accumulate. To supplement declining wild populations, therefore, repeat use of captive-reared organisms for reproduction of captive-reared progenies should be carefully reconsidered.

References and Notes

1. M. L. Cuenco, T. W. H. Barkman, P. R. Mundy, in *Genetic Conservation of Salmonid Fishes*, J. G. Cloud, G. H. Thorgaard, Eds. (Plenum Press, New York, 1993), pp. 269–294.

2. P. J. S. Olney, G. M. Mace, A. Feistner, *Creative Conservation: Interactive Management of Wild and Captive Animals* (Chapman & Hall, London, ed. 1, 1994).
3. R. Frankham, D. A. Briscoe, J. D. Ballou, *Introduction to Conservation Genetics* (Cambridge Univ. Press, Cambridge, 2002).
4. M. Lynch, M. O' Hely, *Conserv. Genet.* **2**, 363 (2001).
5. M. J. Ford, *Conserv. Biol.* **16**, 815 (2002).
6. D. Goodman, *Can. J. Fish. Aquat. Sci.* **62**, 374 (2005).
7. W. R. Heard, "An estimate of total 1992 hatchery releases of the North Pacific Ocean and adjacent seas." [North Pacific Anadromous Fish Commission Doc. 154, Auke Bay Fisheries Laboratory, Alaska Fisheries Science Center, National Marine Fisheries Service (NMFS), National Oceanic and Atmospheric Administration (NOAA), Juneau, AK, 1995].
8. X. Augerot, D. N. Foley, *Atlas of Pacific Salmon: The First Map-Based Status Assessment of Salmon in the North Pacific* (Univ. of California Press, Berkeley, CA, 2005).
9. R. N. Williams, *Return to the River: Restoring Salmon to the Columbia River* (Elsevier Academic Press, Amsterdam, 2006).
10. I. A. Fleming *et al.*, *Proc. R. Soc. London Ser. B* **267**, 1517 (2000).
11. I. A. Fleming, E. Peterson, *Nord. J. Freshw. Res.* **75**, 71 (2001).
12. B. Berejikian, M. J. Ford, "Review of relative fitness of hatchery and natural salmon." (NMFS-NWFSC-61, Northwest Fisheries Science Center, Seattle, WA, 2004).
13. R. R. Reisenbichler, J. D. McIntyre, *Can. J. Fish. Res. Board* **34**, 123 (1977).
14. D. D. Heath, J. W. Heath, C. A. Bryden, R. M. Johnson, C. W. Fox, *Science* **299**, 1738 (2003).
15. T. N. Pearsons, A. L. Fritts, J. L. Scott, *Can. J. Fish. Aquat. Sci.* **64**, 803 (2007).
16. A. L. Fritts, J. L. Scott, T. N. Pearsons, *Can. J. Fish. Aquat. Sci.* **64**, 813 (2007).
17. H. Araki, W. R. Ardren, E. Olsen, B. Cooper, M. S. Blouin, *Conserv. Biol.* **21**, 181 (2007).
18. B. A. Berejikian, E. P. Tezak, S. L. Schroder, C. M. Knudsen, J. J. Hard, *ICES J. Mar. Sci.* **54**, 1040 (1997).
19. Methods are available as supporting material on *Science* Online.
20. H. Araki, M. S. Blouin, *Mol. Ecol.* **14**, 4097 (2005).
21. M. J. Hercus, A. A. Hoffmann, *Proc. R. Soc. London Ser. B* **267**, 2105 (2000).
22. A. Kyneb, S. Toft, *Ecol. Entomol.* **31**, 322 (2006).
23. D. Reznick, *Evolution Int. J. Org. Evolution* **35**, 941 (1981).
24. J. Lindström, *Trends Ecol. Evol.* **14**, 343 (1999).
25. "Report for the meeting held August 20 to September 2, 2004" (Salmon Recovery Science Review Panel, Northwest Fisheries Science Center, Seattle, 2004).

26. We thank R. S. Waples, M. Ford, and four anonymous reviewers for helpful discussions, W. R. Ardren, C. Criscione, R. VanDam and the Center for Genome Research and Biocomputing in Oregon State University for help with laboratory work and E. Olsen, R. French, J. Gidley, and staff of the Oregon Department of Fish and Wildlife (ODFW) for technical help and advice. This research was funded by contracts to M.S.B. from the Bonneville Power Administration and the ODFW.

Supporting Online Material

www.sciencemag.org/cgi/content/full/318/5847/100/DC1

Methods
SOM Text
Tables S1 to S5
Appendix
References

24 May 2007; accepted 21 August 2007
10.1126/science.1145621

Glia Promote Local Synaptogenesis Through UNC-6 (Netrin) Signaling in *C. elegans*

Daniel A. Colón-Ramos,[1] Milica A. Margeta,[1,2] Kang Shen[1,2]*

Neural circuits are assembled through the coordinated innervation of pre- and postsynaptic partners. We show that connectivity between two interneurons, AIY and RIA, in *Caenorhabditis elegans* is orchestrated by a pair of glial cells that express UNC-6 (netrin). In the postsynaptic neuron RIA, the netrin receptor UNC-40 (DCC, deleted in colorectal cancer) plays a conventional guidance role, directing outgrowth of the RIA process ventrally toward the glia. In the presynaptic neuron AIY, UNC-40 (DCC) plays an unexpected and previously uncharacterized role: It cell-autonomously promotes assembly of presynaptic terminals in the immediate vicinity of the glial cell endfeet. These results indicate that netrin can be used both for guidance and local synaptogenesis and suggest that glial cells can function as guideposts during the assembly of neural circuits in vivo.

Neural circuit formation requires an intricate orchestration of multiple developmental events, including cell migration, axon guidance, dendritic growth, synaptic target selection, and synaptogenesis (*1*–*3*). These developmental events are coordinated in pre- and postsynaptic neuronal partners to form the functional neural circuits that underlie behaviors. Although the organization and specificity of these neural circuits is well documented, the cellular and molecular mechanisms that underlie their precise development are not well understood.

To explore how precise neural connectivity is achieved, we studied the synaptic connections between two interneurons in the *C. elegans* brain: presynaptic AIY and postsynaptic RIA. These two interneurons navigate complex cellular environments, discriminating among multiple potential targets before finding and innervating each other at a discrete region of their respective processes (*4*). We generated single-cell fluorescent markers to visualize AIY-RIA connectivity in vivo and observed a discrete clustering of presynaptic AIY markers in a segment of the process we termed zone 2. This zone appears to be the specialized presynaptic region where AIY forms synapses onto RIA, as well as RIB and AIZ neurons. First, the fluorescently labeled presynaptic proteins RAB-3, ELKS-1, and SYD-2 are all more concentrated in zone 2 than in other regions of the axon (Figs. 1A and 2B and fig. S4A). Second, these markers cluster at the exact location at which AIY to RIA synapses are seen in electron micrographs of wild-type animals (fig. S1M) (*5*). Third, this region has a wider diameter than other regions of the axon, a property that we found to be uniquely associated with the presynaptic region of AIY in electron micrographs (fig. S1, A and M to Q). These combined properties were taken as evidence of presynaptic differentiation and were very reproducible across animals (Fig. 1 and fig. S1).

Reconstructions of electron microscropy (EM) micrographs (*5*) revealed that AIY has three distinct anatomical regions throughout its process: a segment proximal to the AIY cell body that is devoid of synapses (zone 1); the synapse-rich region where AIY forms synapses onto RIA, AIZ, and RIB just as the AIY process turns dorsally (zone 2); and a distal axon segment within the nerve ring that has four to eight small presynaptic specializations (zone 3).

To identify the molecular signals that direct this precise innervation, we performed a visual genetic screen for mutants with an abnormal synapse distribution in AIY. From this screen, we isolated the *wy81* mutation, an allele of *unc-40* (fig. S2). UNC-40 (DCC, deleted in colorectal cancer) is a transmembrane immunoglobulin superfamily protein that is a receptor for the axon guidance molecule UNC-6 (netrin) (*6*, *7*). *unc-40* animals had no detectable axon guidance defects in AIY except for an axon truncation defect observed in 7.8% of the animals ($n = 153$ animals; fig. S3). However, they showed a highly penetrant defect in the presynaptic specialization of AIY at zone 2: 95.3% of *unc-40(wy81)* animals displayed a severe reduction of active zone markers ELKS-1::YFP (yellow fluorescent protein) and SYD-2::GFP (green fluorescent protein) and a synaptic vesicle marker, mCherry::RAB-3, in zone 2 ($n = 128$ animals; Fig. 2, A to K, and fig. S4). In addition, the AIY axon diameter in zone 2 failed to widen into the characteristic presynaptic varicosity seen in wild-type animals (fig. S1). By contrast, in the more-dorsal zone 3 synaptic regions, *unc-40* animals had normal or increased levels of synaptic vesicle proteins and a normal or increased diameter (Fig. 2, F to I, and fig. S1). These defects suggest a specific defect in the presynaptic differentiation of AIY in zone 2, although a detailed analysis of AIY synaptic ultrastructure and function could

[1]Department of Biological Sciences, Stanford University, 144 Herrin Laboratories, Stanford, CA 94305–5020, USA. [2]Neurosciences Program, Stanford University, Stanford, CA 94305–5020, USA.

*To whom correspondence should be addressed. E-mail: kangshen@stanford.edu

reveal abnormalities in other AIY synapses. Although *unc-40* animals do not have substantial AIY axon guidance defects, RIA axon guidance is severely affected in *unc-40* mutants: RIA processes fail to extend ventrally to create the loop that is innervated by AIY in zone 2 (95.8% penetrant, $n = 191$ animals; fig. S3).

To identify the cell(s) in which *unc-40* functions to direct AIY-RIA innervation, we analyzed *unc-40* mosaic animals that retain an unstable rescuing array in subsets of cells (*8*). Interestingly, only when the array was retained in the AIY interneuron did we observe significant rescue of the AIY presynaptic patterning defects ($P < 0.001$; Fig. 2, L to M, and figs. S5 and S6). Retention of the array in the closely related interneuron RIB or RIM (RIB/RIM) (*9*) did not result in rescue. Retention in the RIA interneuron resulted in rescue of the RIA axon guidance defect but not of the AIY presynaptic phenotype (fig. S7).

Together, these data indicate that axon guidance of RIA and patterning of presynaptic specializations in AIY are independent, cell-autonomous events. These mosaic analyses are also consistent with the observation that UNC-40 (DCC) is endogenously expressed in AIY interneurons (fig. S6) and indicate a previously uncharacterized role for UNC-40 (DCC) in specifying AIY presynaptic terminals in a cell-autonomous manner.

To determine how UNC-40 (DCC) directs presynaptic assembly in AIY, we examined its subcellular localization. Consistent with UNC-40 (DCC) playing a role in the presynaptic patterning of AIY, we observed that UNC-40 (DCC) is enriched in zones 2 and 3, the regions where presynaptic sites are assembled (Fig. 3, A and C; 71.5% animals with enriched localization, $n = 214$ animals). This enrichment is dependent on UNC-6 (netrin), because UNC-40 (DCC) failed to concentrate at the presynaptic sites of AIY in *unc-6* animals (Fig. 3, B and C; 87.6% with diffuse localization, $n = 201$ animals). Consistent with this observation, in *unc-6* animals circuit assembly between AIY and RIA is abnormal, phenocopying the *unc-40* mutant defect (fig. S8).

During neurulation, when AIY-RIA innervation takes place, UNC-6 (netrin) is exclusively expressed by ventral cephalic sheath cells (VCSCs) at the nerve ring (*10*). VCSCs are non-neuronal cells that are morphologically similar to vertebrate astrocytes (*11*). Mosaic analysis using an *unc-6* rescuing construct showed that expression of UNC-6 (netrin) by VCSCs regulates the pattern of AIY presynapses (fig. S8B, $P < 0.001$).

VCSCs have slender processes that enter the nerve ring and terminate at specific synaptic sites, one of them being zone 2, the region where AIY innervates RIA (*4*). We investigated the physical relations between the VCSCs, AIY, and RIA and observed that the VCSCs project endfeet to the anterior end of the ventral nerve cord and form deeply invaginated membrane lamellae that ensheath the zone 2 region where AIY innervates RIA. The relative positioning of the VCSC endfeet with respect to AIY and RIA is extremely stereotyped across animals, revealing a tight and reproducible anatomical relation between the UNC-6–secreting VCSCs and the AIY-RIA synapses (Fig. 3, D to J, and fig. S1).

To test further whether the precise anatomical relation between the sheath cells and AIY-RIA synapses is instructive in mediating AIY:RIA innervation, we identified mutants that disrupt sheath cell morphology. We found that mutations in *unc-34*/enabled, a regulator of the actin cytoskeleton, altered the morphology of cephalic sheath cells: 47.8% of the *unc-34* animals have distended endfeet, which project further posteriorly ($n = 94$ animals; Fig. 4, A and D, and fig. S9A). In these *unc-34* animals, the distended VCSCs ectopically ensheath zone 1 of AIY in addition to zones 2 and 3 (Fig. 4, A and D). Also in these animals, we observed a change in the distribution of UNC-40 (DCC), which ectopically localized to zone 1 (Fig. 4, E to G). Furthermore, there was a concomitant change in the distribution of AIY presynapses: ectopic AIY presynaptic specializations now formed in zone 1, the region of overlap with distended sheath cell endfeet where ectopic UNC-40 localized (Fig. 4, B and D). Moreover, RIA axon guidance changed accordingly, with the RIA postsynaptic loop extending further posteriorly to the region covered by the sheath cell endfeet ($P < 0.001$; Fig. 4, C and D, and fig. S9A).

An epistasis analysis confirmed that the displacement of presynaptic sites observed in *unc-34* animals is an UNC-40 (DCC)–dependent event (fig. S9, B to D). These observations are consistent with a model whereby UNC-34 (enabled) affects presynaptic patterning in AIY by altering sheath cell morphology, which then affects localized UNC-6 (netrin) secretion, UNC-40 (DCC) localization, and presynaptic assembly.

Together our data strongly suggest that glia act as guideposts in directing circuit assembly between AIY and RIA. The glial cells mark a neurospatial coordinate in the *C. elegans* nerve ring through the secretion of UNC-6 (netrin). This in turn signals to AIY and RIA neurons through UNC-40 (DCC). UNC-40 (DCC) simultaneously activates two different and independent pathways in each neuron, orchestrating presynaptic assembly in AIY and axon guidance of postsynaptic RIA to the glial-specified location.

How can the same receptor and ligand elicit diverse cellular responses in distinct neurons? UNC-40 (DCC) has been reported to regulate diverse developmental processes like cell migration, neuronal polarization, and axon guidance, all of which involve an initial polarization event that may be mediated by netrin signaling (*6*, *7*, *12*–*15*). The patterning of AIY presynaptic regions can also be considered a local polarization event, through which AIY transforms a region of its plasma membrane into a specialized presynaptic area. Other guidance molecules, such as the Eph family of receptors and their ephrin ligands, have been shown to play roles in growth cone guidance as well as the development of mature excitatory synapses (*16*). In ephrin-mediated signaling, distinct cellular responses are likely generated by the developmental context and by diverse downstream targets (*17*). Similar mechanisms could explain the distinct cellular responses to UNC-40 (DCC) signaling.

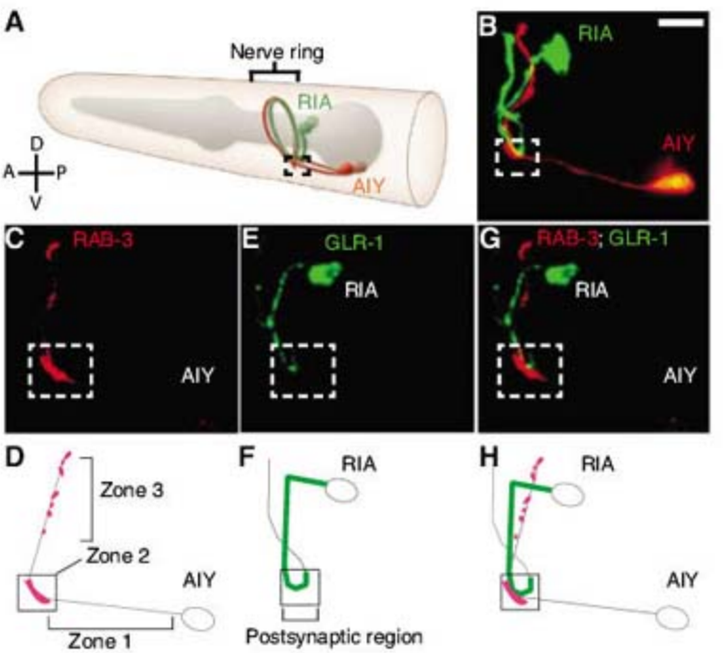

Fig. 1. AIY and RIA innervate at a specific spatial coordinate in the nerve ring. **(A)** Schematic diagram of the morphology of the presynaptic AIY and postsynaptic RIA neurons in the nerve ring (brackets). Modified image adapted from www.wormatlas.org with permission. **(B)** Representative adult animal expressing cytoplasmic fluorophores specifically in AIY (red) and RIA (green). In all images, the dashed box (zone 2 in text) delineates a spatial coordinate in the wild-type nerve ring where the RIA and the AIY interneurons converge and synapse onto each other. **(C to H)** Confocal micrographs and corresponding diagrams demonstrating the colocalization of AIY presynaptic vesicles [CFP::RAB-3 and pseudocolored red in (C)] with postsynaptic RIA glutamate receptors [GLR-1::YFP and pseudocolored green in (E)] in zone 2 (dashed box). Double labels are shown in (G). Schematic diagrams [(D), (F), and (H)] show the relation between AIY presynaptic terminals and the RIA postsynaptic region, which was highly reproducible across animals ($n > 500$). Scale bars, 5 μm.

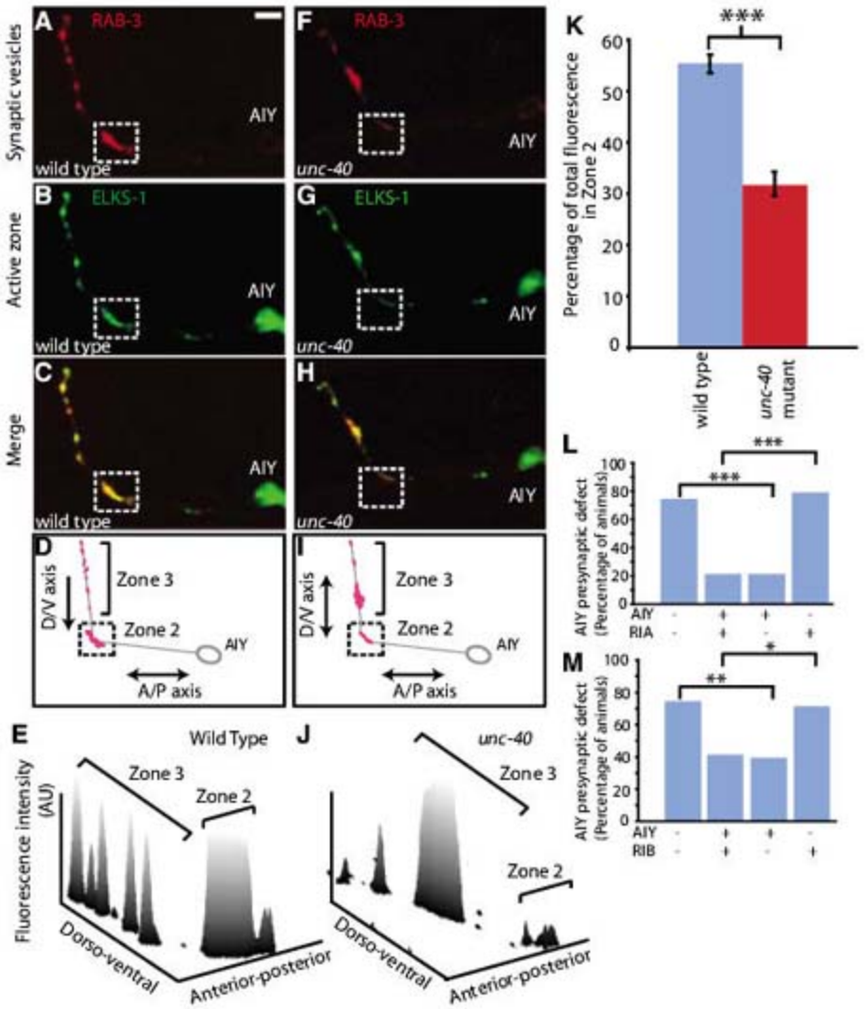

Fig. 2. UNC-40 (DCC) is required for correct presynaptic patterning in AIY. (**A** to **J**) Distribution of presynaptic sites of AIY in wild-type [(A) to (E)] or *unc-40* [(F) to (J)] animals. Confocal micrographs demonstrate the colocalization and patterning of AIY presynaptic vesicles [mCherry::RAB-3 pseudocolored red in (A) and (F)] and active zones [ELKS-1/ERC::YFP pseudocolored green in (B) and (G)] in a representative wild-type [(A) to (C)] or *unc-40* [(F) to (H)] animal, evident in the double-label merge images [(C) and (H)] and represented in the diagram of presynaptic site distribution [(D) and (I)]. Three-dimension line scan profiles of the fluorescence intensity (arbitrary units, AU) distribution in (A) and (F). (**K**) Quantification comparing the relative distribution of synaptic vesicle fluorescence in wild-type (blue; $n = 20$ neurons) versus *unc-40* animals (red; $n = 31$ neurons). Error bars represent standard error, and the asterisk represents statistical significance ($P < 0.001$). (**L** and **M**) *unc-40 (e271)* animals expressing an unstable transgene containing an *unc-40* rescuing construct, and cytoplasmic cell-specific markers in AIY and RIA (L) or RIB/RIM (M) were scored for retention of the transgene and rescue of the AIY presynaptic phenotype. ***$P <$ 0.001, **$P < 0.01$, and *$P < 0.05$ between indicated groups. Scale bars, 5 μm.

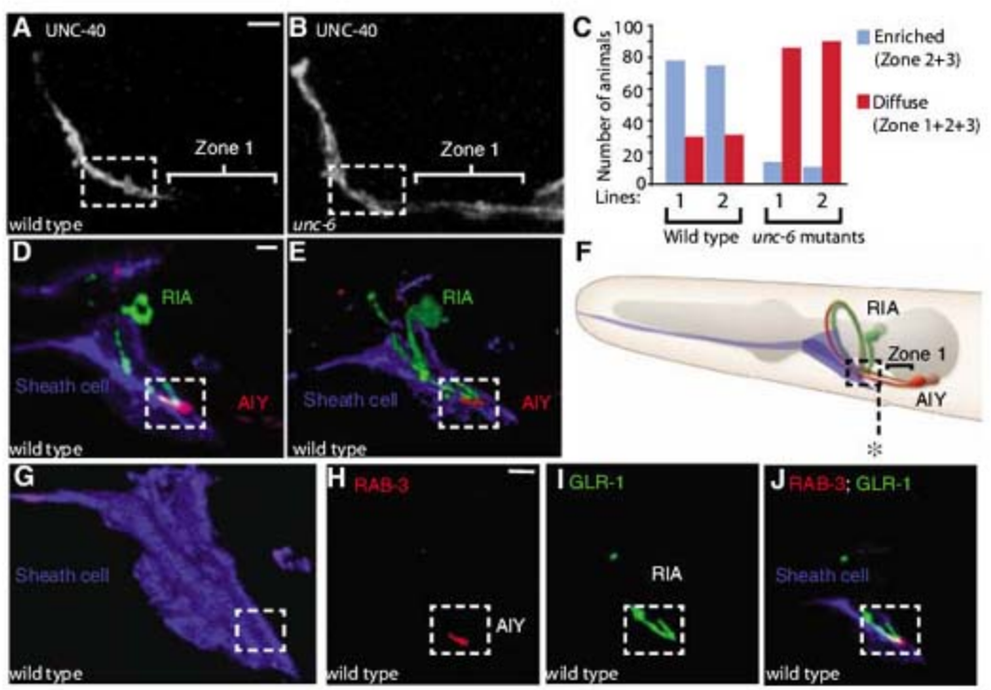

Fig. 3. Ventral cephalic sheath cells control UNC-40 (DCC) enrichment in presynaptic regions by secreting UNC-6 (netrin). (**A** and **B**) Localization of UNC-40::GFP in AIY of a representative wild-type (A) or *unc-6* (B) animal. Note UNC-40:GFP enrichment in zones 2 and 3 in wild-type animals [(A) dashed box], as compared to diffuse localization in *unc-6* animals (B). (**C**) Quantification of the enrichment of UNC-40::GFP in the presynaptic regions of wild-type versus *unc-6* animals. Two different transgenic lines (lines 1 or 2), both expressing UNC-40::GFP, were scored. (**D**) Projection of confocal micrographs obtained from a representative animal simultaneously expressing *hlh-17::mCherry* (to label ventral cephalic sheath cells and pseudocolored blue), *ttx-3::cfp::rab-3* (to label presynapses in AIY and pseudocolored red), and *glr-3::glr-1::yfp* (to label the glutamate receptors in RIA and pseudocolored green). (**E**) Volume rendering of (D) showing the relative positioning of the glial-like ventral cephalic sheath cells with respect to the region of innervation between AIY and RIA (*29*). (**F**) Diagram of (D) and (E). The asterisk marks the posterior extension of the sheath cell. (**G**) Volume rendering of the ventral sheath cell in (D). Note the groove in the boxed region where AIY and RIA are ensheathed by the ventral cephalic sheath cells and innervate each other. (**H** and **I**) Single confocal plane of (D), with presynaptic vesicles in AIY [labeled with cyan fluorescent protein (CFP)::RAB-3 and pseudocolored red in (H)], glutamate receptors in RIA [labeled with GLR-1:YFP and pseudocolored green in (I)] and a triple label including expression of the mCherry cytoplasmic fluorophore in the sheath cells [pseudocolored blue in (J)]. This anatomical relation was extremely stereotyped across animals ($n > 500$). Scale bars, 5 μm.

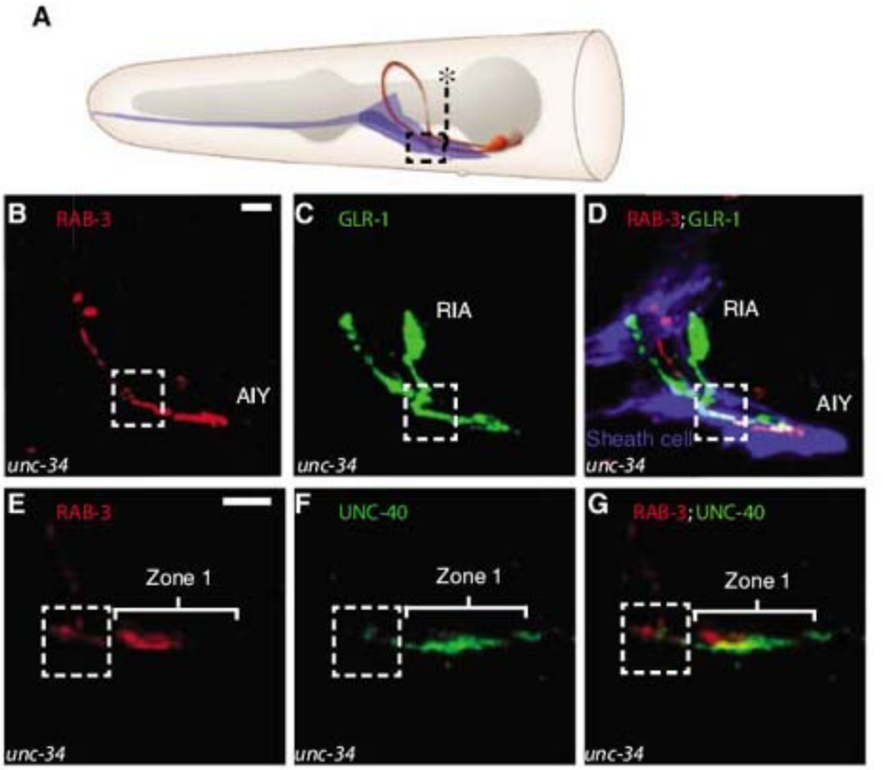

Fig. 4. Repositioning of the sheath cells affects RIA axon guidance and AIY presynapses. (**A**) Diagram showing the distended positioning of the ventral cephalic sheath cell in *unc-34* animals. The asterisk marks the normal posterior boundary of a wild-type sheath cell (see Fig. 3F for comparison). In *unc-34*, animals sheath cells abnormally distend posteriorly in 47.9% of animals (n = 94 animals). (**B** to **D**) Confocal micrographs obtained from a representative *unc-34* animal simultaneously expressing *ttx-3::cfp::rab-3* [to label presynapses in AIY and pseudocolored red in (B) and (D)], *glr-3::glr-1::yfp* [to label the glutamate receptors in RIA and pseudocolored green in (C) and (D)], and *hlh-17::mCherry* [to label the ventral cephalic sheath cells and pseudocolored blue in (D)]. Note abnormal posterior extension of the sheath cell endfeet, corresponding ectopic AIY presynapses in zone 1, and distended RIA axon in the area now covered by the distended sheath cell (compare with Fig. 3D). (**E** to **G**) Confocal micrographs obtained from a representative *unc-34* animal simultaneously expressing *ttx-3::mCherry::rab-3* [to label presynapses in AIY and pseudocolored red in (E) and (G)] and *ttx-3::unc-40::gfp* [to label the UNC-40 (DCC) receptors in AIY and pseudocolored green in (F) and (G)]. Scale bars, 5 μm.

Although cell-specific events in AIY and RIA happen independently of each other, their simultaneous regulation by a single molecule allows coordinated circuit assembly. UNC-6 (netrin) is a secreted chemotropic factor that can act as a long-range chemical cue or a short-range signaling molecule, depending on the developmental context (*18*–*20*). Given the close anatomical relation between the source of UNC-6 (netrin) (VCSCs) and the AIY:RIA synapses, it is likely that UNC-6 (netrin) acts as a short-range signaling molecule in this pathway, specifying microenvironments that promote UNC-40 (DCC) enrichment and synaptogenesis. Indeed, vertebrate astrocytes have been shown to be functionally compartmentalized into subcellular microdomains, which may be important in regulating localized secretion of signaling molecules regulating synaptic assembly and function (*21*). Furthermore, UNC-6 (netrin) has been reported to mediate adhesive interactions and function as a short-range target recognition molecule in other developmental events (*18*, *19*, *22*).

Our study is consistent with observations made in vertebrates and highlights the importance of glial cells in specifying precise neural connectivity. The fact that dissociated cultured neurons can form functional synapses in the absence of glial cells suggests that pre- and postsynaptic neurons are sufficient to assemble chemical synapses. However, growing evidence suggests that glia are essential regulators of synaptic assembly and function in vivo (*11*, *23*–*26*). For instance, astrocyte-secreted thrombospondin increases the density of synapses in the mammalian central nervous system (*23*, *27*).

Our data show that glia can also specify neural connectivity in vivo by marking a neurospatial coordinate, which achieves precise circuit assembly by controlling both synaptic partner choices and the location of innervation. Such stereotyped synaptic assembly gives rise to highly organized neuropil structures such as the nematode nerve ring. Similarly organized neuropil structures are also evident throughout the vertebrate central nervous system, exemplified by the stratified organization of the inner plexiform layer of the vertebrate retina and the glomeruli in the olfactory bulb (*2*, *28*). The roles observed here for glia in *C. elegans* may be evolutionarily conserved, such that proteins with multifunctional roles in spatial patterning, like UNC-40 (DCC), would detect the localized expression of glial signals and thus orchestrate the formation of neural circuits.

References and Notes

1. R. Salie, V. Niederkofler, S. Arber, *Neuron* **45**, 189 (2005).
2. R. Juttner, F. G. Rathjen, *Cell. Mol. Life Sci.* **62**, 2811 (2005).
3. C. L. Waites, A. M. Craig, C. C. Garner, *Annu. Rev. Neurosci.* **28**, 251 (2005).
4. J. G. White, E. Southgate, J. N. Thomson, S. Brenner, *Philos. Trans. R. Soc. London Ser. B* **314**, 1 (1986).
5. J. G. White, E. Southgate, J. N. Thomson, S. Brenner, *Cold Spring Harbor Symp. Quant. Biol.* **48**, 633 (1983).
6. S. S. Chan *et al.*, *Cell* **87**, 187 (1996).
7. K. Keino-Masu *et al.*, *Cell* **87**, 175 (1996).
8. J. Yochem, R. K. Herman, *Development* **130**, 4761 (2003).
9. Materials and methods are available on *Science* Online.
10. W. G. Wadsworth, H. Bhatt, E. M. Hedgecock, *Neuron* **16**, 35 (1996).
11. S. Shaham, *Curr. Opin. Neurobiol.* **16**, 522 (2006).
12. C. E. Adler, R. D. Fetter, C. I. Bargmann, *Nat. Neurosci.* **9**, 511 (2006).
13. E. M. Hedgecock, J. G. Culotti, D. H. Hall, *Neuron* **4**, 61 (1990).
14. E. D. Leonardo *et al.*, *Cold Spring Harbor Symp. Quant. Biol.* **62**, 467 (1997).
15. E. Bloch-Gallego, F. Ezan, M. Tessier-Lavigne, C. Sotelo, *J. Neurosci.* **19**, 4407 (1999).
16. M. B. Dalva *et al.*, *Cell* **103**, 945 (2000).
17. K. K. Murai, E. B. Pasquale, *Neuroscientist* **10**, 304 (2004).
18. K. A. Baker, S. W. Moore, A. A. Jarjour, T. E. Kennedy, *Curr. Opin. Neurobiol.* **16**, 529 (2006).
19. P. Strickland, G. C. Shin, A. Plump, M. Tessier-Lavigne, L. Hinck, *Development* **133**, 823 (2006).
20. M. Brankatschk, B. J. Dickson, *Nat. Neurosci.* **9**, 188 (2006).
21. P. G. Haydon, G. Carmignoto, *Physiol. Rev.* **86**, 1009 (2006).
22. M. L. Winberg, K. J. Mitchell, C. S. Goodman, *Cell* **93**, 581 (1998).
23. N. J. Allen, B. A. Barres, *Curr. Opin. Neurobiol.* **15**, 542 (2005).
24. M. R. Freeman, *Curr. Opin. Neurobiol.* **16**, 119 (2006).
25. P. Jourdain *et al.*, *Nat. Neurosci.* **10**, 331 (2007).
26. H. Nishida, S. Okabe, *J. Neurosci.* **27**, 331 (2007).
27. K. S. Christopherson *et al.*, *Cell* **120**, 421 (2005).
28. T. Komiyama, L. Luo, *Curr. Opin. Neurobiol.* **16**, 67 (2006).

29. We thank G. Wang, C. Johnson, J. Audhya, M. Nonet, Y. Kohara, J. Kaplan, G. Garriga, E. Lundquist, the *Caenorhabditis* Genetic Center, and the Japanese National BioResource Project for strains and reagents; D. Hall and Z. Altun for diagrams used in the figures; C. Bargmann for helpful discussions and generous sharing of advice and reagents; C. Gao and Frank Chen for technical assistance; and S. Margolis, L. Looger, J. Irazoqui, B. Barres, and members of the Shen lab for thoughtful comments on the manuscript. This work was funded by grants to K.S. from the following: the McKnight Endowment Fund, the W. M. Keck Foundation, and the Searle Scholar program. M.A.M. was supported by the Stanford Medical Scientist Training Program and NIH grant GM007365. D.A.C.-R. was supported by the Damon Runyon Foundation and NIH grant K99 NS057931-01.

Supporting Online Material

www.sciencemag.org/cgi/content/full/318/5847/103/DC1
Materials and Methods
Figs. S1 to S9

13 April 2007; accepted 24 August 2007
10.1126/science.1143762

Chimpanzees Are Rational Maximizers in an Ultimatum Game

Keith Jensen,* Josep Call, Michael Tomasello

Traditional models of economic decision-making assume that people are self-interested rational maximizers. Empirical research has demonstrated, however, that people will take into account the interests of others and are sensitive to norms of cooperation and fairness. In one of the most robust tests of this finding, the ultimatum game, individuals will reject a proposed division of a monetary windfall, at a cost to themselves, if they perceive it as unfair. Here we show that in an ultimatum game, humans' closest living relatives, chimpanzees (*Pan troglodytes*), are rational maximizers and are not sensitive to fairness. These results support the hypothesis that other-regarding preferences and aversion to inequitable outcomes, which play key roles in human social organization, distinguish us from our closest living relatives.

Humans are able to live in very large groups and to cooperate with unrelated individuals whom they expect never to encounter again, conditions that make the standard mechanisms for cooperation unlikely (*1*), namely kin selection (*2*) and reciprocal altruism (*3*). Nevertheless, people help others, sometimes at great personal cost. But people are not obligate altruists; they do not tolerate abuse of their generosity. Not only will they punish or shun individuals who free-ride or exploit them, they will do so even if they themselves do not benefit from correcting the behavior of norm violators (*4*). The willingness both to cooperate and to punish noncooperators has been termed strong reciprocity (*5*) and has been claimed to be uniquely human (*6*). To cooperate in these ways, humans must be more than self-regarding rational decision-makers; they must also, at least to some degree, have concern for outcomes and behaviors affecting others (other-regarding preferences) (*4*) as well as a general concern for norms of fairness (*7*, *8*).

The benchmark test for examining sensitivity to fairness and other-regarding preferences is the ultimatum game (*9*). In the standard version of the game, two anonymous individuals are assigned the roles of proposer and responder. The proposer is offered a sum of money and can decide whether to divide this windfall with the responder. The crucial feature of the ultimatum game is that the responder can accept or reject the proposer's offer. If the responder accepts it, both players receive the proposed division; if the responder rejects it, both get nothing. The canonical economic model of pure self-interest predicts that the proposer will offer the smallest share possible and that the responder will accept any nonzero offer. This is not what happens. Although the specifics vary across culture and setting, the basic finding is that proposers typically make offers of 40 to 50% and responders routinely reject offers under 20% (*10*). These findings suggest that responders are sensitive to unfairness and punish proposers who make inequitable offers by rejecting those offers at a cost to themselves, and knowing this, proposers make strategic offers that are less likely to be refused.

The ultimatum game has been used in dozens, possibly hundreds of studies, including various human cultures (*11*) and children (*12*). Testing the ultimatum game on other species would be an important contribution to the debate on the evolution and possible uniqueness of human cooperation (*6*). Chimpanzees are our closest extant relatives and engage in cooperative behavior such as group hunting, coalitionary aggression, and territorial patrols (*13*). Furthermore, in experiments they have been shown to coordinate their behavior (*14*) and to provide help (*15*, *16*). However, there is ongoing debate about whether chimpanzees are sensitive to, and tolerant of, unfairness (*17*) or whether they simply attend to their own expectations with no regard for what others receive (*18*). Additionally, experiments have failed to reveal other-regarding preferences when food was involved (*19*, *20*) other than to punish direct theft (*21*). Having chimpanzees play the ultimatum game would address these conflicting findings on fairness and negative reciprocity and allow direct comparisons to humans.

In the current study, we tested chimpanzees in a mini-ultimatum game. The mini-ultimatum game is a reduced form of the ultimatum game in which proposers are given a choice between making one of two pre-set offers which the responder can then accept or reject (*22*). In one such study (*23*), there were four different games. In all games, the proposer had as one option an amount that would typically be rejected by a human responder as unfair, namely 80% for the proposer and 20% for the responder (8/2 offer; the proposer received the amount to the left of the slash and the responder received the amount to the right). In the 5/5 (fair) game, the proposer

Max Planck Institute for Evolutionary Anthropology, Deutscher Platz 6, D-04103, Leipzig, Germany.

*To whom correspondence should be addressed. E-mail: jensen@eva.mpg.de

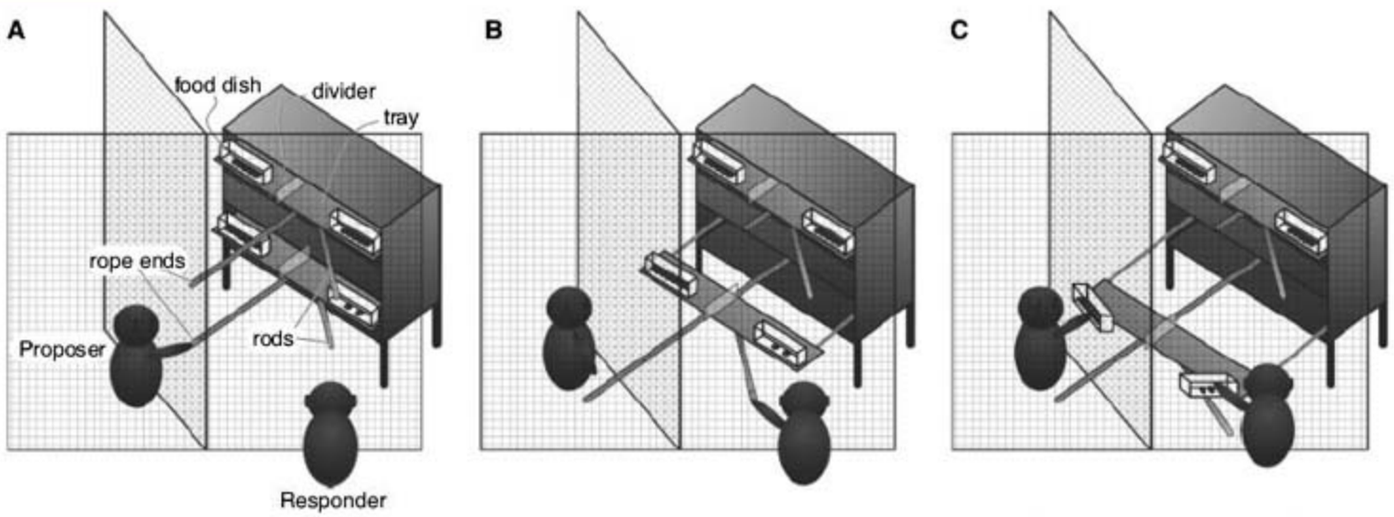

Fig. 1. Illustration of the testing environment. The proposer, who makes the first choice, sits to the responder's left. The apparatus, which has two sliding trays connected by a single rope, is outside of the cages. **(A)** By first sliding a Plexiglas panel (not shown) to access one rope end and by then pulling it, the proposer draws one of the baited trays halfway toward the two subjects. **(B)** The responder can then pull the attached rod, now within reach, to bring the proposed food tray to the cage mesh so that **(C)** both subjects can eat from their respective food dishes (clearly separated by a translucent divider).

was faced with the choice of 8/2 versus 5/5. The other games were 8/2 versus 2/8 (unfair versus hyperfair), 8/2 versus 8/2 (no choice), and 8/2 versus 10/0 (unfair versus hyperunfair). Human responders rejected the 8/2 offer most when the alternative was fair (5/5 game), less when the alternative was hyperfair (2/8 game), even less when there was no alternative (8/2 game), and hardly at all when the alternative was for the proposer to be even more selfish (10/0 game) (*23*). The differential rejection of unfair outcomes across the games suggests that people are not sensitive solely to unfair distributions (*7*) nor solely to unfair intent (*24*) but to a combination of both (*8*). If chimpanzees are sensitive to unfairness and are negatively reciprocal, they would behave like *Homo reciprocans* (*25*), whereas if they accept any nonzero offer regardless of alternatives for the proposer, they will be more like the hypothetical *Homo economicus* (*26*).

Subjects were 11 chimpanzees from a group-housed colony at the Wolfgang Köhler Primate Research Center (*27*). The proposer sat to the left of the responder, who was in an adjacent cage in an L-shaped arrangement. The test apparatus, which was outside of the cages, had two sliding trays. On each tray were two dishes with raisins, separated by translucent dividers: one for the proposer and the other for the responder (Fig. 1). Proposers would first choose one of the two trays by pulling it halfway to the cages (as far as it would go); responders could accept the offer by pulling the proposed tray the remaining distance (via the rod which came into reach only as a result of the proposer's pull) or could reject it by not pulling at all within 1 min. The responder's acceptance led to both subjects being able to reach the food in their respective dishes. Rejection led to both getting nothing, because the experimenter would remove all food dishes after the trial ended. There were four games (as in the study described above), all played within a single session: 2/8, 5/5, 8/2, and 10/0—each versus 8/2. The order of games was counterbalanced across subjects.

The most important finding is that responders tended to accept any offer. As can be seen in Fig. 2, responders rejected 8/2 offers at overall low rates (from 5 to 14% of the time). There was a trend toward different rejection rates of 8/2 offers across the four games (Friedman's χ^2_3 test = 6.643, $P = 0.069$). However, all paired comparisons were nonsignificant, indicating that, crucially, chimpanzees rejected 8/2 offers equally often regardless of the alternatives available to the proposers (*27*). Moreover, this trend toward rejections was in the opposite direction of the finding for humans (*23*). When proposers offered non-8/2 alternatives (available in all but the 8/2 game), responders accepted them differentially across the games (Friedman's χ^2_2 test = 10.00, $P = 0.012$). In line with the principle of self-interest to accept any nonzero offer, responders rejected 10/0 offers (in which the responder receives nothing) more often than 5/5 offers [Wilcoxon T^+ test = 28.00, $n = 8$ (1 tie), $P = 0.016$] and marginally more often than 2/8 offers [Wilcoxon T^+ test = 15.00, $n = 7$ (2 ties), $P = 0.063$]. Indeed, the only offers rejected by responders more than 0% of the time were 10/0 offers (one-sample t test $t_9 = 4.735$, $P = 0.001$). In short, responders did not reject unfair offers when the proposer had the option of making a fair offer; they accepted almost all nonzero offers; and they reliably rejected only offers of zero. As can be seen in Fig. 3, these results contrast strongly with those of adult humans, who reject 8/2 offers most often when a fair (5/5) option is available for the proposer and least often when the alternative for the responder is even more selfish than the 8/2 option (10/0) (*23*). Furthermore, unlike human responders, who report being angry when confronted with unfair offers (*28*), chimpanzee responders showed signs of arousal [displays and tantrums (*13*, *29*)] in less than 2% of the test trials (all occurrences were by one individual in all trials of a single session), whereas in a previous study in which the subjects had food taken away from them, these same individuals exhibited tantrums or displays 40% of the time (*21*).

Consistent with previous studies on chimpanzees (*19*, *20*), proposers did not appear to take outcomes affecting the responder into account. When given the opportunity, proposers did not make fair offers (Fig. 2) [see also (*27*), and fig. S1]. Given the propensity of responders to accept any nonzero offer, it is not surprising that chimpanzee proposers acted according to traditional economic models of self-interest. However, it is perhaps surprising that proposers made zero offers to the responders, given that these offers were rejected at the highest rate (Fig. 2); chimpanzees are certainly capable of distinguishing two pieces of food from zero when choosing for themselves (*30*).

To rule out more trivial interpretations of our results, it was necessary to demonstrate that responders and proposers understood the critical features of the task. To this end, we conducted familiarization and probe trials as well as a follow-up study. First, sensitivity to fairness in the ultimatum game requires that responders and proposers each know what the other gains. We

Game	Proposer Offers	Payoffs: Proposer	Payoffs: Responder	Responder Rejections
5/5	39 (75%)	8	2	2 (5%)
	13 (25%)	5	5	0 (0%)
2/8	45 (87%)	8	2	3 (7%)
	7 (13%)	2	8	0 (0%)
8/2	53 (100%)	8	2	6 (11%)
		8	2	
10/0	29 (54%)	8	2	4 (14%)
	25 (46%)	10	0	11 (44%)

Fig. 2. Offers made by proposers and rejections by responders in the four games. In each game, the proposer could choose between two payoff options: 8/2 (8 raisins for the proposer and 2 for the responder) and an alternate [2/8 (2 for the proposer and 8 for the responder), 5/5 (5 for the proposer and 5 for the responder), 8/2 (8 for the proposer and 2 for the responder), and 10/0 (10 for the proposer and 0 for the responder)]. Results on the left show the total number and corresponding percentage of offers for each option made by proposers in each game. (Trials in which the proposer did not participate are not included, therefore the total number of offers varies across the games; percentages are therefore based on the total number of offers for each option out of the total number of trials played for each game.) Results on the right indicate the total number of each offer rejected and the corresponding percentage of rejections out of the total number of offers for each game.

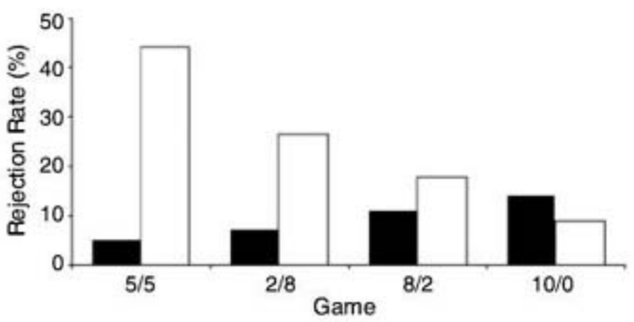

Fig. 3. Rejection rates (% of trials) of 8/2 offers in the four games for chimpanzees in this study (black bars) and for human participants (white bars) [data are from (*23*)].

therefore ran follow-up probe trials to determine whether the chimpanzees were capable of attending to the amount of food available to the partner. Subjects were tested alone, and they had to look into the distal food dishes to correctly choose the tray that would yield the largest payoff from the partner's position before going through the open door to the adjacent cage to get it. They chose correctly at greater than chance levels, demonstrating that they would have been capable of seeing payoffs to the partner (*27*). Second, in inhibition probe trials, we found that subjects could inhibit pulling the rod when it led to no food gain about 64% of the time, about the same rate of pulling as in the 10/0 condition, suggesting that some of the failure to reject zero offers was due, at least some of the time, to an inability to inhibit a natural tendency to pull. Third, in discrimination probe trials, responders could distinguish between all offers available to them (fig. S2), and proposers could do so for all but 10/0 versus 8/2 (fig. S1) (*31*), demonstrating that subjects were able to make maximizing choices.

Our subjects were from a single social group, they did not interact anonymously, and they played both roles in the game. However, anonymous one-shot games are used in experiments with humans to decrease the likelihood of making fair offers or accepting unfair offers (*32*, *33*), and so if anything, our experimental design should have been skewed in favor of finding fairness sensitivity. The fact that chimpanzees in this study did not punish other individuals for making unfair offers may be in part a reflection of the fact that active food sharing is rare in this species (*34*) and may also be because they were unwilling to pay a cost to punish.

We gave chimpanzees the most widely recognized test for a sensitivity to fairness, the ultimatum game, and found that they did not systematically make fair offers to conspecifics, nor did they systematically refuse to accept unfair offers from conspecifics even though they could discriminate between the quantities available to themselves and their partners. It thus would seem that in this context, one of humans' closest living relatives behaves according to traditional economic models of self-interest, unlike humans, and that this species does not share the human sensitivity to fairness.

References and Notes

1. R. Boyd, P. J. Richerson, *J. Theor. Biol.* **132**, 337 (1988).
2. W. D. Hamilton, *J. Theor. Biol.* **7**, 1 (1964).
3. R. Trivers, *Q. Rev. Biol.* **46**, 35 (1971).
4. R. Boyd, H. Gintis, S. Bowles, P. J. Richerson, *Proc. Natl. Acad. Sci. U.S.A.* **100**, 3531 (2003).
5. H. Gintis, *J. Theor. Biol.* **206**, 169 (2000).
6. E. Fehr, U. Fischbacher, *Nature* **425**, 785 (2003).
7. E. Fehr, K. M. Schmidt, *Q. J. Econ.* **114**, 817 (1999).
8. A. Falk, U. Fischbacher, *Games Econ. Behav.* **54**, 293 (2006).
9. W. Güth, R. Schmittberger, B. Schwarze, *J. Econ. Behav. Organ.* **3**, 367 (1982).
10. C. F. Camerer, *Behavioral Game Theory—Experiments in Strategic Interaction* (Princeton Univ. Press, Princeton, NJ, 2003).
11. J. Henrich *et al.*, *Science* **312**, 1767 (2006).
12. J. K. Murnighan, M. S. Saxon, *J. Econ. Psych.* **19**, 415 (1998).
13. J. Goodall, *The Chimpanzees of Gombe* (Harvard Univ. Press, Cambridge, MA, 1986).
14. A. P. Melis, B. Hare, M. Tomasello, *Anim. Behav.* **72**, 275 (2006).
15. F. Warneken, M. Tomasello, *Science* **311**, 1301 (2006).
16. F. Warneken, B. Hare, A. P. Melis, D. Hanus, M. Tomasello, *PLoS Biol.* **5**, e184 (2007).
17. S. F. Brosnan, H. C. Schiff, F. B. M. de Waal, *Proc. R. Soc. London Ser. B* **272**, 253 (2005).
18. J. Bräuer, J. Call, M. Tomasello, *Proc. R. Soc. London Ser. B* **273**, 3123 (2006).
19. J. B. Silk *et al.*, *Nature* **437**, 1357 (2005).
20. K. Jensen, B. Hare, J. Call, M. Tomasello, *Proc. R. Soc. London Ser. B* **273**, 1013 (2006).
21. K. Jensen, J. Call, M. Tomasello, *Proc. Natl. Acad. Sci. U.S.A.* **104**, 13046 (2007).
22. G. E. Bolton, R. Zwick, *Games Econ. Behav.* **10**, 95 (1995).
23. A. Falk, E. Fehr, U. Fischbacher, *Econ. Inq.* **41**, 20 (2003).
24. M. Rabin, *Am. Econ. Rev.* **83**, 1281 (1993).
25. E. Fehr, S. Gächter, *Eur. Econ. Rev.* **42**, 845 (1998).
26. R. H. Frank, *Am. Econ. Rev.* **77**, 593 (1987).
27. Additional details on the methods and results can be found in the supporting material on *Science* Online.
28. M. Pillutla, J. Murnighan, *Organ. Behav. Hum. Decision Processes* **68**, 208 (1996).
29. T. Nishida, T. Kano, J. Goodall, W. C. McGrew, M. Nakamura, *Anthropol. Sci.* **107**, 141 (1999).
30. S. T. Boysen, G. G. Berntson, *J. Comp. Psych.* **103**, 23 (1989).
31. However, the same subjects could discriminate 10 from 8 in a previous study (*35*), and chimpanzees can reliably discriminate 0 from 2 (*30*), which they would have done had they attended to responder outcomes.
32. M. Shinada, T. Yamagishi, Y. Ohmura, *Evol. Hum. Behav.* **25**, 379 (2004).
33. K. J. Haley, D. M. T. Fessler, *Evol. Hum. Behav.* **26**, 245 (2005).
34. J. Stevens, D. Stephens, *Behav. Ecol.* **13**, 393 (2002).
35. D. Hanus, J. Call, *J. Comp. Psych.* **121**, 241 (2007).

36. We thank the keepers of the Leipzig zoo, notably S. Leideritz, D. Geissler, N. Schenk, and "Mozart" Herrmann for their help; G. Sandler for reliability coding; R. Mundry for statistical advice; and two anonymous reviewers for helpful comments.

Supporting Online Material

www.sciencemag.org/cgi/content/full/318/5847/107/DC1
Materials and Methods
SOM Text
Figs. S1 and S2
References
Movies S1 and S2

30 May 2007; accepted 16 August 2007
10.1126/science.1145850

Widespread Role for the Flowering-Time Regulators FCA and FPA in RNA-Mediated Chromatin Silencing

Isabel Bäurle,[1]* Lisa Smith,[2]† David C. Baulcombe,[2]‡ Caroline Dean[1]*

The RRM-domain proteins FCA and FPA have previously been characterized as flowering-time regulators in *Arabidopsis*. We show that they are required for RNA-mediated chromatin silencing of a range of loci in the genome. At some target loci, FCA and FPA promote asymmetric DNA methylation, whereas at others they function in parallel to DNA methylation. Female gametophytic development and early embryonic development are particularly susceptible to malfunctions in FCA and FPA. We propose that *FCA* and *FPA* regulate chromatin silencing of single and low-copy genes and interact in a locus-dependent manner with the canonical small interfering RNA–directed DNA methylation pathway to regulate common targets.

Heterochromatin in many organisms is characterized by extensive DNA methylation and histone modifications (*1*). Plants display cytosine methylation in CG, CNG (N = any nucleotide), and CHH (H = A, C, or T) sequence contexts. In *Arabidopsis*, small interfering RNAs (siRNAs) are involved in localizing and maintaining these chromatin modifications in processes requiring *RNA-DEPENDENT RNA POLYMERASE2* (*RDR2*), *DICER-LIKE3* (*DCL3*), *ARGONAUTE4* (*AGO4*), and the two RNA polymerase IV isoforms, Pol IVa and b (*2*–*9*).

To identify further components required for siRNA-mediated chromatin silencing, we used a reporter system in which the *Arabidopsis* phytoene desaturase (*PDS*) gene is silenced in response to a homologous inverted repeat (*SUC-PDS*) (*10*). Two mutants that partially suppressed the silencing of *PDS* (Fig. 1, A, B, C, and E) showed late flowering that was reversible by vernalization. The silencing and flowering phenotypes cosegregated, and the mutations mapped to chromosomes 2 and 4. The flowering phenotype suggested involvement of *FPA* and *FCA*, two members of the autonomous pathway (*11*), mapping to those genomic regions. Sequencing revealed a premature termination codon in *FPA* (Trp^{98}*, G to A, *fpa-8*) and *FCA* (Gln^{537}*, C to T, *fca-11*). The flowering defect was confirmed by complementation analysis with previously known flowering mutants (*fca-9*, *fpa-7*, and *fve-3*; Fig. 1F), which also showed *PDS* silencing (fig. S1). Thus, *FCA* and *FPA* are required

for efficient *PDS* silencing in the presence of *SUC-PDS*.

FCA and FPA contain multiple RNA recognition motif (RRM) RNA binding domains (*12*, *13*), which are known to bind single-stranded RNA, but share no other sequence homology. FCA negatively regulates its own expression through alternative polyadenylation site usage (*14*). Late flowering in *fca* and *fpa* is due to overexpression of the major repressor of flowering in *Arabidopsis*, *FLOWERING LOCUS C* (*FLC*) (*11*). *FCA* and *FPA* do not appear to regulate *PDS* in the absence of the silencing trigger, which suggests that the presence of the transgene makes the endogenous *PDS* a target of *FCA* and *FPA*.

Because FCA and FPA both contain RRM domains, we hypothesized that they act partially redundantly; consistent with this, an *fca-11 fpa-8* double mutant showed no *PDS* silencing (Fig. 1D). Components of the siRNA chromatin-silencing pathway (the Pol IVa largest subunit NRPD1a and RDR2) also suppress *PDS* silencing completely (*10*). Both *nrpd1a-5* and *fca-11 fpa-8* double mutants showed reduced *SUC-PDS* and higher *PDS* mRNA levels (Fig. 1G and fig. S2) (*10*). *PDS* siRNA levels were reduced in *rdr2-5*, *nrpd1a-5*, and *fca-11 fpa-8* mutants, but not in *fca-11* or *fpa-8* single mutants (Fig. 1H).

Bisulfite sequencing was used to investigate whether *PDS* silencing corresponded to DNA methylation at the endogenous *PDS* locus. We found non-CG methylation (CNG and CHH) at the endogenous *PDS* locus in a region complementary to the hairpin in *SUC-PDS* leaves, but not in wild-type leaves (Fig. 1I and table S1). CG sites were highly methylated in both the wild type and mutants. In *nrpd1a-5* and *fca-11 fpa-8* mutants, loss of siRNA coincided with loss of asymmetric DNA methylation (Fig. 1I and table S1). CHH methylation was also compromised in *fca-11* and *fpa-8* single mutants, although *PDS* siRNA levels were unaffected (Fig. 1, H and I). These results suggest a dual role for *FCA* and *FPA*: (i) They act together with *NRPD1a* and *RDR2* and redundantly with each other to amplify siRNAs derived from the transgene locus; (ii) they act in the perception and interpretation of the silencing signal at the target locus. Mutants in two other members of the autonomous pathway—the MSI1 homolog *FVE* and the putative histone demethylase *FLD* (*15*, *16*)—also suppressed *PDS* silencing (fig. S1), which indicates that multiple components of the autonomous pathway are involved in this process.

Transposons, retroelements, and intergenic transcripts are endogenous targets of chromatin-silencing pathways (*5*–*8*, *17*). Expression of the *AtSN1* retroelement and the *AtMu1* DNA transposon were also controlled by FCA and FPA (Fig. 2A). *AtSN1* was reactivated very strongly in *fpa-8*, *fca-11 fpa-8*, and *nrpd1a-5* mutant seedlings, but not in *fca-11*. In contrast, *AtMu1* was slightly derepressed in *fca-11* and *fpa-8* single mutants and more strongly in *fca-11 fpa-8*. *AtMu1* reactivation in *fca-11 fpa-8* was similar to that in *nrpd1a-5*. An intergenic transcript flanked by a solo long terminal repeat (LTR), *IG/LINE*, was also up-regulated in *fca-11 fpa-8*, albeit to a lesser extent than in *nrpd1a-5* (Fig. 2A). Together, these findings indicate that *FCA* and *FPA* have a widespread role in the regulation of endogenous loci known to be silenced at the level of transcription and dependent on siRNA.

We next investigated whether this transcriptional reactivation correlated with loss of corresponding siRNA. *AtSN1* and *AtMu1* siRNAs were detected at wild-type levels in *fca-9*, *fpa-7*, and *fca-9 fpa-7*, but were absent from *nrpd1a-3* mutant seedlings (Fig. 2B). Corresponding results were obtained for other siRNAs. Thus, despite their role in the amplification of *PDS* siRNA, *FCA* and *FPA* do not generally act in NRPD1a-dependent siRNA production. There was no change in DNA methylation at the *AtSN1* locus in *fca fpa* (Fig. 2C, fig. S3, A and B, and table S2). However, bisulfite sequencing indicated a reduction of ~50% in asymmetric (CHH) DNA methylation at *AtMu1* in *fca fpa*, whereas CG and CNG methylation were not affected (Fig. 2C, fig. S3B, and table S2). Likewise, asymmetric DNA methylation at the solo LTR was reduced (fig. S3C). Maintenance of asymmetric DNA methylation requires the continued presence of the trigger, whereas symmetric DNA methylation can be maintained through cell divisions in the absence of the trigger. Silencing at these loci is also associated with changed histone tail modifications such as increased H3 K9 dimethylation and reduced H3 K4 dimethylation (*5*, *8*, *17*). Using chromatin immunoprecipitation, we did not find any pronounced alteration in these marks in *fca-9 fpa-7*.

Heterochromatic loci are targeted by multiple silencing pathways, and their contribution at individual loci differs considerably (*18*–*20*). This is corroborated by our finding that silencing of *AtSN1*, *AtMu1*, *IG/LINE*, and *PDS* in the presence of *SUC-PDS* differentially requires

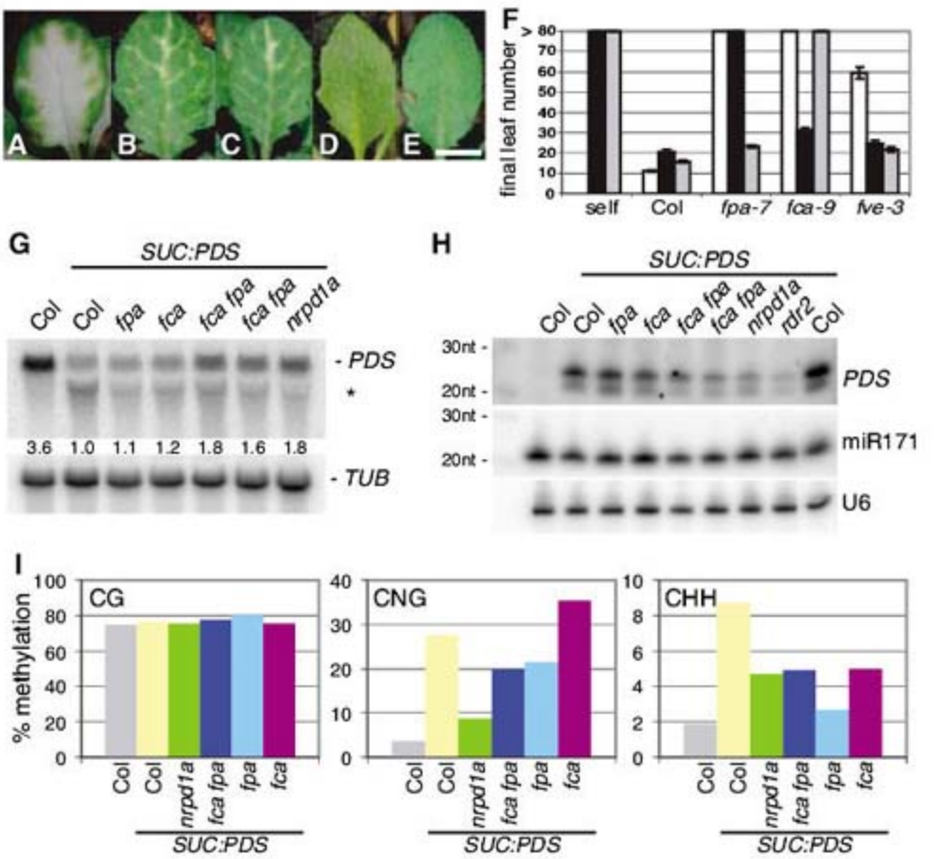

Fig. 1. *FCA* and *FPA* suppress *SUC-PDS*–induced silencing of *PDS*. (**A** to **E**) Leaf phenotypes in *SUC-PDS* background grown in long days. (A) Col, (B) *fpa-8*, (C) *fca-11*, (D) *fca-11 fpa-8*, (E) no transgene. Scale bar, 5 mm. (**F**) Complementation analysis: average flowering time (±SEM) of F_1 progeny of crosses between the indicated mutations (white, selfed) and *fpa-8* (black) or *fca-11* (gray). (**G**) RNA gel blot analysis of *PDS* mRNA detecting endogenous *PDS* (*PDS*) and *SUC-PDS* mRNA (*). Numbers indicate relative expression of *PDS* averaged over two experiments. (**H**) RNA gel blot analysis of *SUC-PDS* siRNA. (**I**) Cytosine methylation at the endogenous *PDS* locus assayed by bisulfite sequencing.

[1]Department of Cell and Developmental Biology, John Innes Centre, Norwich NR4 7UH, UK. [2]Sainsbury Laboratory, Colney Lane, Norwich NR4 7UH, UK.

†Present address: Max Planck Institute for Developmental Biology, Spemannstrasse 37-39, 72076 Tübingen, Germany. ‡Present address: Department of Plant Sciences, University of Cambridge, Downing Street, Cambridge CB2 3EA, UK. *To whom correspondence should be addressed. E-mail: isabel.baurle@bbsrc.ac.uk; caroline.dean@bbsrc.ac.uk

FCA and *FPA*. *PDS* silencing is associated with target DNA methylation and siRNA production through mechanisms that are dependent on both the siRNA chromatin-silencing pathway and *fca fpa*. Derepression of *AtMu1* and *IG/LINE* in *fca fpa* mutants coincides with loss of DNA methylation but not siRNAs, whereas both are lost in mutants of the siRNA chromatin-silencing pathway. Despite much stronger reactivation of *AtSN1* in *fca fpa*, neither DNA methylation nor siRNA accumulation was affected. Our findings are consistent with the idea that transcription can be reactivated in the presence of DNA methylation, as was established for the *morpheus' molecule 1* (*mom1*) mutation (*19*, *21*). Despite this similarity, it seems unlikely that *FCA* and *FPA* generally act together with *MOM1*, because *AtSN1* and *AtMu1* are not misregulated in *mom1* (*22*).

To investigate how *FCA* and *FPA* relate to the chromatin siRNA amplification pathway including *Pol IVa*, *RDR2*, and *DCL3*, we analyzed the release of silencing in double mutants (Fig. 2D). All double mutants showed much higher reactivation of *AtSN1* and *AtMu1* than any of the single mutants, which suggests that *FCA* and *FPA* do not act downstream of the siRNA amplification pathway, but rather in parallel. Similarly, transposon reactivation was greatly enhanced in *five nrpd1a* double mutants relative to either of the single mutants (fig. S3D). Strikingly, although *FCA* is dispensable for *AtSN1* silencing in the wild type, the loss of *FCA* in *nrpd1a*, *rdr2*, or *dcl3* mutant backgrounds greatly enhanced the release of *AtSN1* silencing.

Our findings predict that perturbation of DNA methylation in *fca fpa* mutants will affect reactivation of target loci differently. At *AtSN1*, where the effect of *FCA* and *FPA* is uncoupled from DNA methylation, enhanced loss of silencing in the presence of the DNA methylation inhibitor 5-aza-deoxycytidine (aza-dC) would be expected. Conversely, at *AtMu1*, where *fca fpa* mutants show reduced DNA methylation, the additional effect of the inhibitor would be small. Our results (Fig. 3A and table S3) are consistent with this prediction, because *fca-9 fpa-7* mutants were more sensitive than the wild type to aza-dC with respect to *AtSN1* reactivation, but less sensitive than the wild type with respect to *AtMu1* reactivation. Also, development of *fca-9 fpa-7* seedlings was strongly perturbed when exposed to aza-dC at concentrations where development of wild-type or *fca-9* seedlings was not abnormal and development of *fpa-7* seedlings was only very slightly abnormal (Fig. 3B and table S4) (*23*).

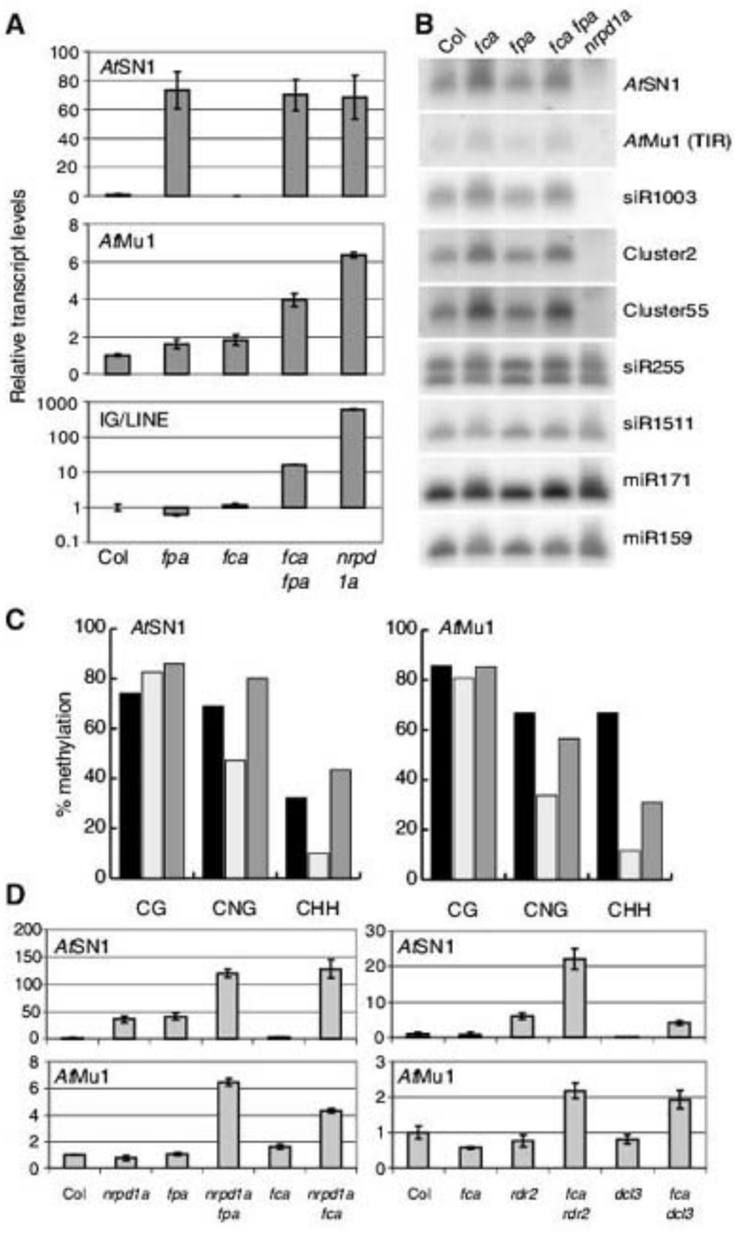

Fig. 2. Reactivation of *AtSN1*, *AtMu1*, and *IG/LINE* in seedlings. (**A**) Quantitative reverse transcription polymerase chain reaction (RT-PCR) on Col, *fpa-8*, *fca-11*, *fca-11 fpa-8*, and *nrpd1a-5*. (**B**) RNA gel blot analysis of trans-acting siRNAs (siR255, siR1511), microRNAs (miR159, miR171), or siRNAs (all other) on Col, *fca-9*, *fpa-7*, *fca-9 fpa-7*, and *nrpd1a-3*. (**C**) Cytosine methylation for Col (black), *nrpd1a-3* (light gray), and *fca-9 fpa-7* (dark gray). (**D**) Quantitative RT-PCR (left: Col, *nrpd1a-3*, *fpa-8*, *nrpd1a-3 fpa-8*, *fca-11*, and *nrpd1a-3 fca-11*; right: Col, *fca-9*, *rdr2-1*, *fca-9 rdr2-1*, *dcl3-1*, and *fca-9 dcl3-1*). *nrpd1a-3* is a weaker allele than *nrpd1a-5* with respect to *AtMu1* reactivation; error bars indicate SD.

Fig. 3, E and F). Together, these data all indicate that silencing does not occur posttranscriptionally but rather cotranscriptionally before any processing occurs.

Taken together, our results show that the nuclear proteins FCA and FPA have a much more widespread role in development and gene silencing than previously anticipated. We propose a model in which FCA and FPA cotran-

fca fpa double mutant plants are late flowering but otherwise largely normal. However, closer examination of *fca-11 fpa-8* siliques revealed that ~20% of developing seeds aborted and ~70% of ovules did not initiate development (fig. S4A and Table 1). When pollinating double mutants with wild-type pollen, no seeds aborted, but the high proportion of undeveloped seeds persisted; this finding suggested that the embryonic lethality was zygotic, whereas the undeveloped seed phenotype was caused by the genotype of the mother plant. When *fca/fca FPA/fpa* ovules were pollinated with wild-type pollen, 34% of seeds appeared undeveloped (Table 1). Microscopic examination of mature ovules did not reveal any abnormalities (fig. S4, B and C), which suggests that the genotype of the female gametophyte determined the undeveloped seed phenotype. Thus, (female) gametophytic and early embryonic development is extremely sensitive to loss of *FCA* and *FPA*. Once these stages are passed successfully, development can proceed largely independently of *FCA* and *FPA*. Whether misregulation of a few key genes or more global genome misorganization causes these defects remains to be investigated.

We propose that the increased transcript levels measured for the targets in *fca fpa* reflect transcriptional reactivation rather than increased cytoplasmic RNA stability. This is supported by the subcellular localization of FPA and FCA: A fully complementing FPA–yellow fluorescent protein (YFP) fusion protein localized to the nucleus (Fig. 3C and fig. S5); FCA is a nuclear protein that interacts with the SWI/SNF chromatin remodeler SWI3B (*14*, *24*). Both proteins associate with the chromatin of their target genes: The FPA-YFP fusion protein localized to the chromatin of *AtMu1* and *FLC* (Fig. 3D); FCA localized to *FLC* chromatin (*25*). Lastly, using an established assay for transcriptional activity (*26*), *FLC* and *AtMu1* unspliced (nascent) transcripts were up-regulated in all backgrounds that caused up-regulation of the spliced transcript, and both unspliced and spliced transcripts were increased similarly (Fig. 3, E and F). Together, these data all indicate that silencing does not occur posttranscriptionally but rather cotranscriptionally before any processing occurs.

scriptionally recognize aberrant RNA and mark it for silencing (fig. S6). A nascent RNA may be made aberrant by the presence of low levels of complementary siRNAs or misconducted processing events. FCA and FPA would then facilitate silencing by recruiting or stabilizing effector complexes. Although the common result of FCA and FPA action is silencing of a target locus, the identity of these effector complexes presumably varies with the contribution of different pathways at individual loci, thus leading to somewhat different silencing signatures. Whereas the majority of functionally characterized RRM-domain proteins act in posttranscriptional RNA processing (*27*), FCA and FPA appear to integrate the state of the nascent RNA with transcription. That this might be a novel function of some RRM-domain proteins is supported by two other reports. The yeast Set1 histone methyltransferase has an RRM domain thought to bind nascent RNA and thereby regulate the methyltransferase activity (*28*). Furthermore, three RRM-domain proteins are required for transcriptional silencing in *Caenorhabditis elegans* cosuppression (*26*).

Although the canonical siRNA-directed chromatin-silencing pathway has been described for repetitive loci, FCA and FPA silence mainly single-copy loci and do not affect silencing of the highly repetitive 5S loci (fig. S7). At a subset of targets, however, these pathways clearly interact. The canonical chromatin-silencing/siRNA amplification pathway involves amplification of siRNAs and shuttling of silencing information between the locus and a nucleolar RNA processing center (*29*, *30*), thereby silencing any sufficiently homologous locus in the genome. In contrast, FCA and FPA may bypass the siRNA amplification step, thereby restricting it to acting in cis. Unraveling the interactions between the different pathways will ultimately enable us to understand what properties in a target commit it to being silenced in a particular way.

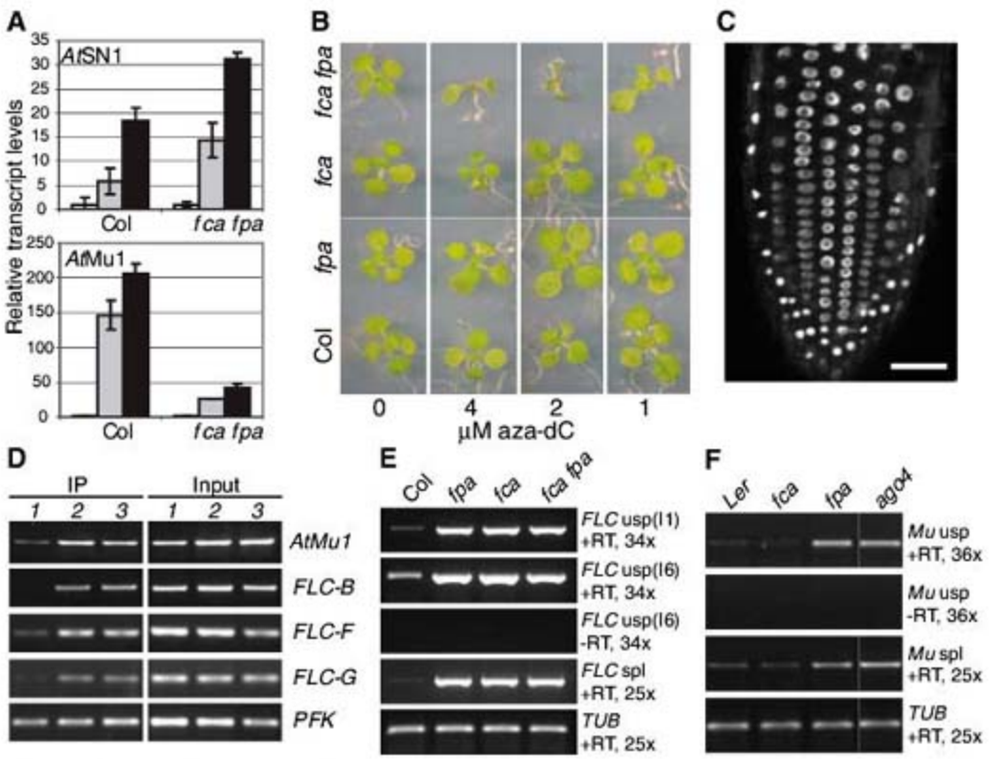

Fig. 3. (**A** and **B**) Aza-dC treatment. (A) Quantitative RT-PCR on Col and *fca-9 fpa-7* seedlings grown on aza-dC (white, mock; gray, 2 µM; black, 4 µM) normalized to the expression level after mock treatment (±SD). (B) Seedlings (Col, *fpa-7*, *fca-9*, and *fca-9 fpa-7*) grown for 14 days on aza-dC. (**C**) An FPA-YFP fusion protein localizes to the nucleus of transgenic *Arabidopsis* seedling roots. Scale bar, 50 µm. (**D**) Chromatin immunoprecipitation from two independent FPA-YFP lines. Lane 1, Col; lane 2, FPA-YFP line 2; lane 3, FPA-YFP line 5. (**E** and **F**) RT-PCR assaying spliced and unspliced transcripts of *FLC* and *AtMu1*.

Table 1. Percentage of aborted and undeveloped seed in *fca-11 fpa-8* mutant lines.

Parental genotype (female × male)	Healthy (%)	Aborted (%)	Undeveloped (%)	*n*
Col (SUC-PDS) selfed	100.0	0.0	0.0	206
fca-11 fpa-8 selfed	21.3	4.7	74.0	572
Col (SUC-PDS) × *fca-11 fpa-8*	82.7	0.0	17.3	572
fca-11 fpa-8 × Col (SUC-PDS)	30.9	0.0	69.1	375
fca-11 selfed	99.1	0.0	0.9	559
fpa-8 selfed	75.0	0.0	25.0	464
fca-11/*fca-11 FPA*/*fpa-8* × Col	63.9	1.6	34.4	244

References and Notes

1. M. Zaratiegui, D. V. Irvine, R. A. Martienssen, *Cell* **128**, 763 (2007).
2. M. A. Matzke, J. A. Birchler, *Nat. Rev. Genet.* **6**, 24 (2005).
3. D. Baulcombe, *Nature* **431**, 356 (2004).
4. R. A. Martienssen, M. Zaratiegui, D. B. Goto, *Trends Genet.* **21**, 450 (2005).
5. Z. Xie *et al.*, *PLoS Biol.* **2**, e104 (2004).
6. A. J. Herr, M. B. Jensen, T. Dalmay, D. C. Baulcombe, *Science* **308**, 118 (2005); published online 3 February 2005 (10.1126/science.1106910).
7. T. Kanno *et al.*, *Nat. Genet.* **37**, 761 (2005).
8. D. Zilberman, X. Cao, S. E. Jacobsen, *Science* **299**, 716 (2003); published online 9 January 2003 (10.1126/science.1079695).
9. Y. Onodera *et al.*, *Cell* **120**, 613 (2005).
10. L. M. Smith *et al.*, *Plant Cell* **19**, 1507 (2007).
11. S. D. Michaels, R. M. Amasino, *Plant Cell* **13**, 935 (2001).
12. F. M. Schomburg, D. A. Patton, D. W. Meinke, R. M. Amasino, *Plant Cell* **13**, 1427 (2001).
13. R. Macknight *et al.*, *Cell* **89**, 737 (1997).
14. V. Quesada, R. Macknight, C. Dean, G. G. Simpson, *EMBO J.* **22**, 3142 (2003).
15. I. Ausin, C. Alonso-Blanco, J. A. Jarillo, L. Ruiz-Garcia, J. M. Martinez-Zapater, *Nat. Genet.* **36**, 162 (2004).
16. Y. He, S. Michaels, R. Amasino, *Science* **302**, 1751 (2003); published online 30 October 2003 (10.1126/science.1091109).
17. B. Huettel *et al.*, *EMBO J.* **25**, 2828 (2006).
18. Z. Lippman, B. May, C. Yordan, T. Singer, R. Martienssen, *PLoS Biol.* **1**, E67 (2003).
19. O. Mittelsten Scheid, A. V. Probst, K. Afsar, J. Paszkowski, *Proc. Natl. Acad. Sci. U.S.A.* **99**, 13659 (2002).
20. Y. Qi *et al.*, *Nature* **443**, 1008 (2006).
21. P. Amedeo, Y. Habu, K. Afsar, O. Mittelsten Scheid, J. Paszkowski, *Nature* **405**, 203 (2000).
22. Y. Habu *et al.*, *EMBO Rep.* **7**, 1279 (2006).
23. High concentrations of aza-dC may cause DNA damage. Currently, we cannot rule out a hypersensitivity of *fca fpa* to DNA damage.
24. T. J. Sarnowski, S. Swiezewski, K. Pawlikowska, S. Kaczanowski, A. Jerzmanowski, *Nucleic Acids Res.* **30**, 3412 (2002).
25. F. Liu *et al.*, *Mol. Cell*, in press.
26. V. J. Robert, T. Sijen, J. van Wolfswinkel, R. H. Plasterk, *Genes Dev.* **19**, 782 (2005).
27. C. Maris, C. Dominguez, F. H. Allain, *FEBS J.* **272**, 2118 (2005).
28. A. Schlichter, B. R. Cairns, *EMBO J.* **24**, 1222 (2005).
29. O. Pontes *et al.*, *Cell* **126**, 79 (2006).
30. C. F. Li *et al.*, *Cell* **126**, 93 (2006).

31. We thank our colleagues for comments and advice, and F. Liu for seed. Supported by a UK Biotechnology and Biological Sciences Research Council grant to the John Innes Centre; UK Natural Environment Research Council grant NE/C507629/1 (C.D.); Gatsby Charitable Foundation and EU training network "Silencing in different organisms," EC contract HPRN-CT-2002-00257 (D.C.B.); and a European Molecular Biology Organization long-term postdoctoral fellowship (I.B.).

Supporting Online Material

www.sciencemag.org/cgi/content/full/318/5847/109/DC1
Materials and Methods
Figs. S1 to S7
Tables S1 to S5
References

15 June 2007; accepted 21 August 2007
10.1126/science.1146565

Methyl Salicylate Is a Critical Mobile Signal for Plant Systemic Acquired Resistance

Sang-Wook Park, Evans Kaimoyo, Dhirendra Kumar,* Stephen Mosher,† Daniel F. Klessig‡

In plants, the mobile signal for systemic acquired resistance (SAR), an organism-wide state of enhanced defense to subsequent infections, has been elusive. By stimulating immune responses in mosaic tobacco plants created by grafting different genetic backgrounds, we showed that the methyl salicylate (MeSA) esterase activity of salicylic acid–binding protein 2 (SABP2), which converts MeSA into salicylic acid (SA), is required for SAR signal perception in systemic tissue, the tissue that does not receive the primary (initial) infection. Moreover, in plants expressing mutant SABP2 with unregulated MeSA esterase activity in SAR signal–generating, primary infected leaves, SAR was compromised and the associated increase in MeSA levels was suppressed in primary infected leaves, their phloem exudates, and systemic leaves. SAR was also blocked when SA methyl transferase (which converts SA to MeSA) was silenced in primary infected leaves, and MeSA treatment of lower leaves induced SAR in upper untreated leaves. Therefore, we conclude that MeSA is a SAR signal in tobacco.

Plants respond to pathogen attack by activating both local and systemic defenses that restrict pathogen growth and spread. In the infected leaf, these defenses often involve a hypersensitive response in which necrotic lesions form at the infection site(s) (*1*); the uninoculated tissues subsequently develop systemic acquired resistance (SAR), a state of heightened defense throughout the plant. SAR is similar to acquired immunity in animals in that it is systemic and long-lasting; it also resembles innate immunity, as it provides broad-spectrum resistance to secondary infection (*1*, *2*).

SAR requires movement through the phloem of a signal from the infected tissue to the systemic tissue (leaves above the primary infected leaves) (*3*). Initially, salicylic acid (SA) was postulated to be this mobile signal because it induces defense responses when applied to plants, moves systemically, is found in phloem exudates of infected leaves, and is required in systemic tissue for SAR (*1*, *2*). However, grafting studies showed that infected, SA-deficient rootstocks could trigger SAR in wild-type scions; such results imply that SA is not a mobile SAR signal (*4*, *5*).

To clarify the role of SA in defense signaling, we identified putative SA-effector proteins in tobacco (*6*–*9*). One of these, SA-binding protein 2 (SABP2), is integral to plant innate immunity, as silencing of *SABP2* suppresses both local resistance to tobacco mosaic virus (TMV) and SAR development (*9*). SABP2 is an esterase in the α/β-fold hydrolase superfamily, with strong preference for methyl salicylate (MeSA). It binds SA with high affinity (dissociation constant K_d = 90 nM), resulting in inhibition of MeSA esterase activity (*10*). This suggests that SABP2 functions by converting biologically inactive MeSA (*11*) [which is synthesized from SA by an SA methyl transferase (SAMT) (*12*)] to active SA; feedback inhibition by SA may modulate this process.

To determine whether SABP2 is involved in generating and transmitting the SAR signal in leaves receiving the primary infection and/or perceiving and responding to it in systemic tissue, we performed grafting studies with wild-type (empty vector control) or *SABP2*-silenced rootstocks and scions (*13*) (Fig. 1A). These experiments are informative only if the signal for gene silencing in *SABP2*-silenced tissue is not graft-transmissible to wild-type tissue; this is demonstrated in Fig. 1B. After TMV inoculation, SAR was observed in wild-type scions grafted onto *SABP2*-silenced or wild-type rootstocks. SAR is manifested as a reduction in the size of lesions formed after secondary TMV infection of systemic leaves (scion leaves of grafted plants) on plants that have received a primary infection (on rootstock leaves of grafted plants), relative to the size of lesions developed by plants that previously received a mock inoculation as the primary infection (Fig. 1, C and D). The reduction in lesion size occurs because SAR elicited by the primary infection enables the plant to restrict viral replication and spread more efficiently the second time it encounters the virus. Conversely, plants containing *SABP2*-silenced scions grafted onto wild-type or *SABP2*-silenced rootstocks failed to develop SAR after TMV infection of the rootstock, as evidenced by large secondary lesions formed regardless of whether the rootstock received a primary TMV infection (Fig. 1, C and D). Suppression of SAR in *SABP2*-silenced scions was accompanied by increased viral replication in systemic tissue (Fig. 1D, lower panel) and reduced expression of the *pathogenesis-related 1* gene, which is associated with SAR development (Fig. 1E). These results indicate that SABP2 is required for SAR in

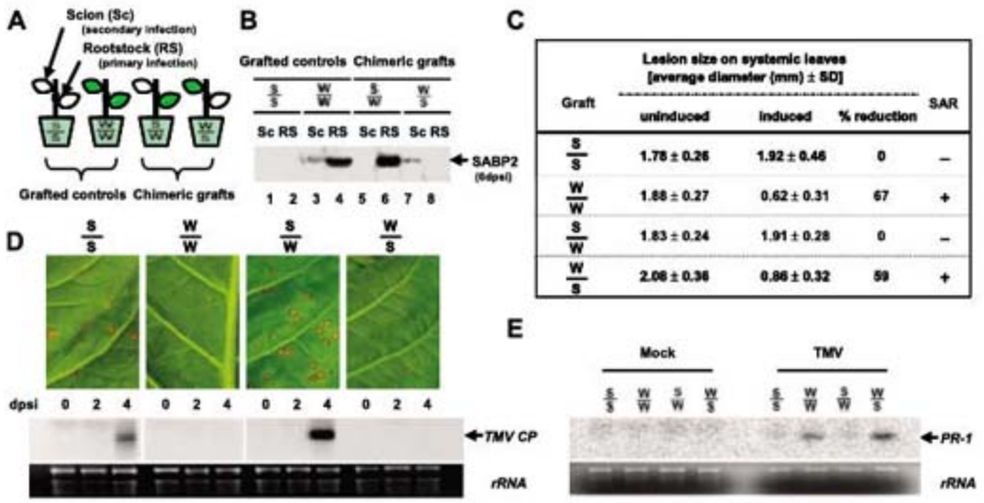

Fig. 1. SABP2 is required for SAR in systemic but not primary infected tobacco leaves. **(A)** Schematic of grafting experiments using wild-type [W; control line C3# expressing an empty vector in *Nicotiana tabacum* cv. Xanthi nc (NN) (*9*)] and *SABP2*-silenced [S; line 1-2# (*9*)] rootstocks (RS) and scions (Sc). **(B)** Immunoblot analysis of SABP2 accumulation in rootstocks and scions of grafted plants (*13*). Nine-week-old plants received a secondary inoculation with TMV at 7 days post primary infection (dppi); SABP2 accumulation was determined at 6 days post secondary infection (dpsi). Note that SABP2 levels are weaker in secondary infected systemic scions at 6 dpsi than in primary infected rootstocks at 13 dppi in controls as well as chimeric grafts. **(C)** Determination of lesion size on scions whose rootstocks received either a mock (uninduced) or TMV (induced) inoculation 7 days before a secondary infection with TMV; lesion sizes were determined at 6 dpsi. **(D)** Upper panel: TMV-induced lesions on scion leaves of the above-described plants at 6 dpsi. Lower panel: RNA blot analysis of TMV *coat protein* (*CP*) transcripts in scion leaves at various times after secondary infection. **(E)** RNA blot of *pathogenesis-related-1* (*PR-1*) expression at 7 dppi (before secondary infection) in grafted scion leaves. Ribosomal RNA (rRNA) is shown as a loading control in (D) and (E).

Boyce Thompson Institute for Plant Research, Tower Road, Ithaca, NY 14853, USA.

*Present address: Department of Biological Sciences, East Tennessee State University, Johnson City, TN 37614, USA. †Present address: Department of Cell and Systems Biology, University of Toronto, Toronto, Ontario M5S 3B2, Canada. ‡To whom correspondence should be addressed. E-mail: dfk8@cornell.edu

systemic tissue, but not for production of a SAR signal in primary infected tissue.

Mutant SABP2 proteins were constructed on the basis of SABP2's three-dimensional structure and produced in *Escherichia coli*; the recombinant proteins were assayed for MeSA esterase activity, SA-binding activity, and SA-feedback inhibition in vitro (table S1). Three mutants were then tested for complementation of SAR in *SABP2*-silenced tobacco: $Ala^{13} \rightarrow$ Leu (A13L), which lacks SA-binding activity and SA-feedback inhibition; $Ser^{81} \rightarrow$ Ala (S81A), which lacks MeSA esterase activity; and $His^{238} \rightarrow$ Ala (H238A), which lacks SA-binding and MeSA esterase activities (Fig. 2A). To prevent RNA interference–mediated silencing of the wild-type or mutant *SABP2* transgenes, we introduced the above mutations into synthetic versions of *SABP2*, *syn1* [formerly *syn* (*14*)] and *syn2*, which share 77% and 60% identity with the native *SABP2* gene, respectively, and are controlled by the estradiol-inducible XVE system (*15*). *syn1* is effectively expressed in *SABP2*-silenced tobacco and restores SAR (*14*). Estradiol treatment of systemic leaves of *SABP2*-silenced plants stably transformed with a *syn* transgene resulted in local synthesis of wild-type or mutant syn SABP2; expression of wild-type *syn1* or *syn2* led to a ~55 to 65% reduction in secondary lesion size, demonstrating that SAR was restored (Fig. 2, B to D). Induction of the A13L mutant in systemic leaves also restored SAR, whereas induction of S81A or H238A did not (these plants had similarly sized primary and secondary lesions and high levels of TMV *coat protein* transcripts in secondary inoculated systemic leaves; Fig. 2, C and D). Thus, SAR requires SABP2's esterase activity, but not its SA-binding activity and SA-feedback inhibition, in systemic leaves.

Although SABP2 is not required in primary infected tissue to generate a mobile SAR signal (Fig. 1 and Fig. 3, A to C), grafted plants containing a wild-type scion and an *SABP2*-silenced rootstock expressing the A13L mutant were SAR-deficient (Fig. 3, A to C). Because the MeSA esterase activity of A13L is not inhibited by SA, whereas that of wild-type SABP2 is, this finding suggests that in wild-type plants, SA-mediated inhibition of SABP2 in the primary infected leaves is critical to allow sufficient MeSA accumulation for SAR induction (Fig. 3D).

Our data argue that MeSA is a mobile SAR signal because SAR requires (i) SABP2's MeSA esterase activity in systemic tissue and (ii) SA-mediated inhibition of this activity in primary infected leaves. This conclusion is supported by gas chromatography–mass spectrometry analyses, which revealed increased MeSA levels in primary infected and, subsequently, systemic leaves of wild-type plants [peaking at 48 and 72 hours post primary infection (hppi), respectively] but not in *SABP2*-silenced plants expressing the A13L mutant in primary infected leaves (Fig. 3D). MeSA levels also increased in phloem (petiole) exudates of primary infected leaves from wild-type plants, peaking at 48 hppi, whereas little increase occurred in plants expressing the A13L mutant (Fig. 3E). In addition, biologically active SA, with or without its biologically inactive conjugated glucoside (SAG), rose in systemic leaves of wild-type plants, whereas little to no rise occurred in SAR-deficient *SABP2*-silenced plants expressing the A13L mutant in primary infected leaves or in *SABP2*-silenced plants (Fig. 3, F and G). Note that the similarity of SA (or SA plus SAG) levels in primary infected leaves of wild-type and *SABP2*-silenced plants expressing A13L (Fig. 3, F and G) was expected because the MeSA level is only 10 to 20% of the SA plus SAG level (Fig. 3, D, F, and G) (*11*); thus, A13L-mediated conversion of most or all of the MeSA to SA would increase SA levels only slightly. Accumulation of SA (or SA plus SAG) in primary leaves of *SABP2*-silenced plants was reduced relative to that in wild-type plants at early times but eventually reached wild-type levels.

In a complementary approach, MeSA levels were reduced by suppressing MeSA biosynthesis via silencing of *NtSAMT1* (fig. S1). Grafting experiments indicate that NtSAMT1 is required in the SAR-signal generating, TMV-infected rootstock, but not in the systemic tissue (i.e., scion) (Fig. 4, A and B). Moreover, treating the lower leaves of wild-type tobacco plants with MeSA induced SAR in the upper, untreated leaves. This required SABP2 in the untreated, but not treated, leaves (Fig. 4, C to E).

SA-deficient rootstocks expressing salicylate hydroxylase (SH) can generate a SAR signal (*4*); therefore, MeSA can act as a mobile signal only if it is not metabolized by SH. Analysis of recombinant SH revealed no activity against MeSA (fig. S2). Moreover, plants expressing SH accumulated MeSA to nearly wild-type levels in primary infected leaves and in systemic leaves, although peak accumulation was delayed ~24 hours (Fig. 3, D and E). MeSA levels in phloem exudates of SH-expressing plants were intermediate between those in wild-type and A13L plants. Because MeSA is synthesized from SA, SA-deficient plants expressing SH might be expected to have very depressed MeSA levels. The similar level of MeSA in SH transgenic and wild-type plants suggests that the kinetic properties of NtSAMT1 and SH are very different, with NtSAMT1 having higher affinity for SA (lower Michaelis-Menten constant K_m) and/or faster kinetics (higher catalytic rate constant k_{cat}) than SH. Alternatively, NtSAMT1 and SH may be in different subcellular locations, with NtSAMT1 having greater (or earlier) access than SH to newly synthesized SA.

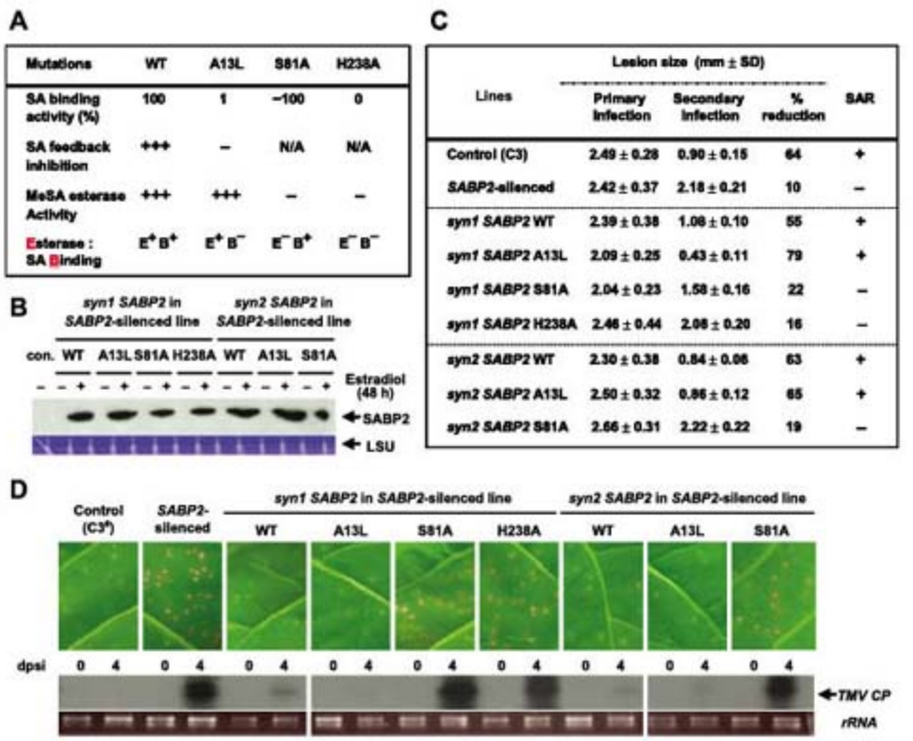

Fig. 2. SABP2's MeSA esterase activity, but not its SA-binding and feedback inhibition activities, is required for SAR in systemic leaves. (**A**) Biochemical characteristics of mutant SABP2 proteins. N/A, not applicable. (**B**) Immunoblot analysis of wild-type or mutant syn SABP2 protein accumulation in 8-week-old stably transformed *SABP2*-silenced tobacco at 0 (–) and 48 hours (+) after treatment with 30 μM estradiol. Expression of endogenous SABP2 was used as a control (con.). The large subunit (LSU) of ribulose bisphosphate carboxylase/oxygenase is shown as a loading control. (**C**) Average lesion size was determined at 5 days post infection (dpi). (**D**) Upper panel: TMV-induced lesions on systemic leaves of plants described in (C) at 5 dpsi. Lower panel: RNA blot analysis of TMV *CP* transcripts in systemic leaves of these plants at 0 and 4 dpsi. For (C) and (D), the transgenes were induced only in systemic leaves (*13*).

The following findings argue that MeSA is a phloem-mobile SAR signal and that SAPB2 is its receptor in systemic tissue: (i) SAR requires SABP2's MeSA esterase activity in the systemic tissue to convert biologically inactive MeSA to active SA (Figs. 1 and 2). (ii) After infection, SA levels rise in the systemic leaves of wild-type plants, whereas little or no rise occurs in SAR-defective, *SABP2*-silenced plants (Fig. 3, F and G). (iii) SAR requires SA-mediated inhibition of this esterase activity in the primary infected leaves (Fig. 3, A and C). (iv) MeSA levels increase after infection in primary infected leaves, and subsequently in phloem exudates of primary infected leaves and in systemic leaves of wild-type plants (Fig. 3, D and E). (v) Reducing MeSA levels in primary infected leaves by expressing the A13L mutant SABP2 with uncontrolled MeSA esterase activity leads to little or no MeSA increase in phloem exudates (Fig. 3E), little or no increase in MeSA and SA in systemic leaves (Fig. 3, D, F, and G), and loss of SAR development (Fig. 3, A to C). (vi) Reducing MeSA levels in primary infected leaves by silencing *NtSAMT1* also results in SAR deficiency (Fig. 4, A and B). (vii) Treating the lower leaves of wild-type tobacco plants with MeSA induces SAR in the upper, untreated leaves. This requires SABP2 in the untreated, but not treated, leaves (Fig. 4, C to E).

MeSA also may be an airborne signal that induces resistance in neighboring plants (*16*). Analyses of the *Arabidopsis dir1-1* and *sfd1* mutants have suggested that the mobile SAR signal is a lipid or lipid derivative (*17*, *18*). Consistent with this possibility, recent studies by Truman *et al.* (*19*) suggest that this lipid-derived signal may be jasmonic acid. It is interesting to note that functional SA analogs induce SAR in both *dir1-1* and *sfd1* mutants (*17*, *18*). Together these studies suggest that a lipid-derived SAR signal works with (or upstream of) MeSA to activate SAR. Thus, there may be two translocated signals that induce SAR: a lipid-derived molecule (perhaps jasmonic acid) and MeSA.

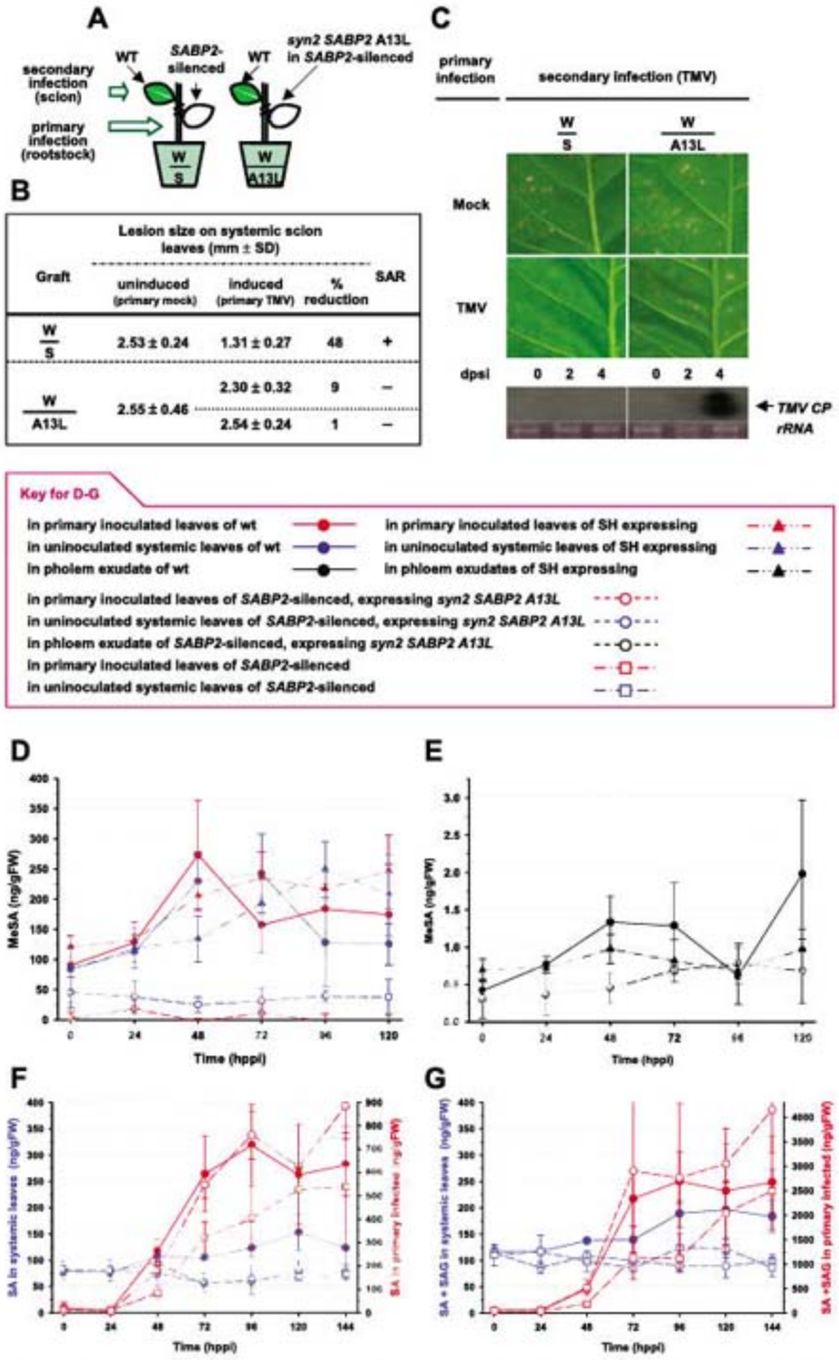

Fig. 3. SAR is compromised by expression of the SABP2 A13L mutant in primary inoculated leaves, and MeSA, SA, and SAG accumulation kinetics after TMV inoculation. **(A)** Schematic of grafting studies using wild-type scions (W, empty vector control) and *SABP2*-silenced (S) rootstocks or *SABP2*-silenced rootstocks expressing the *syn2 SABP2 A13L* transgene (A13L). **(B)** Average lesion size on scion leaves at 5 dpsi. SABP2 A13L synthesis was induced in the rootstocks by estradiol treatment 24 hours before primary inoculation. **(C)** Upper panel: TMV-induced lesions on scion leaves of plants described in (B) at 5 dpsi. Lower panel: analysis of TMV *CP* transcripts in scions at 0, 2, and 4 dpsi. **(D)** MeSA levels in primary inoculated leaves (red) and uninoculated systemic leaves (blue). **(E)** MeSA levels in phloem (petiole) exudates from primary inoculated leaves. **(F** and **G)** SA levels (F) and SA plus SAG levels (G) in primary inoculated leaves (red) and uninoculated systemic leaves (blue). For (D) to (G), the *SABP2 A13L* transgene was induced only in the primary inoculated leaves with estradiol at 24 hours before inoculation. Colors denote measurements in primary leaves (red), secondary leaves (blue), or phloem (black). Solid circles, wild-type plants; open circles, *SABP2*-silenced plants expressing *syn2 SABP2 A13L*; triangles, SA-deficient plants expressing salicylate hydroxylase (SH); squares, *SABP2*-silenced plants.

References and Notes

1. D. Dempsey, J. Shah, D. F. Klessig, *Crit. Rev. Plant Sci.* **18**, 547 (1999).
2. W. E. Durrant, X. Dong, *Annu. Rev. Phytopathol.* **42**, 185 (2004).
3. A. E. Jenns, J. Kuć, *Phytopathology* **69**, 753 (1979).
4. B. Vernooij *et al.*, *Plant Cell* **6**, 959 (1994).
5. J. A. Pallas, N. L. Paiva, C. Lamb, R. A. Dixon, *Plant J.* **10**, 281 (1996).
6. Z. Chen, H. Silva, D. F. Klessig, *Science* **262**, 1883 (1993).
7. D. H. Slaymaker *et al.*, *Proc. Natl. Acad. Sci. U.S.A.* **99**, 11640 (2002).
8. H. Du, D. F. Klessig, *Plant Physiol.* **113**, 1319 (1997).
9. D. Kumar, D. F. Klessig, *Proc. Natl. Acad. Sci. U.S.A.* **100**, 16101 (2003).
10. F. Forouhar *et al.*, *Proc. Natl. Acad. Sci. U.S.A.* **102**, 1773 (2005).
11. M. Seskar, V. Shulaev, I. Raskin, *Plant Physiol.* **116**, 387 (1998).
12. N. Dudareva, R. A. Raguso, J. Wang, J. R. Ross, E. Pichersky, *Plant Physiol.* **116**, 599 (1998).
13. See supporting material on *Science* Online.
14. D. Kumar, C. Gustafsson, D. F. Klessig, *Plant J.* **45**, 863 (2006).
15. J. Zuo, Q.-W. Niu, N.-H. Chua, *Plant J.* **24**, 265 (2000).
16. V. Shulaev, P. Silverman, I. Raskin, *Nature* **385**, 718 (1997).
17. A. M. Maldonado, P. Doerner, R. A. Dixon, C. J. Lamb, R. K. Cameron, *Nature* **419**, 399 (2002).
18. A. Nandi, R. Welti, J. Shah, *Plant Cell* **16**, 465 (2004).
19. W. Truman, M. H. Bennett, I. Kubigsteltig, C. Turnbull, M. Grant, *Proc. Natl. Acad. Sci. U.S.A.* **104**, 1075 (2007).

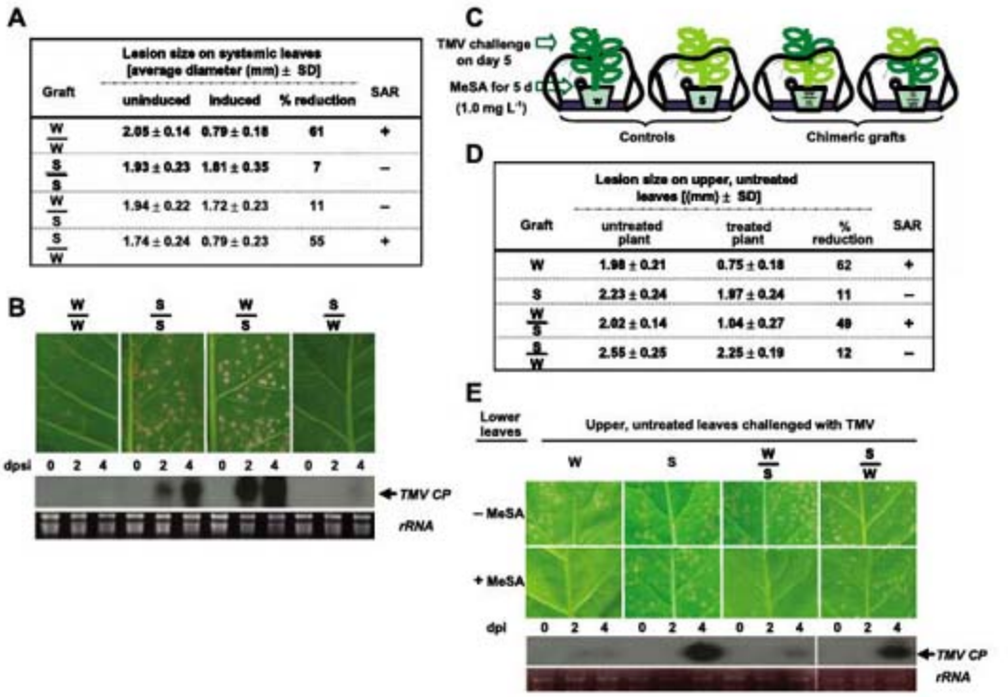

Fig. 4. *NtSAMT1*-silenced tobacco plants are SAR-deficient, and MeSA induces SAR in untreated tissue. (**A**) Determination of lesion size on scions whose rootstocks received either a mock (uninduced) or TMV (induced) inoculation 6 days before a secondary infection with TMV (W, empty vector control; S, *NtSAMT1*-silenced line). (**B**) Upper panel: TMV-induced lesions on scion leaves of the above-described plants at 5 dpsi. Lower panel: RNA blot analysis of TMV *CP* transcripts in scion leaves of these plants at 0, 2, and 4 dpsi. See Fig. 1 legend for details. (**C**) Schematic for MeSA treatment of wild-type (W, empty vector control) and *SABP2*-silenced (S) tobacco. The lower parts of plants (8 weeks old) were treated for 5 days in gas-tight sealed plastic film chambers containing air with or without supplementation with MeSA. After this incubation, the upper, untreated leaves were inoculated with TMV. (**D**) Lesion size on upper, untreated leaves of plants described in (C) at 5 dpi; untreated plants were exposed only to air, whereas treated plants received air supplemented once at the start of the experiment with MeSA (1.0 mg/liter) on the lower leaves. (**E**) Upper panel: TMV-induced lesions on the untreated leaves of plants described in (C) at 5 dpi. Lower panel: RNA blot analysis of TMV *CP* transcripts in untreated leaves at 0, 2, and 4 dpi.

20. We thank L. Tong for advice regarding SABP2 mutational analysis, A. Kessler for advice on GC/MS analyses, N.-H. Chua for estradiol-inducible pER8 vector, DNA2.0 Inc. for synthesizing *syn2 SABP2*, J. Ryals for the transgenic NahG-10 tobacco line encoding a salicylate hydroxylase (*4*), and D. Dempsey for critical comment on the manuscript. Supported by NSF grants IOB-0525360 and DBI-0500550 (D.F.K.).

Supporting Online Material

www.sciencemag.org/cgi/content/full/318/5847/113/DC1
Materials and Methods
Figs. S1 and S2
Table S1
References

27 June 2007; accepted 29 August 2007
10.1126/science.1147113

In Situ Imaging of the Endogenous CD8 T Cell Response to Infection

Kamal M. Khanna, Jeffery T. McNamara, Leo Lefrançois*

Mounting a protective immune response is critically dependent on the orchestrated movement of cells within lymphoid organs. We report here the visualization, using major histocompatability complex class I tetramers, of the CD8-positive (CD8) T cell response in the spleens of mice to *Listeria monocytogenes* infection. A multistage pathway was revealed that included initial activation at the borders of the B and T cell zones followed by cluster formation with antigen-presenting cells leading to CD8 T cell exit to the red pulp via bridging channels. Strikingly, many memory CD8 T cells localized to the B cell zones and, when challenged, underwent rapid migration to the T cell zones where proliferation occurred, followed by egress via bridging channels in parallel with the primary response. Thus, the ability to track endogenous immune responses has uncovered both distinct and overlapping mechanisms and anatomical locations driving primary and secondary immune responses.

An effective immune response depends on the large-scale, but carefully regulated, movement of cells within and between lymphoid and peripheral tissues. In recent years, our understanding of events in secondary lymphoid tissues has been advanced by the use of multiphoton microscopy to visualize lymphocyte movement (*1*–*4*). Nevertheless, much remains to be elucidated about the microanatomy of antigen-specific primary and memory CD8 T cell responses, with relatively limited data currently available from in situ visualization of endogenous CD8 T cell responses (*5*–*7*). Indeed, because of technical difficulties with intravital imaging of the spleen, intravital microscopic analysis of immune responses has been limited to the lymph node and has only elucidated the properties of clonal, single-avidity T cell receptor (TCR) transgenic T cells after transfer of large numbers of cells. Because it is known that increasing naïve T cell precursor frequency affects immune responses (*8*) and that each TCR transgenic T cell exhibits distinct physiological characteristics (*9*), these data should be interpreted with these caveats in mind. Thus, determining the anatomical location and migration of endogenous antigen-specific T cells in lymphoid tissues during primary and secondary immune responses remains an important goal.

To achieve this objective, we used staining with major histocompatability complex (MHC) class I tetramers, which allows in situ identification and localization of clonally diverse endogenous antigen-specific CD8 T cells (*7*). This approach avoids the complications associated with adoptive transfer of TCR transgenic T cells and challenge with model antigens. With this technique, we systematically examined the CD8 T cell response to primary and secondary infection with *Listeria monocytogenes* (LM), which is primarily induced in the spleen (*10*). C57BL/6 mice were infected intravenously with 1×10^6 colony-forming units (CFU) of an attenuated *actA*-deficient strain of LM that had been engineered to express the exogenous antigen ovalbumin

Department of Immunology, University of Connecticut, Farmington, CT 06030, U.S.A.

*To whom correspondence should be addressed. E-mail: Llefranc@neuron.uchc.edu

(LM-OVA) (*11*–*13*). This allowed generation of a robust ova-specific CD8 T cell response that can be readily followed by using tetramers. At days 3, 4, and 5 post infection (PI), the spleen from each mouse was cut in two equal halves with one half used for imaging studies and the other for flow cytometric comparison. Tetramer-positive (tet^+) CD8 T cells that displayed characteristics of activation were detected by 3 days (Fig. 1A), with tet^+ cells expanding almost 14-fold from day 3 to day 5 (Fig. 1A). Phenotypic analysis revealed up-regulation of the activation markers CD11a and PD1 by day 3 (Fig. 1A), while CD69 expression was elevated on a portion of tet^+ cells at day 3 PI, but was lost by day 4 (Fig. 1A). CD127 down-regulation on tet^+ cells was a late event, occurring at day 4 PI after the down-regulation of CD62L (Fig. 1A).

Having framed the overall kinetics of the early CD8 T cell response, we undertook imaging of the splenic response in situ. Splenic architecture is organized into two distinct compartments: white pulp (WP) and red pulp (RP) (Fig. 1B) (*14*). The WP includes the B cell follicles and a T cell area, the periarteriolar lymphoid sheath (PALS). The RP is a blood-filled space between each WP lymphoid follicle and the next; it contains a complex venous system, reticular fibroblasts, macrophages, and some lymphocytes. The marginal zone (MZ) separates the WP from the RP, surrounds the B cell follicles and is populated with B cells expressing high levels of surface immunoglobulin IgM, dendritic cells (DCs), and macrophages (*14*). Tet^+ CD8 T cells were essentially undetectable in the spleen of uninfected mice (Fig. 1B). However, at 3 days PI, but not earlier, small numbers of tet^+ CD8 T cells could be readily detected (Fig. 1C) as clusters, primarily at the border of the T cell–B cell zones of the splenic WP and in the MZ (Fig. 1C and inset). These tet^+ cells were also in close contact with $CD11c^+$ DC (Fig. 1D), with many exhibiting apparent polarization of TCR and CD8 co-receptors toward the contact areas with DC, consistent with an immunological synapse (Fig. 1, D and E; see movie S1). Some tet^+ cells were also detected in the RP, MZ (white arrows) or the B cell areas [yellow arrow in (fig. S1A)]. Four days PI (24 hours later), a substantial increase in tet^+ CD8 T cells was noted, with a majority (>80%) now located in the PALS (Fig. 2A and fig. S2). Tet^+ CD8 T cells were localized in only a small number of lymphoid follicles; other follicles appeared devoid of proliferating tet^+ CD8 T cells (fig. S3), which suggested that CD8 T cell activation and proliferation occurred in a limited number of foci.

By 5 days PI, tet^+ CD8 T cells continued to proliferate (Fig. 1A) and were located along the border of the T cell and B cell zones (>40%) or in the MZ (>50%) in discrete clusters (Fig. 2, B and C, and fig. S2). $CD11c^+$ DCs were concentrated within these clusters (Fig. 2C) and, in many cases, formed apparent synapses with tet+ CD8 T cells [(Fig. 2C, bottom), arrowheads in magnifications of boxed region above, and (fig. S4)]. Because antigen presentation occurs for ~10 days after infection (fig. S5), we tested whether the clustering and TCR reorganization of CD8 T cells relatively late in the response was antigen-dependent. To do so, we used the 25D-1.16 monoclonal antibody (mAb) (*15*) that recognizes SIINFEKL bound to $H\text{-}2K^b$ to block antigen recognition. mAb treatment on days 0 or 3 PI blocked cluster formation (fig. S6A) and expansion to some extent (fig. S6C). Although some tet^+ CD8 T cell clusters were present in the spleens of mice treated with mAb at 4 days PI, TCR or CD8 co-receptor polarization was not evident [(fig. S6B), arrowheads, left versus right]. These data demonstrated that secondary antigen-dependent interactions occurred between CD8 T cells and DCs.

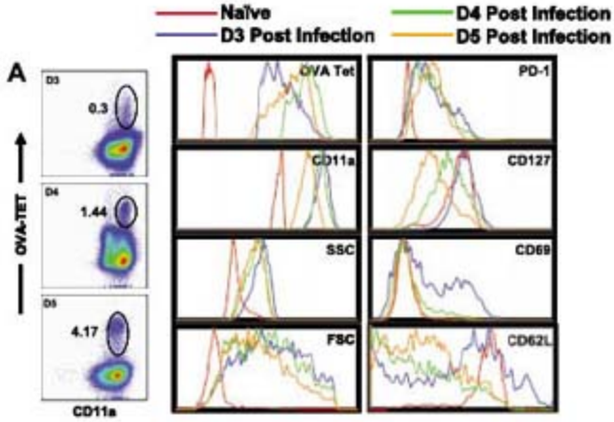

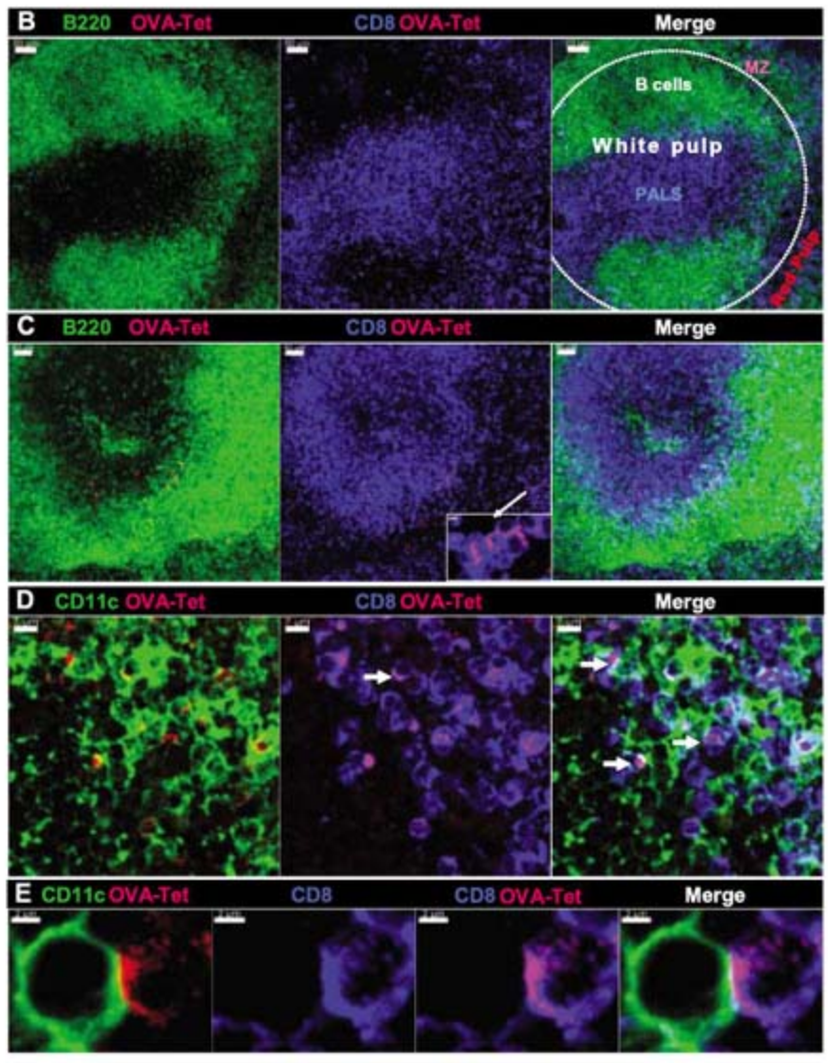

Fig. 1. Time course of the early splenic response to LM infection and imaging of early events in situ. (**A**) Flow cytometric and microscopic analysis of mouse spleen at 3, 4, and 5 days PI. Dot plots represent gated CD8 T cells and histograms, gated tet^+ $CD8^+$ cells. The values represent tet^+ cells as a percentage of CD8 T cells. Gated $CD8^+CD11a^{lo}CD62L^{hi}$ represent naive cells. (**B** to **E**) Thick sections were stained with K^b-OVA tetramer and the indicated mAb, and multiple sections from each spleen were analyzed by confocal microscopy. B220, a CD45 isoform preferentially expressed by B cells. (B) Uninfected spleen with regions marked. MZ, marginal zone. The image was acquired by using a 20× 0.75 numerical aperture (NA) objective; a 24-μm merged z-stack is shown. (C) Splenic tissue 3 days PI. Note small clusters of tet^+ CD8 T cells. (Magnified cluster of tet^+ CD8 T cells in the MZ shown in inset.) A 20-μm merged z-stack is shown. (D) Cluster of tet^+ CD8 T cells interacting with $CD11c^+$ DC 3 days PI. Image acquired by using a 40× 1.2 NA water objective; a 12-μm merged z-stack is shown. [Gallery of individual z-sections shown in (fig. S1B).] (E) Magnified view of a tet^+ CD8 T cell in contact with a $CD11c^+$ DC. Image acquired by using a 40× 1.2 NA water objective (also see movie S1). The data are representative of three different experiments with two or three mice each.

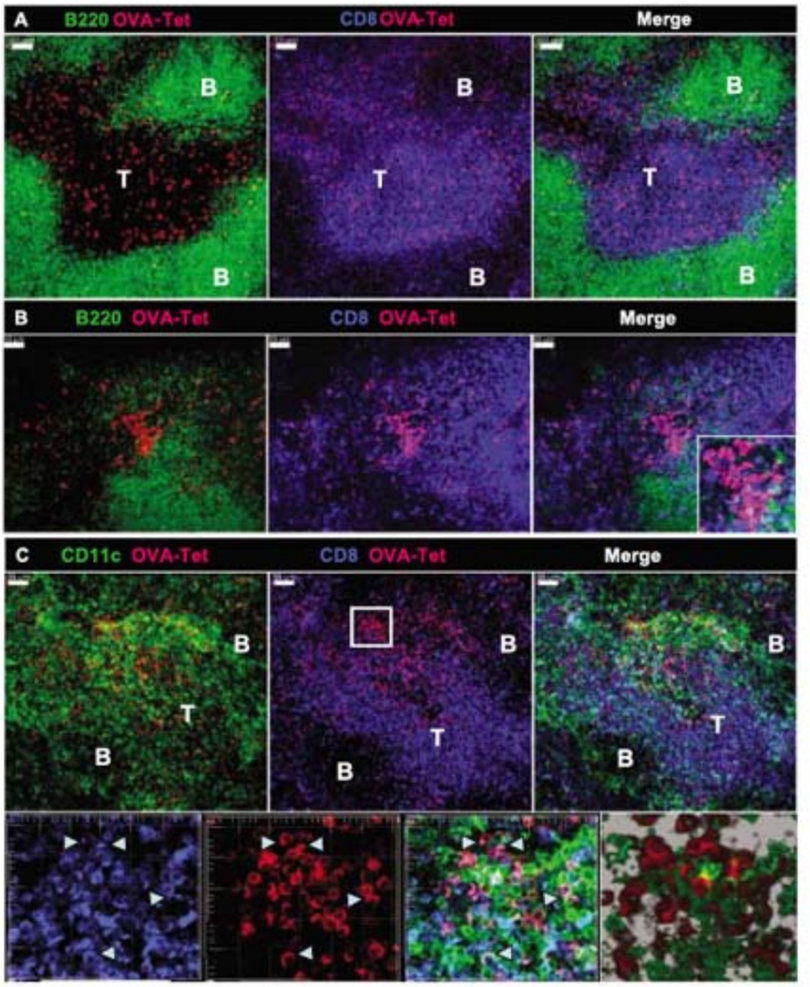

Fig. 2. Localization of antigen-specific CD8 T cells 4 and 5 days PI. (**A**) CD8 T cells localize to the PALS 4 days PI. (**B** and **C**) Clusters of antigen-specific CD8 T cells localize along the border of the T and B cell zones 5 days PI in multiple thick sections from each spleen. (B) Cluster of tet$^+$ CD8 T cells on the T cell–B cell zone border. (C) Tet$^+$ CD8 T cells cluster with CD11c$^+$ DC. (Top) A 32-μm merged z-stack. (Bottom) Three-dimensional (3D) reconstruction of a 24-μm z-stack represents the magnified view of the boxed region in the top middle. Arrowheads indicate TCR and CD8 co-receptor polarization toward the adjacent CD11c$^+$ DCs. (Bottom, far right) A rendered 3D-reconstruction. T, T cell zone; B, B cell zone. All images acquired by using a 20× 0.75 NA objective. The data are representative of five different experiments with two or three mice each.

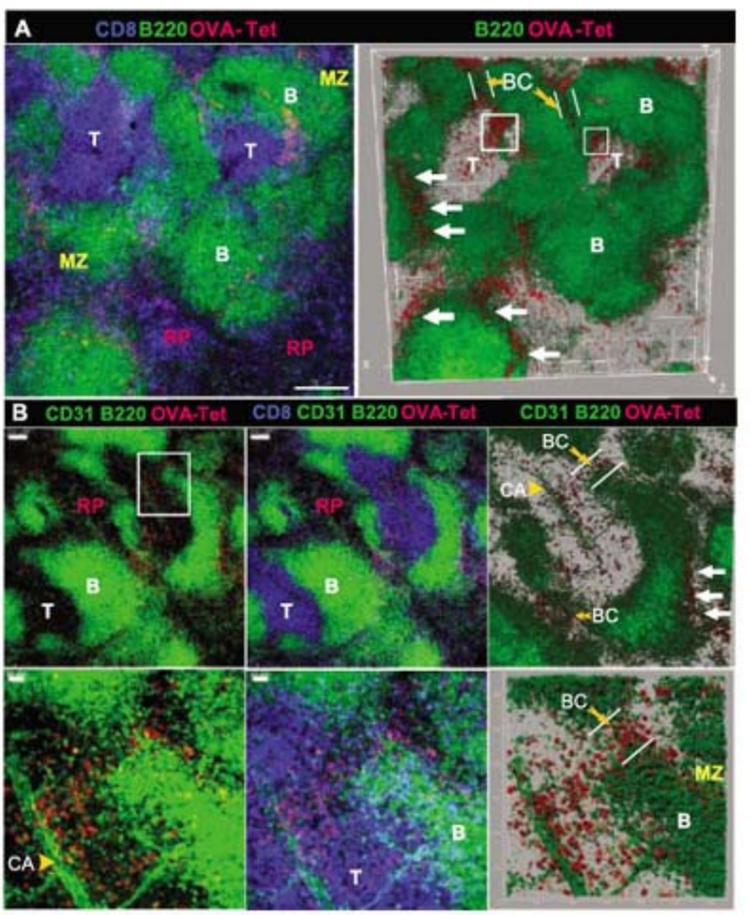

Fig. 3. Antigen-specific CD8 T cells exit the white pulp via bridging channels. Multiple thick sections from each spleen, 5 days PI, were stained with K^b-OVA tetramer and the indicated mAb. (**A**) Low-power view of spleen. Rendered 3D reconstruction (right) of the 110-μm merged z-stack (left) of a spleen fragment shows multiple clusters of tet$^+$ CD8 T cells along the border of the B–T cell zones and the MZ. (**B**) Spleen section stained (CD31-specific, green) for blood vessels (arrows) to identify the central arteriole (CA) and associated branches (see also fig. S6). The image shows two bridging channels (BC, yellow arrows) through which tet$^+$ CD8 cells exit the PALS into the MZ (top). (Bottom) Magnified views of the BC boxed top left. (Top and bottom, far right) Rendered 3D reconstructions are shown. (Top) Images acquired by using a 10× 0.45 NA water objective and (bottom) by using a 40× 1.2 NA water objective; both are 30-μm merged z-stacks. MZ, marginal zone; RP, red pulp. Also see fig. S6 and movie S3. The data are representative of five different experiments with two or three mice each.

The route that antigen-specific CD8 T cells follow to exit the WP is not known (*14*, *16*) but examination of the location of tet$^+$ CD8 T cells at days 5 and 6 PI clearly revealed this pathway (Fig. 3 and figs. S7 and S8, and movie S2). At 5 days PI, clusters as well as individual tet$^+$ cells were located in regions originally described as bridging channels (*16*, *17*) that apparently connect the PALS to the MZ/RP (Fig. 3, A and B) and are often associated with the central arteriole and its branches (fig. S7 and movie S2). tet$^+$ CD8 T cells egressed the PALS via the bridging channels and followed a relatively uniform path in the MZ (Fig. 3, A and B, right, and Fig. 3B, white arrows, magnified lower panels). By 6 days PI, most of the tet$^+$ population (>80%) had exited the PALS and was localized in the RP and/or the MZ (fig. S8, A and B), and by 7 days PI, nearly all (>90%) of the cells were located in the RP. Although a more detailed analysis is required, the CD8 T cell response to VSV infection was characterized by similar anatomical events, though at a more rapid pace (fig. S9, A, B, and C). Thus, although the kinetics of the CD8 response may be distinct between different infections, responding splenic CD8 T cells appear to follow a prescribed pathway driving immune response initiation, expansion, and exit.

Knowing the anatomy of the primary response to LM infection, we set out to define the location of resting and reactivated memory cells derived from that response. Image analysis 30 days after infection revealed that over 60% of tet$^+$ memory CD8 cells were embedded in the B cell follicles (Fig. 4A and figs. S2 and S10, and movie S3). In addition, memory cells were also present in the MZ and RP (~30%; fig. S2), as previously suggested by adoptive transfer studies (*18*, *19*). Intranasal influenza virus infection also resulted in the appearance of flu-specific memory cells in B cell follicles (Fig. 4B), which suggested that this was a general characteristic of

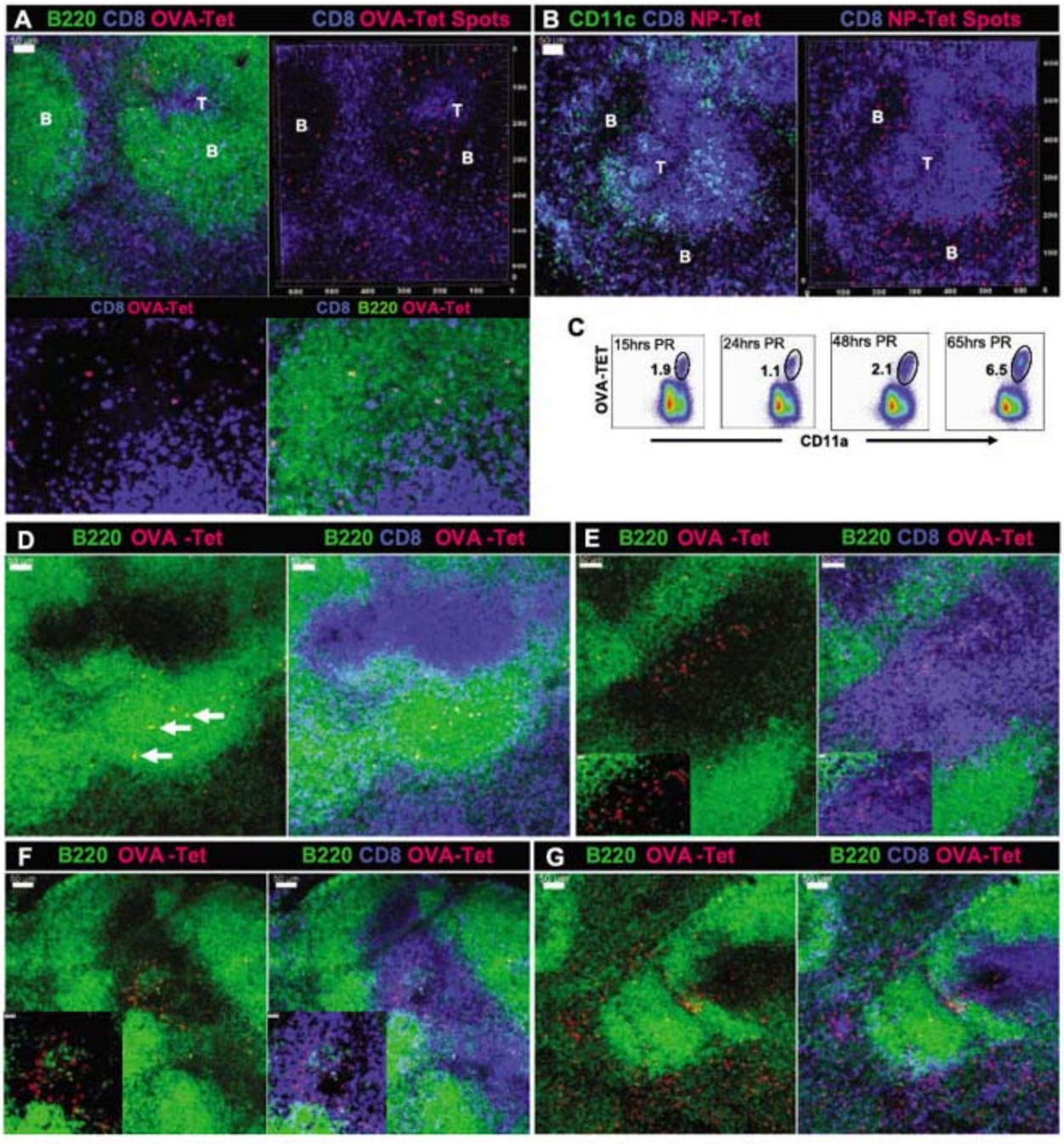

Fig. 4. Memory tet$^+$ CD8 T cells localized to the B cell follicles, MZ and RP rapidly undergo local migration after infection. Multiple thick sections from each spleen, 30 days PI, were stained with K^b-OVA tetramer and the indicated mAb. (**A**) (Top left) A 36-μm merged z-stack image acquired by using a 20× 0.75 NA objective. The data are representative of six different experiments. (Top right) A 3D reconstruction of the z-stack shown at left. The SpotCheck function of Imaris was used to quantify the number of OVA-specific memory CD8 T cells (red spots, 41 cells) in the 37.1-mm^3 volume of spleen shown. (Bottom) Magnified view of a B cell follicle of the splenic white pulp, an 18-μm merged z-stack. The data are representative of six different experiments with two or three mice each. (**B**) NP-specific memory CD8 T cells also localize to the B cell follicles. Spleen sections from mice infected 35 days earlier with 300 times the 50% egg infective dose (EID_{50}) of HKx31 influenza virus intranasally were stained with NP-tetramer and the indicated mAb. (Right) A 3D reconstruction of the 35-μm z-stack shown at left and acquired by using a 20× 0.75 NA objective. SpotCheck analysis revealed 104 NP-specific memory CD8 T cells in the 40.4 mm^3 volume of spleen shown. The data are representative of two different experiments with two mice each. (**C** to **G**) Mice infected 30 days previously were infected with 1×10^4 CFU of LM-OVA. At the indicated times post recall (PR), halves of the spleen were used for flow cytometry (C) or imaging [(D) and (E)]. Dot plots represent gated CD8 T cells. The values represent OVA-tet$^+$ cells as a percentage of CD8 T cells. (D) At 15 hours PR. (E) At 24 hours PR. (F) At 48 hours PR. (G) At 65 hours PR. The data are representative of two different experiments with two mice each.

early memory CD8 T cells. To determine the effect of secondary antigen encounter on memory cells, LM-primed mice were reinfected with LM, and spleens were analyzed (Fig. 4, C to G). At 5 (Fig S11A) and 15 hours (Fig. 4, C and D) post-challenge, the tet^+ memory cells remained in the RP and B cell areas. In contrast, 24 hours post-challenge, tet^+ cells had relocated to the margins of the PALS (Fig. 4E), and by 48 hours, cells were centrally located in the T cell zones (Fig. 4F). Note that unlike the cells in the primary infection, virtually all lymphoid follicles (PALS) were populated with responding tet^+ CD8 T cells (compare Fig. 2A with fig. S11B), which suggests that precursor frequency may dictate the extent of follicle involvement. Events up to this point occurred in the absence of T cell expansion (Fig. 4C), an unexpected result given the rapidity with which memory T cells are believed to be reactivated. By 65 hours post recall, the tet^+ CD8 cells had proliferated (Fig. 4C), and most had exited the PALS and were localized to RP and MZ (Fig. 4G). Movement of memory T cells into the PALS after secondary infection was antigen-specific because infection with wild-type LM had no effect (fig. S12, A and B).

Although previous studies have examined splenic lymphoid architecture, the anatomical events driving primary and secondary CD8 T cell responses to infection have not been clearly delineated. The technique we used did not allow us to quantify movement of individual cells, but allowed us to examine large areas of tissue with relative ease, which is difficult to achieve using other imaging procedures. At the population level, our kinetic analysis clearly revealed a stepwise progression of cellular movements leading to CD8 T cell expansion, exit from the spleen, and localization of resulting memory CD8 T cells in discrete splenic locales. Before this, these events had not been visualized. Imaging also revealed previously unappreciated secondary encounters of daughter CD8 T cells with antigen-bearing DC in large clusters. These findings align with a recent study that concluded that prolonged interactions between CD4 T cells and antigen-presenting cells (APCs) can occur at lower T cell frequencies (*4*). Thus, the contention that only a single brief encounter with an APC is needed to drive CD8 T cell activation (*20*, *21*), although it occurs in experimental systems using TCR transgenic T cells, may not represent in situ events during infection. In contrast, memory CD8 T cells appeared not to undergo secondary activation events and large cluster formation, but upon reactivation, rapidly moved from the B cell follicles to the RP via bridging channels. Therefore, these results lend evidence for a novel mechanism in which B cells or other follicular APCs induced memory CD8 T cell activation. It will be of considerable interest to determine the localization of memory cells as the population undergoes development and maturation.

Overall, the methodical examination of large areas of tissue without disturbing the integrity of structures or the localization of cellular compartments within the organ added a new dimension to the analysis of immune responses. These studies will set the stage for identification of the factors, such as chemokines and other inflammatory mediators, that control the processes driving each anatomical phase of the response. In addition, by comparing the anatomy of different types of immunizations the importance of each step in mounting a protective immune response can be determined. Thus, by monitoring how anatomical relations change during the initiation, expansion, and memory phases of an antimicrobial immune response, we have obtained an understanding of how a productive immune response takes place in vivo, and this information will provide clues to improving vaccine design.

References and Notes

1. M. J. Miller, S. H. Wei, I. Parker, M. D. Cahalan, *Science* **296**, 1869 (2002).
2. P. Bousso, E. Robey, *Nat. Immunol.* **4**, 579 (2003).
3. T. R. Mempel, S. E. Henrickson, U. H. von Andrian, *Nature* **427**, 154 (2004).
4. Z. Garcia *et al.*, *Proc. Natl. Acad. Sci. U.S.A.* **104**, 4553 (2007).
5. P. J. Skinner, M. A. Daniels, C. S. Schmidt, S. C. Jameson, A. T. Haase, *J. Immunol.* **165**, 613 (2000).
6. D. B. McGavern, U. Christen, M. B. Oldstone, *Nat. Immunol.* **3**, 918 (2002).
7. K. M. Khanna, R. H. Bonneau, P. R. Kinchington, R. L. Hendricks, *Immunity* **18**, 593 (2003).
8. A. L. Marzo *et al.*, *Nat. Immunol.* **6**, 793 (2005).
9. Y. Hao, N. Legrand, A. A. Freitas, *J. Exp. Med.* **203**, 1643 (2006).
10. K. D. Klonowski *et al.*, *J. Immunol.* **177**, 6738 (2006).
11. Materials and methods are available as supporting material on *Science* Online.
12. C. Pope *et al.*, *J. Immunol.* **166**, 3402 (2001).
13. J. S. Haring, G. A. Corbin, J. T. Harty, *J. Immunol.* **174**, 6791 (2005).
14. R. E. Mebius, G. Kraal, *Nat. Rev. Immunol.* **5**, 606 (2005).
15. A. Porgador, J. W. Yewdell, Y. Deng, J. R. Bennink, R. N. Germain, *Immunity* **6**, 715 (1997).
16. J. Mitchell, *Immunology* **24**, 93 (1973).
17. W. van Ewijk, T. H. van der Kwast, *Cell Tissue Res.* **212**, 497 (1980).
18. C. Potsch, D. Vohringer, H. Pircher, *Eur. J. Immunol.* **29**, 3562 (1999).
19. H. Unsoeld, D. Voehringer, S. Krautwald, H. Pircher, *J. Immunol.* **173**, 3013 (2004).
20. M. J. Van Stipdonk, E. E. Lemmens, S. P. Schoenberger, *Nat. Immunol.* **2**, 423 (2001).
21. S. M. Kaech, R. Ahmed, *Nat. Immunol.* **2**, 415 (2001).

22. K.M.K is a Damon Runyon Fellow supported by the Damon Runyon Cancer Research Foundation (DRG-1886-05), and by NIH grants AI41576 and AI56172 (LL). We gratefully acknowledge the assistance of A. Cowan and the Center for Cell Analysis and Modeling.

Supporting Online Material

www.sciencemag.org/cgi/content/full/318/5847/116/DC1
Materials and Methods
Figs. S1 to S11
References
Movies S1 to S3

11 June 2007; accepted 30 August 2007
10.1126/science.1146291

Automatic Potentiometric Titrator

The Aquacounter COM-300A automatic titrator performs pH, acid/base, complexometric, redox, Karl Fischer, photometric, and ion-selective electrode measurements as well as non-aqueous titrations. The unit can also determine total acid/total base in oils. Additional features include a statistics package for one-touch calculations. It can store up to 50 results in memory or download results to a laptop or desktop computer. An optional Karl Fischer kit is available for moisture determination.

JM Science For information 800-495-1678 www.jmscience.com

Human Adipose-Derived Stem Cells

The Poietics Human Adipose-Derived Stem Cell (ADSC) system, for use in adult stem cell research, provides laboratories with ready-to-use cells and media for research in areas such as tissue repair, wound healing, cell differentiation, osteoporosis, insulin resistance, and obesity. The system contains cryopreserved normal human adipose-derived stem cells and an optimized ADSC growth media kit for cell growth and expansion. Research has indicated that when exposed to specific growth conditions in vitro, these cells can demonstrate various characteristics suggestive of cells from tissues such as fat, bone, cartilage, nerve, muscle, and blood vessels to some extent.

Lonza Group For information 800-638-8174 www.lonzabioscience.com

Ultra-High Pressure Liquid Chromatography

New ultra-high pressure liquid chromatography (UHPLC) methods provide higher resolution than traditional HPLC methods. To take full advantage of this superior resolution, it is important that samples, mobile phases, and buffers are properly prepared. Millipore provides syringe filters, membranes, and holders in many configurations that are designed to maximize UHPLC performance. These devices minimize column clogging and have low extractables, low binding, and low hold-up volumes to optimize sample preparation. Millex syringe filters ensure minimal signal-to-noise ratios and clean baselines. They have a broad chemical compatibility and low hold-up volumes, making them a convenient means of clarifying and/or removing small particles from samples prior to UHPLC analysis. Millipore Express Plus membrane is the first asymmetrical polyethersulfone (PES) membrane available for ultrafast filtration in laboratory applications. It enables the rapid filtration of additives, buffers, and other aqueous solutions. This membrane is available as 25-mm and 47-mm cut disks with 0.22 mm pore sizes as well as Steritop vacuum filter cups and syringe filter devices. MultiScreen Solvinert Plates are optimized for drug discovery applications, including total drug analysis. They come in both deep-well and standard volumes and are available in a choice of either chemically resistant hydrophobic or hydrophilic PTFE membranes.

Millipore For information 800-MILLIPORE www.millipore.com/bioscience

Assay Development Service

A comprehensive assay development service is available for high-performance, highly sensitive assays in advanced cellular science and drug discovery research. Whether it involves developing custom assays, increasing densities from 96-well to 384-well or 1536-well, or converting outdated assay technologies to next-generation platforms, the assay development service can fast-track development of application-specific assays for pharmaceutical or research customers. The service offers comprehensive assay solutions for high-value g-protein coupled receptor and kinase cell-based screening including sensitive, high-throughput platforms such as the AlphaScreen, AequoScreen, DELFIA, and LANCE technologies. Reporter gene assays are available featuring Steadylite Plus and Britelite Plus technologies. The assay development service can also provide miniaturization of tough-to-automate immunoassays.

PerkinElmer For information 781-237-5100 www.perkinelmer.com

Cell Surface Protein Isolation

Sulfo-NHS-SS-Biotin can be used to label cell surface proteins and isolate them for further analysis, including protein immunoblotting. An amine-reactive biotinylation reagent that is soluble in water but impermeable to plasma membranes, it can label adherent and non-adherent mammalian cells. Sulfo-NHS-SS-Biotin has a disulfide bond in the spacer arm that permits the cleavage of the biotin moiety from the protein, making its interaction with a streptavidin purification column reversible. Cells are lysed and applied to a streptavidin agarose column. Unlabeled intracellular proteins are washed away and the biotin-labeled cell surface proteins are then released by reduction of the disulfide bond with dithiothreitol.

Genotech/G-Biosciences For information 800-628-7730 www.GBiosciences.com

Freeze Dryers

The Benchtop K Series Freeze Dryers were developed to meet the demand for a research freeze dryer that would provide a full range of laboratory processing capabilities. The K Series offers a wide range of options and accessories with condenser temperatures from −55°C to −105°C. This wide range of condenser temperatures provides the drying power required to freeze-dry all aqueous and most organic-based samples. The freeze dryers are efficient and easy to operate, with a microprocessor controller providing a user-friendly interface with full function control. A graphical wave LED displays system status while a backlit synoptic LCD enables at-a-glance monitoring of all operations. Powerful software provides complete data collection and historical trending of the freeze drying cycle.

SP Industries For information 800-523-2327 www.SPindustries.com

Newly offered instrumentation, apparatus, and laboratory materials of interest to researchers in all disciplines in academic, industrial, and government organizations are featured in this space. Emphasis is given to purpose, chief characteristics, and availability of products and materials. Endorsement by *Science* or AAAS of any products or materials mentioned is not implied. Additional information may be obtained from the manufacturer or supplier.

Science Careers
From the journal Science AAAS

Classified Advertising

From life on Mars to life sciences

For full advertising details, go to www.sciencecareers.org and click on **For Advertisers,** or call one of our representatives.

United States & Canada

E-mail: advertise@sciencecareers.org
Fax: 202-289-6742

IAN KING Recruitment Sales Manager
Phone: 202-326-6528

ALLISON MILLAR
Industry–US & Canada
Phone: 202-326-6572

ALEXIS FLEMING
Northeast Academic
Phone: 202-326-6578

TINA BURKS
Southeast Academic
Phone: 202-326-6577

DARYL ANDERSON
Midwest/Canada Academic
Phone: 202-326-6543

NICHOLAS HINTIBIDZE
West Academic
Phone: 202-326-6533

Europe & International

E-mail: ads@science-int.co.uk
Fax: +44 (0) 1223 326532

TRACY HOLMES Sales Manager
Phone: +44 (0) 1223 326525

ALEX PALMER
Phone: +44 (0) 1223 326527

ALESSANDRA SORGENTE
Phone: +44 (0) 1223 326529

MARIUM HUDDA
Phone: +44 (0) 1223 326517

LOUISE MOORE
Phone: +44 (0) 1223 326528

Japan

JASON HANNAFORD
Phone: +81 (0) 52-757-5360
E-mail: jhannaford@sciencemag.jp
Fax: +81 (0) 52-757-5361

To subscribe to *Science*:
In U.S./Canada call 202-326-6417 or 1-800-731-4939
In the rest of the world call +44 (0) 1223-326-515

Science makes every effort to screen its ads for offensive and/or discriminatory language in accordance with U.S. and non-U.S. law. Since we are an international journal, you may see ads from non-U.S. countries that request applications from specific demographic groups. Since U.S. law does not apply to other countries we try to accommodate recruiting practices of other countries. However, we encourage our readers to alert us to any ads that they feel are discriminatory or offensive.

POSITIONS OPEN

EXERCISE BIOLOGIST

Washington State University Program in Health Sciences (Exercise Physiology and Metabolism) invites applications for a nine-month, full-time, permanent, tenure-track appointment at the level of **ASSISTANT or ASSOCIATE PROFESSOR** (depending on qualifications) located at the WSU Spokane campus. Position is available August 2008. Position description: The successful candidate will be expected to teach, maintain a focused line of research with significant extramural funding, and participate in the service missions of the University. Required qualifications include a doctoral degree in a relevant area before first date of employment and evidence of scholarly productivity with potential for extramural funding. Preferred qualifications include postdoctoral experience in an area relevant to exercise biology with research emphasis in, but not limited to, cellular signaling, molecular, genomic, and/or proteomic approaches to address the role of exercise in chronic disease prevention or management, and excellent communication skills. Salary will be commensurate with qualifications and experience. Applicant screening begins November 1, 2007.

To apply, send the following items to the **Search Committee Clerical Manager** (see below): letter of application addressing qualifications and responsibilities, curriculum vitae, names of three references with mail and e-mail addresses and telephone numbers, narrative of research plan, including information on grant applications recently submitted (abstract, agency to which it was submitted, amount requested, status of funding) and planned (title, brief summary), and statement of teaching philosophy. References will not be contacted until candidate approval is secured.

Send information to: **Saren Kennedy, Search Committee Clerical Manager, Attn: E. Carolyn Johnson, Ph.D., Fellow of the American College of Sports Medicine, College of Pharmacy, Washington State University Spokane, P.O. Box 1495, Spokane, WA 99210-1495. Telephone: 509-358-7630; fax: 509-358-7627; e-mail: saren@wsu.edu** (PDF format preferred).

For more information contact: **E. Carolyn Johnson, Ph.D., Fellow of the American College of Sports Medicine, Search Committee Chair, Associate Professor, Program in Health Sciences (Exercise Physiology and Metabolism), College of Pharmacy, Washington State University Spokane, P.O. Box 1495, Spokane, WA 99210-1495. Telephone: 509-368-6733; e-mail: ecarolj@mail.wsu.edu.**

The complete job description is available at **websites: http:// www.phs.spokane.wsu.edu** and **http:// www.chr.wsu.edu.** *WSU is an Equal Employment Opportunity/Affirmative Action Educator and Employer.*

For more than 130 years, Lilly has been dedicated to meeting the health care needs of people in the United States and around the world. We address these needs primarily by developing innovative medicines; investing a higher percentage of our sales in research and development than any other major pharmaceutical company. If you are interested in being considered for employment with a "Best in Class" pharmaceutical company, please review the following opportunity: job identification number 50306254 - Lilly seeks a **PRINCIPAL RESEARCH SCIENTIST** in Indianapolis, Indiana, in the bioinformatics group to design, develop, implement, and maintain bioinformatics tools to accelerate the drug discovery pipeline. Candidate will prioritize gene pools to obtain biologically relevant information from microarray experimental data, and will apply bioscientific principles in analyzing enormous and highly complex groups of data to determine how to best use and understand the data to develop new drugs. Must have Ph.D. in microbiology, biology, or related field and relevant experience. Salary range: $105,000 to $163,000, depending upon qualifications. Please submit resume to **website: http://www.lilly.com/careers** and cite the relevant job title and job identification number in your submission. *Lilly is an Equal Opportunity Employer that values the strength diversity brings to the workplace.*

POSITIONS OPEN

RUTGERS CAMDEN

RUTGERS UNIVERSITY, CAMDEN
Department of Mathematical Sciences
Joseph and Loretta Lopez Endowed Chair in Mathematics

Applications and nominations are invited for the **JOSEPH and LORETTA LOPEZ CHAIR in MATHEMATICS.** The Department seeks a distinguished Scholar in mathematics with international reputation, well-established research and teaching record, and demonstrated ability to generate external funding. This endowed Chair is the first at the Camden Campus of Rutgers University. It is a tenured faculty position and the Chair is for a five-year renewable term. The holder of this Chair will be a senior faculty member and a vigorous participant in the research, instruction, and service work of the Department of Mathematical Sciences. The holder will also be expected to play a vital role in the campus' growing program in computational biology and the recently established Center for Computational and Integrative Biology. As such, applicants must demonstrate evidence of research in the areas of mathematical and/or computational biology.

The appointment will commence on July 1, 2008, and is at the rank of **ASSOCIATE or FULL PROFESSOR.** The Department will begin reviewing applications on December 17, 2007, and continue its review until the position is filled. Applications should be sent to:

Professor Gabor Toth
Chair, Search Committee
Department of Mathematical Sciences
Rutgers University, Camden
Camden, NJ 08102

Applicants should also arrange for at least four letters of recommendation to be sent.

Rutgers University, Camden, is an Affirmative Action/Equal Opportunity Employer and encourages applications from women and minority group members.

BRANDEIS UNIVERSITY
Department of Chemistry Faculty Positions

The Department of Chemistry at Brandeis University is seeking creative individuals for faculty positions in all areas of chemistry, beginning fall 2008. We expect to appoint at the rank of tenure-track **ASSISTANT PROFESSOR,** but a more advanced appointment for candidates with exceptional qualifications may be considered, with the level of appointment depending upon qualifications. The successful applicants are expected to establish vigorous, externally funded research programs and be enthusiastic teachers.

The Department of Chemistry anticipates a number of searches over the next several years, and is part of a vibrant and interactive scientific community. Resources include state of the art nuclear magnetic resonance, X-ray crystallography, mass spectrometry, and electron microscopy facilities; new research buildings are under construction. The suburban campus is located in the Route 128 technology corridor just 20 minutes from Boston and Cambridge. For information about the Department, visit **website: http:// www.chem.brandeis.edu.**

Applicants at the Assistant level (tenure track) should submit curriculum vitae, description of their research plans, and arrange for three letters of recommendation addressed to the **Search Committee** at **e-mail: chmsrch@brandeis.edu** (preferred) or **Search Committee Chair, Department of Chemistry M.S. 015, Brandeis University, 415 South Street, Waltham, MA 02454-9110.** Senior applicants should provide curriculum vitae, brief description of their research program, and the names of three potential referees. First consideration will be given to applications received by November 1, 2007. *Brandeis University is an Equal Opportunity Employer, committed to building a culturally diverse intellectual community, and strongly encourages applications from women and minorities.*

MEANINGFUL MENTORING:
NATIVE AMERICAN AND LATINO SUCCESS STORIES

Early and sustained interventions which strongly feature mentoring are essential in helping Native American and Latino students navigate an unfamiliar academic system that is dominated by majority culture and practices. Throughout students' educational progression and well into their initial strides upon donning the doctoral gown, they depend upon a clearly marked career map, research training opportunities, professional skills development, peer networks, and role models. These factors can mean the difference between successfully reaching their goals and taking missteps ending in an impassable career detour.
By Lin M. Hundt and Jenny Kurzweil

Maria Elena Zavala, director for the California State University, Northridge Minority Access to Research Careers and Minority Biomedical Research Support programs.

Claudia Benítez-Nelson and son

Talia Martin

"I was never lost. They really helped me through, every step of the way."

In a class of 100 students, I might have one minority student," says **Claudia Benítez-Nelson,** describing the abysmally low minority participation in even her most introductory marine science courses.

Benítez-Nelson, associate professor in the Department of Geological Sciences and undergraduate director for the Marine Science Program at the University of South Carolina (USC), could be relating statistics from a science program in most any field at any college in the nation. The low participation of Native Americans and Latinos in science research careers is no secret. According to the latest data available from the National Science Foundation, while Latinos, Native Americans, Alaska Natives, and Native Hawaiians/Pacific Islanders comprise nearly 17 percent of the population in the United States only 4 percent of the science and engineering Ph.D.s granted in 2004 went to Hispanic/Latinos and 0.3 percent to Native Americans/Alaska Natives (National Science Foundation, Division of Science Resources Statistics, Survey of Earned Doctorates, 1997–2004. http://www.nsf.gov/statistics/wmpd/tables/tabf-6.xls). And, while significant shifts in participation continue to be elusive, many of the keys to change are in place thanks to national efforts and federally funded diversity programs at most institutions.

Mapping the Path to a Science Career

Many minority students enter university with tremendous trepidation about whether they belong, doubts about their chances of success, and a conspicuous lack of knowledge about the college experience. **Talia Martin,** a Native American of the Shoshone-Bannock tribes and a recent graduate in chemistry from the University of Kansas (KU), was the first in her family to earn a college degree. Martin initially learned how to navigate college and approach faculty for mentoring support through the 500 Nations Bridges to the Future Program at Haskell Indian Nations University. One of the many multifaceted programs funded by the Minority Opportunities in Research (MORE) division at the National Institute of General Medical Sciences (NIGMS), the 500 Nations Bridges Program provides research opportunities in KU labs for students at Haskell who are interested in transferring to four-year research universities. Once Martin had transferred to KU, she got involved with the McNair Scholars Program that prepares traditionally underrepresented students for graduate study through continued research opportunities. Martin credits participation in mentoring-focused programs as critical to connecting her to faculty mentors and helping her succeed as an undergraduate. The mentors gave her direction. "I was never lost. They really helped me through, every step of the way—whether it be getting to class, passing my classes, or finding a goal in life and academia."

A lack of understanding of any number of decisions along the path can lead to lack of minority students' retention within the science education pipeline, not to mention indelibly affecting career options. To counter this lack of knowledge, **Debra E. Stalk,** Kahnawake Mohawk, created the Native American Mentoring Program (NAMP) of the Sackler Institute of Graduate Biomedical Sciences at the New York University (NYU) School of Medicine.

Reaching out nationally, NAMP helps Native American students become competitively prepared to enter graduate programs in their area of interest. She finds, however, that students aren't the only ones who lack an understanding of the current realities of a science education. She says, "Because the numbers of Native American students are so small continued »

CREDIT: (BOTTOM) KU UNIVERSITY RELATIONS

UPCOMING FEATURES

Top Employers Survey— October 12
Careers in Neuroscience — October 26
Focus on Diversity 3 — November 16

at undergraduate [institutions], oftentimes advisers are under this misimpression that these students will be eligible for any medical school or graduate training program they apply to, just by virtue of being a native student in college." Thus, another facet of NAMP is providing training to undergraduate advisers, so that they can offer accurate career counseling to their minority students.

Developing Science Research Expertise

The more generalized mentoring elements of programs like NAMP, Bridge, and McNair Scholars are accompanied in many instances by exposure of underrepresented minority students to hands-on research experience. In developing their scientific expertise in the lab, minority students lay the foundation for a research career by significantly increasing their chances of getting into competitive graduate programs.

Maria Elena Zavala, professor of biology at California State University, Northridge, is the program director for the CSUN Minority Access to Research Careers (MARC) and Minority Biomedical Research Support (MBRS) programs through MORE. Both MARC and MBRS focus on bringing students into the lab. MARC is a competitive honors program that provides lab research opportunities in addition to mentoring-focused workshops and curricula. MBRS funding, in general, allows faculty to establish research programs that create opportunities for students to work as part of a research team. Zavala notes that MARC/MBRS programs are like an apprenticeship. "The way we do science is by learning from others; it is easier if someone directs you in that hands-on approach. Having students work in the lab is one way of imparting knowledge; it is also a way of imparting behavior."

Because most of her Latino and Native American students haven't grown up with professional scientists as parents, prior to entering her mentoring program Zavala's students haven't had someone to make the general guidelines for pursuing the scientific career path clear to them. Thus, Zavala's mentoring introduces her students to research as an intellectual and social pursuit, including concepts of scientific ethics, responsibility, and appropriate conduct.

Important research opportunities for minority science students are also available outside the traditional academic setting through industry internships and fellowships. **Lino Gonzalez,** a research scientist at Genentech, believes that these research opportunities are particularly important for Latino and Native American students who have had little, if any, exposure to the high technology world and how science is conducted in such an environment. Therefore, Gonzalez believes that "diversifying [students'] scientific experiences during the undergraduate years with both academic and industrial research can help shape life-long goals for their graduate and professional lives." In his experience, for students interested in industry, the connections they develop during internships can be invaluable. "I have seen many former intern students return after they complete their graduate studies to apply for full-time positions," says Gonzalez.

The All Nations Louis Stokes Alliance for Minority Participation program (All Nations LSAMP), funded through the National Science Foundation (NSF), is another endeavor to engage underrepresented minority students, specifically Native Americans, in research. All Nations LSAMP, housed at Salish Kootenai College, serves as a funding clearinghouse for 25 tribal colleges and 11 other predominantly Native American–serving universities, to start up and sustain science and research programs that meet the particular needs of the communities they serve. "For example," **Zetra Wheeler,** Blackfeet, the program manager for All Nations LSAMP, explains, "Salish Kootenai College used the previous phase LSAMP funds to help develop its four-year forestry program since the reservation is covered in timber and is a source of income."

For Native American students on reservations and in rural areas that want to pursue a career in academia or industry, participating in conventional lab research is crucial for their next steps. These careers, however, will take them away from home, a compromise that as Wheeler explains many Native American students are reluctant to make. As the most underrepresented group within the scientific arena, Native American communities have a deep need for increased representation within the mainstream scientific work force. At the same time, there is a significant gap in scientific expertise to tackle pressing concerns within the community, such as management of tribal lands and natural resources, and culturally relevant health care and public health awareness. Through the diversity of the programs funded by All Nations LSAMP, Native American students are provided opportunities for scientific preparation that address both areas of concern. continued »

All Nations Louis Stokes Alliance for Minority Participation (All Nations LSAMP)
www.anamp.org

American Indian Science and Engineering Society (AISES)
www.aises.org

Annual Biomedical Research Conference for Minority Students (ABRCMS)
www.abrcms.org

California State University, Northridge
www.csun.edu

David Geffen School of Medicine, University of California, Los Angeles
www.dgsom.healthsciences.ucla.edu

Genentech, Inc. College Programs
www.gene.com/gene/careers/college/programs.jsp

Haskell Indian Nations University
www.haskell.edu/haskell

Institutional Research and Academic Career Development Award (IRACDA) Program
www.nigms.nih.gov/Training/Mechanisms/CareerDev/MOREInstRes.htm

Minority Access to Research Careers (MARC)
www.nigms.nih.gov/Minority/MARC

Minority Biomedical Research Support (MBRS)
www.nigms.nih.gov/Minority/MBRS

National Institute of General Medical Sciences, Minority Opportunities in Research Division
www.nigms.nih.gov/Minority

National Postdoctoral Association
www.nationalpostdoc.org

National Science Foundation
www.nsf.gov

National Science Foundation Graduate Teaching Fellows in K-12 Education (GK-12) Program
www.nsf.gov/funding/pgm_summ.jsp?pims_id=5472

Native American Mentoring Program (NAMP), Sackler Institute of Graduate Biomedical Sciences, New York University School of Medicine
www.med.nyu.edu/sackler/namp

University of Pennsylvania (Penn) Biomedical Postdoctoral Programs (BPP)
www.med.upenn.edu/postdoc

Salish Kootenai College
www.skc.edu

ScienceQuest Program, University of South Carolina
www.geol.sc.edu/cbnelson/ScienceWeb/index.htm

Society for Advancement of Chicanos and Native Americans in Science (SACNAS)
www.sacnas.org

SACNAS Minority Postdoc Community
www.minoritypostdoc.org

University of Kansas (KU)
www.ku.edu

University of Kansas 500 Nations Bridges to the Future Program
www2.ku.edu/~bridge

University of Kansas McNair Scholars Program
www2.ku.edu/~mcnair

Professional Skills for Professional Advancement

In addition to the scientific preparation that mentors and mentoring programs offer, doctorates and doctoral aspirants alike need training in the professional (nonbench) skills that form a foundation to science career advancement. In the University of Pennsylvania's Biomedical Postdoctoral Programs (BPP), this translates to ongoing workshops that start with conventional aspects of professionalism from communication skills for grant writing and job interviews to leadership skills for managing a lab and working with a research team. The program also addresses fundamentals that minority postdocs may never even have considered to be part of their professional training—like which utensils to use during the course of a business lunch.

Ivonne Vidal Pizarro, the former recruitment and diversity coordinator for BPP, categorizes shortfalls in professional training opportunities and support services for postdocs as the missing links in the minority science pipeline. According to Vidal Pizarro, who is now at the American Association for Cancer Research in the position of scientist, program administrator, the postdoctoral stage is overlooked by those looking at the advancement of Native Americans and Latinos in the sciences. "If you really want to bump up the numbers of faculty members that come from underrepresented minority groups, then you need to address postdoctoral issues."

And those issues are by no means uncomplicated. Recent recipients of a doctorate often find themselves, in fact, at one of the most precarious junctures in their career. While postdoctoral training has become practically a requirement for academic employment in many fields, the large majority of postdocs will be unable to obtain a faculty position at the end of their postdoctoral tenure. In such a tight job market, for Latino and Native American scientists, postdoctoral appointment choices and planning, professional skills development, and support systems are especially crucial.

"The value of peer-to-peer networks is to ameliorate the difficulties that minorities can face in majority settings by sharing experiences with and finding empathy from sympathetic colleagues."
–Alberto Roca

In the trajectory of a successful scientific career, communicating one's research results goes hand in hand with establishing aptitude in conducting that research. Annual minority science conferences, such as the Society for Advancement of Chicanos and Native Americans in Science (SACNAS), the American Indian Science and Engineering Society (AISES), and the NIGMS-funded Annual Biomedical Research Conference for Minority Students (ABRCMS), provide excellent multidisciplinary forums for students to receive guidance in the art of public speaking and the craft of scientific inquiry.

Gustavo Miranda, a research scientist at the David Geffen School of Medicine at the University of California, Los Angeles, chairs the student poster presentations program at the SACNAS conference, where over 500 students present their work annually. He affirms that conferences like SACNAS provide "early training for how to handle the nuances of professional presentations." Miranda has observed that when attending large, discipline-specific conferences minority students can get lost in the crowd, feel insignificant and out of place. "At conferences like SACNAS, students connect with mentors and role models from their same ethnic background and progressive majority scientists." In Miranda's view, these interactions with mentors, that recognize the value of underrepresented minority communities in producing a competitive scientific work force, provide minority students with scientific preparation that they cannot get elsewhere.

Peer-to-Peer Networking on a National Scope

Efforts at individual institutions to support the needs of the burgeoning postdoctoral community have been joined by a growing number of national programs and organizations. Many are self-initiated by postdocs desperate for support. The National Postdoctoral Association (NPA) was formed in 2003 to provide advocacy for and national coalescence among postdoctoral scholars. Similarly, the SACNAS Postdoc Committee and Minority Postdoc Community website are the conception of SACNAS postdocs, resulting in postdoctoral networking activities and an interactive virtual community across geographical barriers.

Whether enhancing their skills via postdoctoral research, on the hunt for employment, or settling into a newly acquired faculty or investigator role, minority scientists are regularly culturally isolated as the only minority in their professional world. **Alberto Roca,** founding member of the SACNAS Postdoc Committee believes, "The value of peer-to-peer networks is to ameliorate the difficulties that minorities can face in majority settings by sharing experiences with and finding empathy from sympathetic colleagues."

Full Circle: Ph.D. to Precollege

In order for increasing numbers of Native Americans and Latinos to arrive at the point where they are seeking a faculty, federal, or industry research position, they must have seen the possibility of such a career well before college entrance exams.

Benítez-Nelson from USC became involved in precollege education, forming the USC ScienceQuest program based on a national model, to address minority students' lack of awareness about and interest in science careers. Having identified the need to reach out to precollege students when they are still quite open to the enjoyment of scientific investigations, Benítez-Nelson focused her after-school science enrichment program on grades four through six.

Benítez-Nelson perceives a direct link between the involvement of minority professional scientists in K-12 education and the promotion of a vibrant minority scientific work force. "If all you see are people who don't look like you, who don't act like you, who don't come from your background, it never occurs to you that it is possible to do these things, too." ScienceQuest, funded by NSF, is recording positive results for the student participants in terms of grades, behavior, and performance in all subject areas, including science. Benítez-Nelson's graduate students are also enriched by the experience; many become inspired to extend their experience in precollege teaching by becoming involved in USC's NSF Graduate Teaching Fellows in K-12 Education (GK-12) Program.

Enduring Needs

Minority mentoring on a national scale is working...to a certain degree. Latino and Native American students are matriculating into and graduating from science programs at an increasing rate; and opportunities at research corporations and federal laboratories are building inroads for nonacademic science careers. Nonetheless, within the echelons of tenure-track faculty at leading research universities, there remains a noticeable lack of change in the representation of minority scientists. Fresh approaches and commitments at the professoriate level, in concert with programs that encourage minority participation in science throughout the education process, may hold the final key to success.

Jenny Kurzweil and Lin M. Hundt are senior editors with SACNAS News.

DOI: 10.1126/science.opms.r0700041

CREDIT: UNIVERSITY OF CALIFORNIA, IRVINE